Donor-Acceptor Systems Based on Axially and Peripherally Substituted Porphyrin Building Blocks

A Thesis

Submitted for the Degree of

DOCTOR OF PHILOSOPHY

By

Poddutoori Prashanth Kumar

School of Chemistry
University of Hyderabad
Hyderabad - 500 046
INDIA

September 2004

Dedicated To

My Beloved Supervisor

Late Prof. Bhaskar G. Maiya

Contents

School of Chemistry
University of Hyderabad
Central University P.O.
Hyderabad 500 046
India

Statement

I hereby declare that the matter embodied in this thesis is the result of investigations carried out by me in the School of Chemistry, University of Hyderabad, Hyderabad, India under the supervision of **Late Prof. Bhaskar G. Maiya**.

In keeping with the general practice of reporting scientific observations, due acknowledgements have been made wherever the work described is based on the findings of other investigators.

Poddutoori Prashanth Kumar

School of Chemistry
University of Hyderabad
Central University P.O.
Hyderabad 500 046
India

Certificate

Certified that the work contained in this thesis entitled **"Donor-Acceptor Systems Based on Axially and Peripherally Substituted Porphyrin Building Blocks"** has been carried out by **Poddutoori Prashanth Kumar** under the supervision of **Late Prof. Bhaskar G. Maiya** and that the same has not been submitted elsewhere for a degree.

Dean
School of Chemistry

DEAN
School of Chemistry
University of Hyd.
Hyderabad-46.

Prof. M. V. Rajasekharan
Thesis Co-Supervisor

Acknowledgements

It gives me immense pleasure to express my deep sense of gratitude and profound respect to my sir **Late Prof. Bhaskar G. Maiya** for introducing me to this field of research and teaching me many principles and techniques. I have learnt a lot from his meticulous planning and implementation, dedication and hard work. My association with him throughout my research tenure in this lab was a rewarding experience, which I never wish to forget.

I express my sincere thanks to Prof. M. V. Rajasekharan, for his help full discussions, suggestions and corrections of the thesis.

I thank Prof. E. D. Jemmis, Dean, School of Chemistry, former Deans and all the faculty members especially Dr. Samudranil Pal, Prof. K. C. Kumara Swamy and Prof. T. P. Radhakrishnan for their help on various occasions.

I thank Prof. V. Krishnan (JNACSR, Bangalore) for his guidance and helpful discussions for writing the thesis. I am grateful to Prof. T. K. Chandrashekar (IIT, Kanpur) for collecting the NMR data for some of the samples.

Also, I would like to thank Prof. J. K. M. Sanders and Dr. N. Bampos, (University of Cambridge, Cambridge, U. K.); Prof. A. Osuka (Kyoto University, Kyoto, Japan) for their help in collecting the NMR and mass (MALDI) data for some of the samples.

I am grateful to Prof. N. Periasamy and Dr. Srirama Koti (TIFR, Mumbai) and I also thank Dr. P. Ramamurthy and Indira Priyadharshini (National Centre for Ultrafast Processes, Chennai) for their kind help in time-resolved fluorescence studies.

Central Drug Research Institute (CDRI), Lucknow is acknowledged for the FAB mass spectral data.

I thank the authorities of Centre for Modelling, Simulation and Design (CMSD) and also the University with Potential for Excellence (UPE) programme of the University of Hyderabad.

I thank my senior Dr. L. Giribabu for his helpful discussions. I thank my labmates Dr. A. Ashok Kumar, Dr. D. Raghunath Reddy, C. V. Sastri, M. Mariappan, G. Premaladha, Tamal Ghosh, A. Narahari and S. Prathap Chandran for creating pleasant atmosphere during my tenure in this laboratory.

I would like to thank Mr. Satyanarayana, Mr. Bhaskar Rao, Mr. Raghavaiah and Mrs. Ayesa Parwez for their technical assistance. I also thank Mr. Shetty and other non-teaching staff of the school of chemistry for their help.

I thank all my **friends** and well wishers for making my stay in the campus a memorable one.

Financial assistance from UGC and CSIR is gratefully acknowledged.

Last, but not the least, I am deeply grateful to my parents, brothers and sister for their love and constant encouragement throughout my career.

Synopsis

This thesis entitled "**Donor-Acceptor Systems Based on Axially and Peripherally Substituted Porphyrin Building Blocks**" deals with the design, synthesis, spectroscopy and photochemical properties of free base and metallo/metalloid porphyrins that are substituted at either axial or peripheral positions with aromatic donor/acceptor subunits. Main observations of the research carried out here include photoinduced electron transfer (PET) and electronic energy transfer (EET) reactions in these D-A systems.

Porphyrins and their metal/metalloid derivatives are a versatile class of compounds having applications in various research areas such as biomimetic photosynthesis, molecular electronics, molecular catalysis, photodynamic therapy etc. A great variety of D-A type porphyrin systems have been built for use in many of these applications, which generally involve PET and EET as the key principles. While majority of the D-A systems have been constructed by linking the donor/acceptor subunits at the porphyrin peripheral (i.e. β-pyrrole and meso) positions, relatively less number of such systems have been synthesized by utilizing the axial site/s on the central metal/ metalloid ion of a porphyrin.

A Chapter in this thesis (Chapter 3) deals with a series of oligomeric porphyrin dimers and trimers in which a main-group element aluminium(III) containing porphyrin is used as the basal scaffolding unit and either free base or metallo-porphyrins are the axial donor/acceptor subunits. The 'axial bonding' idea has been further extended to the design of a novel terpyridine containing tin(IV) and phosphorus(V) porphyrin triads **[L^1Sn(O-ptp)$_2$]** and **[L^1P(O-ptp)$_2$]$^+$** (Chapter 4). Detailed studies on the chemistry, electrochemistry and photochemistry of these triads have been carried out. Next, the 'peripheral' positions have been utilized to construct a series of D-A systems (Chapter 5), where ruthenium (II)

bis-terpyridine complex has been connected to the meso phenyl of free base or zinc(II) porphyrins *via* ethylene spacer. Details of EET and PET reactions occurring in these dyads and triads have been investigated. Finally, a systematic investigation has been carried out on the spectral and photophysical properties of molecular dyads in which free base porphyrin or its copper(II)/zinc(II) analogues has been covalently linked to donor pyrene or acceptor anthraquinone subunits through azomethine bridge at meso phenyl ring (Chapter 6).

The work embodied in this thesis has been divided into seven Chapters. A brief, Chapter-wise account of the results is presented below.

Chapter 1. Introduction

Recent literature on various axial/peripheral-bonding type, porphyrin based D-A systems highlighting their PET and EET reactions have been reviewed in this Chapter.

Chapter 2. Material and methods

This Chapter presents a list of chemicals, a general description of the synthetic procedures and details of X-ray crystallographic, spectroscopic, electrochemical and photophysical techniques employed during the research work.

Chapter 3. Aluminium(III) porphyrin based dimers and trimers: Synthesis, spectroscopy and photochemistry.

The well-known oxophilicity of aluminium(III) ion and the well-defined redox and photochemical properties of aluminium(III) porphyrins have been exploited to synthesize functionally-active, 'axial-bonding' type free base-aluminium(III) porphyrin dimer (**H_2-Al**) and free base-[aluminium(III)

porphyrin]$_2$ trimer (**H_2-Al_2**) as well as the corresponding copper(II) (**Cu-Al, Cu-Al_2**) and zinc(II) (**Zn-Al, Zn-Al_2**) derivatives, Fig. 1.

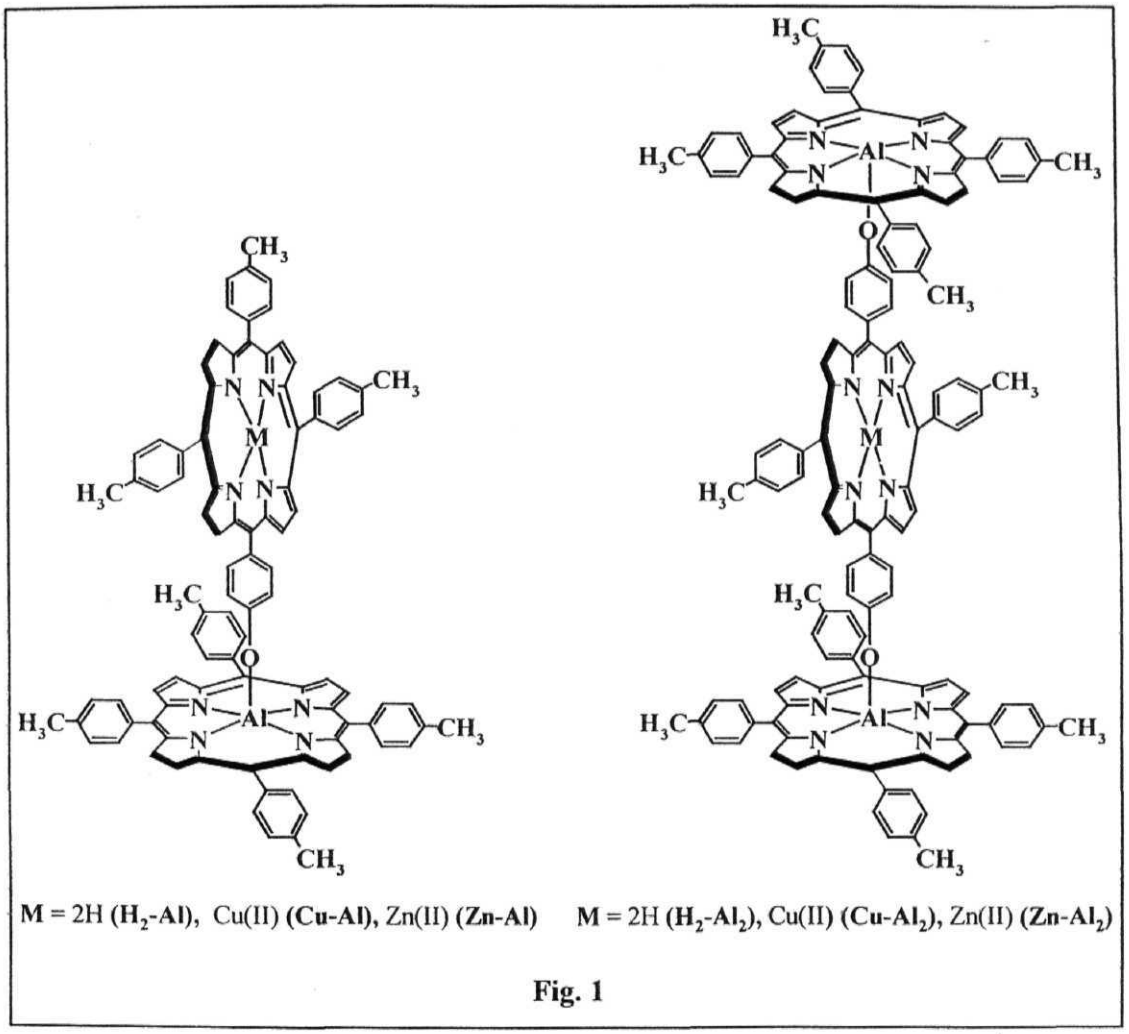

Fig. 1

These dimeric and trimeric species have been fully characterized by the mass (MALDI), UV-visible, proton nuclear magnetic resonance (1D and ^{1}H-^{1}H COSY) and electron spin resonance spectroscopies and also by the differential pulse voltammetric method. Comparison of their spectroscopic and electrochemical data with those of the corresponding monomeric porphyrins reveals that there are no apparent ring-to-ring interactions in these 'vertically' linked dimers and trimers. The fluorescence quantum yields and singlet state life times were found to be lower for **H_2-Al** and **H_2-Al_2** in comparison with those of

the monomeric chromophores. Electronic energy transfer from the aluminium(III) porphyrin to the free base subunit is detected in both **H_2-Al** and **H_2-Al_2**. On the other hand, efficiency of the PET from the singlet Al(III) porphyrin to the free base cannot be neglected altogether in high polarity solvents.

Finally, a comparison is made between the presently reported aluminium(III) porphyrin based arrays and the previously reported analogous arrays based on tin(IV), germanium(IV) and phosphorus(V) porphyrins with regard to their architectural features, spectroscopic properties and photochemical activities.

Chapter 4. Synthesis and characterization of axial bis(terpyridoxy) Sn(IV) and P(V) porphyrins: Modulation of EET and PET by transition metal ions.

The 'axial-bonding' theme is further utilized in this Chapter to synthesize tin(IV) and phosphorus(V) porphyrin based terpyridine containing **[L^1Sn(O-ptp)$_2$]** and **[L^1P(O-ptp)$_2$]$^+$** triads, Fig. 2. These triads have been fully characterized by the mass (MALDI), UV-visible, proton nuclear magnetic resonance (1D and ^{1}H-^{1}H COSY) and also by the cyclic- and differential pulse voltammetric methods. The fine and dark red crystals of **[L^1Sn(O-ptp)$_2$]** was obtained and the crystallographic data have been collected and solved.

The UV-visible data of these triads suggest that in **[L^1Sn(O-ptp)$_2$]** there does not exists π-π interaction between **ptp** subunit and porphyrin moiety whereas in compound **[L^1P(O-ptp)$_2$]$^+$** there exists intramolecular π-π interactions. In the steady state fluorescence studies, based on thermodynamic considerations and singlet state energy data the quenching of fluorescence when excitation is at 555 nm due to a PET from the ground state terpyridine to the singlet porphyrin. Whereas excitation at 280/300 nm results in a PET from the excited state

terpyridine to the ground state porphyrin competing with an EET from the terpyridine to the porphyrin in both the D-A systems.

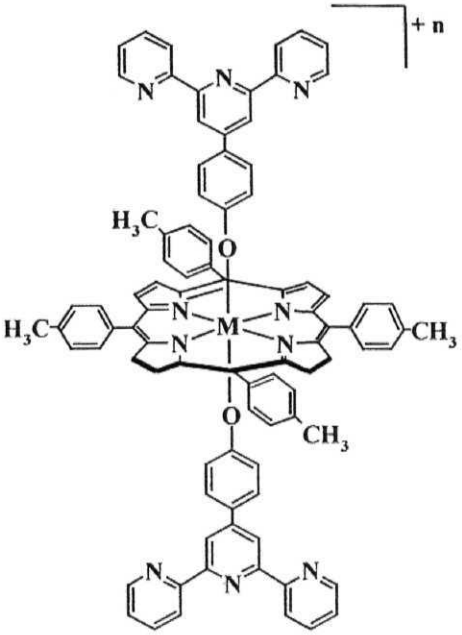

M = Sn(IV), n = 0, **[L^{1}Sn(O-ptp)$_2$]**
M = P(V), n = 1, **[L^{1}P(O-ptp)$_2$]$^+$**

Fig. 2

Further the complexation of **[L^{1}P(O-ptp)$_2$]$^+$** with transition metal ions have been studied in detail by means of ^{1}H NMR, UV-visible and fluorescence spectroscopies. This was complexed with variety of transition metals such as **Zn^{2+}**, **Cd^{2+}**, **Hg^{2+}**, **Cu^{2+}**, **Cu^{1+}**, **Ag^{1+}**, **Ni^{2+}**, **Co^{2+}**, **Fe^{2+}** and **Mn^{2+}** ions by using their corresponding acetates/triflates/chlorides. In the steady state fluorescence studies, it was observed that fluorescence quantum yields are increased upon successive addition of **Zn^{2+}**or **Cd^{2+}** ions, whereas quantum yields are decreased with paramagnetic metals (i.e. **Cu^{2+}**, **Ni^{2+}**, **Co^{2+}** and **Fe^{2+}**). When excited at 566 nm with addition of **Zn^{2+}** or **Cd^{2+}**, PET process was inhibited from ground state of **ptp** subunit to excited state of porphyrin, results enhancement in porphyrin fluorescence. On the other hand when excited at the isosbestic point at 300 nm, PET was suppressed and EET from excited **ptp** subunit to the ground state of porphyrin was enhanced.

Chapter 5. Porphyrin dyads and triads with ruthenium(II) bis-terpyridine complex: Synthesis, spectroscopy and photochemistry.

In the previous Chapter both PET and EET reactions occurred when terpyridine is connected axially to either Sn(IV) or P(V) porphyrin. It is of interest

to see whether such PET and EET reactions take place when terpyridine subunits are linked at the meso-phenyl position(s) of porphyrin ring. For this reason, we have designed and synthesized molecular dyads and triads in which the acceptor ruthenium(II) bis-terpyridine complex have been connected *via* ethylene bridges of free base or Zn(II) porphyrins (Fig. 3).

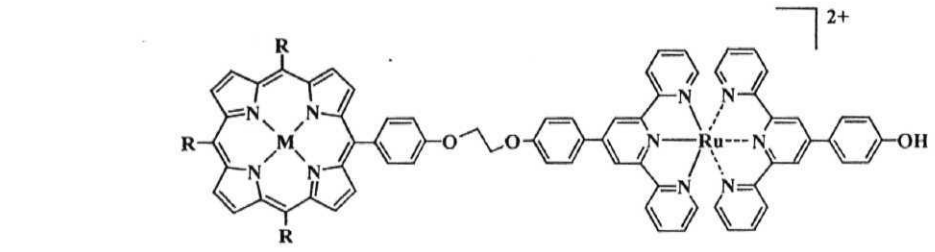

R = tolyl, M = 2H (**[H_2Ru](PF_6)$_2$**), Zn(II) (**[ZnRu](PF_6)$_2$**)

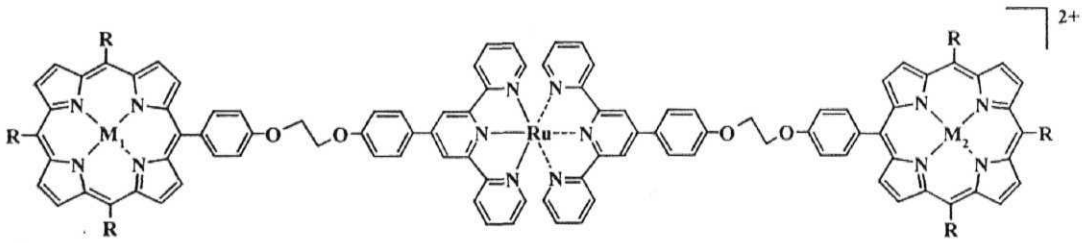

R = tolyl, M_1 = M_2 = 2H (**[H_2RuH_2](PF_6)$_2$**); M_1 = M_2 = Zn(II) (**[ZnRuZn](PF_6)$_2$**);

M_1 = Zn(II), M_2 = 2H (**[ZnRuH_2](PF_6)$_2$**)

Fig. 3

These dyads (**H_2Ru, ZnRu**) and triads (**H_2RuH_2, ZnRuH_2** and **ZnRuZn**), with -OCH_2CH_2O- spacer/s have been synthesized in good to moderate yields. They have been fully characterized by mass (MALDI), UV-visible and ^{1}H NMR spectroscopic methods. A comparison of UV-visible and ^{1}H NMR of these D-A systems with those of individual reference compounds reveals that there exist no electronic communication in ground states between porphyrin and **[Ru]**$^{2+}$ complex.

Their photophysical properties have also been investigated and the results are interpreted in terms of intramolecular electron and energy transfer mechanisms. In the case of $[ZnRu]^{2+}/[ZnRuZn]^{2+}$, deactivation of S_1 occurs essentially by electron transfer to give the CT level that then deactivates to the ground state. In the case of $[H_2Ru]^{2+}/[H_2RuH_2]^{2+}$ we could not find any cosidarable energy or electron processes. Similar to the dyads $[H_2Ru]^{2+}$ and $[ZnRu]^{2+}$, $[ZnRuH_2]^{2+}$ also exhibit same singlet state properties but the additional quenching is explained by energy transfer from singlet excited state of zinc(II) porphyrin to free base porphyrin.

Chapter 6. Porphyrin-pyrene and porphyrin-anthraquinone dyads: Synthesis, spectroscopy and photochemistry

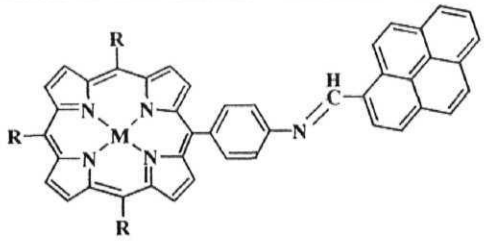

M = 2H (**H_2-Py**), Cu(II) (**Cu-Py**), Zn(II) (**Zn-Py**)

R = tolyl

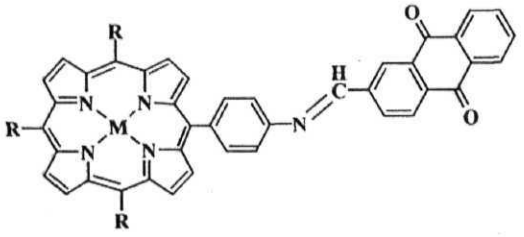

M = 2H (**H_2-AQ**), Cu(II) (**Cu-AQ**), Zn(II) (**Zn-AQ**)

Fig. 4

It is interesting to see whether PET and EET reactions occurred when either donor or acceptor molecules are connected at the peripheral positions of porphyrin. For this reason, we have constructed free base, copper(II) and zinc(II) derivatives of a 'porphyrin-pyrene' and 'porphyrin-anthraquinone' conjugates (**H_2-Py**, **Cu-Py**, **Zn-Py**, **H_2-AQ**, **Cu-AQ** and **Zn-AQ**) having an azomethine group separating the two subunits have been synthesized and fully characterized by mass (FAB), IR, UV-visible, ^{1}H NMR and ESR

spectroscopies and also by the cyclic and differential pulse voltammetric methods. An analysis of the data reveals that the spectral and electrochemical properties of the individual chromophoric entities are retained and that there exists no specific π-π interaction between the porphyrin, pyrene or anthraquinone subunits in these dyads.

Excitation of **H_2-Py** and **Zn-Py** derivatives at 550 nm results in no quenching of fluorescence due to the porphyrin moiety, but that at 290 nm results in a quenching of fluorescence due to the appended pyrene moiety. An intramolecular EET mechanism is proposed for the substantial decrease in fluorescence in both **H_2-Py** and **Zn-Py** derivatives. The fluorescence life times (τ) of the porphyrin parts of both **H_2-Py** and **Zn-Py** (λ_{ex} = 411 nm) remained quite similar to those of **H_2TTP** and **ZnTTP** but those of their pyrene subunits (λ_{ex} = 290 nm) were found to be considerably shorter in comparison with the lifetime of pyrene.

H_2-AQ and **Zn-AQ** were shown to exhibit substantial quenching (84-97%) of the porphyrin fluorescence as measured against the monomeric analogues in steady-state fluorescence experiments. Thermodynamic considerations based on the redox potential and singlet state energy data indicate an intramolecular PET from the excited state of porphyrin to anthraquinone in both derivatives. Time-resolved fluorescence decay experiments were fit to 2-3 exponentials. From the time-resolved fluorescence data, the electron-transfer rate constants were calculated and k_{ET} values were found to dependent upon the solvent.

Chapter 7. Conclusions

This Chapter presents general conclusions based on the investigations carried out in this work.

CHAPTER 1

Introduction

The recent resurgence witnessed in the chemistry of porphyrin and related macrocyclic compounds is mostly due to the potential applications of these species in research areas such as biomimetic photosynthesis, molecular electronics, supramolecular catalysis, organic synthesis, magnetic resonance imaging (MRI), photodynamic therapy (PDT) etc. A variety of donor-acceptor (D-A) type porphyrin systems have been built for use in many of these applications, which generally involve photoinduced electron transfer (PET) and excitation energy transfer (EET) as the key principles. While majority of the D-A systems have been constructed by linking the donor/acceptor subunits at the porphyrin peripheral (i.e. β-pyrrole and meso) positions, relatively less D-A systems have been synthesized by utilizing the axial site/s (central metal/non metal ion) of a porphyrin. This thesis deals with the design, synthesis and PET and EET reactions of D-A systems in which the donor/acceptor subunits are connected to the meso and axial sites of metal/metalloid porphyrin.

1.1 Basic theory of PET and EET reactions

Molecules, upon photoexcitation become powerful donors or acceptors and hence, can be involved in electron and/or energy transfer reactions. Photoinduced electron transfer reaction has attracted the interest of chemists in many respects that include synthesis of organic molecules, development of solar energy storage/conversion systems and understanding of natural/artificial photosynthetic systems.[1-4] Similarly, excitation energy transfer reactions are also important from the point of view of photosynthetic antenna function,[5] polymer

photophysics,[6] molecular electronic devices etc.[7,8] Equally significant is the theoretical understanding of the electron and energy transfer reactions and, this has added further impetus to the study of these important processes.[9-14] Fig. 1.1 depicts pathways through which electron and energy transfer processes can occur. In electron transfer, the excited state (*) can act either as a donor (D) or as an acceptor (A) whereas in energy transfer, the excited state will always be a donor.

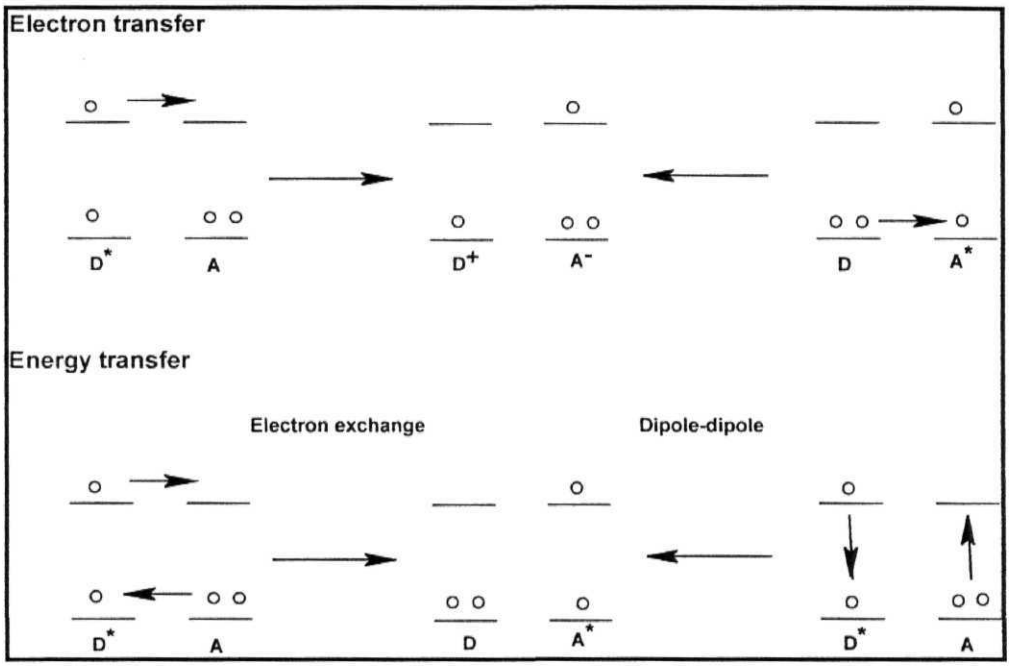

Fig. 1.1 Electron and energy transfer involving excited donor (**D***) and acceptor (**A***) systems.

Marcus theory of electron transfer process provides a convenient way of discussing certain key aspects involved in the PET reactions.[9-12] According to this theory, the rate constant for electron transfer (k_{ET}) is given by the expression

$$k_{ET} = \frac{k_{el}\, \nu_n \exp(-\Delta G^0 + \lambda)}{4\, k_B T} \qquad (1.1)$$

Here, k_{el} is the electronic transmission coefficient, ν_n is the frequency of nuclear motion through the transition state, ΔG^0 is the standard Gibb's free energy change for the overall ET reaction, λ is the reorganization energy needed to orient the initial complex to have a suitable configuration for electron transfer, k_B is the Boltzman's constant and T, the absolute temperature. $\Delta G^{\#}$ is the free energy of activation, and it is related to ΔG^0 and λ, the reorganization energy, by the expression

$$\Delta G^{\#} = \frac{(\lambda + \Delta G^0)^2}{4\lambda} \tag{1.2}$$

For exoergic reactions, when $-\Delta G^0 < 0$, k_{ET} increases with increasing exoergicity. It reaches a maximum at $-\Delta G^0 = \lambda$ and decreases again when $-\Delta G^0 > \lambda$. This region of decrease of k_{ET} with respect to increasing exoergicity is termed as the "Marcus inverted region".

Electronic energy transfer reactions can, in principle, operate by two mechanisms:

(i) Dipole-dipole mechanism which involves mutual Columbic interaction of electrons (Forster's theory) [13]

(ii) Exchange mechanism which involves mutual exchange of electrons (Dexter's theory) [14]

Forster has developed an expression for the rate of electronic energy transfer due to dipole-dipole interaction in terms of the experimentally obtainable parameters. According to this theory, the rate constant for energy transfer, k_{EnT}, is given by eqn. 1.3.

$$k_{EnT} = \frac{8.8x10^{-25}\kappa^2\phi_D}{n^4\tau_D R^6}\int F_D(\bar{\nu})\varepsilon_A(\bar{\nu})\bar{\nu}^{-4}d\bar{\nu} \tag{1.3}$$

In the above equation, $\bar{\nu}$ is the wave number, $F_D(\bar{\nu})$ is the spectral distribution of the donor emission in quanta normalized to unity, $\varepsilon_A(\bar{\nu})$ is the molar extinction coefficient for the acceptor absorption and n is the refractive index of the solvent. κ^2 is a function of relative orientation of transition dipole moments of the donor and the acceptor. ϕ_D is the quantum yield of donor emission, τ_D is the donor emission lifetime (in seconds) and R is the distance between the donor and acceptor molecules (in centimeters).

From the photophysical point of view, the fundamental processes that originate from the singlet state are depicted in Fig. 1.2.

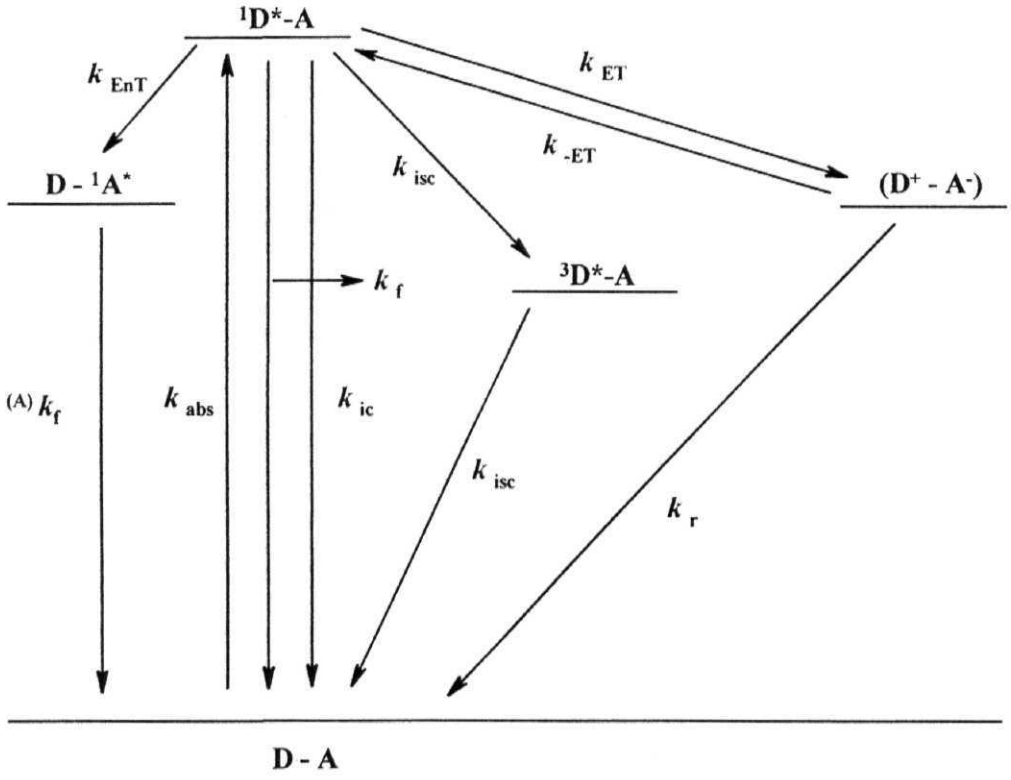

Fig. 1.2 Fundamental processes originating from the singlet excited state.

Here, superscripts 1 and 3 refer to the singlet and the triplet states, respectively. k_f ($^{(A)}k_f$), k_{ic}, k_{isc}, k_{ET}, k_{-ET}, k_r and k_{EnT} are the rate constants for fluorescence, internal

conversion, intersystem crossing, forward electron transfer, reverse electron transfer, charge recombination and energy transfer reactions, respectively. For an efficient electron/energy transfer to occur, k_{ET} and k_{EnT} have to compete with other processes *viz.* fluorescence, internal conversion, intersystem crossing etc.

Table 1.1 summarizes determinants of EET and PET reactions derived from the theories of electron and energy transfer reactions as well as the processes competing with these reactions discussed above.

Table 1.1

Determinants of electron and energy transfer	
Electron transfer	Distance and orientation (electronic coupling, orbital overlap); Free energy change (driving force); Reorganization in D and A; Orientation polarization of medium
Excitation energy transfer	Distance and orientation (coupling of excited states); Spectral overlap of emission and absorption of D and A; refractive index of the medium.
Processes competing with electron and energy transfer	
Electron transfer	(i) Nonradiative relaxation of D* by photoisomerization and other conformational changes; Excited state proton transfer; Intersystem crossing; Chemical reactions. (ii) Back reaction to the ground state D-A
Excitation energy transfer	Same as (i)

1.2 PET and EET in biological and abiological systems

As mentioned in the previous section, many applications of porphyrins rely on the photochemical characteristics of these macrocyclic compounds. In

recent years, considerable development that has taken place in areas such as biomimetic photosynthesis, photodynamic therapy and molecule based opto-electronics seems to have provided greater impetus to research related to photochemistry of porphyrins. A brief introduction to these biological and abiological issues, as applied to the theme of the present thesis is presented below.

Photosynthesis is responsible for our oxygenic atmosphere. Both PET and EET are important and prevalent phenomena in natural photosynthesis. For example, antenna function of the photosynthetic systems involves singlet-singlet (s-s) energy transfer between two chlorophyll (*Chl*) molecules and also that between carotenoids (*Car*) and *Chl*. In addition, carotenoids provide photoprotection by rapidly quenching the triplet states of *Chl* by triplet-triplet (t-t) energy transfer thus preventing *Chl* sensitized production of singlet oxygen.

The electron transfer events of photosynthesis take place within a highly specialized reaction center (RC) complex. Detailed structural information for several bacterial reaction centers are now available from X-ray crystallographic investigations.[15-24] The RC of *Rhodobacter spheroides* (RhS) is known to comprise of four bacteriochlorophylls (*BChl*) including those of the so-called 'special pair', two bacteriopheophytins (*BPhe*), two quinones (*Q*) and a carotenoid polyene. In addition, this RC has two branches – L and M. The photosynthetic process begins within the reaction center by excitation of the "special pair" *BChl*. This excitation usually occurs through s-s energy transfer from antenna molecules. Within 2 - 4 ps of excitation, singlet state of the special pair donates an electron to one of the *BPhe* molecules with a quantum yield of essentially unity. The *Bphe* radical anion transfers this electron to the neighbouring *Q*, again with a quantum yield of ~1. The net result of this multistep electron transfer sequence is the generation of a spatially separated, charge transfer state comprising the oxidized 'special pair' and the reduced quinone.

A detailed understanding of these natural reactions has been greatly aided by studies of electron and energy transfer in synthetic model systems. A great number of free base and metallo/metalloid porphyrins substituted with donor/ acceptor moieties have been synthesized as photosynthetic model systems; a number of reviews/monographs on this topic are now available.[1,5, 25-39]

Currently, design of molecule based optical devices is receiving worldwide attention. Molecular rectifiers, transistors, wires, photodiodes etc. are being designed by utilizing the chemistry of excited- and charge transfer states of both inorganic and organic molecules.[7,8,39] Porphyrin-based D-A systems and arrays are also being developed as molecule based electronic/optoelectronic devices such as, for example, 'molecular wires'.[40-45]

This Chapter provides a survey of the recent literature on porphyrin-based 'axial/peripheral-bonding' type D-A systems, arrays etc., as relevant to the present study.

1.3 Covalently/non-covalently linked porphyrin oligomers

A great variety of covalently/non-covalently linked porphyrin dimers and higher oligomers have been reported in the literature and multistep energy- and electron transfer reactions have been elucidated in some of these systems. In the following discussion, recent studies on the oligomeric porphyrins are highlighted.

1.3.1 Linear oligomers

Among the first examples of linear dimers are those which have been developed by Kong and Loach and also by Boxer and Bucks.[46-48] Linear porphyrin oligomers formed by conjugated bridging of porphyrin subunits have been the focus of current interest for their potential application in non-linear optics, organic semiconductors and light harvesting antenna systems.

Osuka and co-workers have been synthesized meso-meso/β-β linked, linear dimeric, trimeric, tetrameric, pentameric, hexameric, nonameric and 12-meric porphyrin arrays.[49-66] In these arrays, they have demonstrated the mutual electronic and excitonic interactions between the individual porphyrin units. The Soret bands of these porphyrin arrays have been observed to be split depending upon the number of porphyrins in a given array. This has been explained in terms of the exciton coupling theory. In addition, absorption bands become increasingly red-shifted and intensified upon increasing the number of porphyrins, reaching into the infrared frequency range. The completely fused 12-meric array **1** has planar, tape-shaped structure and it displays extremely red-shifted absorption bands, reflecting the extensively conjugated electronic system. With an increase in the number of porphyrins in this series of arrays, the fluorescence spectra also become broader and red-shifted without significant decrease in the fluorescence quantum yield, reflecting their stretched conformations that do not allow the formation of a singlet-excitation-energy trapping site.

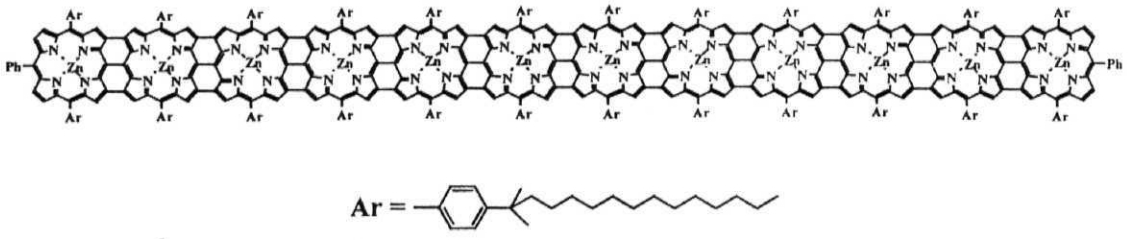

1

The same group has also reported 1,4-phenylene-linked zinc(II) porphyrin oligomers and demonstrated excitonic interactions between the porphyrin units.[67,68] While similar meso-meso linked porphyrin trimers have been reported by Segawa and co-workers[69], acetylenyl bridged porphyrin arrays have been

reported by Therien and co-workers.[70-76] In the latter arrays, efficient electronic interactions between the porphyrinic subunits has been demonstrated by the application of fluorescence and absorption spectroscopies and also by electrochemistry.

Burrell *et al.* have synthesized linear trimers **2** *via* aldehyde appended porphyrin subunits.[77] The utility of aldehyde appended porphyrin unit as a building block for construction of larger linear arrays has also been demonstrated.[78]

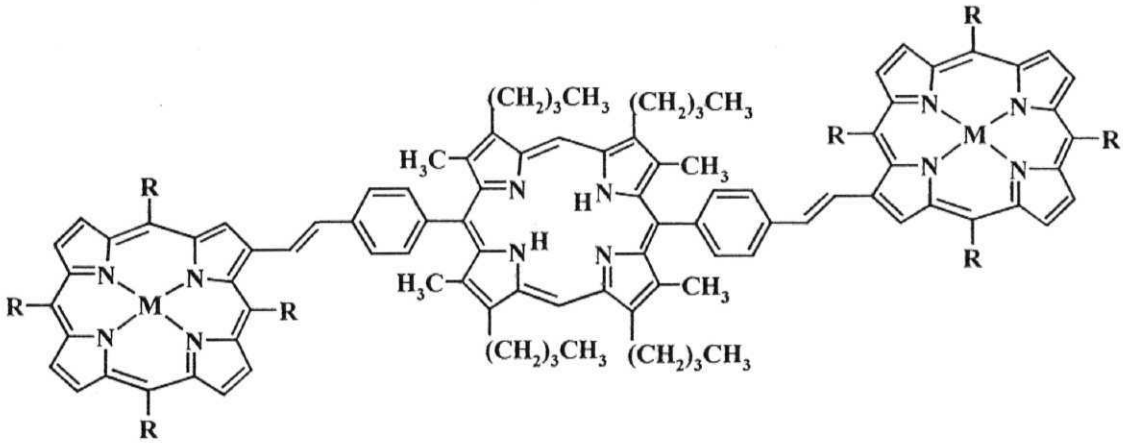

R = phenyl, M = 2H **(2a),** M = Ni(II) **(2b)**

Krishnan and Sen have reported novel hybrid porphyrin trimers **3** in which the monomers bear different metal centers and/or different peripheral substituents.[79] The Q and B bands in the UV-visible spectra of these trimers are red-shifted and broadened in comparison with corresponding monomers. It has been reported that fluorescence due to the distal free base porphyrin is quenched by the non-fluorescent octabromoporphyrin due to spin-orbit coupling or other non-radiative deactivation mechanisms.

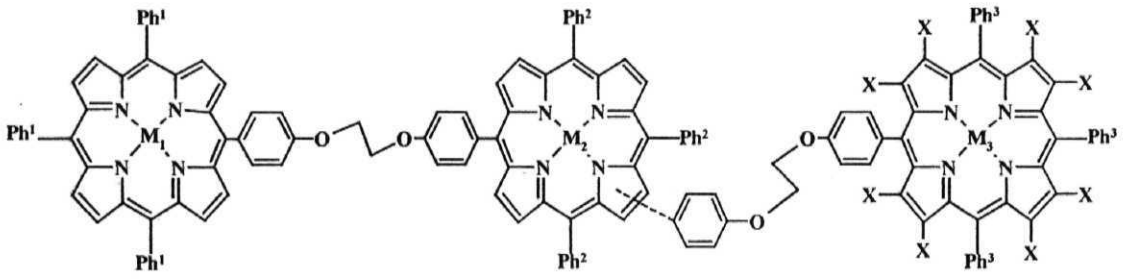

3

$Ph^1 = Ph^2 = Ph^3$ = phenyl, X = H, M_1 = 2H M_2 = 2H M_3 = 2H
M_1 = 2H M_2 = Cu(II) M_3 = Co(II)
M_1 = 2H M_2 = Cu(II) M_3 = Ag(II)
M_1 = 2H M_2 = Cu(II) M_3 = Zn(II)
M_1 = Ni(II) M_2 = 2H M_3 = Co(II)
M_1 = Co(II) M_2 = Cu(II) M_3 = Zn(II)
M_1 = Zn(II) M_2 = Cu(II) M_3 = Ag(II)

Ph^1 = 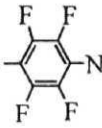 , $Ph^2 = Ph^3$ = phenyl, X = Br, $M_1 = M_2 = M_3$ = 2H

Ph^1 = 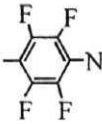 , Ph^2 = phenyl, Ph^3 = 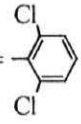 , X = H, $M_1 = M_2 = M_3$ = 2H

Crossley and co-workers[41-45] have synthesized linear and bent porphyrin arrays by fusing individual porphyrin units through rigid aromatic units. Compound **4** is an illustrative example. Crossley and co-workers have also discussed relationship between the inter-ring coupling responsible for electron or hole conduction and oligomer size in this class of arrays. The advantage of this system is that it is completely rigid, spans large distances and possesses a sizable, switchable electronic coupling between its ends.

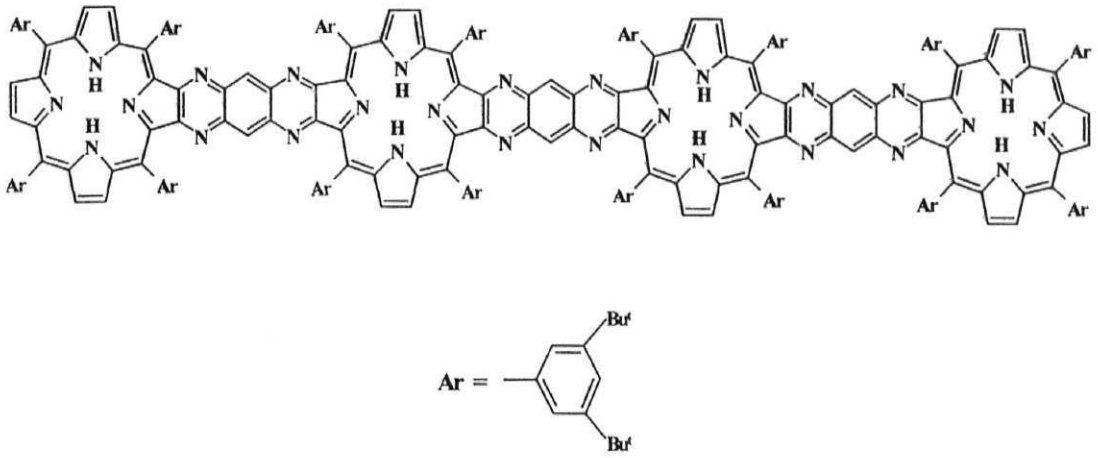

4

1.3.2 Branched oligomeric porphyrin arrays

Based on the architecture of antenna chlorophyll systems, porphyrin oligomers have been fashioned to generate the so-called "light-harvesting arrays". A number of conformationally restricted porphyrins such as face-to-face porphyrins, stacked porphyrins and other similarly rigidly linked systems have been studied.[80-99] These are mostly dimeric systems and will not be discussed here.

Crossley *et al.* reported a series of first, third and fifth generation dendrimers consisting of 4, 16 and 64 porphyrin chromophores.[100] In these dendrimers, they have observed a depolarization of the fluorescence as compared to the monoporphyrin model compound, indicating that electronic energy transfer takes place between the chromophores within the dendrimers. Aida and coworkers have reported a series of first, second and third generation of zinc(II) porphyrin dendrimers having a free base porphyrin core. By the application of pico and femto second time-resolved fluorescence spectroscopic techniques, they have demonstrated that the quenching of zinc(II) porphyrin fluorescence increases as the dendrimer generation increases.[101,102]

Pentameric porphyrins comprising a central porphyrin that is covalently linked to four others are among the interesting examples of the branched chain oligomeric arrays. These have been designed to serve as light harvesting models and for use in potential photovoltaic cells. The ether-bridged pentameric arrays **5a, 5b** and **5c** were first reported by Milgrom.[103] Harriman and co-workers have demonstrated an efficient Forster-type EET from the antenna zinc(II) porphyrins to the central free base porphyrin in these systems.[104]

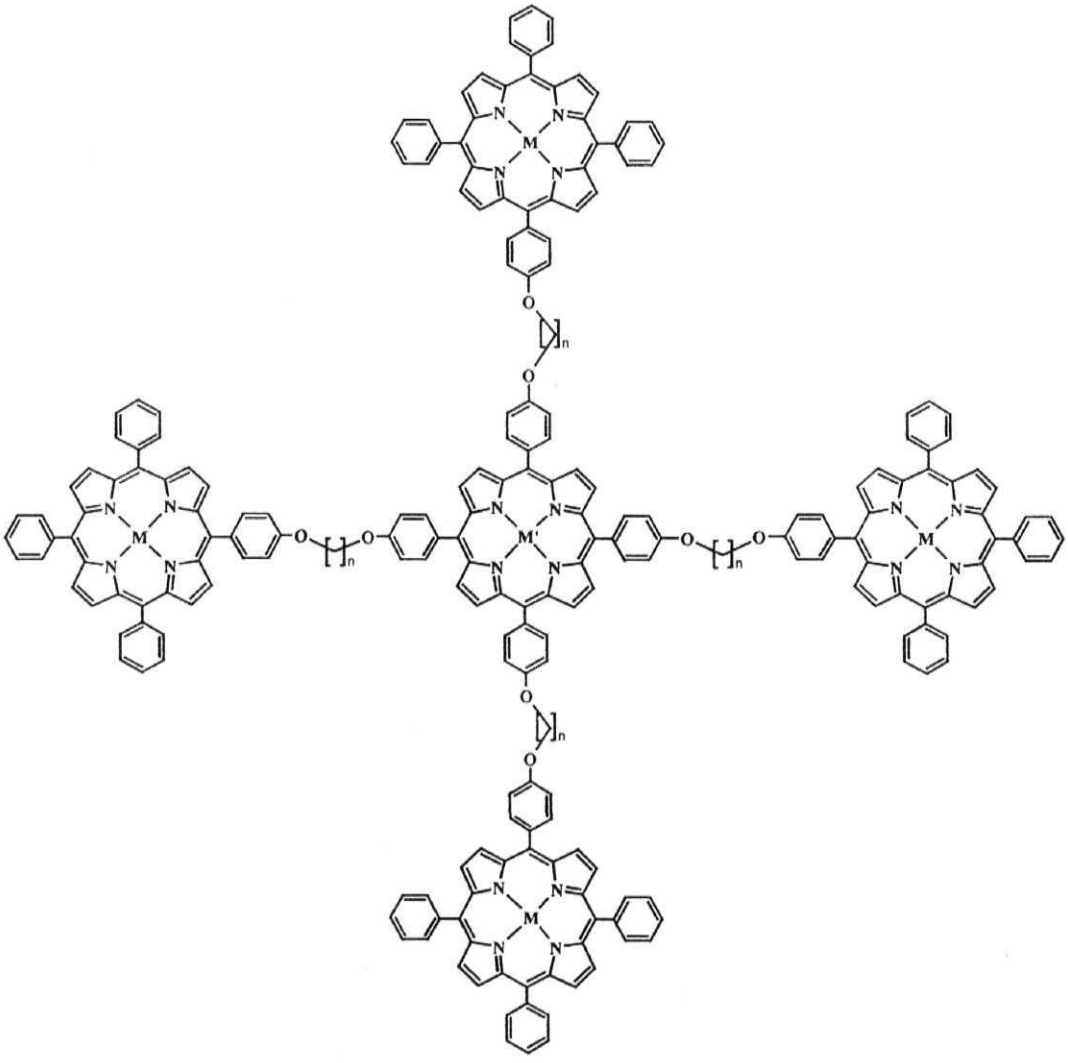

n = 3, M = M′ = Zn(II) (**5a**); M = 2H, M′ = Zn(II) (**5b**); M = Zn(II), M′ = 2H (**5c**)

Wennerstrom *et al.* have further modified the architecture of **5** and designed a more rigid pentamer incorporating the phenyl bridges.[105] Similarly, with a view to increase the conjugation between the porphyrin subunits, a diarylethyne bridged array was synthesized.[106-108] This pentameric array[106] has been tailored in such a way that the centre-to-centre inter-porphyrin distances are ~20 A°, making the porphyrin units close enough for rapid energy transfer but far enough to preclude any competing electron transfer quenching reactions. Detailed spectral and electrochemical studies have been carried out on the zinc(II) and free base derivatives of this system.[109]

Sakata and coworkers have reported an aryl linked henicosamer porphyrin array **6** which they termed as "a mandala-patterened bandanna" porphryin.[110] The compound has been characterized by MALDI-TOF and scanning and tunneling microscopic techniques.

Osuka and coworkers have reported several meso-meso linked 'windmill and grid like' porphyrin arrays having potential application as light harvesting antenna complexes.[111] Array **7** is an illustrative example. In the UV-visible spectra of these arrays, the Soret band gets split due to exciton interaction between the individual porphyrin units. Steady state fluorescence spectra of these arrays show dual emission emanating from the peripheral porphyrin rings and the diporphyrin core. The reduced fluorescence intensity of peripheral porphyrin rings suggested a singlet-singlet energy transfer to diporphyrin core.

Sanders *et al.* reported synthesis, binding and photophysical properties of flexible nine-porphyrin array.[112, 113] The absorption spectrum was approximated as a superposition of spectra of the constituent monomeric porphyrins, suggesting a relatively weak electronic interaction between the porphyrins. The luminescence properties indicate that both the fluorescence quantum yield and lifetime of the singlet excited state of the zinc(II) porphyrin units are reduced 2.5 fold relative to

a monomeric zinc(II) porphyrin. Furthermore, excitation spectra demonstrate a parallel sensitization of the fluorescence of the free base porphyrin by the zinc(II) porphyrin. These results show that energy is transferred from the peripheral zinc(II) porphyrin to the core free base porphyrin.

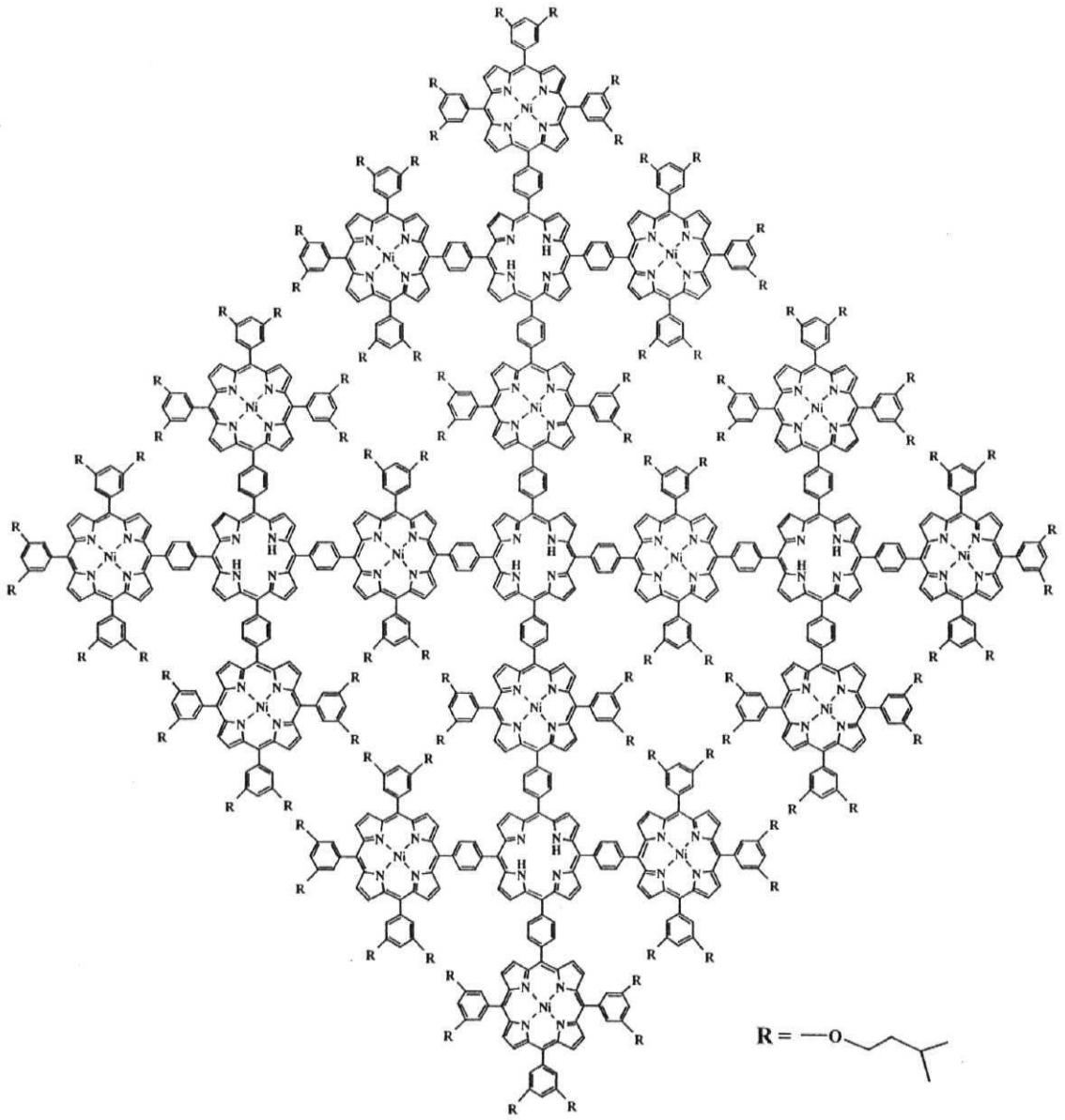

6

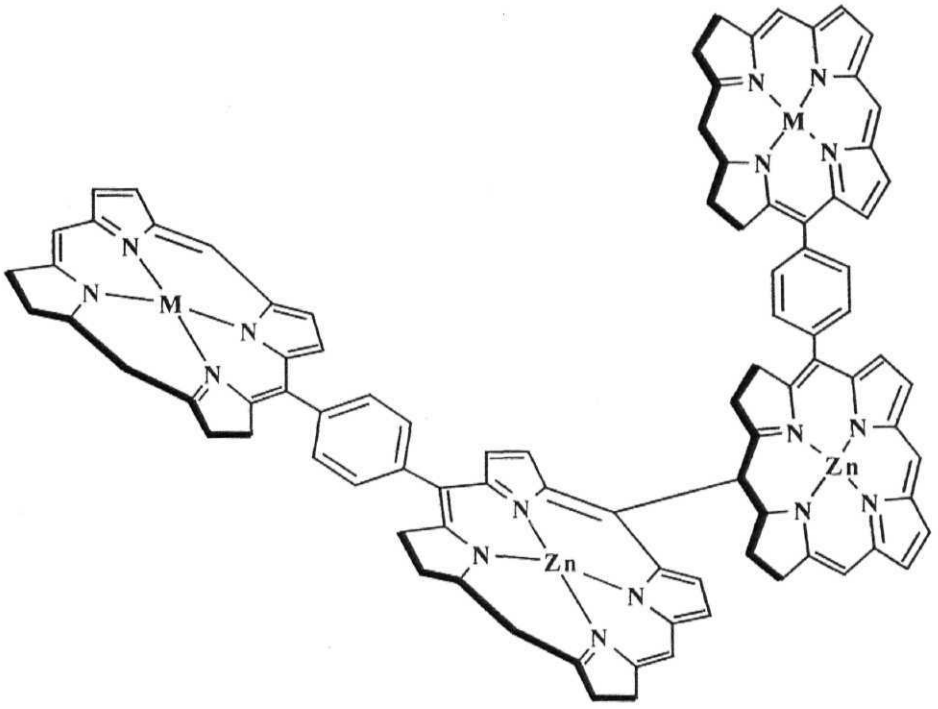

M = Zn(II) (**7a**), M = Ni(II) **(7b)**

1.3.3 Cyclic oligomeric porphyrin arrays

Cyclic porphyrin oligomers have been synthesized in an effort towards mimicking the conformation of the photosynthetic reaction center and enzymatic catalysis.[114-125] Dubowchik and Hamilton have reported cyclic tetrameric and hexameric entities in their efforts to mimic bacterial photosynthetic reaction center.[114-116] During their studies on supramolecular catalysis using macrocyclic systems, Sanders and co-workers have developed an 'extended conjugation' approach to synthesize various oligomeric porphyrins.[119-125] In an effort to create a system in which convergent binding sites are positioned in such a way that substrate molecules can be held in close proximity, they have synthesized a cyclic porphyrin system **8** in which four zinc(II) porphyrins have been covalently linked by extended conjugation.[121]

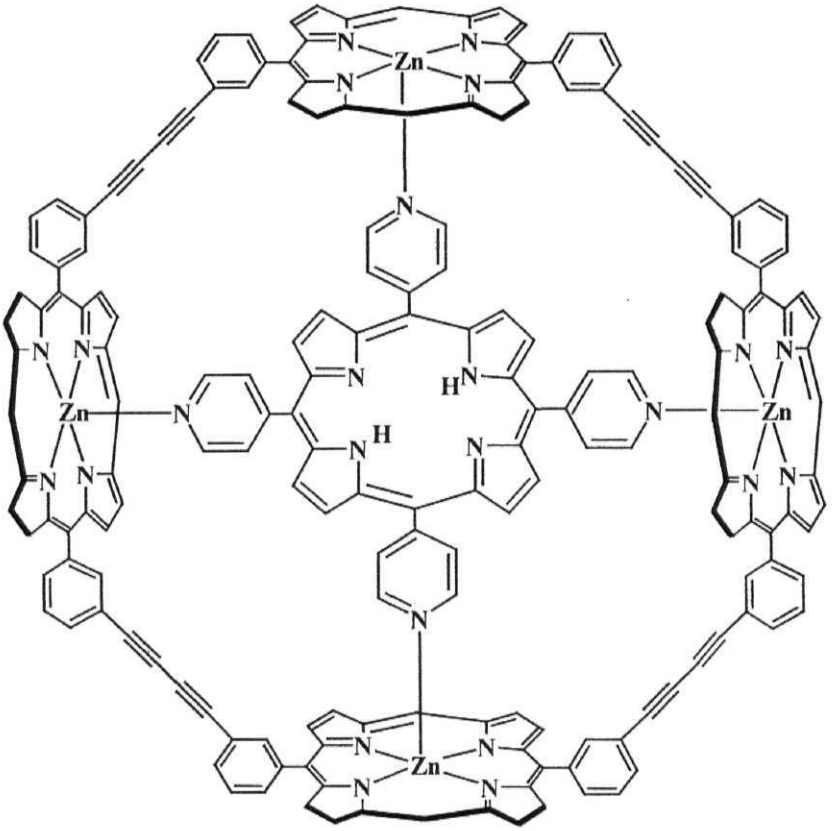

8

Osuka and coworkers have reported 126-mer, 512-mer, 768-mer and 1024-mer porphyrin arrays *via* Ag(I)-promoted oxidative coupling reaction.[126] A cyclic hexamer **9** consisting of three zinc(II) porphyrins which can accommodate a star shaped guest (a trimeric free base porphyrin) inside its cavity has been reported by Gossuer and co-workers[127-129] Singlet excited state energy transfer from the zinc(II) chelates to free base porphyrins has been observed in these arrays and an overall intramolecular energy transfer efficiency was estimated to be 98%. Lindsey *et al.* have reported a light harvesting cyclic arrays of seven porphyrins in a 'wheel and spoke' architecture.[130,131] Here, a shape-persistent cyclic array of zinc(II) porphyrins provides an effective host for a dipyridyl-

substituted free base porphyrin, yielding a self-assembled structure. Energy transfer occurs quantitatively from the uncoordinated to the pyridyl-coordinated zinc(II) porphyrins in this cyclic array. On the other hand, EET from the coordinated zinc(II) porphyrin to the guest free base porphyrin is less efficient and is attributed to a Forster process.

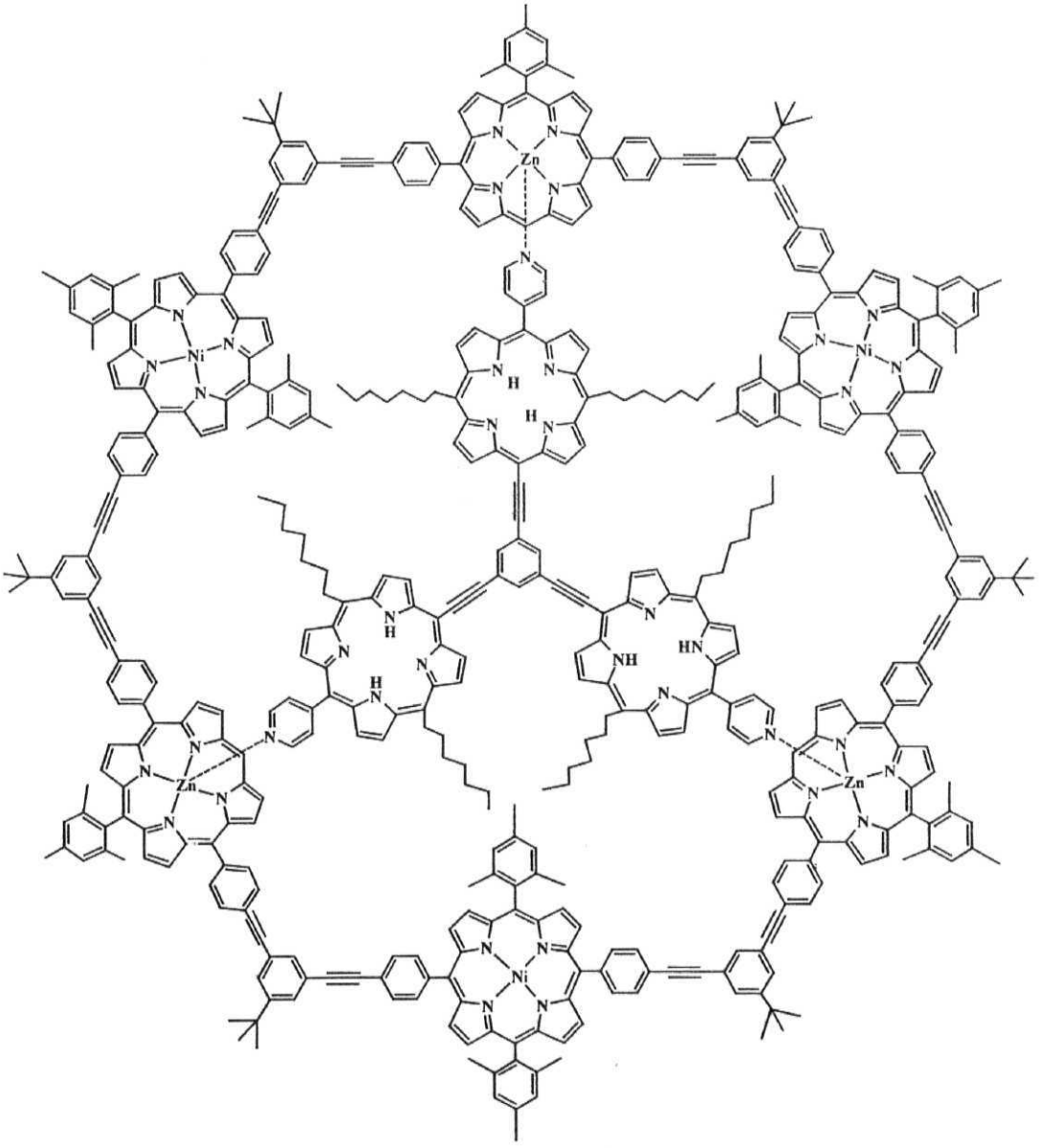

9

The same group recently reported a wheel type dodecameric porphyrin array **10**.[132] The absorption spectrum exhibits a split in the Soret band and Q-bands, which are red-shifted compared with that of starting compound as a consequence of exciton coupling with the neighboring porphyrins. In steady state

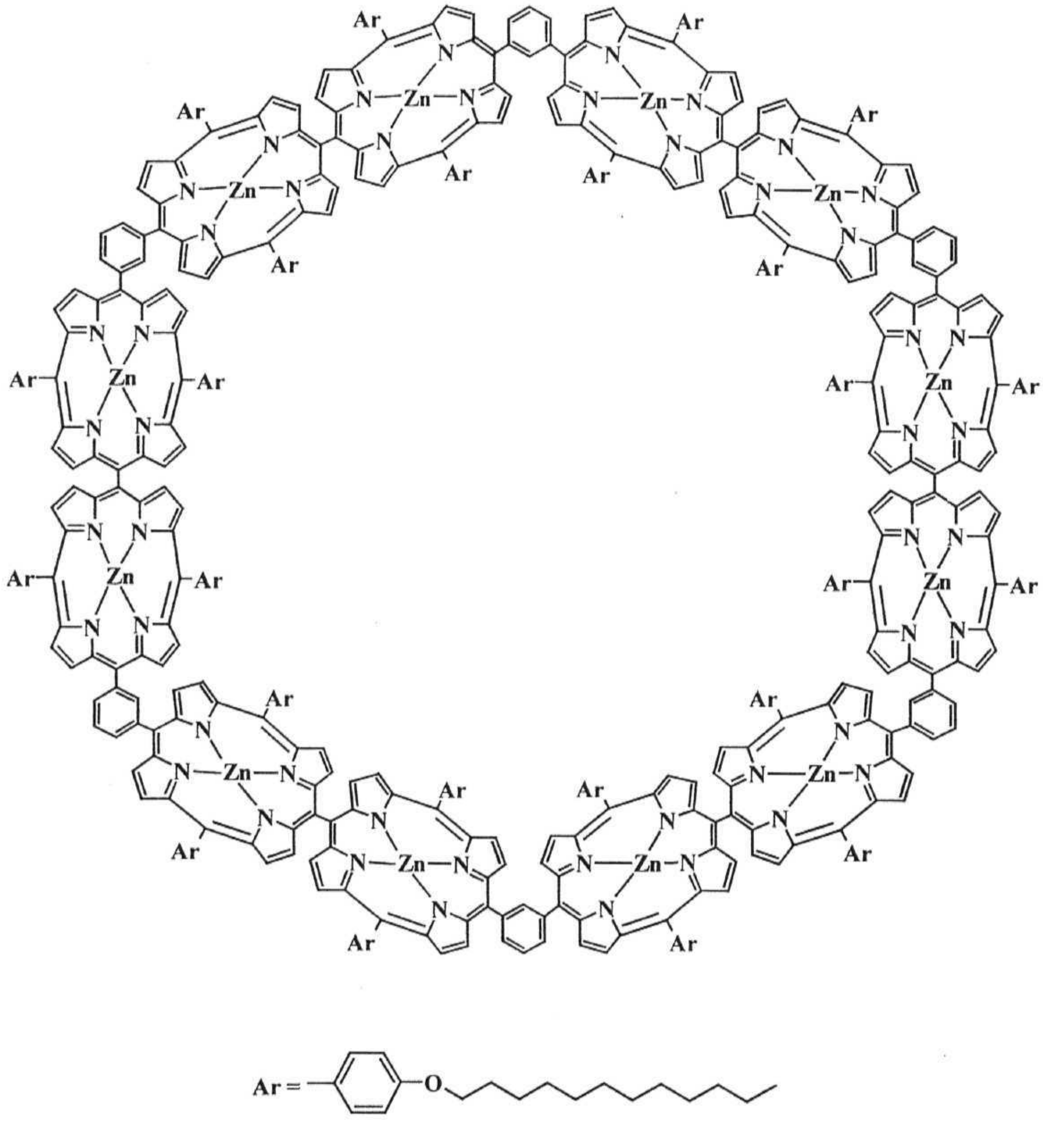

10

fluorescence studies, this porphyrin is found to emit with nearly the same quantum yield as those of linear arrays, indicating no serious quenching in the singlet excited state. The fluorescence and transient absorption anisotropy decay measurements, have been shown to be pertinent as a model of photosynthetic antenna in terms of very efficient excitation energy hopping along the array without encountering an energy sink.

1.4 D-A systems involving covalent linkage at the porphyrin peripheral position/s

The first quinone substituted trimer was synthesized by Sessler and co-workers.[133,134] Porphyrin → quinone electron transfer in this system is over a distance comparable to that found in the natural photosynthetic reaction centers and has been shown to be efficient enough to use this system as a model for studying long range electron transfer mechanisms. In an analogous study, Osuka *et al.* have reported tetrads consisting of 1,2-phenylene-bridged zinc diporphyrin, zinc(II) porphyrin, pyromellitimide and quinone.[135]

Earlier reports on EET and PET reactions of porphyrin-based D-A systems are abound with studies on covalently linked complexes and these have been reviewed in many recent accounts.[1,2,5,24-38] Kong and Loach have synthesized the ester linked porphyrin-quinone (P-Q) dyad in 1978[46] and the corresponding amide linked dyad was reported in 1979 by Tabushi and co-workers.[136] These latter systems were subsequently investigated for their photophysical properties by Ho *et al.*[137] Since then, a number of porphyrin based D-A systems have been synthesized and their photophysical properties studied in detail. Discussion on a few recent examples follows.

Therien and co-workers have reported distance dependence of electron transfer in a rigid, cofacially compressed, π-stacked porphyrin-bridge-quinone

systems **11**.[138,139] Photoinduced charge separation and thermal charge recombination reactions of **11** were investigated by visible pump/probe-IR transient absorption spectroscopy.

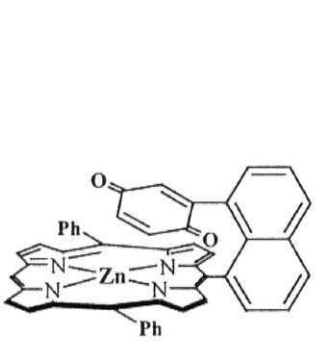

11a

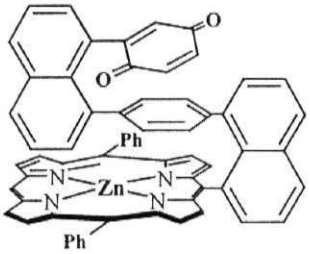

11b

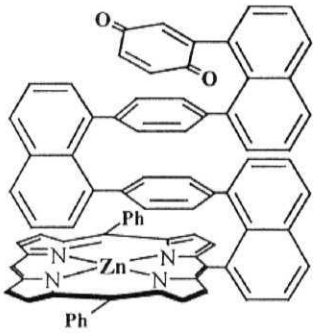

11c

Moderelli *et al.* reported porphyrin-containing benzoquinone-terminated, rigid polyphenylene dendrimers.[140] Steady-state absorption measurements for these dendrimers showed Soret and Q-band absorptions typical of free base porphyrins. Preliminary steady-state fluorescence measurements of these dendrimers indicate quenching of the S_1 state of the free base porphyrin in all benzoquinone-containing dendrimers that is attributed to efficient electron-transfer from the excited porphyrin to the benzoquinone end-groups. The amount of fluorescence quenching was in good agreement with the number of benzoquinone groups at the dendrimer periphery and the distance between the porphyrin and benzoquinone groups as calculated by semiempirical (AM1) molecular orbital calculations

Hayashi *et al.* have reported the D-A system **12** in which a quinone is connected through peptide bonds to the one of the propionate side chain of the porphyrin.[141] Both steady state fluorescence and transient spectroscopic

measurements have suggested that an intramolecular electron transfer from photoexcited zinc(II) porphyrin to the covalently linked quinone takes place in the system.

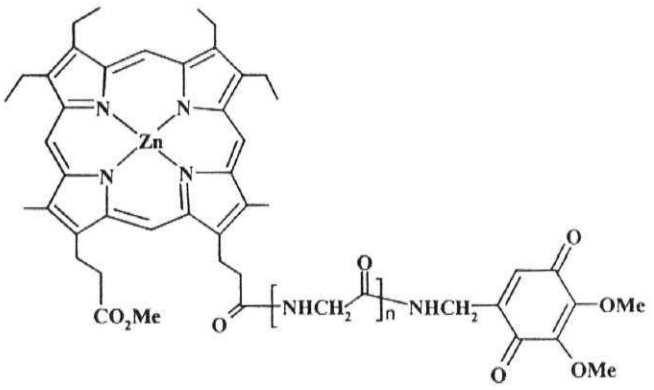

n = 0 (**12a**), n = 1 (**12b**), n = 2 (**12c**)

Gust, Moore and their co-workers have reported triads, tetrads and pentads based on carotene, porphyrin and quinone subunits.[142] One example is the tetrad system **13**, which consists of two covalently linked porphyrin moieties: one containing a zinc(II) ion (P_{Zn}) and other present as the free base (P). The metallated porphyrin bears a carotenoid (C) polyene and other a diquinone species (Q_A-Q_B). The carotenoid absorbs light in spectral regions where the porphyrin does not absorb strongly and transfers singlet excitation energy to the porphyrin. Excitation of the free base porphyrin of the pentad yields an initial charge separated state, $\mathbf{C\text{-}P_{Zn}\text{-}P^{+\cdot}\text{-}Q_A^{-\cdot}\text{-}Q_B}$, and subsequent electron transfer steps lead to a final charge separated state $\mathbf{C\text{-}P_{Zn}\text{-}P^{+\cdot}\text{-}Q_A\text{-}Q_B^{-\cdot}}$ with an overall quantum yield of 0.83.

Porphyrins substituted with multiple crown ether voids have been investigated in great detail.[143-149] A recent study has investigated a porphyrin substituted with a redox active crown ether (**14**) as a biomimetic model. Folding

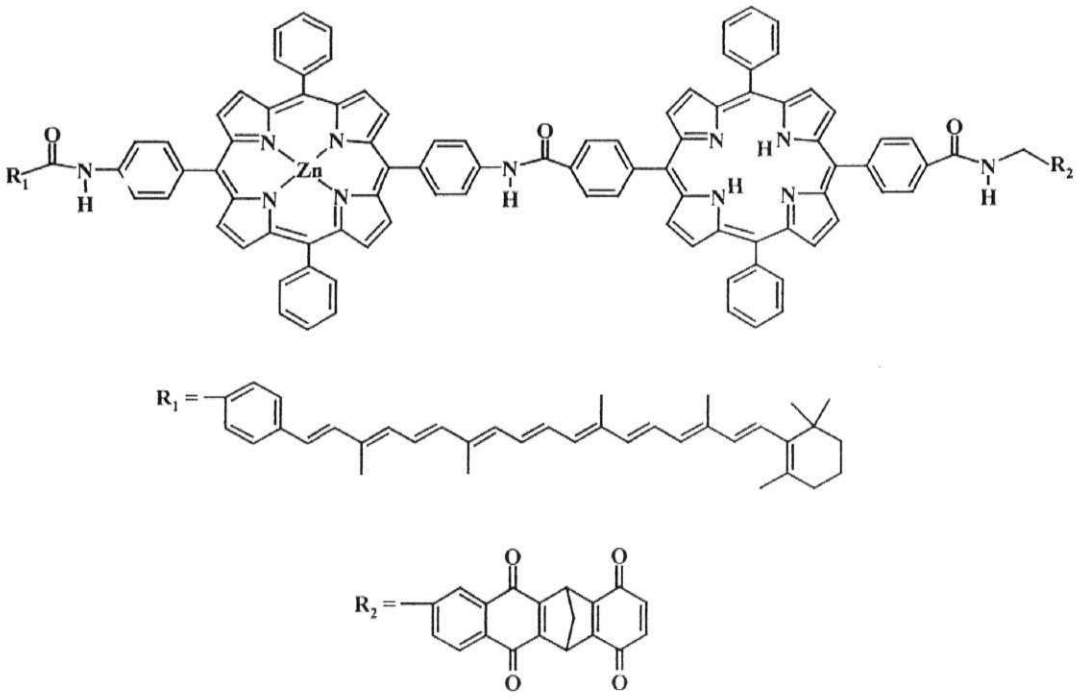

13

of the crown-ether-quinone moiety towards the porphyrin and 'intramolecular' PET has been demonstrated in this system at the room temperature.[149] At low temperatures, however, PET has been shown to be absent.

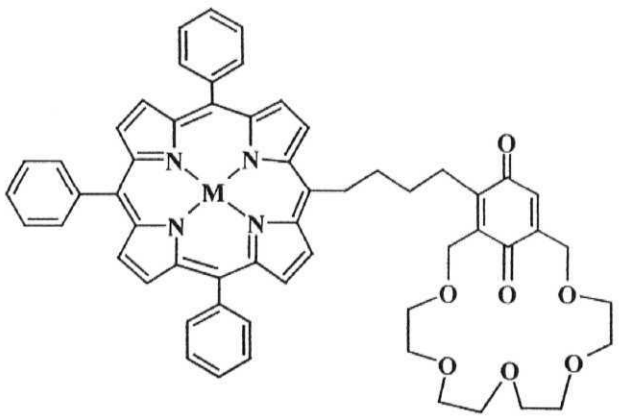

M = 2H (**14a**), M = Zn(II) (**14b**)

In an attempt to mimic photosynthetic energy transfer reactions and to develop molecular devices, porphyrin systems, as energy acceptors, have been covalently linked to carotenoid, cyanine dye and anthracene donor subunits to generate molecular dyads.[5] Lindsey *et al.* have synthesized a series of porphyrin-cyanine dye dyads to mimic the phycobilisome action of photosynthesis.[150]

Sirish and Maiya have reported a series of anthracene-porphyrin dyad molecules in which the anthracene is covalently linked to a tetraarylporphyrin at the ortho, meta, or para position of a meso aryl ring **(15)**.[151] Results of steady-state fluorescence have revealed singlet-singlet energy transfer from the anthracene to the porphyrin. In order to further probe the mechanistic details involved in the PET reactions of the porphyrin-acceptor complexes, D-A systems in which a porphyrin is connected to an acceptor other than a quinone (viz., nitroaromatics, viologens, pyromellitimides) have also been studied. Photochemistry of these systems has been discussed in recent reviews.[5,12] Sirish and Maiya have linked a 3,5-dinitrobenzene moiety *via* an ester bridge, to either ortho, meta or para position of one of the phenyl groups of free base or Zn(II) porphyrin **(16)**.[152] Steady-state and transient spectroscopic studies have revealed the occurrence of PET from singlet porphyrin to the appended nitroaromatic acceptor moiety.

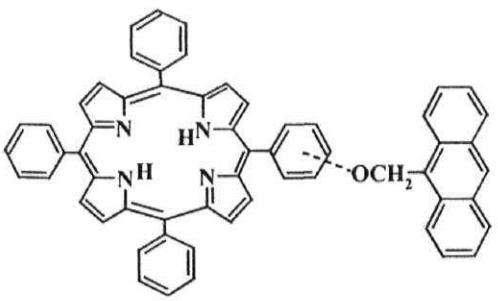

15

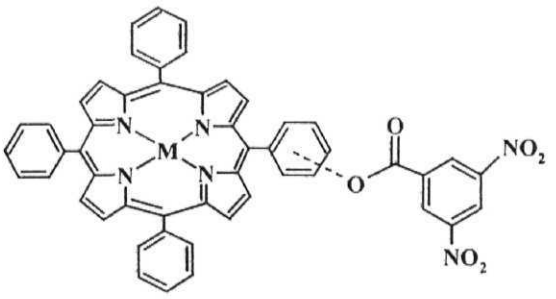

M = 2H **(16a)**, M = Zn(II) **(16b)**

Lindsey and Holten group have synthesized light harvesting arrays comprised of a porphyrin bearing multiple perylene-monoimide systems.[153] It was found that there is a energy transfer from the excited state perylene to porphyrin. Wasielewski *et al.* have reported the D-A system in which a perylene-3,4-dicarboximide is connected to the meso-position of the zinc(II) porphyrin.[154] Same group have reported two zinc(II) porphyrins in which a pyromellitimide (PI) acceptor is attached to the para position of a *meso*-phenyl group of the porphyrin (**17a**) or to that of a β-phenyl group of the porphyrin (**17b**).[155] Transient absorption studies show that efficient electron transfer occurs from S_2 of Zn(II) porphyrin to PI acceptor. Moreover, the results show that while charge separation from S_1 is about 6 times faster for PI attached to the **17a** than for PI attached to the **17b**, the opposite is observed for charge separation from S_2. Subsequent charge recombination is 2.6-2.8 times faster for PI attached to the **17a** relative to that of the **17b**. Comparisons of rates between 2-methyltetrahydrofuran and toluene have shown that the ordering of rates is the same for both solvents, although the rate ratios are larger in 2-methyltetrahydrofuran than in toluene.

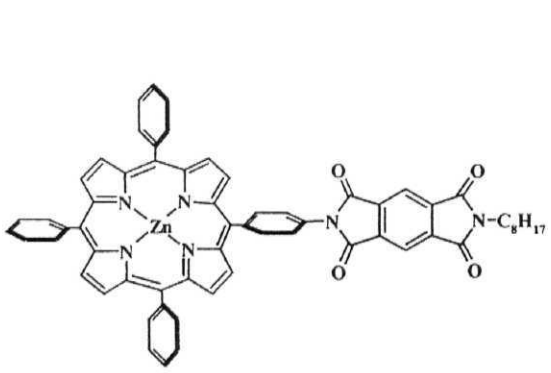

17a

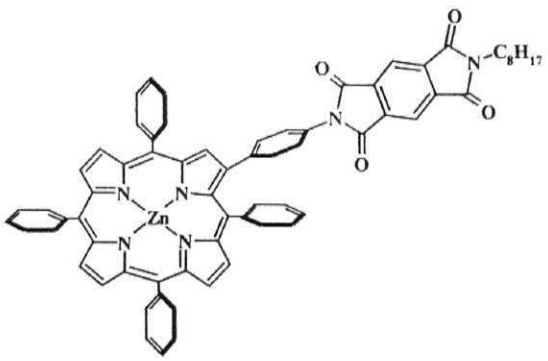

17b

More recently, fullerenes have been covalently linked to porphyrins.[156-162] For example, Sakata and co-workers have synthesized cis and trans porphyrin-

$(C_{60})_2$ triad molecules which show a PET reaction from singlet excited state of the porphyrin to the appended C_{60}.[162] Gust and Moore have reported carotene-porphyrin-fullerene triad.

1.5 D-A Systems involving axial substitution of porphyrins

Donor/acceptor subunits can be connected at the axial sites of a metallo/metalloid (M) porphyrin *via* M–N, M–O etc. bonds characterized by either coordinative or covalent interactions.

1.5.1 M–N bonded D-A systems

Most examples of porphyrin-based 'axial-bonding' type D-A systems assembled *via* coordinative interactions involve axial ligation of pyridine ligands to metalloporphyrin units.

An early, laser flash photolysis study by Langford and co-workers indicated that, upon irradiation, zinc(II) tetraphenylporphyrin transferred an electron to the axially bound pyridine.[163] The charge transfer state was proven to be accessible from the π-π^* triplet state of zinc(II) porphyrin with a time constant of *ca.* 3 ns.

Otsuki *et al.* and others have reported energy gap,[164-169] and dependence of the electron transfer rate on geometry in supramolecular D-A assemblies. Complex **18** is a illustrative example for geometric change dependence D-A system. Complexation of pyridine nitrogen with the zinc(II) center in these systems was confirmed by UV-visible and NMR spectroscopic methods. It has been found that an efficient electron transfer occurs from zinc(II) porphyrin to stilbazole-pyromellitic diimide conjugate in **18-cis**, whereas no electron transfer is detected for **18-trans**, representing a photoswitchable photoinduced electron transfer system based on a geometric change. The same group has further reported

that a zinc(II) porphyrin/free base porphyrin conjugate that is axially coordinated by phenylazopyridine provides a switch for intramolecular energy transfer, with reversible complexation/decomplexation as a switching protocol.[164]

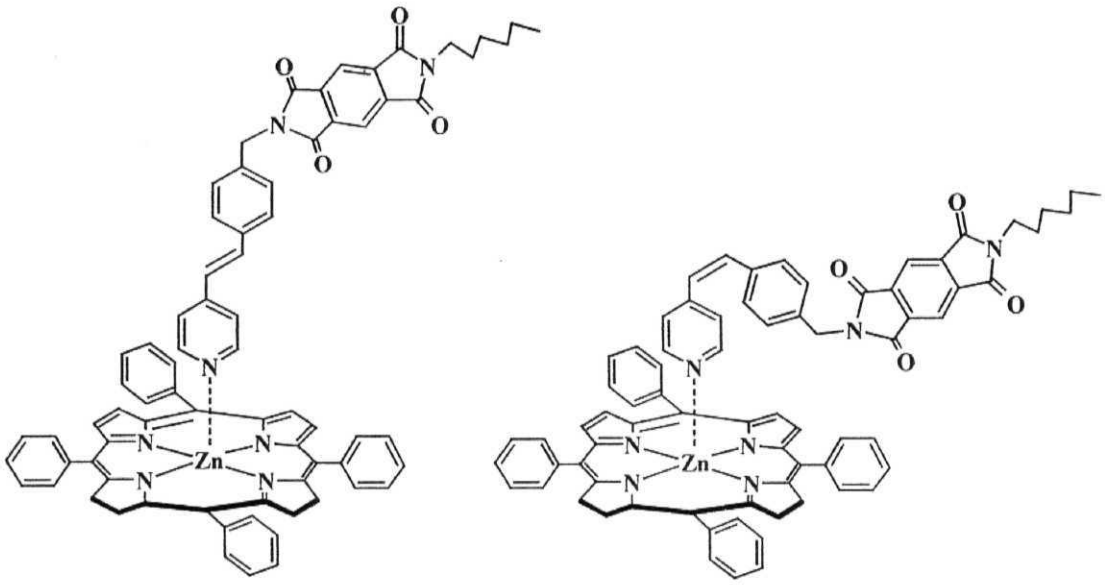

18-trans **18-cis**

Recently D'souza and Ito have reported the first example of a working model of the photosynthetic antenna-reaction center complex, constructed via self-assembled supramolecular methodology.[170] For this, a supramolecular triad **19** is assembled by axially coordinating imidazole-appended fulleropyrrolidine to the zinc center of a covalently linked zinc(II) porphyrin-boron dipyrrin dyad. Selective excitation of the boron dipyrrin moiety in the boron dipyrrin-zinc(II) porphyrin dyad resulted in efficient energy transfer creating singlet excited zinc(II) porphyrin. Upon forming the supramolecular triad, the excited zinc(II) porphyrin resulted in efficient electron transfer to the coordinated fullerenes, resulting in a charge-separated state. The important feature of the present model system is its relative "simplicity" because of the supramolecular approach utilized

to mimic rather complex, "combined antenna-reaction center" events of photosynthesis.

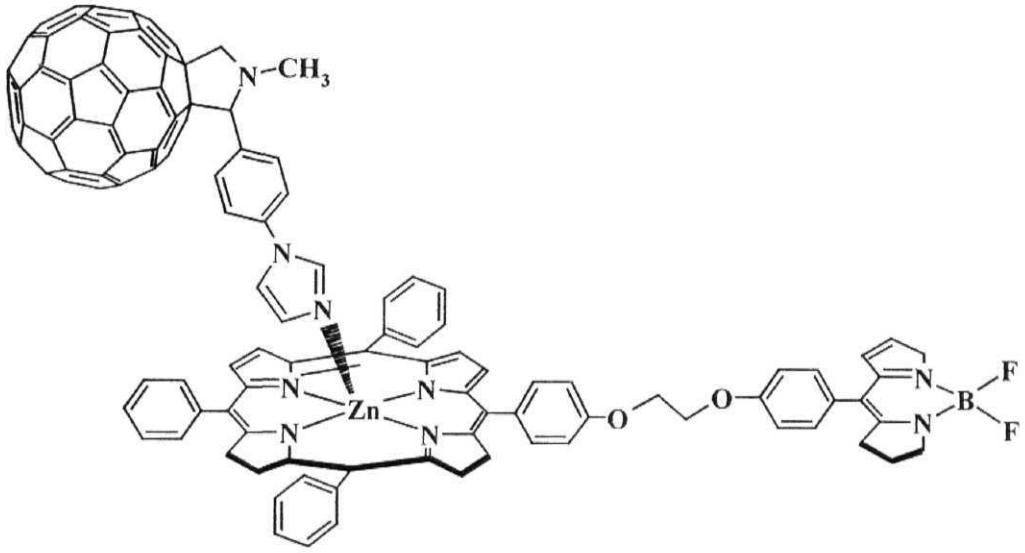

19

The D'Souza group and also others have reported porphyrin-fullerene D-A systems.[171-184] Dyad **20a** in which a pyridine appended fullerene is axially ligated to the zinc(II) porphyrin through coordinative interaction, forms an illustrative example. UV-visible and ^{1}H NMR spectral studies revealed a 1:1 complex formation between the pyridine-fullerene and zinc(II) porphyrin. Singlet emission studies have showed efficient fluorescence quenching due to the occurrence of a PET from the singlet excited zinc(II) porphyrin to the axially positioned fullerene The estimated rate constant for this electron transfer was found to be $(2.4\pm0.3)\times10^8$ s^{-1}. Guldi and co-workers have reported a similar system, **20b**.[182] UV-visible spectral studies with **20b** revealed a noticeable red shift of the two Q-bands as well as a minor broadening of the Soret band compared to the uncomplexed porphyrin. The fluorescence quantum yield and the singlet state

lifetime were both found to be substantially lower for this dyad in comparison with those of the free porphyrin. PET from the singlet excited zinc(II) porphyrin to the axially positioned fullerene has been invoked to explain the observed fluorescence quenching in this complex.

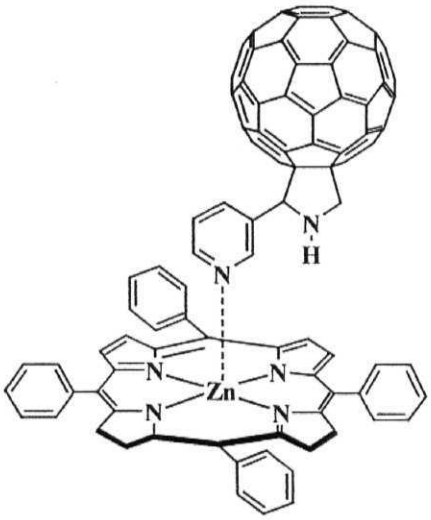

20a

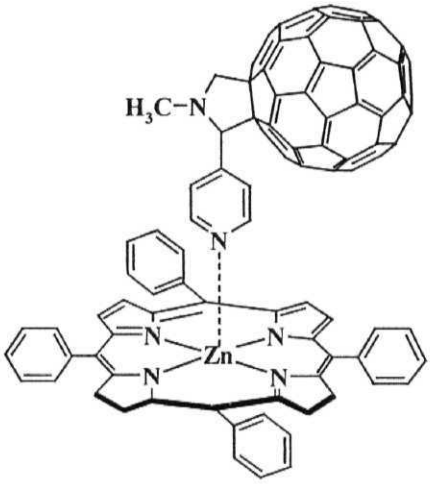

20b

The 'donor-spacer-acceptor' complex **21**, in which a pyromellitimide group with a pendant pyridyl group is axially ligated to a zinc(II) porphyrin fragment, has been reported by Hunter *et al.*[185,186] Electron transfer has been observed to occur from the excited state porphyrin to the pyromellitimide in this complex.

Imamura and co-workers have reported ruthenium(II) porphyrin dimers and trimers.[187-189] More recently the same group reported rhodium(III) porphyrin cyclic tetramer (**22**) and cofacial dimer (**23**).[187] These oligomers were formed by self assembly of rhodium(III) pyridylporphyrins. The Soret bands of both oligomers were significantly broadened by excitonic interactions between the porphyrin units, compared to those observed for a corresponding constituent

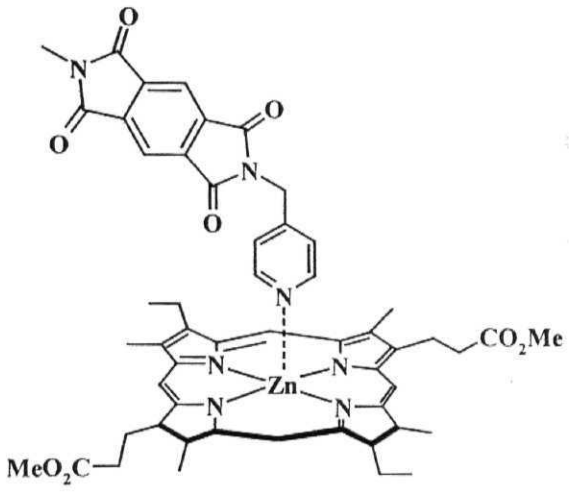

21

compounds. Stepwise oxidation of the porphyrin rings in the oligomers was observed by cyclic voltammetry. The oligomers are very stable in solution, and they slowly undergo reactions with pyridine to give corresponding monomer complexes only at high temperatures. Photochemistry of these systems has not been investigated.

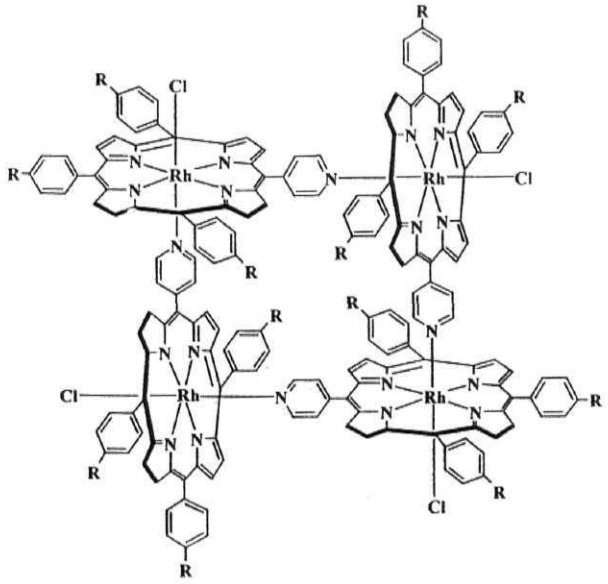

R = -CH_3 (**22**)

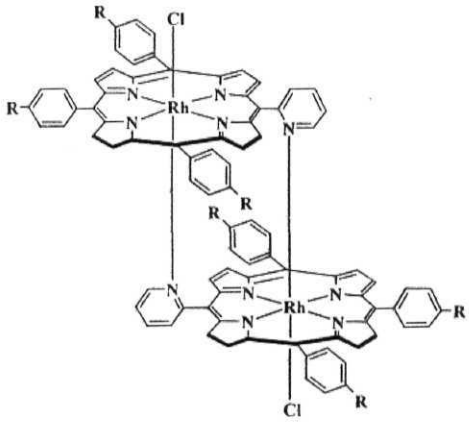

R = -*t*-Bu (**23**)

Chichak and Branda have reported two multicomponent arrays formed through the self-assembly of a central transition metal complex of terpyridine or bipyridine with ruthenium(II) porphyrins *via* axial coordination, **24.**[190,191] The absorption spectra in the UV-visible region of these complexes have been reported to be essentially the sum of those of their individual constituents. Steady state emission results have been interpreted in terms of a PET from bis(terpyridine) core to ruthenium(II) porphyrin.

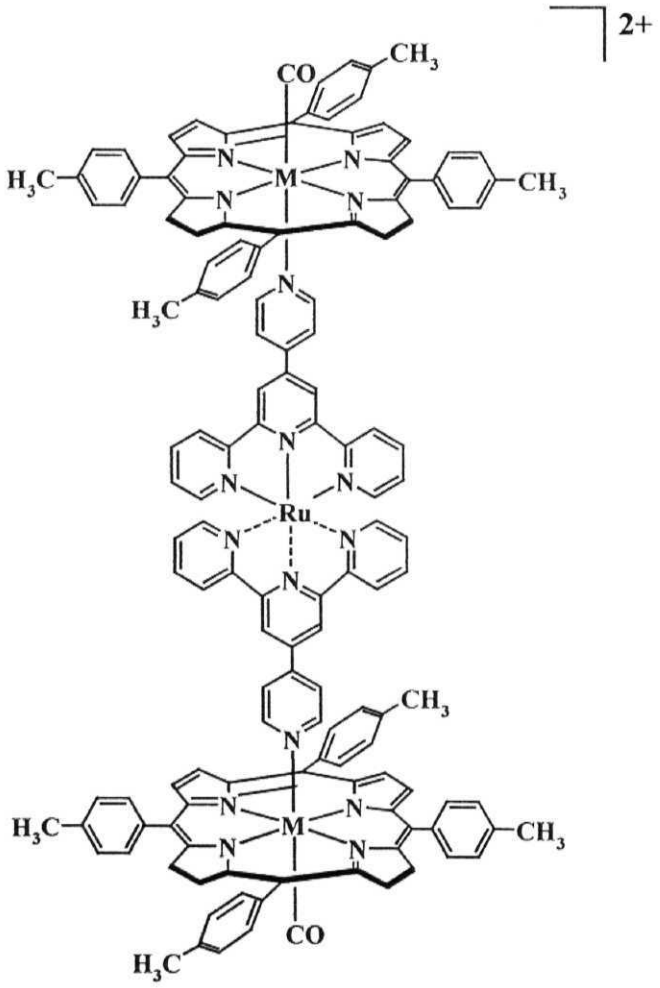

M = Ru(II) (**24a**), Os(II) (**24b**)

In an elegant study, Sanders and co-workers have synthesized a host of cyclic trinulcear porphyrins with a view to construct models for enzyme catalysis.[192,193] They have investigated binding properties of a range of pyridine ligands with these systems.[194-204] Representative examples are trimeric hosts **25** which have spacious cavities and bind pyridyl ligands such as, for example, 2,4,6-tri-4-pyridyl-s-triazine, as shown for **25b**. It was further demonstrated that both **25a** and **25b** dramatically accelerate Diels-Alder reactions of the attached dienes and dienophiles with a stereoselectivity that depended on the cavity size.[193,205-207] For example, cyclic 1,1,2-trimer **(25a)** favored the formation of *endo* adduct and 2,2,2-trimer **(25b)** favored the *exo* adduct. Cyclic trinulcear porphyrin catalyzed acyl transfer reactions have also been reported by the same group.[123]

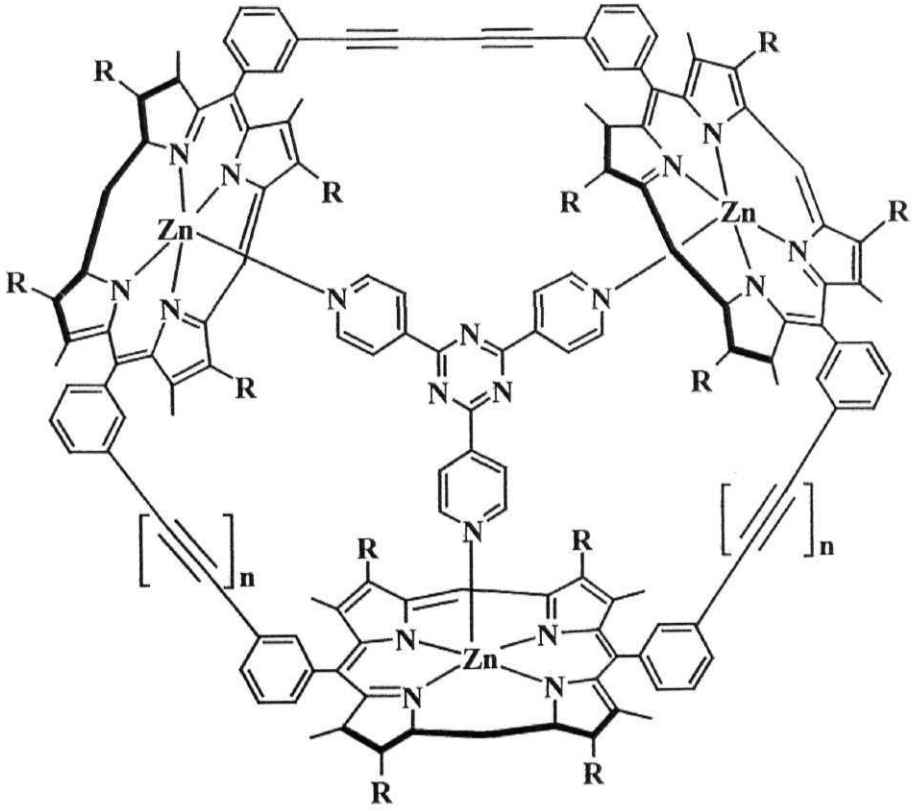

R = ethyl, n = 1 **(25a)**, n = 2 **(25b)**

1.5.2 M–O bonded D-A systems

Shimidzu and co-workers have reported a series of "wheel-and-axle" type phosphorus(V) porphyrin arrays in which porphyrin units are linked to each other *via* the central phosphorus(V) ions.[208-212] The excited state properties of a few compounds in this series of oligomers have been investigated. Singlet lifetimes of these 'wheel-and-axle' type dimers have been reported to decrease with increasing solvent polarity. The decrease in lifetime suggested the enhancement of non-radiative decay through the charge transfer (CT) state. In addition, the trimers showed strong fluorescence quenching than that of the corresponding dimers. Electrochemically synthesized D-A polymers, which contain axial oligothiophene (electron donor) and basal phosphorus(V) porphyrin (electron acceptor) subunits have also been reported.[213]

Segawa and co-workers have reported a series of center-to-edge type phosphorus porphyrin arrays of the type **26** in which porphyrin units are linked axially to each other *via* the central phosphorus(V) ions.[214] In these systems, the excited state charge transfer was considered to be responsible for the quenching of fluorescence. The same group has reported axially substituted dialkoxo phosphorus(V) porphyrin derivatives.[215] Photochemistry of these systems has not been investigated.

Rao and Maiya have reported aryloxo derivatives of phosphorus(V) porphyrin-based trimers and D-A systems.[216,217] While steady state fluorescence data of the former systems have been analyzed in terms of energy transfer from the phosphorus(V) porphyrin to the axial porphyrin subunits and a PET in the reverse direction, those of the latter systems has been interpreted in terms of a PET reaction from the axial aryloxo 'donor' ligands to the singlet phosphorus(V) porphyrin.

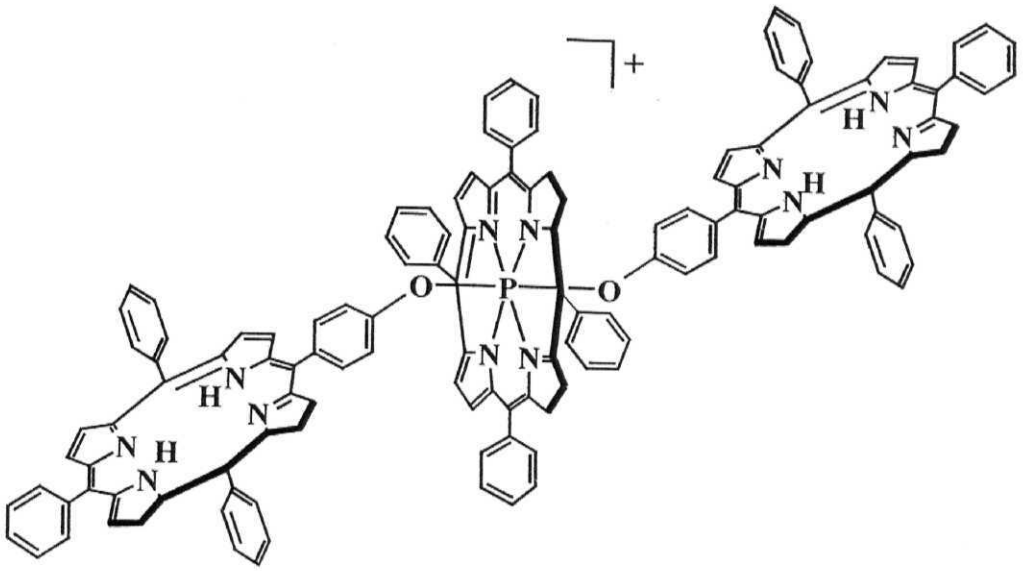

26a

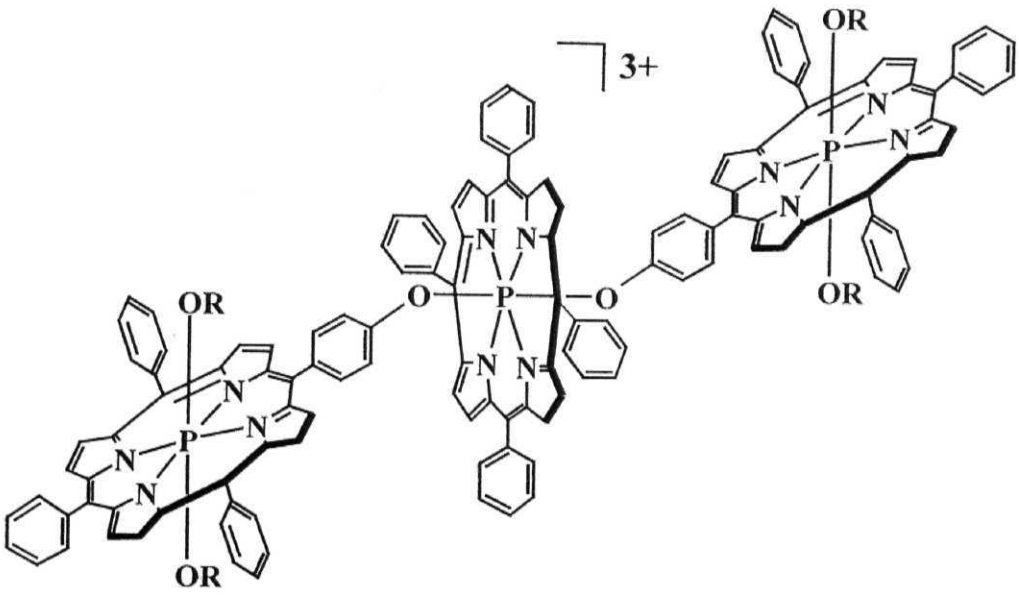

26b

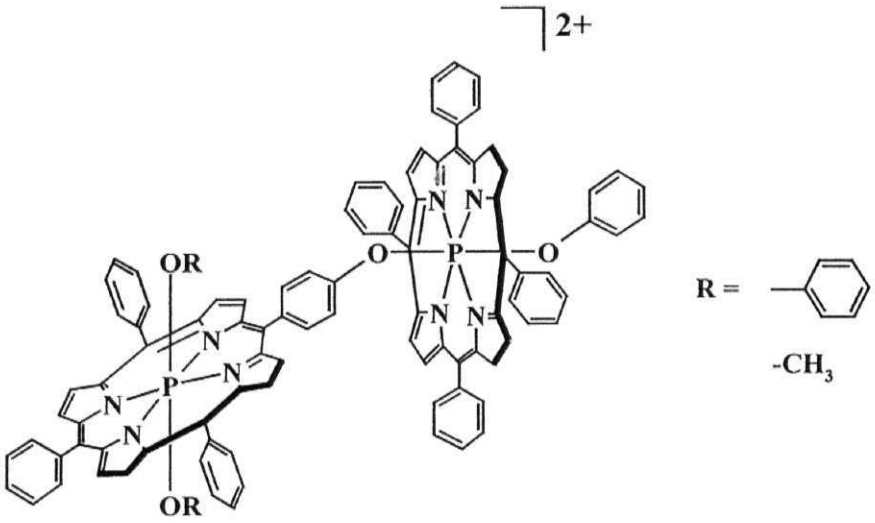

26c

Hirakawa and Segawa have reported phosphorus(V) porphyrin-pyrene triads in which two pyrene subunits are connected to a central phosphorus(V) ion through various bridges as in **27** and **28.** These triads are characterized by π - π interaction between the pyrene and porphyrin moieties. As a result, emission from the photoexcited states of both the pyrene and the porphyrin subunits were quenched through energy and/or electron transfer process.[218]

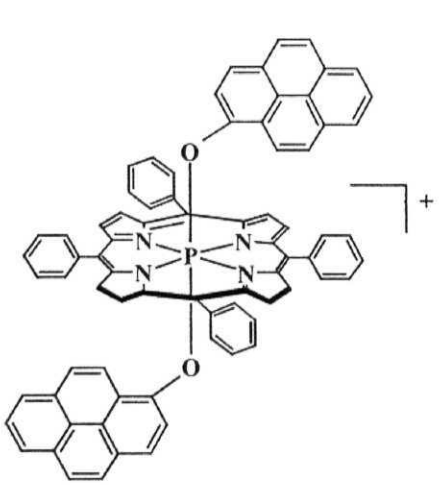

27

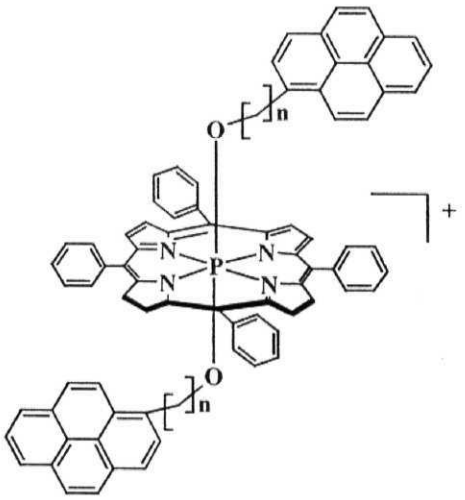

n = 1 **(28a),** n = 2 **(28b)**

Goh and Czuchajowski have reported synthesis of novel axial dinucleoside bearing phosphorus(V) porphyrins.[219] In these complexes, phosphorus(V) porphyrin units are axially connected through the 5′-O-thymidine-3′-O bridges.

The scope of carboxylate binding by tin(IV) porphyrins and the solution geometries of the resulting complexes **(29)** have been explored using NMR spectroscopy by Hawley *et al.*[220] Sanders and co-workers have suggested the use of 'axial-bonding' type tin(IV) porphyrins as NMR shift reagents and as supramolecular protecting groups.[221]

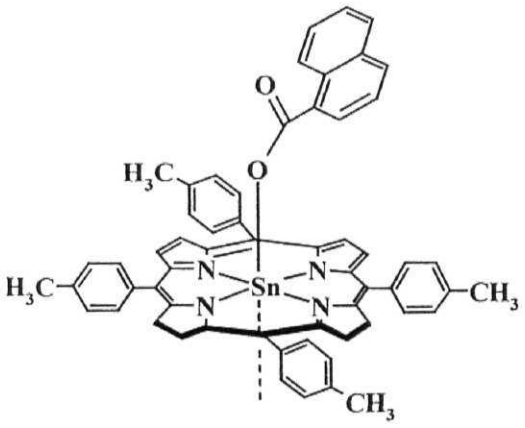

29a

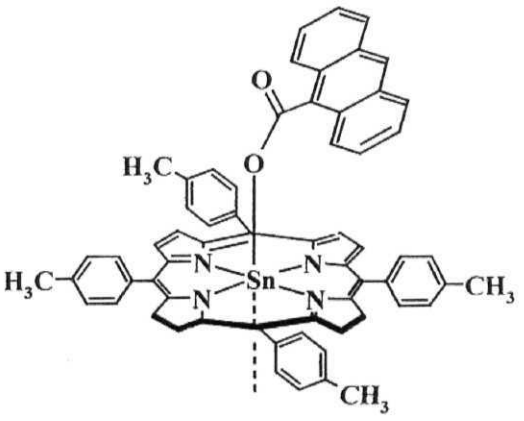

29b

In an interesting study, Webb and Sanders have reported a series of cyclic, mixed-metalloporphyrin trimers **(30)** having cavities lined with different carboxylate groups.[222] The influence of these carboxylate-lined cavities on the binding of pyridyl ligands to the ruthenium(II) centers of these hosts was investigated. The rich hydrogen-bonding environment provided by a D-quinate-lined cavity **30e** was found to enhance the binding of 4-methanolpyridine to the ruthenium(II) center.

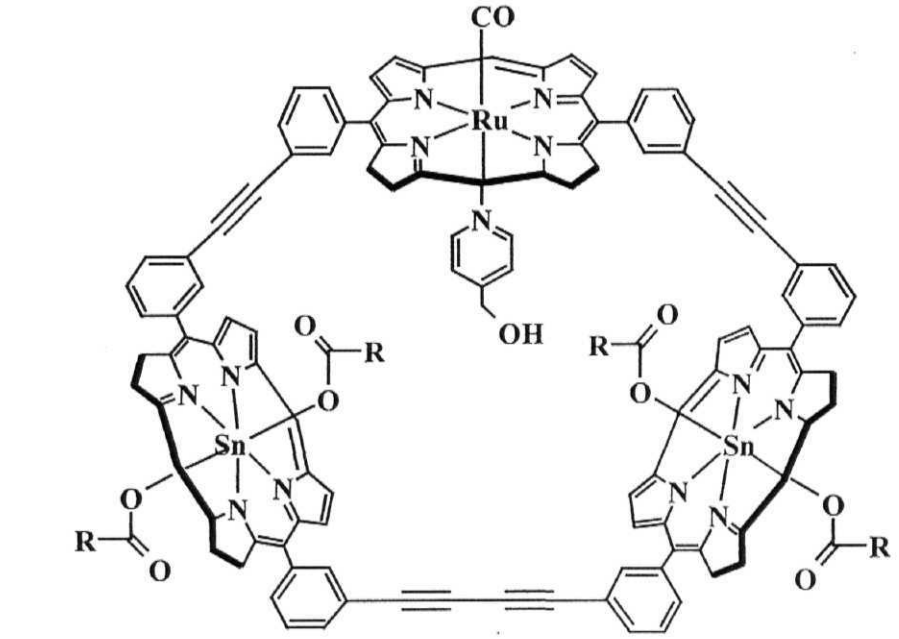

R = Et

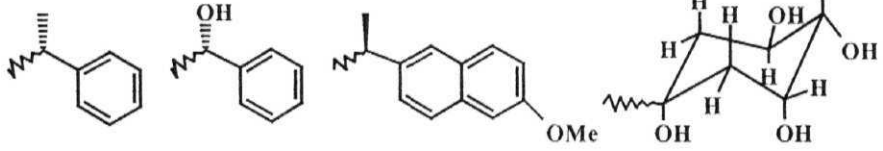

30a **30b** **30c** **30d** **30e**

Shiragami *et al.* reported antimony(V) porphyrin systems bearing axial aryl groups. Fluorescence spectra of (2-naphthoxy)polyoxalkoxyantimony(V) tetraphenylporphyrin complex **(31)**[223,224] were analyzed under the excitation of naphthoxy and porphyrin chromophores. The excitation energy of naphthoxy chromophore was observed to be transferred to the porphyrin moiety with nearly equal rates irrespective of methylene bridge length. The emission of porphyrin chromophore was quenched by naphthoxy chromophore with rate constants of 10^7 – 10^{10} s^{-1} depending on both the solvent used and the length of the methylene bridge. Under excitation of the naphthoxy chromophore of the triad system involving porphyrin, 2-naphthoxy and 4-methoxyphenoxy chromophores, the

excited singlet state of the porphyrin chromophore generated by the energy transfer from the naphthoxy chromophore was quenched by the naphthoxy and the methoxyphenoxy chromophores *via* non-radiative processes involving electron transfer.

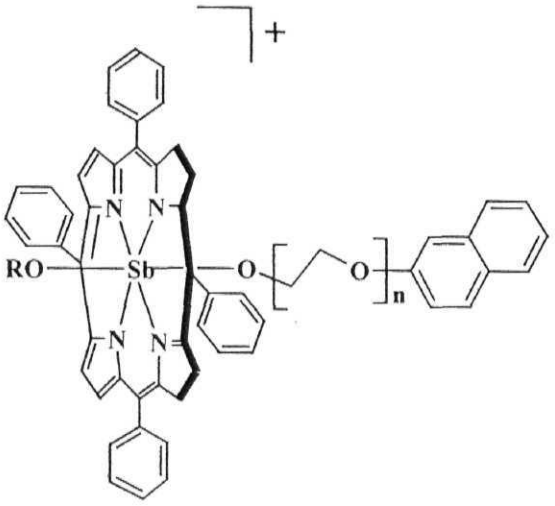

R = H, n = 1 (**31a**); R = H, n = 2 (**31b**); R = H, n = 3 (**31c**); R = 4-OMe-C_6H_4-, n = 1 (**31d**)

1.5.3 Both M–N and M–O bond containing D-A Systems

Sanders and co-workers have reported heterometallic oligoporphyrins, **32** and **33**, using cooperative Ru–N / Zn–N and Sn–O coordination.[225-227] These oligomers were designed to exploit the complementary geometries and cooperative binding properties of tailor-made metalloporphyrin building blocks.

Recently, a photochemically-functional, axial-bonding type hybrid porphyrin trimer, **34**, has been self-assembled by an advantageous utilization of the well-known hard and soft acid-base (HSAB) principle and metal ion recognition by a ditopic ligand.[228] Steady state emission results have been interpreted in terms of a PET from the axial ruthenium(II) porphyrin to the

excited state of the basal tin(IV) porphyrin. Extending on the same theme, Fallon *et al.* have reported porphyrin trimers, **35**.[229-231] Photochemistry of these systems has not been investigated.

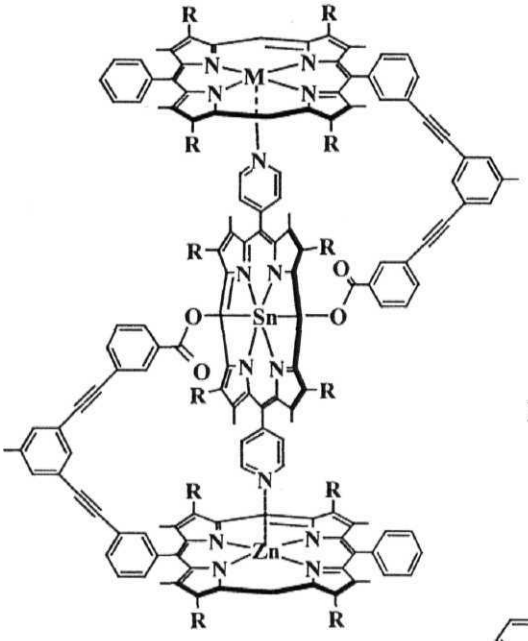

M = Zn(II) (**32a**), M = Ru(II) (**32b**)

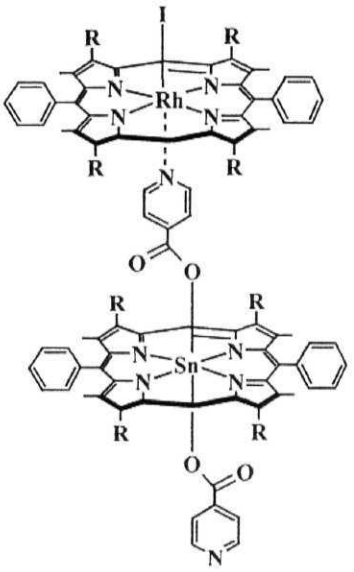

R = hexyl

33a

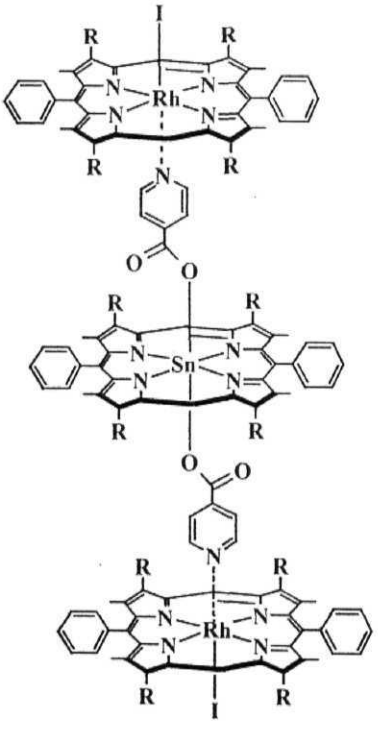

33b

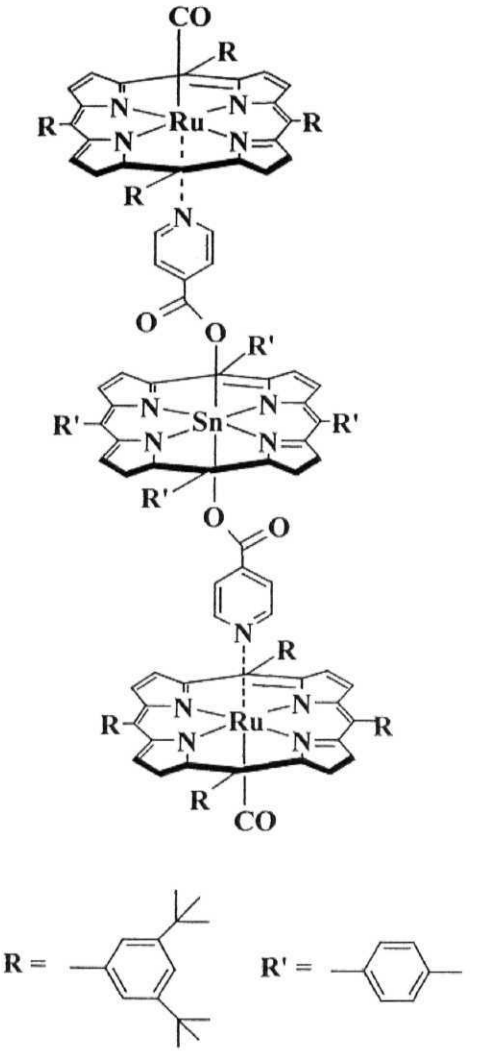

34

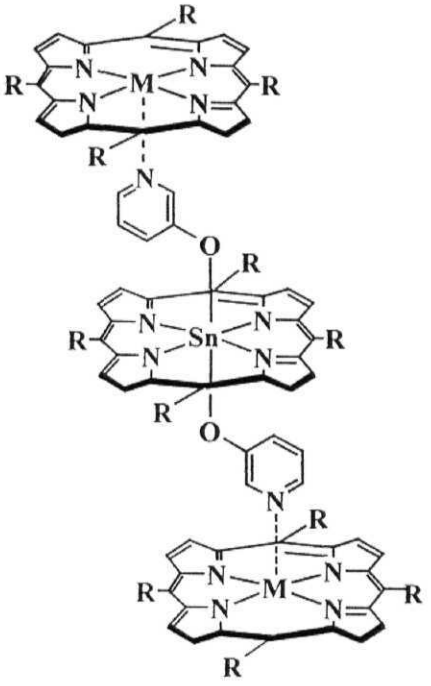

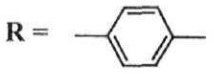

M = Zn(II) (**35a**), M = Ru(II) (**35b**)

1.6 Summary

The basic principles involved in electron and energy transfer reactions and also a discussion on the recent porphyrin based D-A systems highlighting their PET and EET reactions as applicable to the subject matter of the present thesis have been presented in this Chapter.

1.7 References

1. *Photoinduced Electron Transfer*, Parts A-D; Fox, M. A., Chanon, M., Eds.; Elsevier: Amsterdam, **1988**.
2. *Photoinduced Electron Transfer* A series in *Topics in Current Chemistry* Mattay, J.; Ed.; Springer-verlag: New York, **1991**.
3. Marcus, R. A.; Sutin, N. *Biochim. Biophys. Acta* **1985**, *811*, 262.
4. *Photosynthesis;* Amesz, J.; Ed.; Elsevier: Amsterdam, **1987**.
5. Gust, D.; Moore, T. A.; Moore, A. L. *Acc. Chem. Res.* **1993**, *26*, 198.
6. Guillet, J. E. in *Polymer Photophysics and Photochemistry*; Cambridge University Press: Cambridge, **1985**.
7. Bloor, D. *Physica Scripta.* **1991**, *39*, 380.
8. Pope, M. *Mol. Cryst. Liq. Cryst.* **1993**, *228*, 1.
9. Marcus, R. A. *J. Chem. Phys.* **1956**, *24*, 966.
10. Marcus, R. A. *J. Chem. Phys.* **1965**, *43*, 679.
11. Marcus, R. A. *in Light Induced Charge Separation in Biology and Chemistry*; Gerischer, H.; Katz, J. J., Eds.; Verlag Chemie: Berlin, **1979**, p. 15.
12. Marcus, R. A. *Angew. Chem., Int. Ed. Engl.* **1993**, *32*, 1111.
13. Forster, Th. *Discuss. Faraday Soc.* **1959**, *27*, 7.
14. Dexter, D. L. *J. Chem. Phys.* **1953**, *21*, 836.
15. Deisenhofer, J.; Epp, O.; Mikki, K.; Huber, R.; Michel, H. *J. Mol. Biol.* **1984**, *180*, 385.
16. Deisenhofer, J.; Epp, O.; Mikki, K.; Huber, R.; Michel, H. *Nature*, **1985**, *318*, 618.
17. Chang, C. H.; Tiede, D.; Tang, J.; Smith, U.; Norris, J.; Schiffer, M. *FEBS Lett.* **1986**, *205*, 82.

18. Allen, J. P.; Feher, G.; Yeates, T. O.; Rees, D. C.; Deisenhofer, J.; Michel, H.; Huber, R. *Proc. Natl. Acad. Sci. USA* **1986**, *83*, 8589.

19. Allen, J. P.; Feher, G.; Yeates, T. O.; Komiya, H.; Rees, D. C. *Proc. Natl. Acad. Sci. USA* **1987**, *84*, 5730.

20. Yeates, T. O.; Komiya, H.; Chirino, A.; Rees, D. C.; Allen, J. P.; Feher, G. *Proc. Natl. Acad. Sci. USA* **1988**, *85*, 7993.

21. El-Kabbani, O.; Chang, C. H.; Tiede, D. M.; Norris, J.; Schiffer, M. *Biochemistry* **1991**, *30*, 5361.

22. Ermler, U.; Fritzsch, G.; Buschanan, S. K.; Michel, H. *Structure* **1994**, *2*, 925.

23. Deisenhofer, J.; Epp, O.; Sinning, I.; Michel, H. *J. Mol. Biol.* **1995**, *246*, 429.

24. Connolly, J. S. In *Photochemical Conversion and Storage of Solar Energy*; Rabani, J., Ed.; The weizman Science Oress : Jerusalem, **1982**, Part A, p. 175.

25. *Photochemistry of Polypyridine and Porphyrin Complexes*; Kalyanasundaram, K.; Academic Press: London, **1992**.

26. Harriman, A. in *Supramolecular Photochemistry*; Balzani, V.; Reidel, D.; Boston, **1987**, p. 207.

27. Wasielewski, M. R. In *Photoinduced Electron Transfer*, Part D, Fox, M. A.; Channon, M.; Eds.; Elsevier: Amsterdam, **1988**, Chapter 1.4.

28. Gust, D.; Moore. T. A. *Science* **1989**, *244*, 35.

29. *The Porphyrins*, Dolphin, D.; Ed.; Academic Press: New York, **1979**, Vols. 1-7.

30. Gust, D.; Moore, T. A. *Top. Curr. Chem.* **1991**, *159*, 103.

31. Wasielewski, M. R. *Chem. Rev.* **1992**, *92*, 435.

32. Fox, M. A. *Photochem. Photobiol.* **1990**, *52*, 617.

33. Kurreck, H.; Huber, M. *Angew. Chem., Int. Ed. Engl.* **1995**, *34*, 849.
34. Morgan, B.; Dolphin, D. *Structure and Bonding* **1987**, *64*, 115.
35. Baldwin, J. E.; Perlmuter, P. *Top. Curr. Chem.* **1984**, *121*, 181.
36. Pullerits, T.; Sundstrom, V. *Acc. Chem. Res.* **1996**, *29*, 381.
37. Hayashi, T.; Ogoshi, H. *Chem. Soc. Rev.* **1997**, *26*, 355.
38. Ward, M. D. *Chem. Soc. Rev.* **1997**, *26*, 365.
39. Yamamoto, M.; Ito, S.; Ohmori, S. *In Photochemical Processes in Organized Molecular Systems*; Honda, K.; Ed: Amsterdam, **1991**; p 329.
40. Anderson, H. L. *Inorg. Chem.* **1994**, *33*, 972.
41. Crossley, M. J.; Burn, P. L. *J. Chem. Soc., Chem. Commun.* **1987**, 39.
42. Crossley, M. J.; Burn, P. L. *J. Chem. Soc., Chem. Commun.* **1991**, 1569.
43. Crossley, M. J.; Govenlock, L. J.; Prashar, J. K. *J. Chem. Soc., Chem. Commun.* **1995**, 2379.
44. Crossley, M. J.; Burn, P. L.; Langford, S. J.; Prashar, J. K. *J. Chem. Soc., Chem. Commun.* **1995**, 1921.
45. Reimers, J. R.; Lu, T. X.; Crossley, M. J.; Hush, N. S. *Chem. Phys. Lett.* **1996**, *256*, 353.
46. Kong, J.; Loach, P. A. In *Frontiers of Biological Energetics: From Electrons to Tissues* Dutton, P. L.; Scarpa, S. Eds.; Academic: New York, Vol.1, p. 73.
47. Anton, J. A.; Kong, J. A.; Loach, P. A. *J. Heterocycl. Chem.* **1976**, *13*, 717.
48. Boxer, S. G.; Bucks, R. R. *J. Am. Chem. Soc.* **1979**, *101*, 1883.
49. Takagi, A.; Yanagawa, Y.; Tsuda, A.; Aratani, N.; Matsumoto, T.; Osuka, A.; Kawai, T. *Chem. Commun.* **2003**, 2986.
50. Yoon, D. H.; Lee, S. B.; Yoo, K.-H.; Kim, J.; Lim, J. K.; Aratani, N.; Tsuda, A.; Osuka, A.; Kim, D. *J. Am. Chem. Soc.* **2003**, *125*, 11062.

51. Aratani, N.; Cho, H. Y.; Ahn, T. K.; Cho, S.; Kim, D.; Sumi, H.; Osuka, A. *J. Am. Chem. Soc.* **2003**, *125*, 9668.
52. Tsuda, A.; Nakano, A.; Osuka, A. *Chem. Commun.* **2003,** 1096.
53. Aratani, N.; Osuka, A.; Cho, H. Y.; Kim, D. *J. Photochem. Photobiol., C: Photochem Rev.* **2002**, *21*, 1.
54. Cho, H. Y.; Jeong, D. H.; Cho, H. S.; Kim, D. Matsuzaki, Y.; Tanaka, K.; Tsuda, A.; Osuka, A. *J. Am. Chem. Soc.* **2002**, *124*, 14642.
55. Jeong, D. H.; Yoon, M.-C.; Jang, S. M.; Kim, D.; Cho, D. W.; Yoshida, N.; Aratani, N.; Osuka, A. *J. Phys. Chem. A* **2002**, *106*, 2359.
56. Song, N. W.; Cho, H. S.; Yoon, M.-C.; Aratani, N.; Osuka, A.; Kim, D. *Bull. Korean Chem. Soc.* **2002**, *23*, 271.
57. Kim, Y. H.; Cho, H. S.; Kim, D.; Kim, S. K.; Yoshida, N.; Osuka, A. *Synth. Metal.* **2001**, *117*, 183.
58. Aratani, N.; Osuka, A. *Org. Lett.* **2001**, *3*, 4213.
59. Tsuda, A.; Osuka, A. *Science* **2001**, *293*, 79.
60. Tsuda, A.; Furuta, H.; Osuka, A. *J. Am. Chem. Soc.* **2001**, *123*, 10304.
61. Piet, J. J.; Taylor, P. N.; Wagewijs, B. R.; Anderson, H. L.; Osuka, A.; Warman, J. M. *J. Phys. Chem. B* **2001**, *105,* 97.
62. Tsuda, A.; Furuta, H.; Osuka, A. *J. Am. Chem. Soc.* **2001**, *123*, 10304.
63. Tsuda, A.; Nakano, A.; Furuta, H.; Yamochi.; Osuka, A. *Angew. Chem., Int. Ed.* **2000**, *39*, 558.
64. Nakano, A.; Osuka, A.; Yamazaki, I.; Yamazaki, T.; Nishimura, Y. *Angew. Chem., Int. Ed. Engl.* **1998**, *37*, 3023.
65. Ogawa, T.; Nishimoto, Y.; Yoshida, N.; Ono. N.; Osuka, A. *Chem. Commun.* **1998**, 337.
66. Osuka, A.; Shimidzu, H. *Angew. Chem., Int. Ed. Engl.* **1997**, *36*, 135.
67. Osuka, A.; Maruyama, K. *Chem. Lett.* **1993**, 949.

68. Osuka, A.; Tanabe, N.; Nakajima, S.; Maruyama, K. *J. Chem. Soc., Perkin Trans. 2* **1996**, 199.

69. Susumu, K.; Shimidzu, T.; Tanaka, K.; Segawa, H. *Tetrahedron Lett.* **1996**, 8399.

70. Susumu, K.; Therien, M. J. *J. Am. Chem. Soc.* **2002**, *124*, 8550.

71. Fletcher, J.; Therien, M. J. *Inorg. Chem.* **2002**, *41*, 331.

72. Fletcher, J. T.; Therien, M. J. *J. Am. Chem. Soc.* **2000**, *122*, 12393.

73. Shediac, R.; Gray, M. H. B.; Uyeda, H. T.; Johnson, R. C.; Hupp, J. T.; Angiolillo, P. J.; Therien, M. J. *J. Am. Chem. Soc.* **2000**, *122*, 7017.

74. Kumble, R.; Palese, S.; Lin, V. S.-Y.; Therien, M. J.; Hochstrasser, R. M. *J. Am. Chem. Soc.* **1998**, *120*, 11489.

75. Lin, V. S.-Y.; Therien, M. J. *Chem. Eur. J.* **1995**, *1*, 645.

76. Lin, V. S.-Y.; DiMagno, S. G.; Therien, M. J. *Science* **1994**, *264*, 1105.

77. Burrell, A. K.; Officer, D. L.; Reid, D. C. W. *Angew. Chem., Int. Ed. Engl.* **1995**, *34*, 900.

78. Higuchi, H.; Shimizu, K.; Ojima, J.; Sugiura, K.-I.; Sakata, Y. *Tetrahedron Lett.* **1995**, *36*, 5359.

79. Sen, A.; Krishnan, V. *Tetrahedron Lett.* **1998**, *39*, 6539.

80. Tran-Thi, T. H.; Lipskier, J. R.; Maillard, P.; Momenteau, M.; Lopez-Castillo, J.-M.; Jay-Gerrin, J.-P. *J. Phys. Chem.* **1992**, *96*, 1073.

81. Wasielewski, M. R.; Niemezyk, M. P.; Svec, W. A. *Tetrahedron Lett.* **1982**, *23*, 3215.

82. Nagata, T.; Osuka, A.; Maruyama, K. *J. Am. Chem. Soc.* **1990**, *112*, 3054.

83. Abdalmuhdi, I.; Chang, C. K. *J. Org. Chem.* **1985**, *50*, 411.

84. Osuka, A.; Ida, K.; Maruyama, K. *Chem. Lett.* **1989**, 741.

85. Osuka, A.; Nagata, T.; Maruyama, K. *Chem. Lett.* **1991**, 481.

86. Osuka, A.; Nakajima, S.; Maruyama, K.; Mataga, N.; Asahi, T.; Yamazaki, I.; Nishimura, Y.; Ohino, T.; Nozaki, K. *J. Am. Chem. Soc.* **1993**, *115*, 5477.

87. Osuka, A.; Yamada, H.; Maruyama, K.; Ohno, T.; Nozaki, K.; Okada, T.; Tanaka, Y.; Mataga, N. *Chem. Lett.* **1995**, 591.

88. Osuka, T.; Taniguchi, S.; Nozaki, K.; Ohno, T.; Mataga, N. *Tetrahedron Lett.* **1995**, *36*, 5781.

89. Osuka, A.; Lin, B.-I.; Maruyama, K. *Chem. Lett.* **1993**, 949.

90. Sazanovich, I. V.; Kirmaier, C.; Hindin, E.; Yu, L.; Bocian, D. F.; Lindsey, J. S.; Holten, D. *J. Am. Chem. Soc.* **2004**, *126*, 2664.

91. Segawa, H.; Senshu, Y.; Nakazaki, J.; Susumu, K. *J. Am. Chem. Soc.* **2004**, *126*, 1354.

92. Chng, L. L.; Chang, C. J.; Nocera, D. G. *J. Org. Chem.* **2003**, *68*, 4075.

93. Sazanovich, I. V.; Balakumar, A.; Muthukumaran, K.; Hindin, E.; Kirmaier, C.; Diers, J. R.; Lindsey, J. S.; Bocian, D. F.; Holten, D. *Inorg. Chem.* **2003**, *42*, 6616.

94. Cho, H. S.; Rhee, H.; Song, J. K.; Min, C.-K.; Takase, M.; Aratani, N.; Cho, S.; Osuka, A.; Joo, T.; Kim, D. *J. Am. Chem. Soc.* **2003**, *125*, 5849.

95. Fukuzumi, S.; Ohkubo, K.; Wenbo, E.; Ou, Z.; Shao, J.; Kadish, K. M.; Hutchison, J. A.; Ghiggino, K. P.; Sintic, P. J.; Crossley, M. J. *J. Am. Chem. Soc.* **2003**, *125*, 14984.

96. Hasobe, T.; Imahori, H.; Yamada, H.; Sato, T.; Ohkubo, K.; Fukuzumi, S. *Nano. Lett.* **2003**, *3*, 409.

97. Blake, I. M.; Krivokapic, A.; Katterle, M.; Anderson, H. L. *Chem. Commun.* **2002**, 1662.

98. Chang, C. J.; Deng, Y.; Peng, S.-M.; Lee, G.-H.; Yeh, C.-Y.; Nocera, D. G. *Inorg. Chem.* **2002**, *41*, 3008.

99. Fletcher, J. T.; Therien, M. J. *J. Am. Chem. Soc.* **2002**, *124*, 4298.

100. Yeow, E. K. L.; Ghiggino, K. P.; Reek, J. N. H.; Crossley, M. J.; Bowman, A. W.; Schenning, A. P. H. J.; Meijer, E. W. *J. Phys. Chem. B* **2000,** *104,* 2596.

101. Choi, M. S.; Aida, T.; Yamazaki, T.; Yamazaki, I. *Chem. Eur. J.* **2002**, *6*, 2667.

102. Choi, M. S.; Aida, T.; Yamazaki, T.; Yamazaki, I. *Angew. Chem., Int. Ed. Engl.* **2001**, *40*, 3194.

103. Milgrom, L. R. *J. Chem. Soc., Perkin Trans. 2* **1983**, 2535.

104. Davila, J.; Harriman, A.; Milgrom, L. R. *Chem. Phys. Lett.* **1987**, *136*, 427.

105. Wennerstrom, O.; Ericsson, H.; Raston, I.; Svensson, S.; Pimlott, W. *Tetrahedron Lett.* **1989**, *30*, 1129.

106. Prathapan, S.; Johnson, T. E.; Lindsey, J. S. *J. Am. Chem. Soc.* **1993**, *115*, 7519.

107. del Rosario, M. B.; Johnson, T. E.; Weghorn, S.; Yu, L.; Rao, P. D.; Diers, J. R.; Yang, S. I.; Kirmaier, C.; Bocian, D. F.; Holten, D.; Lindsey, J. S. *J. Mater. Chem.* **2002**, *12*, 65.

108. Loewe, R. S.; Lammi, R. K.; Diers, J. R.; Kirmaier, C.; Bocian, D. F.; Holten, D.; Lindsey, J. S. *J. Mater. Chem.* **2002**, *12*, 1530.

109. Seth, J.; Palaniappn, V.; Johnson, T. E.; Prathapan, S.; Lindsey, J. S. *J. Am. Chem. Soc.* **1995**, *117*, 5231.

110. Sugiura, K.; Tanaka, H.; Matsumoto, T.; Kawai, T.; Sakata, Y. *Chem. Lett.* **1999**, 1193.

111. Nakano, A.; Osuka, A.; Yamazaki, I.; Yamazaki, T.; Nishimura, Y. Itaya, A.; Murakami, M.; Miyasaka, M. *Chem. Eur. J.* **2001**, *7*, 3134.

112. Mak, C. C.; Bampos, N.; Sanders, J. K. M. *Angew. Chem., Int. Ed. Engl.* **1998**, *37*, 3020.

113. Mak, C. C.; Pomeranc, D.; Montalti, M.; Prodi, L.; Sanders, J. K. M. *Chem. Commun.* **1999**, 1083.

114. Dubowchik, G. M.; Hamilton, A. D. *Chem. Commun.* **1986**, 1392.

115. Dubowchik, G. M.; Hamilton, A. D. *Chem. Commun.* **1986**, 665.

116. Dubowchik, G. M.; Hamilton, A. D. *Chem. Commun.* **1987**, 293.

117. Screen, T. E. O.; Thorne, J. R. G.; Denning, R. G.; Bucknall, D. G.; Anderson, H. L. *J. Am. Chem. Soc.* **2002**, *124*, 9712.

118. Taylor, P. N.; Anderson, H. L. *J. Am. Chem. Soc.* **1999**, *121*, 11538.

119. Anderson, H. L.; Hunter, C. A.; Sanders. J. K. M. *Chem. Commun.* **1989**, 226.

120. Anderson, H. L.; Hunter, C. A.; Meah, M. N.; Sanders, J. K. M. *J. Am. Chem. Soc.* **1990**, *112*, 5780.

121. Anderson, S.; Anderson, H. L.; Sanders, J. K. M. *Acc. Chem. Res.* **1993**, *26*, 469.

122. Vidal-Ferran, A.; Muuler, C. M.; Sanders, J. K. M. *Chem. Commun.* **1994**, 2657.

123. Mackay, L. G.; Wylie, R. S.; Sanders, J. K. M. *J. Am. Chem. Soc.* **1994**, *116*, 3141.

124. Anderson, S.; Anderson, H. L.; Bashall, A.; McPartlin, M.; Sanders, J. K. M. *Angew. Chem., Int. Ed. Engl.* **1995**, *34*, 1096.

125. Marty, M.; Clyde-Watson, Z.; Twyman, L. J.; Nakash, M.; Sanders, J. K. M. *Chem. Commun.* **1998**, 2265.

126. Nakano, A.; Osuka, A.; Yamazaki, I.; Yamazaki, T.; Nishimura, Y. *Angew. Chem., Int. Ed. Engl.* **1998**, *37*, 3023.

127. Rucareanu, S.; Mongin, O.; Schuwey, A.; Hoyler, N.; Gossauer, A. *J. Org. Chem.* **2001**, *66*, 4973.

128. Mongin, O.; Hoyler, N.; Gossauer, A. *Eur. J. Org. Chem.* **2000**, 1193.

129. Mongin, O.; Schuwey, A.; Vallot. M. A.; Gossauer, A. *Tetrahedron Lett.* **1999**, *40*, 8347.

130. Kin-ya, T.; Yu, L.; Wei. L.; Bocian, D.; Lindsey, J. S. *J. Org. Chem.* **2003**, *68*, 8199.

131. Ambroise, A.; Li, J.; Yu, L.; Lindsey, J. S. *Org. Lett.* **2000**, *2*, 2563.

132. Peng, X.; Aratani, N.; Takagi, A.; Matsumoto, T.; Kawai, T.; Hwang, I.–W.; Ahn, T. K.; Kim, D.; Osuka, A. *J. Am. Chem. Soc.* **2004**, *126*, 4468.

133. Sessler, J. L.; Capuano, V. L. *Angew. Chem., Int. Ed. Engl.* **1990**, *29*, 1134.

134. Sessler, J. L.; Capuano, V. L.; Harriman, A. *J. Am. Chem. Soc.* **1993**, *115*, 4618.

135. Osuka, A.; Yamada, H.; Maruyama, K.; Ohno, T.; Nozaki, K.; Okada, T.; Tanaka, Y.; Mataga. *Chem. Lett.* **1995**, 591.

136. Tabushi, I.; Koga, N.; Yanagita, M. *Tetrahedron Lett.* **1979**, *29*, 257.

137. Ho, T. F.; McIntosh, A. R.; Bolton, J. R. *Nature*, **1980**, *286*, 254.

138. Rubtsov, I. V.; Kang, Y. K.; Redmore, N. P.; Allen, R. M.; Zheng, J.; Beratan, D. N.; Therien, M. J. *J. Am. Soc. Chem.* **2004**, *126*, 5022.

139. Kang, Y. K.; Rubtsov, I. V.; Iovine, P. M.; Chen, J.; Therein, M. J. *J Am. Chem. Soc.* **2002**, *124*, 8275.

140. Capitosti, G. J.; Guerrero, C. D.; Binkley Jr, D. E.; Rajesh, C. S.; Modarelli, D. A. *J. Org. Chem.* **2003**, *68*, 247.

141. Hayashi, T.; Takimura, T.; Ohara, T.; Hitomi, Y.; Ogoshi, H. *Chem. Commun.* **1995**, 2503.

142. Gust, D.; Moore, T. A.; Moore, A. L.; Lee, S.; Bittersmann, E.; Luttrull, D. K.; Rehms, A. A.; Degraziano, J. M.; Ma, X. C.; Gao, F.; Belford, R. E.; Trier, T. T. *Science* **1990**, *24*, 199.

143. Hung, S.; Macpherson, A. N.; Lin, S.; Liddell, P. A.; Seely, G. R.; Moore, A. L.; Moore, T. A.; Gust, D. *J. Am. Chem. Soc.* **1995**, *117*, 1657.

144. Thanabal, V.; Krishnan, V. *J. Am. Chem. Soc.* **1982**, *104*, 3643.

145. Maiya, B. G.; Krishnan, V. *Inorg. Chem.* **1985**, *24*, 3253.

146. Chandrashekar, T. K.; van Willigen, H.; Ebersole, M. H. *J. Phys. Chem.* **1985**, *89*, 3453.

147. van Willigen, H.; Chandrashekar, T. K. *J. Am. Chem. Soc.* **1986**, *108*, 709.

148. Lehn, J.-M. *Supramolecular Photochemistry*, Balzani, V.; Ed.; NATO ASI Ser. C, **1987**, Vol. 24, p. 29f.

149. Sun, L.; van Gersdorff, J.; Niethammer, D.; Tian, P.; Kurreck, H. *Angew. Chem., Int. Ed. Engl.* **1994**, *33*, 2318.

150. Lindsey, J. S.; Brown, P. A.; Siesel, D. A. *Tetrahedron* **1989**, *45*, 4845.

151. Sirish, M.; Maiya, B. G. *J. Photochem. Photobiol. A: Chem.* **1996**, *93*, 129.

152. Sirish, M.; Maiya, B. G. *J. Photochem. Photobiol. A: Chem.* **1994**, *77*, 189.

153. Kin-ya, T.; Loewe, R. S.; Kirmaier, C.; Schwartz, J. K.; Retsek, J. L.; Bocian, D. F.; Holten, D.; Lindsey, J. S. *J. Org. Chem.* **2002**, *67*, 6519.

154. Hayes, R. T.; Walsh, C. J.; Wasielewski, M. R. *J. Phys. Chem. A* **2004**, *108*, 3253.

155. Hayes, R. T.; Walsh, C. J.; Wasielewski, M. R. *J. Phys. Chem. A* **2004**, *108*, 2375.

156. Schuster, D. I.; Li, K.; Guldi, D. M.; Ramey. J. *Org. Lett.* **2004**, *6*, 1919.

157. Imahori, H. *Org. Biomol. Chem.* **2004**, *2*, 1425.

158. Kashiwagi, Y.; Ohkubo, K.; McDonald, J. A.; Blake, I. M.; Crossley, M. J.; Araki, Y.; Ito, O.; Imahori, H.; Fukuzumi, S. *Org. Lett.* **2003**, *5*, 2719.

159. Liddel, P. A.; Sumida, J. P.; Macpherson, A. N.; Noss, L.; Seely, G. R.; Clark, K. N.; Moore, A. L.; Moore, T. A.; Gust, D. *Photochem. Photobiol.* **1994**, *60*, 537.

160. Maruyama, H.; Fujiwara, M.; Tanaka, K. *Chem. Lett.* **1998**, 805.

161. Smirnov, S. N.; Liddell, P. A.; Vlassiouk, I. V.; Teslja, A.; Kuciauskas, D.; Braun, C. L.; Moore, A. L.; Moore, T. A.; Gust, D. *J. Phys. Chem. A* **2003**, *107*, 7567.

162. Higashida, S.; Imahori, H.; Kaneda, T.; Sakata, Y. *Chem. Lett.* **1998**, 605.

163. Crouch, A. M.; Sharma, D. K.; Langford, C. H. *Chem. Commun.* **1988**, 307.

164. Otsuki, J.; Suka, A.; Yamazaki, K.; Abe, H.; Araki, Y.; Ito, O. *Chem. Commun.* **2004**, 1290.

165. Mataga, N.; Taniguchi, S.; Chosrowjan, H.; Osuka, A.; Yoshida, N. *Chem. Phys.* **2003**, *295*, 215.

166. Otsuki, J.; Takatsuki, M.; Kaneko, M.; Miwa, H.; Takido, T.; Seno, M.; Okamoto, K.; Imahori, H.; Fujitsuka, M.; Araki, Y.; Ito, O.; Fukuzumi, S. *J. Phys. Chem. A* **2003**, *107*, 379.

167. Otuski, J.; Harada, K.; Toyama, K.; Hirose, Y.; Araki, K.; Seno, M.; Takatera, K.; Watanabe, T. *Chem. Commun.* **1998**, 1515.

168. Otsuki, J.; Yasuda, A.; Takido, T. *Chem. Commun.* **2003**, 608.

169. Otuski, J.; Harada, K.; Araki, K. *Chem. Lett.* **1999**, 269.

170. D'Souza, F.; Smith, P. M.; Zandler, M. E.; McCarty, A. L.; Itou, M.; Araki, Y.; Ito, O. *J. Am. Chem. Soc.* **2004**, *126*, 7898.

171. D'Souza, F.; Deviprasad, G. R.; Zandler, M. E.; Honangm, V. T.; Klykov, A.; Vanstipdonk, M.; Perera, A.; El-Khouly, M. E.; Fujitsuka, M.; Ito, O. *J. Phys. Chem. A* **2002**, *106*, 3243.

172. D'Souza, F.; Deviprasad, G. R.; Rahman, M. S.; Choi, J. *Inorg. Chem.* **1999**, *38*, 2157.

173. D'Souza, F.; Deviprasad, G. R.; Zandler, M. E.; El-Khouly, M. E.; Fujitsuka, M.; Ito, O. *J. Phys. Chem. A* **2003**, *107*, 4801.

174. Deviprasad, G. R.; D'Souza, F. *Chem. Commun.* **2000**, 1915.

175. El-Khouly, M. E.; Gadde. S.; Deviprasad, G. R.; Fujitsuka, M.; Ito, O.; D'Souza, F. *J. Porphyrins Phthalocyanines* **2003**, *7*, 1.

176. El-Khouly, M. E.; Rogers, L. M.; Zandler, M. E.; Gadde, S.; Fujitsuka, M.; Ito, O.; D'Souza, F. *Chem. Phys. Chem.* **2003**, *4*, 474.

177. Tkachenko, N. V.; Lemmetyinen, H.; Sonoda, J.; Ohkubo, K.; Sato, T.; Imahori, H.; Fukuzumi, S. *J. Phys. Chem A* **2003**, *107*, 8834.

178. Yin, G.; Xu, D.; Xu, Z. *Chem. Phys. Lett.* **2002**, *365*, 232.

179. Wilson, S. R.; MacMahon, S.; Tat, F. T.; Jarowski, P. D.; Schuster, D. I. *Chem. Commun.* **2003**, 226.

180. D'Souza, F.; Rath, N. P.; Deviprasad, G. R.; Zandler, M. E. *Chem. Commun.* **2001**, 267.

181. Armaroli, N.; Diederich, F.; Echegoyen, L.; Habicher, T.; Flamigni, L.; Marconi, G.; Nierengarten, J.-F. *New. J. Chem.* **1999**, *23*, 77.

182. Ros, D. T.; Prato, M.; Guldi, D. M.; Alessio, E.; Ruzzi, M.; Pasimeni, L. *Chem. Commun.* **1999**, 635.

183. D'Souza, F.; Deviprasad, G. R.; El-Khouly, M. E.; Fujitsuka, M.; Ito, O. *J. Am. Chem. Soc.* **2001**, *123*, 5277.

184. D'Souza, F.; Zandler, M. E.; Deviprasad, G. R.; Kutner, W. *J. Phys. Chem. A* **2000**, *104*, 6887.

185. Hunter, C. A.; Sanders, J. K. M.; Beddard, G. S.; Evans, S. *Chem. Commun.* **1989**, 1765.

186. Hunter, C. A.; Hyde, R. K. *Angew. Chem., Int. Ed.* **1996**, *35*, 1936.

187. Fukushima, K.; Funatsu, K.; Ichimura, A.; Sasaki, Y.; Suzuki, M.; Fujihara, T.; Tsuge, K.; Imamura, T. *Inorg. Chem.* **2003**, *42*, 3187.

188. Kimura, A.; Fantasu, K.; Imamura, T.; Kido, H.; Sasaki, Y. *Chem. Lett.* **1995**, 207.

189. Fantasu, K.; Kimura, A.; Imamura, T.; Ichimura, A.; Sasaki, Y. *Inorg. Chem.* **1997**, *36*, 1625.

190. Chichak, K.; Branda, N. R. *Chem. Commun.* **1999**, 523.

191. Chichak, K.; Branda, N. R. *Chem. Commun.* **2000**, 1211.

192. Kelly, T. R.; Zhao, C.; Bridger, G. J. *J. Am. Chem. Soc.* **1989,** *111*, 3744.

193. Bonar-Law, R. P.; Mackay, L. G.; Walter, C. J.; Marvaud, V.; Sanders, J. K. M. *Pure Appl. Chem.* **1994**, *66*, 803.

194. Kieran, A. L.; Bond, A. D.; Belenguer, A. M.; Sanders, J. K. M. *Chem. Commun.* **2003**, 2674.

195. Anderson, H. L.; Sanders, J. K. M. *Chem. Commun.* **1989**, 1714.

196. Anderson, H. L.; Sanders, J. K. M. *Angew. Chem., Int. Ed.* **1990**, *29*, 1400.

197. Vidal-Ferran, A.; Muller, C. M.; Sanders, J. K. M. *Chem. Commun.* **1996**, 1849.

198. Anderson, H. L.; Anderson, S.; Sanders, J. K. M. *J. Chem. Soc., Perkin Trans 1* **1995**, 2231.

199. Anderson, S.; Anderson, H. L.; Sanders, J. K. M. *J. Chem. Soc., Perkin Trans 1* **1995**, 2255.

200. McCallein, D. W. J.; Sanders, J. K. M. *J. Am. Chem. Soc.* **1995**, *117*, 6611.

201. Vidal-Ferran, A.; Clyde-Watson, Z.; Bampos, N.; Sanders, J. K. M. *J. Org. Chem.* **1997**, *62*, 240.

202. Marvaud, V.; Vidal-Ferran, A.; Webb, S. J.; Sanders, J. K. M. *J. Chem. Soc., Dalton Trans.* **1997**, 985.

203. Vidal-Ferran, A.; Bampos, N.; Sanders, J. K. M. *Inorg. Chem.* **1997**, *36*, 6117.

204. Clyde-Watson, Z.; Bampos, N.; Sanders, J. K. M. *New. J. Chem.* **1998**, 1135.

205. Walter, C. J.; Anderson, H. L.; Sanders, J. K. M. *Chem. Commun.* **1993**, 458.

206. Walter, C. J.; Sanders, J. K. M. *Angew. Chem., Int. Ed.* **1995**, *34*, 217.

207. Clyde-Watson, Z.; Vidal-Ferran, A.; Twyman, L. J.; Walter, C. J.; McCallien, D. W. J.; Fanni, S.; Bampos, N.; Wylie, S.; Sanders, J. K. M. *New. J. Chem.* **1998**, *22*, 493.

208. Shimadzu, T.; Segawa, H. *Thin Solid Films* **1996**, *273*, 14.

209. Susumu, K.; Kunimoto, K.; Segawa, H.; Shimidzu. *J. Phys. Chem.* **1995**, *99*, 29.

210. Segawa, H.; Kunimoto, K.; Susumu, K.; Taniguchi, M.; Shimidzu, T. *J. Am. Chem. Soc.* **1994**, *116*, 11193.

211. Susumu, K.; Segawa, H.; Shimidzu, T. *Chem. Lett.* **1995**, 929.

212. Susumu, K.; Kunimoto, K.; Segawa, H.; Shimidzu, T. *J. Photochem. Photobiol. A: Chem.* **1995**, *92*, 39.

213. Segawa, H.; Nakayama, N.; Shimidzu, T. *Chem. Commun.* **1992**, 784.

214. Susumu, K.; Tanaka, K.; Shimidzu, T.; Takeuchi, Y.; Segawa, H. *J. Chem. Soc., Perkin Trans. 2* **1999**, 1521.

215. Segawa, H.; Kunimoto, K.; Nakamoto, A.; Shimidzu, T. *J. Chem. Soc., Perkin Trans. 1* **1982**, 939.

216. Rao, T. A.; Maiya, B. G. *Chem. Commun.* **1995**, 939.

217. Rao, T. A.; Maiya, B. G. *Inorg. Chem.* **1996**, *35*, 4829.

218. Hirakawa, K.; Segawa, H. *J. Photochem. Photobiol. A: Chem.* **1999**, *123*, 67.

219. Goh, G, K.-M.; Czuchajowski, L. *J. Porphyrins Phthalocyanines* **1997**, *1*, 281.

220. Hawley, J. C.; Bampos, N.; Abraham, R. J.; Sanders, J. K. M. *Chem. Commun.* **1998**, 661.

221. Tong, Y.; Hamilton, D. G.; Meillon. J.-C.; Sanders, J. K. M. *Org. Lett.* **1999**, *1*, 1343.

222. Webb, S. J.; Sanders, J. K. M. *Inorg. Chem.* **2000**, *39*, 5920.

223. Andou, Y.; Shiragami, T.; Shima, K.; Yasuda, M. *J. Photochem. Photobiol. A: Chem.* **2002**, *147*, 191.

224. Shiragami, T.; Andou, Y.; Hamasuna, Y.; Yamaguchi, F.; Shima, K.; Yasuda, M. *Bull. Chem. Soc. Jpn.* **2002**, *75*, 1577.

225. Redman, J. E.; Feeder, N.; Teat, S. J.; Sanders, J. K. M. *Inorg. Chem.* **2001**, *40*, 2486.

226. Kim, H.-J.; Bampos, N.; Sanders, J. K. M. *J. Am. Chem. Soc.* **1999**, *121*, 8120.

227. Stulz, E.; Mak, C. C.; Sanders, J. K. M. *J. Chem. Soc., Dalton Trans.* **2001**, 604.

228. Maiya, B. G.; Bampos, N.; Kumar, A. A.; Feeder, N.; Sanders, J. K. M. *New J. Chem.* **2001**, *25*, 797.

229. Fallon, G. D.; Langford, S. J.; Lee, M. A.-P.; Lygris, E. *Inorg. Chem. Commun.* **2002**, *5*, 715.

230. Fallon, G. D.; Lee, M. A.-P.; Langford, S. J.; Nichols, P. J. *Org. Lett.* **2002**, *4*, 1895.

231. Fallon, G. D.; Lee, M. A.-P.; Langford, S. J. *Acta. Cryst. E.* **2001**, *5*, m564.

CHAPTER 2

Materials and Methods

2.1 Introduction

This Chapter presents a listing of all the chemicals and other materials employed at various stages of the research work. Procedures followed for the purification of solvents and chemicals are also given here. Further, a brief discussion of the physicochemical techniques employed during the course of the investigation is presented.

2.2 Materials

Pyrrole, Ruthenium trichloride trihydrate, ammoniumhexafluorophosphate (NH_4PF_6), tetrabutylammonium perchlorate (TBAP) and pyrene were purchased from Aldrich Chemical Co. (U.S.A). Pyrrole was distilled over KOH before use.

4-methylbenzaldehyde, 1,2-dibromoethane and 2-acetylpyridine were purchased from Sisco Chem. (India).

4-hydroxybenzaldehyde, *p*-Cresol and aluminium(III) chloride were procured from E. Merck (India). $AlCl_3$ was sublimed prior to use.

2,3-dichloro-5,6-dicyano-1,4-benzoquinone (DDQ) was purchased from Wilson Laboratories (India).

4-Acetamidobenzaldehyde, copper(II) triflate and zinc(II) triflate were purchased from Acros Organics (India). 1-pyrenecarboxaldehyde and 2-methylanthraquinone were purchased from Lancaster (India). LR grade ferrous(II) chloride was obtained from Fluka (U. S. A).

LR grade metal acetates and AR grade mineral acids such as hydrochloric acid, nitric acid and sulfuric acid used were acquired from either Ranbaxy (India) or from B.D.H. (India).

Tin(II)dichloride dihydrate, ammonium acetate, acetamide, NaOH, potassium chloride, potassium hydroxide, potassium carbonate and sodium bicarbonate were of LR grade and were obtained from B.D.H. (India). $SnCl_2.2H_2O$ was purified by stirring with acetic acid and acetic anhydride at room temperature under nitrogen for 4 h. The solid was filtered under nitrogen and washed with dry ether.[1]

The drying agents used were calcium chloride, sodium sulfate and magnesium sulfate were obtained from either B.D.H. (India) or Qualigens (India) and were of LR grade.

Phosphorus oxychloride and calcium hydride were obtained from Spectrochem (India). $POCl_3$ was distilled prior to use.

Aluminium oxide (basic and neutral) and silica gel (100 - 200 mesh size) for column chromatography were procured from Acme Synthetic Chemicals (India) and were used as such. All other common chemicals were purchased from locally available sources.

Nitrogen gas was obtained from Indian Oxygen Limited (India). It was further purified and dried by passing it through alkaline pyrogallol solution, sulfuric acid, and potassium hydroxide pellets.

2.3 Solvents

The common solvents employed during the research work were purified according to the standard procedures.[1,2]

Acetic acid, acetic anhydride and propanoic acid were purchased from Ranbaxy (India).

Pyridine, triethylamine were obtained from Ranbaxy (India). Pyridine was dried over potassium hydroxide pellets and distilled over calcium hydride under nitrogen before use.

Benzene, toluene and cyclohexane were obtained from Ranbaxy (India) and they were dry distillated over sodium metal and benzoquinone under nitrogen and stored over sodium wire.

DMF, DMSO and benzonitrile were obtained from E. Merck (India). They were purified by flash vacuum distillation over calcium hydride or P_2O_5.

Acetonitrile was obtained from S.d. Fine-Chem. Ltd. (India). It was distilled over calcium hydride prior to use.

Chloroform, methylene chloride and methanol were of LR grade from B.D.H. (India) and were used for synthetic or chromatographic purposes. These solvents were extensively purified as described below, for spectroscopic purposes.

The LR grade methylene chloride was washed twice with sulfuric acid and then with water. This was washed twice with sodium bicarbonate solution and then with water. The solvent was dried over calcium chloride and distilled over phosphorus pentoxide. It was stored over basic alumina until use. Chloroform (LR) was washed 3 - 4 times with water, stored over calcium chloride overnight and distilled over phosphorus pentoxide. It was stored in the dark over basic alumina. Methanol (LR) was initially purified by distillation through an efficient fractionating column then warmed with magnesium turnings and iodine until the color of iodine has disappeared and all the magnesium was converted to magnesium methoxide. Finally it was distilled off and stored over Linde type 4Å molecular sieves until use.

Trifluoro acetic acid, $BF_3.O(Et)_2$ were purchased from E-Merck (India).

Acetone, ethanol and tetrahydrofuran were purified according to the known procedures.[1,2]

$CDCl_3$, CD_3OD, DMSO-d_6 and CD_3CN were obtained from Aldrich Chemicals (U.S.A.).

2.4 Physical methods

The various porphyrins and other compounds synthesized during this study were characterized and investigated using mass (FAB, MALDI-TOF), infrared (IR), electronic absorption and emission, proton nuclear magnetic resonance (^1H and ^1H-^1H COSY NMR) spectroscopies and electrochemical (cyclic- and differential pulse voltammetry) methods. These methods are briefly alluded to below.

The FAB mass spectra were recorded on a JEOL SX 102/DA-6000 mass spectrometer/data system using xenon (6 kV, 10 mA) as the FAB gas. The accelerating voltage was 10 kV and the spectra were recorded at room temperature. m-Nitrobenzyl alcohol (NBA) was used as the matrix. MALDI-TOF spectra were recorded on a Kompact MALDI 4 mass spectrometer (Kratos Analytical Ltd). The instrument was operated in reflection time of flight mode with an accelerating potential of 20 KV and in the negative ion recording mode.

The IR spectra were recorded on a Jasco Model 5300 FT-IR spectrophotometer. The spectra of the solid samples were recorded by dispersing the sample in Nujol mull or as KBr wafers.

The UV-visible spectra were recorded with either a Shimadzu model 160A or a Shimadzu model UV-3101PC UV-vis spectrophotometer. A matched pair of quartz cuvettes were employed (path length = 1 cm each). Concentrations of the various investigated compounds employed for this purpose ranged from ca. 2 x 10^{-6} (porphyrin Soret band) to 5 x 10^{-5} M (porphyrin Q- and other bands / bands due to other compounds).

Steady state fluorescence spectra were recorded either on a Spex Model Fluoromax–3 or a Jasco Model FP 777 spectrofluorometer using a 1 cm quartz cell. Right angle detection technique was employed for these measurements. The excitation and emission slit widths employed were either 3 or 5 nm. Concentration of the samples was adjusted such that the optical densities at the excitation wavelengths were less than ca. 0.2 for emission spectra and ~ 1 x 10^{-7} M (or the optical density at the emission wavelength, $\lambda_{em} < 0.2$) for excitation spectra. A Rhodamine 6G quantum counter was employed for spectral corrections at wavelengths < 600 nm. Fluorescence quantum yields (ϕ) were estimated by integrating the areas under the fluorescence curves using the expression of Austin and Gouterman.[3]

$$\phi_{sample} = \frac{O.D_{standard} \times A_{sample}}{O.D_{sample} \times A_{standard}} \times \phi_{standard} \qquad (2.1)$$

Here, A is area under the emission spectral curve and O.D. is optical density of the compound at the wavelength of exciting light. ϕ_{sample} and $\phi_{standard}$ are the fluorescence quantum yields of the sample under investigation and the standard used, respectively. The fluorescence standards employed were 5,10,15,20-tetraphenylporphyrin (**H_2TPP**) (ϕ_f = 0.13 in CH_2Cl_2), 5,10,15,20-tetraphenylporphyrinatozinc(II) (**ZnTPP**) (ϕ_f = 0.036 in CH_2Cl_2),[4,5] pyrene (ϕ_f = 0.32 in cyclohexane)[6] and 4′-(p-methoxyphenyl)-2,2′:6′,2″–terpyridine (**OMe-ptp**) (ϕ_f = 0.28 in CH_2Cl_2).[7] Refractive index corrections have been employed while estimating the ϕ values in various solvents.[8]

Fluorescence lifetimes were measured by the time correlated single photon counting (TCSPC) method, as described previously.[9,10] Briefly, the samples were

excited by 4 ps laser (Nd/YAG pumped Rhodamine 6G dye laser) pulses at a repletion rate of 800 KHz. The fluorescence was detected at the magic angle (54.7^0) with respect to polarization of the incident beam by a microchannel plate photomultiplier (MCP-PMT, R2809). The count rate employed was typically 2 x 10^4 s^{-1}. The excitation wavelength was fixed at 575 nm and the fluorescence was collected at 650 nm. Deconvolution of the data was carried out by the method of iterative reconvolution of the instrument response function and the assumed decay function. The goodness of fit of the experimental data to the assumed decay function was judged by the standard statistical tests (i. e. random distribution of weighted residuals, the autocorrelation function and the values of reduced χ^2). The error estimates of the lifetimes, obtained by single/bi- exponential fits, were ~ 10%. Although no specific effort has been made here to estimate the error limit on the relative amplitudes (A_i), it is believed that they should be less than 2 - 3%.

^{1}H NMR spectra were recorded with either a Bruker NR-200 AF-FT or a Bruker DRX-400 spectrometer using $CDCl_3$ or CD_3CN or DMSO-d_6 as the solvent. Tetramethylsilane (TMS) was the internal standard employed while recording these samples. The sample concentration was typically ~ 1 - 3 x 10^{-3} M. The proton decoupled ^{31}P NMR spectra were also recorded with the Bruker NR-200 AF-FT or Bruker DRX-400 instrument mentioned above albeit, with an operating frequency of 80.5 MHz and with 85% H_3PO_4 as an external standard.

ESR spectra were run on a JEOL JES-FA200 X-band ESR spectrometer for the copper(II) systems in toluene at 100 ± 3 K. Diphenylpicrylhydrazide (DPPH) was used as the g-marker.

Cyclic- and differential pulse voltammetric experiments were performed on a CH Instruments model CHI 620A electrochemical analyzer. Tetrabutylammonium perchlorate (TBAP) was used as the supporting electrolyte

in all the cases. The working and the auxillary (counter) electrodes employed were always platinum and the reference electrode chosen was a saturated calomel electrode (SCE). A salt bridge containing the same concentration of base electrolyte as that of the bulk solution was positioned between the nitrogen-purged bulk-test-solution and the reference electrode to reduce the effect due to liquid junction potentials. Fc^+/Fc (Fc = ferrocene) couple was used to calibrate the redox potential values and it could be reversibly oxidized under these experimental conditions.

2.5 NMR titrations

A solution of a given metal ion was titrated against a given porphyrin (3 – 4.5 x 10^{-3} M) in CD_3CN or DMSO-d_6. The [porphyrin]:[metal] ratio was varied between 1:0 to 1:10. Initial concentration of the porphyrin was contained in all the ligand solutions to minimize the dilution effect.

2.6 Absorption and Fluorescence titrations

Absorption titration of a given porphyrin with a given metal ion was carried out in the following way. CH_3CN or DMSO solution containing the constant concentration of porphyrin was taken in a cuvette and titrated with increasing volume of a concentrated solution of the metal ion. The ligand solutions also contained the porphyrin at its initial concentration so as to maintain the porphyrin concentration constant throughout the titration. The binding constants were calculated using below eqn. 2.2.[11]

$$\Delta A / b = (S_t K \Delta\varepsilon [L]) / (1 + K [L]) \qquad (2.2),$$

where, ΔA refers to the change in absorbance from initial value at the required wavelength, b is cuvette path length (in cm), S_t is total concentration of porphyrin, K is the apparent binding constant, $\Delta\varepsilon$ is change in extinction coefficient between free and bound porphyrin and [L] is concentration of the titrating metal ion.

In an analogous manner, steady state fluorescence titrations were carried out by exciting the solutions at constant concentration of porphyrin with metal ions. The excitation wavelength (λ_{ex}) was typically 566/300 nm and the intensities were monitored at the emission maximum (λ_{em}) in each case. The binding constants (K) were calculated by below shown eqn. 2.3.[12]

$$F/F_0 = (1 + (k_{11}/k_s)K[L])/(1 + K[L]) \qquad (2.3),$$

where F_0 is the initial fluorescence intensity and F, the fluorescence intensity after each metal ion addition. Here, k_{11} is proportionality constant of the bound complex, k_s is the the proportionality constant for porphyrin and K is the binding constant.

2.7 X-ray crystallography

The X-ray intensity data were measured at 100(2) K on a Bruker SMART APEX CCD area detector system equipped with a graphite monochromator and a Mo Kα fine-focus sealed tube (λ = 0.71073Å) operated at 1500 W power (50 kV, 30 mA). The detector was placed at a distance of 4.995 cm from the crystal. Data were corrected for absorption effects using the multi-scan technique (SADABS). XTAL 3.4 version was employed for the data reduction. The solution and refinement for the data were obtained using SHELXL-97[13, 14] program.

2.8 General considerations

Error estimation of the data, reconstruction of various spectra, calculations of rate constants, various regression analysis etc., that appear throughout this dissertation, have been carried out on an IBM compatible PC Pentium IV computer using the available in-house software/Origin 6.0 software package.

At all times, care was taken to avoid the entry of direct, ambient light into the samples in the spectroscopic and electrochemical experiments. Unless otherwise specified, all experiments were carried out at the an ambient temperature (ca. 293 ± 3 K).

All hazardous chemicals were handled with appropriate precaution. Protective gloves, goggles, and safety mask were employed to minimize exposure to obnoxious chemicals, ultraviolet light etc.

The following are the standard error limits involved in various measurements (unless otherwise stated):

λ_{max}	± 1 nm
ε	± 10%
λ_{em}	± 2 nm
ϕ	± 10%
τ	± 10%
$E_{1/2}$	± 0.1 V
δ	± 0.01 ppm
J	± 1 Hz

2.9 Summary

This Chapter presents a brief account of various solvents and chemicals used in this study. A description of the spectroscopic and other physical methods employed during this study is also given.

2.10 References

1. *Vogel's Text Book of Practical Organic Chemistry* (Revised by Furniss, B. S.; Hannaford, A. J.; Smith, P. W. G.; Tatchell, A. R.), 5th ed.; Longmann (ELBS): Essex (U.K.), **1991**.
2. Perrin, D. D.; Armarego, W. L. F.; Perrin, D. R. *Purification of Laboratory Chemicals*, Pergamon: Oxford, **1980**.
3. Austin, E.; Gouterman, M. *Bioinorg. Chem.* **1978**, *9*, 281.
4. Quimby, D. J.; Longo, F. R. *J. Am. Chem. Soc.* **1975**, *97*, 5111.
5. Harriman, A.; Davila, J. *Tetrahedron* **1989**, *45*, 4737.
6. Berlman, I. B. In *Handbook of Fluorescence Spectra of Aromatic Molecules*; Academic press: New York, **1971**.
7. Mutai, T.; Cheon, J.-D.; Arita, S.; Araki, K. *J. Chem. Soc., Perkin Trans. 2* **2001**, 1045.
8. Lackowicz, J. R. *Principles of Fluorescence Spectroscopy*; Plenum press: New York, **1983**.
9. Jayanthi, S. S.; Ramamurthy, P. *Phys. Chem. Chem. Phys.* **1999**, 4751.
10. Bortolus, P.; Monti, S. *J. Phys. Chem.* **1979**, *83*, 648.
11. Connors, K. A. *Binding constants:* John Wiley and Sons: New York, **1987**, p. 141.
12. Connors, K. A. *Binding constants:* John Wiley and Sons: New York, **1987**, p. 340.

13. Sheldrick, G. M. *SHELXS97 - Program for Crystal Structure Solution*; University of Gottingen, **1997**.

14. Sheldrick, G. M. *SHELXL97 - Program for Crystal Structure Refinement*; University of Gottingen, **1997**.

CHAPTER 3

Aluminium(III) porphyrin based dimers and trimers: Synthesis, spectroscopy and photochemistry

3.1 Introduction

Currently, a great variety of molecular arrays based on metalloporphyrin species are being investigated in relation to their utility in research areas such as biomimetic photosynthesis, molecular electronics/photonics, molecular catalysis etc.[1-33] In contrast, less attention seems to have been paid towards analogous species based on the main-group/metalloid ion containing porphyrins. Only phosphorus(V) (P(V)), tin (IV) (Sn(IV)), antimony(V) (Sb(V)) and gallium (III) (Ga(III)) porphyrin based 'axial-bonding' type cyclic/noncyclic oligomers have been reported so far, with the majority of them having been constructed by utilizing the oxophilicity of the central metalloid ion.[34-49] Aluminium(III) (Al(III)) ion is also oxophilic[50,51] but, to the best of our knowledge, functionally-active Al(III) porphyrin based molecular arrays have never been synthesized. On the other hand, monomeric Al(III) porphyrins are known to possess rich redox and photochemical activities and, in addition, have received attention as catalysts for various organic transformations.[52-56] We sought to harness the well-known strength of Al-O bond and the well-defined redox and photochemical properties of Al(III) porphyrins to build functionally active molecular arrays. Results of our efforts in this direction are discussed in this Chapter which reports the synthesis, characterization and photochemical properties of three dimeric (**H_2-Al**, **Cu-Al** and **Zn-Al**) and three trimeric (**H_2-Al_2**, **Cu-Al_2** and **Zn-Al_2**) 'axial-bonding' type systems based on the Al(III) porphyrin scaffold, Schemes 3.1 & 3.2.

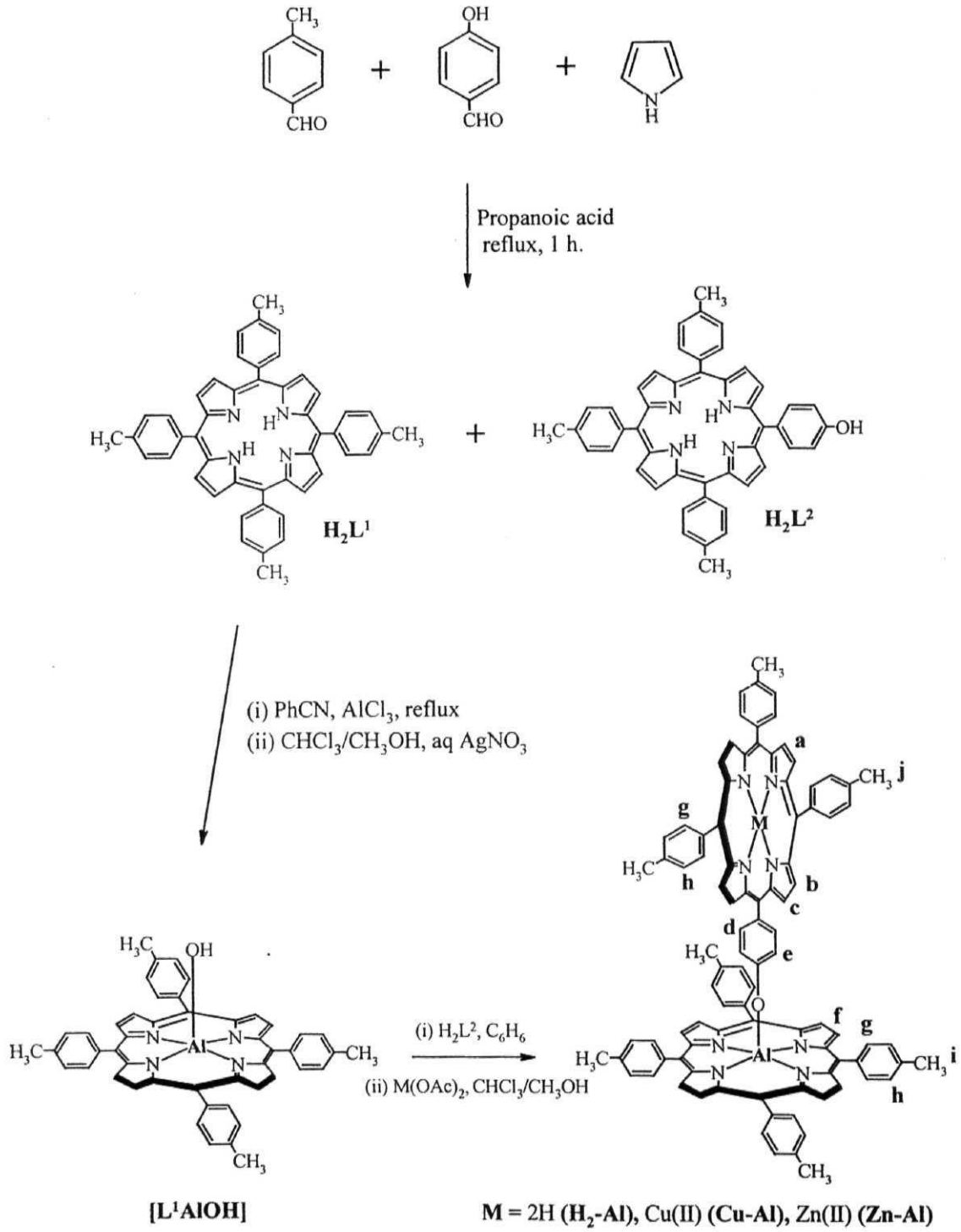

Scheme 3.1 Synthesis of 'axial-bonding' type aluminium(III) dimer.

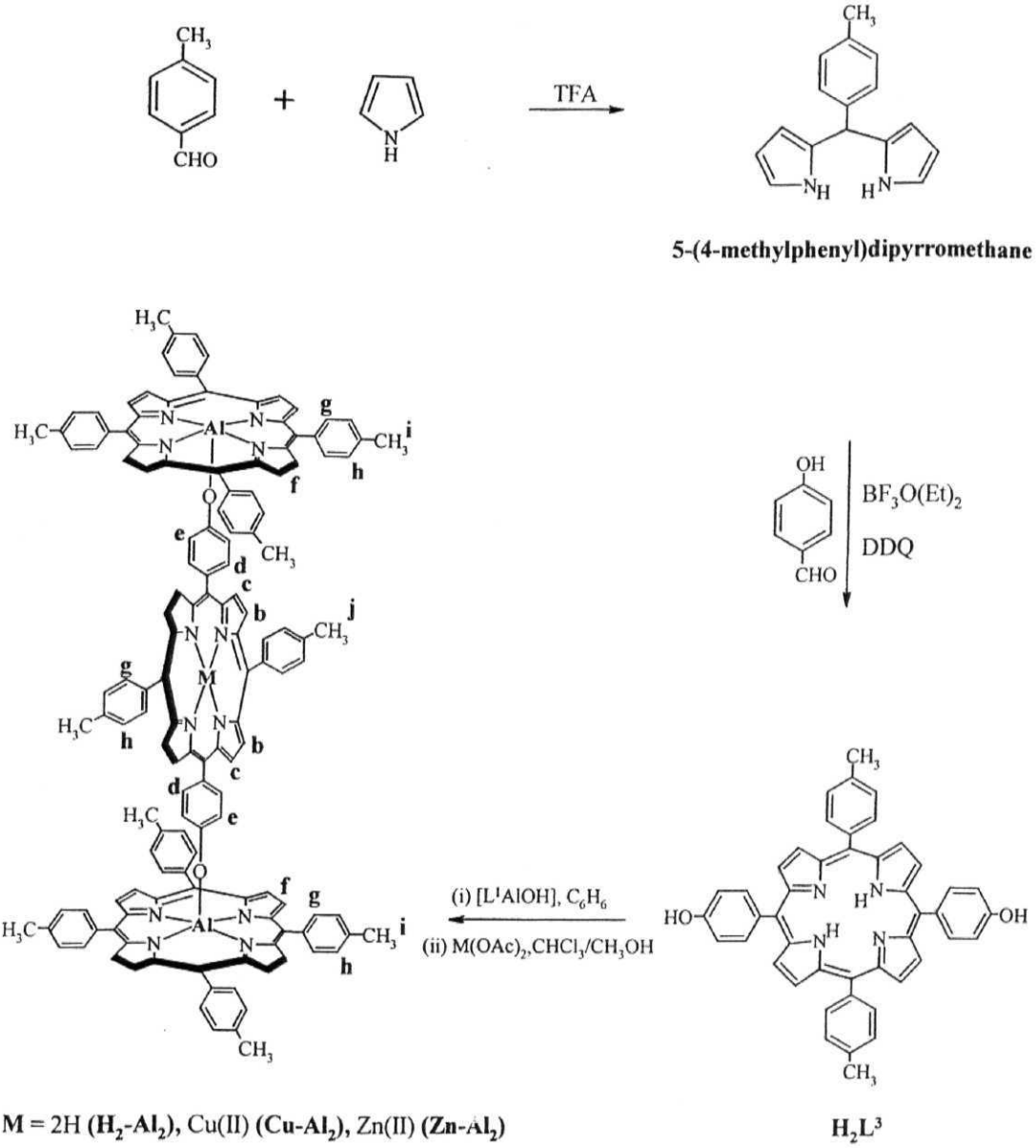

Scheme 3.2 Synthesis of 'axial-bonding' type aluminium(III) trimer.

3.2 Experimental details

5,10,15,20-tetraphenylporphyrin (**H_2TPP**) and 5,10,15,20-tetraphenyl porphyrinatocopper(II)/zinc(II) **(CuTPP/ZnTPP)**, reference compounds employed during this investigation, was synthesized by reported procedures.[57,58]

3.2.1 Synthesis of 5,10,15,20-tetra(4-methylphenyl)porphyrin [H_2L^1] and 5-(4-hydroxyphenyl)-10,15,20-tri(4-methylphenyl)porphyrin [H_2L^2] [59,60]

These compounds were prepared according to reported procedures. 6.1 g (50 mmol) of 4-hydroxybenzaldehyde in 350 ml of propanoic acid was stirred at 120°C for 30 min. To the resulting solution, 12 g (100 mmol) of 4-methylbenzaldehyde followed by 10.5 g (157 mmol) of pyrrole were added. The mixture was refluxed for 45 min., left overnight at 10°C and filtered. The black-violet residue was washed several times with hot water, followed by methanol and purified by chromatography on basic alumina column. Elution with chloroform gave 5,10,15,20-tetra(4-methylphenyl)porphyrin (H_2L^1). Elution with chloroform-methanol (95:5, v/v) gave the product H_2L^2. Overall yield of H_2L^1+H_2L^2 = 9%, out of which 6% is that due to H_2L^2.

3.2.2 Synthesis of 5,10,15,20-tetra(4-methylphenyl)porphyrinatocopper(II)/ zinc(II) [CuL^1/ZnL^1]

CuL^1 and ZnL^1 were prepared by metallating H_2L^1 with the corresponding metal(II) acetates by the standard methods.[58] Typically, 100 mg (0.15 mmol) of H_2L^1 and ~100 mg of either copper(II) acetate or zinc(II) acetate were stirred in $CHCl_3/CH_3OH$ mixture for 1 h. The solvents were evaporated and the residue was washed with water and dried. Purification by column chromatography (silica, 100-200 mesh) furnished the pure product in each case. Yields: CuL^1 = 98 mg (0.13 mmol, 90%) and ZnL^1 = 100 mg (0.14 mmol, 95%).

3.2.3 Synthesis of 5-(4-methylphenyl)dipyrromethane [61]

A solution of 4-methylbenzaldehyde (500 mg, 4.15 mmol) and pyrrole (2.8 ml, 40 mmol) was degassed by bubbling nitrogen for 10 min. Trifluoroacetic acid (TFA) (0.08 ml, 0.1 mmol) was then added to this deaerated solution and it

was stirred for 15 min. at room temperature, at which point no starting aldehyde was seen to be present (TLC analysis). The mixture was diluted with CH_2Cl_2 (50 ml), washed with 0.1 M aqueous NaOH and then with water and finally, dried over anhydrous Na_2SO_4. The unreacted pyrrole was removed by vacuum distillation at room temperature. The resulting yellow amorphous solid was dissolved in minimal quantity of the CH_2Cl_2 and loaded onto a silica gel column. Elution with hexane-ethylacetate-triethylamine (80:20:1, v/v) gave pure sample of 5-(4-methylphenyl)dipyrromethane. Yield = 750 mg (3.17 mmol, 76%).

3.2.4 Synthesis of 5,15-bis(4-hydroxyphenyl)-10,20-bis(4-methylphenyl) porphyrin [H_2L^3]

This compound was synthesized according to a reported procedure.[62] A solution containing 4-hydroxybenzaldehyde (240 mg, 1.96 mmol) and 5-(4-methylphenyl)dipyrromethane (510 mg, 2.16 mmol) in 250 ml of $CHCl_3$ was purged with nitrogen for 10 min. and then a catalytic amount of $BF_3.O(Et)_2$ was added. The resulting solution was stirred for 1 h. at room temperature and 2,3-dichloro-5,6-dicyano-1,4-benzoquinone (DDQ) (1.02 g, 4.5 mmol) was added. The mixture was stirred at room temperature for an additional h. and then the solvent was evaporated. The crude product was loaded onto a silica gel column. Elution with $CHCl_3$ - CH_3OH (98:2, v/v) gave pure sample of **H_2L^3**. Yield = 200 mg (0.30 mmol, 13%).

3.2.5 Synthesis of 5,10,15,20-tetra(4-methylphenyl)porphyrinatohydroxide aluminium(III) [L^1AlOH] [63,64]

H_2L^1 (500 mg, 0.74 mmol) was vigorously refluxed for 1-2 h. with anhydrous aluminium chloride (500 mg, 3.76 mmol) in dry benzonitrile (80 ml). The reflux was continued until no further change of the absorption spectrum was

detected. If the metal insertion was incomplete, the mixture was refluxed again addition of some anhydrous aluminium chloride. The mixture was allowed to cool than filtered and excess hexane was added to the filtrate for completion of precipitation. A trace of methanol facilitates precipitation of **[L^1AlCl]** from oily solution, which often appeared upon addition of hexane. The precipitate was collected by filtration, washed with hexane, and then dissolved in methanol (30 – 40 ml). After filtration of the methanol solution, 3 M HCl was added for precipitation of the complex. The precipitate were collected on a filter, washed with 3 M HCl, dissolved in a smallest amount of acetone, and then precipitated by the addition of hexane. Reddish purple crystals thus obtained were of **[L^1AlCl]**.

The above chloride complex was converted into the corresponding hydroxide complex by shaking the mixture of chloroform and methanol solution of **[L^1AlCl]** with aqueous solution of $AgNO_3$. After removal of aqueous phase the residue was dried and chromatographed on basic alumina. Elution with 2:1 mixture of benzene and tetrahydrofuran gave the desired hydroxo-compound, **[L^1AlOH]**. Yield = 450 mg (0.63 mmol, 85%).

3.2.6 Synthesis of 'free base porphyrin-aluminium(III) porphyrin' dimer [H_2-Al]

A solution containing 100 mg (0.14 mmol) of **[L^1AlOH]** and 280 mg (0.42 mmol) of **H_2L^2** in 30 ml of dry C_6H_6 was refluxed under the nitrogen atmosphere for 12 h. The solvent was removed under vacuum and the crude product was chromatographed on alumina (neutral, activity 1). Elution with $CHCl_3$-hexane (60:40, v/v) separated the desired (aryloxo) aluminium(III) derivative as a purple-coloured band. The solvents were removed under reduced pressure and the resulting solid was precipitated twice from CH_2Cl_2-hexane to give the pure product. Yield = 110 mg (0.081 mmol, 62%).

3.2.7 Synthesis of 'metallo porphyrin-aluminium(III) porphyrin' dimer [Cu/Zn-Al]

Dimers **Cu-Al** and **Zn-Al** were prepared by metallating **H_2-Al** with the corresponding metal(II) acetates by standard methods.[58] Typically, 100 mg (0.07 mmol) of **H_2-Al** and ~100 mg of either copper(II) acetate or zinc(II) acetate were stirred in $CHCl_3/CH_3OH$ mixture for 0.5 – 1 h. The solvents were evaporated and the residue was washed with water and dried. Purification by column chromatography ($CHCl_3$; alumina, activity 1) furnished the pure product in each case. Yields ranged typically from 70 to 80%.

3.2.8 Synthesis of 'free base porphyrin-(aluminium(III) porphyrin)$_2$' trimer [H_2-Al_2]

This trimer was prepared by refluxing a dry C_6H_6 solution (50 ml) containing 100 mg (0.14 mmol) of **H_2L^3** and 570 mg (0.80 mmol) of **[L^1AlOH]** under nitrogen atmosphere for 12 h. The work-up of the reaction mixture as described above for **H_2-Al** furnished 190 mg (0.10 mmol, 65%) yield of the trimer in pure form.

3.2.9 Synthesis of 'metallo porphyrin-(aluminium(III) porphyrin)$_2$' trimer [Cu/Zn-Al_2]

Trimers **Cu-Al_2** and **Zn-Al_2** were prepared by metallating **H_2-Al_2** with the corresponding metal(II) acetates as described above for **Cu-Al** and **Zn-Al**. Yields ranged typically from 70 to 80%.

3.3 Results and discussion

The well-known oxophilicity of aluminium(III) ion and the well-defined redox and photochemical properties of aluminium(III) porphyrins have been

exploited to synthesize functionally-active, 'axial-bonding' type free base-aluminium(III) porphyrin dimer (**H_2-Al**) and free base-[aluminium(III) porphyrin]$_2$ trimer (**H_2-Al_2**) as well as the corresponding copper(II) (**Cu-Al, Cu-Al_2**) and zinc(II) (**Zn-Al, Zn-Al_2**) derivatives. Details of spectroscopic, electrochemical and fluorescence properties of these dimeric and trimeric species are described below. Finally, a comparison is made between the presently synthesized aluminium(III) porphyrin based arrays and the previously reported analogous arrays based on tin(IV), germanium(IV) and phosphorus(V) porphyrins with regard to their architectural features, spectroscopic properties and photochemical activities.[65,66]

3.3.1 Design and Synthesis

Relying largely on oxophilicity of the Al(III) ion, synthesis of **H_2-Al** and **H_2-Al_2** and also their Cu(II) and Zn(II) derivatives has been accomplished here, in good-to-moderate yields, following a step-wise protocol that we had adopted earlier for the synthesis P(V), Sn(IV) and Ge(IV) porphyrin trimers.[65,66] There, however, exist important differences between these old and new arrays with regard to their design and architectural features. These are: (i) Reaction of the **[L^1AlOH]** with excess **H_2L^2** provides an easy access to a dimeric porphyrin, and this is not the case with the P(V), Sn(IV) and Ge(IV) porphyrins. Having been endowed with two axial hydroxy/chloro groups, these latter metalloid porphyrins reacted with excess **H_2L^2** invariably yielding the trimeric species. (ii) On the other hand, synthesis of trimer **H_2-Al_2** has been achieved here by the reaction of **[L^1AlOH]** with the meso trans-dihydroxy porphyrin **H_2L^3**. Thus, trimers derived from the Al(III) porphyrin contain two metalloid porphyrins, whereas the other trimers posses only one metalloid porphyrin in their respective architectures. (iii) Consequently, the gross topological features of the trimeric species derived from

the Al(III) porphyrin are also quite different from that derived from the P(V)/Sn(IV)/Ge(IV) porphyrin species, as illustrated in Fig. 3.1.

The above considerations permit us to probe the role of structural features on the spectroscopic properties and photochemical functions of the Al(III) porphyrin based arrays on one hand, and the P(V), Sn(IV) and Ge(IV) porphyrin based arrays on the other. In addition, the availability of both **H_2-Al** and **H_2-Al_2** (and also the corresponding copper(II) and zinc(II) derivatives) provides an opportunity to compare and contrast properties of the dimeric and trimeric porphyrins that belong to the same 'class'. We have attempted to address these issues while presenting the spectroscopic, redox and photochemical data of these new arrays.

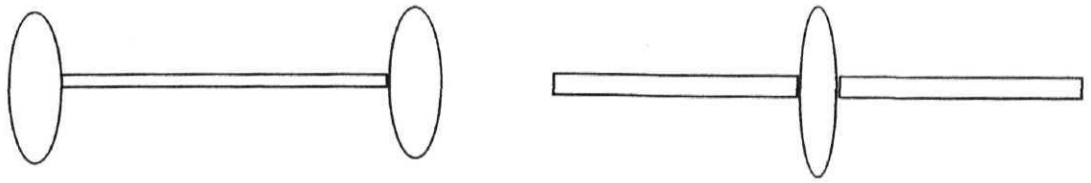

(a) (b)

Fig. 3.1 Topological features of the trimeric species derived from (a) Al(III) porphyrin and (b) P(V)/Sn(IV)/Ge(IV) porphyrin.

3.3.2 Ground state properties

These dimeric and trimeric species have been fully characterized by the mass (MALDI), UV-visible, proton nuclear magnetic resonance (1D and ^1H-^1H COSY), electron spin resonance spectroscopies and also by the cyclic and differential pulse voltammetric methods.

MALDI mass spectra for **H_2-Al**: $(M+H)^+ = 1368$, $(M- C_{47}H_{35}N_4O)^+ = 696$ and **H_2-Al_2**: $(M)^+ = 2064$, $(M- C_{48}H_{36}N_4Al)^+ = 1369$, $(C_{48}H_{36}N_4Al)^+ = 696$. The

mass spectrum of both **H_2-Al** and **H_2-Al_2** showed a low intensity peak ascribable to the parent M^+ ion in each case. However, the peaks due to those fragments obtained upon elimination of the axial free-base porphyrin/s were found to be intense as is the case with the axial-bonding type, penta- and hexa-coordinated metalloid porphyrins previously investigated by several workers including us.[65-70]

The UV-visible data of the new dimers, trimers and those of the corresponding monomeric species **H_2L^1**, **CuL^1**, **ZnL^1**, **H_2L^2**, **H_2L^3** and **[L^1AlOH]** are summarized in Table 3.1. Representative spectra of free-base containing dimer **H_2-Al** and trimer **H_2-Al_2** are illustrated in Fig. 3.2. Dilute solutions containing 1:1 or 1:2 molar equivalents of **H_2L^2/[L^1AlOH]** or **H_2L^3/[L^1AlOH]** generate UV-visible spectra that are close to the sum of the individual spectra in each case and compare very favourably to the spectra of **H_2-Al** or **H_2-Al_2**, with difference of very minor shifts in the wavelengths of maximum absorption (λ_{max}) values. It was

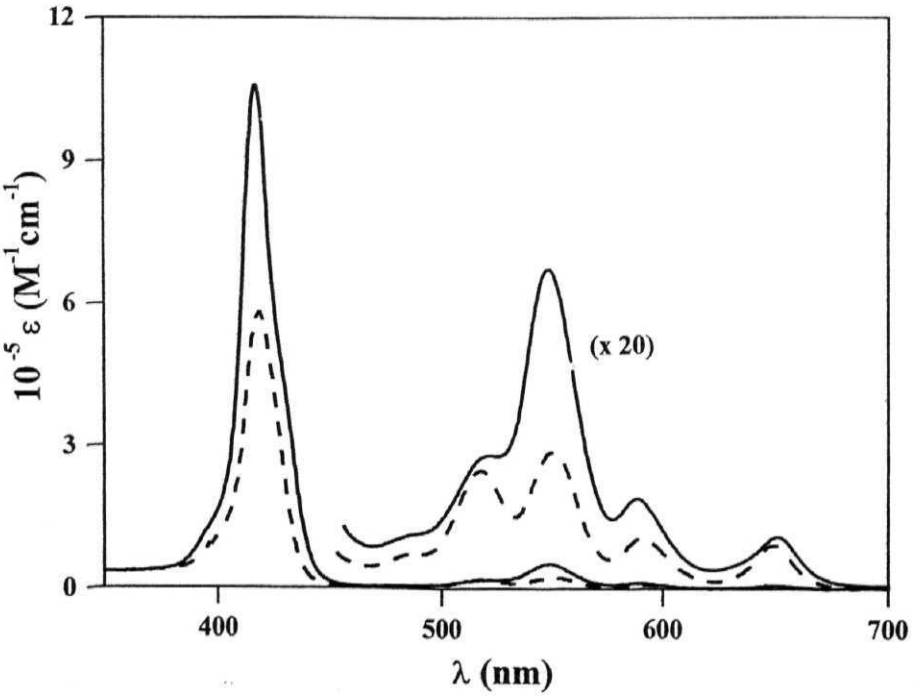

Fig. 3.2 UV-visible spectra of **H_2-Al** (-------) and **H_2-Al_2** (——) in CH_2Cl_2.

noticed, however, that the corresponding molar extinction coefficient values (ε) of the trimeric species are invariably higher than those of the dimers, as illustrated in Fig. 3.2 for **H_2-Al** and **H_2-Al_2**. Analogous results have been obtained for dimers **Cu-Al** and **Zn-Al** and trimers **Cu-Al_2** and **Zn-Al_2**.

Table 3.1 UV-visible data of the dimers, trimers and their constituent monomeric porphyrins [a]

Compd.	λ_{max}, nm (log ε)	
	B-band	**Q-bands**
H_2L^1	419 (5.58)	516 (3.95), 552 (3.72), 592 (3.47), 648 (3.44)
H_2L^2	420 (5.57)	516 (4.04), 552 (3.89), 592 (3.63), 648 (3.59)
H_2L^3	420 (5.48)	517 (3.83), 552 (3.65), 592 (3.36), 648 (3.34)
[L^1Al OH]	418 (5.62)	548 (4.09), 587 (3.44)
CuL^1	416 (5.72)	539 (4.29)
ZnL^1	420 (5.48)	548 (4.38), 587 (3.75)
H_2-Al	419 (5.76)	517 (4.09), 551 (4.16), 591 (3.73), 649 (3.66)
Cu-Al	417 (5.93)	543 (4.75), 580 (4.01)
Zn-Al	419 (5.58)	549 (4.30), 600 (3.88)
H_2-Al_2	417 (6.28)	522 (4.57), 549 (4.97), 588 (4.41), 652 (4.03)
Cu-Al_2	417 (5.75)	549 (4.51), 600 (4.09)
Zn-Al_2	417 (5.72)	548 (4.34), 588 (3.70)

(a) Spectra were measured in CH_2Cl_2. Error limits: λ_{max}, ± 1 nm, log ε, ± 10%

All of the above features seen in the UV-visible spectra of these arrays, while establishing, to a certain extent, their structural integrities, reflect the lack of any exciton coupling interaction between the individual porphyrin units.[71]

Exciton coupling is known to occur when there is complete delocalization of the excitation over the entire super-molecule and excitation of any particular component of the molecule is not possible. For example, various types of covalently or non-covalently linked porphyrin dimers (e.g. face-to-face, slipped etc) and aggregates, that are characterized by π-π interaction between the constituent units in them, have been reported to show distinct UV-visible spectra compared to those off the corresponding monomeric analogues.[35,39,72-74] In particular, λ_{max} and ε values of the Q- and more importantly, Soret bands (B-band) of these dimer/aggregates have been reported to be sensitive to the strength of interaction between the monomeric π-planes and geometry of the ensembles. In contrast, UV-visible spectra of the dimeric and trimeric systems reported here are quite similar to those of the monomeric porphyrins forming them. Thus, UV-visible data reveals that there exists minimum interaction between the individual porphyrins in these arrays.

ESR parameters of **Cu-Al** and **Cu-Al$_2$** and those of corresponding reference compound **CuTPP** in toluene (100 ± 3 K) are summarized in Table 3.2. The spectra were analyzed using the spin-hamiltonians reported for the **CuTPP.**[75-77] From the data given in Table 3.2 suggest that the spectral parameters ($g_{\parallel}$, $g_{\perp}$ and $A_{\parallel}^{Cu}$, $A_{\perp}^{Cu}$, $A_{\parallel}^{N}$ and $A_{\perp}^{N}$ (x 10^4 cm^{-1}) of **Cu-Al** and **Cu-Al$_2$** are indistinguishable from those of **CuTPP** values. Invariance of g and A values in comparison with those of **CuTPP** shows that the super molecular perturbation has no significant influence on the ESR parameters.

ESR spectral features of the covalently linked oligomeric porphyrins have been investigated in great details.[78,79] For systems characterized by direct metal-metal (M-M) interaction, it has been observed that the g and A values in the ESR spectra are drastically altered in comparison with the corresponding monomeric reference porphyrins. Invariance of g and A values in comparison with those of

CuTPP in the ESR spectra of the dimer and trimer reported here are suggestive of the absence of any M-M interaction between their constitute subunits. Thus, both the ESR and UV-visible data indicate that there exists minimum interaction between the individual porphyrins in these arrays.

Table 3.2 ESR spectral data in toluene, 100 ± 3 K [a]

Compd.	(x 10^4 cm^{-1})					
	$g_{\|\|}$	$g_{\perp}$	$A_{\|\|}^{Cu}$	$A_{\perp}^{Cu}$	$A_{\|\|}^{N}$	$A_{\perp}^{N}$
CuTPP	2.187	2.032	214	33.2	15.0	16.6
Cu-Al	2.172	2.030	211	33.4	15.7	16.7
Cu-Al_2	2.164	2.037	212	33.8	15.1	16.9

(a) Error limits: g = ± 0.005; A = ± 10%.

Redox potentials of these arrays have been measured in CH_2Cl_2, 0.1 M TBAP and Table 3.3 summarizes the redox potential data along with that of the relevant monomeric analogues. Each array undergoes up to two to three reduction steps and up to three to four oxidation steps in CH_2Cl_2, 0.1 M TBAP. Wave-analysis of the corresponding cyclic voltammetric responses suggested that, in general, the first two oxidation and also the first two reduction steps are reversible (i_{pc}/i_{pa} = 0.9 - 1.0) and diffusion controlled ($i_{pc}/\upsilon^{1/2}$ = constant in the scan rate (υ) range 50 - 500 mV/s) one-electron transfer (ΔE_P = 60 - 70 mV; ΔE_P = 65 ± 3 mV for Fc^+/Fc couple) reactions. The subsequent steps are either quasi-reversible ($E_{pa} - E_{pc}$ = 90 - 200 mV and i_{pc}/i_{pa} = 0.5 - 0.8 in the scan rate of 100 - 500 mV S^{-1}) or totally irreversible.[80]

Analysis of the data given in Table 3.3 reveals that electrochemical redox potentials of the **H_2-Al** and **H_2-Al_2** are in the same range as those of the corresponding monomeric free-base and Al(III) porphyrins. This is not the case for the previously reported covalently or non-covalently linked porphyrin oligomers that are characterized by π-π interaction between the constituent chromophoric units in them. Those oligomers have been reported to show distinct electrochemical properties quite different from those of the corresponding monomeric analogues. In particularly the oxidation and reduction potentials of these oligomers have been reported to be sensitive to the strength of interaction between the monomeric π-planes.[35,39,73,74]

Nonetheless, it is interesting to note that oxidation and reduction potentials of the present arrays are dependent on the metal ion present (or the absent of it) in the cavities of the constituent monomers thus enabling a facile modulation of the ground state properties. As will be shown in the next section, the excited state redox properties of these arrays are also dependent on the type of metal/metalloid ion present in the porphyrin cavities. Finally, energies of the possible charge transfer states (i.e. $E_{CT}(\mathbf{Al^+M^-}) = E_{1/2}^{ox}(\mathbf{Al}) - E_{1/2}^{red}(\mathbf{M})$ and $E_{CT}(\mathbf{Al^-M^+}) = E_{1/2}^{ox}(\mathbf{M}) - E_{1/2}^{red}(\mathbf{Al})$ where M = H_2, Zn(II)) of the photoactive arrays, as evaluated from the redox potentials data are also summarized Table 3.3. These E_{CT} values are useful quantities in analyzing the photochemical data of dimers and trimers, as will be discussed in the next section of this Chapter.

The ^{1}H NMR spectral data of the diamagnetic dimers and trimers along with those of the individual unlinked monomers are summarized in Table 3.4 and the spectra of **H_2-Al** and **H_2-Al_2** are shown in Fig. 3.3. Spectra were analyzed based on the resonance position and integrated intensity data as well as the proton-to-proton connectivity information revealed in the COSY spectra (Fig. 3.4) to arrive at the structure of these arrays.

Table 3.3 Redox potential data of the dimers, trimers and the corresponding monomers in CH_2Cl_2, 0.1 M TBAP [a]

Compd.	Potential ($E_{1/2}$) mV vs SCE		E_{CT} ($Al^+H_2^-$) (eV)	E_{CT} ($H_2^+Al^-$) (eV)
	Oxidation	Reduction		
H_2L^1	1130, 1370	-1030, -1350	-	-
L^1Cu	1193, 1485	-1008, -1500	-	-
L^1Zn	900, 1210	-1375, -1540	-	-
[L^1AlOH]	1076, 1305, 1620	-1010, -1405	-	-
[L^1Al(O-*p*-cre)] [b]	1140, 1250	-1070, -1305	-	-
H_2-Al	1010, 1100, 1310, 1495	-1060, -1425	2.07	2.16
Cu-Al	1080, 1370, 1580	-1197, -1410	-	-
Zn-Al	882, 1070, 1325, 1460	-1220, -1430, -1615	-	-
H_2-Al_2	900, 1060, 1290, 1650	-1130, -1400	2.03	2.19
Cu-Al_2	1165, 1410, 1570	-1235, -1520	-	-
Zn-Al_2	810, 1030, 1315, 1450	-960, -1210, -1505	-	-

(a) Error limits: $E_{1/2}$, ± 15 mV (b) Data on **[L^1Al(O-*p*-Cre)]**, where **O-*p*-Cre** is the axially ligated *p*-cresol group, is given for comparison.

In the ^{1}H NMR spectra of dimer **H_2-Al** (Fig. 3.3A), all the eight pyrrole-β protons **f** of the aluminium(III) porphyrin resonate at 9.10 ppm (s, 8H). On the other hand, pyrrole-β proton signals of the axial free base porphyrin seem to be shifted to the upfield region (compared to those on **H_2L^2**) and also split into a

singlet 8.71 (s, 4H) and a pair of doublets 8.52 (d, 2H) and 8.12 (d, 2H) with J_{HH} = 4.9 Hz. Thus, two pyrrole-β of the protons **b** and two others of the protons **c** (both facing the aluminium(III) porphyrin, see Scheme 3.1), being differently affected by the ring current of the aluminium(III) porphyrin,[81] resonate as two separate doublets. The remaining four pyrrole-β protons **a** on the free base resonate as a singlet. In principle, these protons are also expected to appear as doublet of doublets. However, given their similar magnetic environments, the difference in chemical shift and coupling constants are very small causing overlap that can look like a singlet at the employed operating frequency of the spectrometer. The ^{1}H NMR spectra of trimer **H_2-Al_2** (see Fig. 3.3B), is nearly identical to the **H_2-Al**. Similar splitting pattern and deshielding effects are observed for the protons on the free base axial porphyrin subunits due to the ring current effect of the two central aluminium(III) porphyrin units for this arrays. All the sixteen pyrrole-β protons **f** (see Scheme 3.2) of the aluminium(III) porphyrin resonate at 9.16 ppm (s, 16H). On the other hand, pyrrole-β proton (**b** & **c**) signals of the axial free base porphyrin shifted to the upfield region (compared to those on H_2L^3) and also split into a pair of doublets 8.45 (d, 4H) and 8.05 (d, 4H) with J_{HH} = 4.3 Hz.

In **H_2-Al**, protons *meta* to the 'oxo' group resonate at 6.63 ppm (d, 2H, protons **d**) those ortho to the 'oxo' group appear at 2.76 ppm (d, 2H, protons **e**)(see the proton connectivity pattern in the 2D NMR spectrum of **H_2-Al**, Fig. 3.4). The Δδ values (i.e. δ(**H_2L^2**) – δ(**H_2-Al**)) for these protons are 4.41 and 1.47 ppm, respectively. The corresponding resonances for **H_2-Al_2** are seen to be further shifted upfield (compared to the corresponding protons on **H_2L^3**) and resonate at 6.57 (d, 4H, protons **d**) and 2.75 (d, 4H, protons **e**) ppm with the Δδ values (i.e. δ(**H_2L^3**) – δ(**H_2-Al_2**)) of 4.50 and 1.53 ppm, respectively (Table 3.4). The higher

$\Delta\delta$ values observed for $\mathbf{H_2\text{-}Al_2}$ in comparison with $\mathbf{H_2\text{-}Al}$ can be traced to the unique topology of this trimer (see Fig. 3.1a).

Another consequence of the topological differences between the dimeric and the trimeric species concerns the ^{1}H NMR resonance pattern and extent of shielding observed for the pyrrole-β protons of their free-base components. This result is similar to that reported for the P(V), Sn(IV) and Ge(IV) porphyrin based trimers and can be accounted for by invoking the porphyrin ring current model.

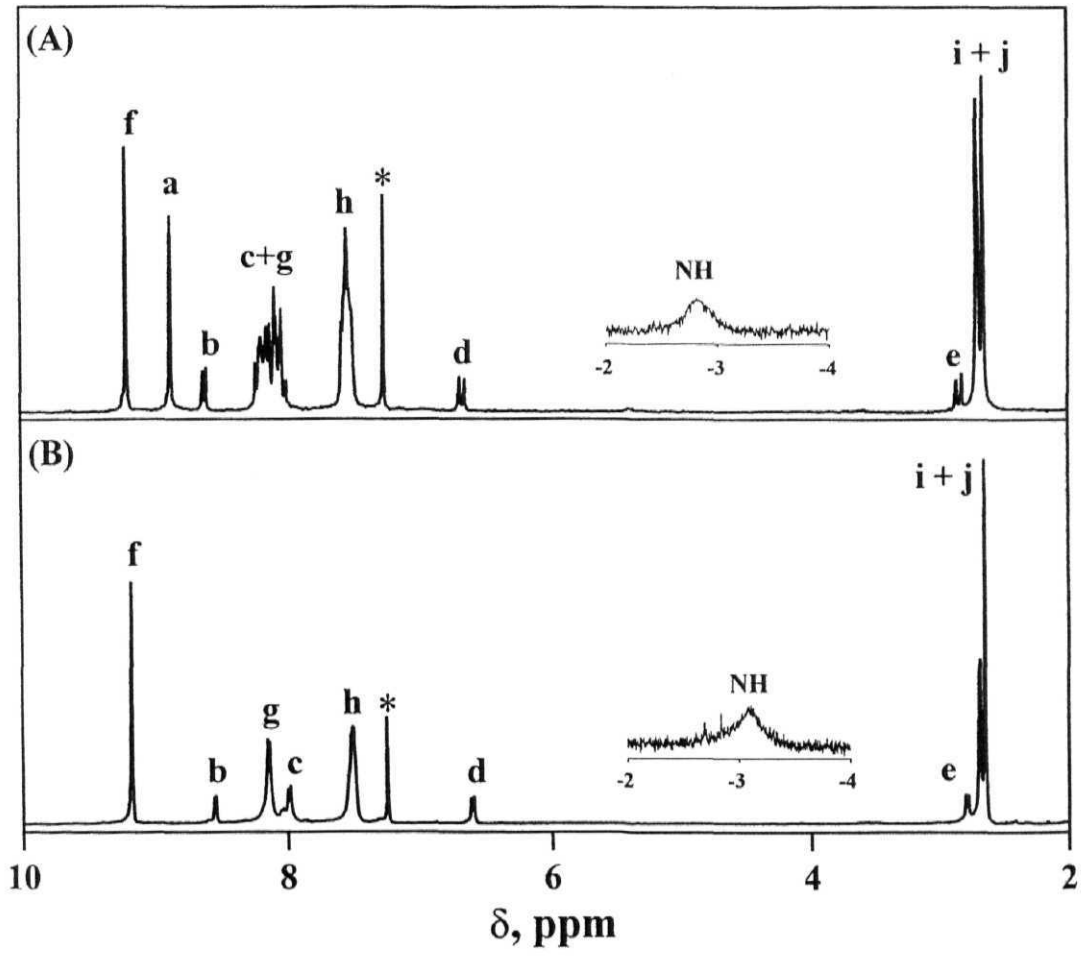

Fig. 3.3 ^{1}H NMR spectrum of (A) $\mathbf{H_2\text{-}Al}$ (200 MHz, 300 K) and (B) $\mathbf{H_2\text{-}Al_2}$ (400 MHz, 300 K) in $CDCl_3$, TMS (* peak is due to solvent).

Table 3.4 ^{1}H NMR data of dimers, trimers and their reference compounds [a]

Compd.	δ, ppm					
	β-pyrrole (Al) (*f*)	β-pyrrole (axial H_2/Zn) [b] (*b, c, a*)	Bridging aryloxo [b] (*d, e*)	-NH [b]	Meso-tolyl (*g, h*)	-CH_3 (*i, j*)
H_2L^2	-	8.86 (s, 8H)	-	-2.76 (s, 2H)	8.11 (d, 6H) 7.56 (d, 6H) J = 7.8 8.06 (d, 2H) 7.18 (d, 2H) J = 8.6 Hz	2.71(s, 9H)
H_2L^3	-	8.86 (s, 8H)	-	-2.75 (s, 2H)	8.10 (m, 8H) 7.55 (d, 4H) J = 7.8 7.21 (d, 4H) J = 8.6 Hz	2.72(s, 6H)
[L^1AlOH]	8.94(s, 8H)	-	-	-	8.01(d, 8H) 7.51(d, 8H) J = 7.8 Hz	2.81(s, 12H)
H_2-Al	9.10 (s, 8H)	8.12 (d, 2H) [0.74] 8.52 (d, 2H) [0.34] J = 4.9 Hz 8.71 (s, 4H) [0.15]	6.63 (d, 2H) [1.47] 2.76 (d, 2H) [4.41] J = 7.7 Hz	-2.86 (s, 2H) [0.10]	8.05 (d, 8H) 7.97 (m, 6H) 7.47 (m, 14H)	2.58 (s, 9H) 2.62 (s, 12H)
Zn-Al	9.11 (s, 8H)	8.31 (d, 2H) [0.59] 8.70 (d, 2H) [0.20] J = 4.7 Hz 8.84 (s, 4H) [0.06]	6.65 (d, 2H) [1.45] 2.84 (d, 2H) [4.34] J = 8.0 Hz	-	8.17 (d, 8H) 8.08 (m, 6H) 7.46 (m, 14H)	2.59 (s, 9H) 2.63 (s, 12H)
H_2-Al_2	9.16 (s, 16H)	8.05 (d, 4H) [0.81] 8.45 (d, 4H) [0.41] J = 4.3 Hz	6.57 (d, 4H) [1.53] 2.75 (d, 4H) [4.50] J = 7.7 Hz	-3.10 (s, 2H) [0.35]	8.03 (d, 16H) 8.00 (m, 4H) 7.50 (m, 20H)	2.65 (s, 6H) 2.69 (s, 24H)
Zn-Al_2	9.17 (s, 16H)	8.30 (d, 4H) [0.60] 8.70 (d, 4H) [0.21] J = 4.9 Hz	6.65 (d, 4H) [1.46] 2.76 (d, 4H) [4.42] J = 7.7 Hz	-	8.25 (d, 16H) 8.16 (m, 4H) 7.53 (m, 20H)	2.66 (s, 6H) 2.70 (s, 24H)

(a) Spectra were run in $CDCl_3$, TMS. Error limits: δ, ± 0.01 ppm, J: ± 1 Hz. (b) Numbers within the square parentheses refer to the Δδ values (i.e. $\delta_{monomer} - \delta_{array}$; see text for details)

The Δδ values for protons **a**, **b** and **c** of **H_2-Al** are 0.15, 0.34, 0.74 ppm in that order. On the other hand, higher Δδ values for protons **b** and **c** (0.41 and 0.81ppm, respectively) are noticed for the trimer **H_2-Al_2**. There is an obvious absence of protons of type **a** in this trimer due to its architectural symmetry; a symmetric resonance pattern (AB) is observed for protons **b** and **c**.

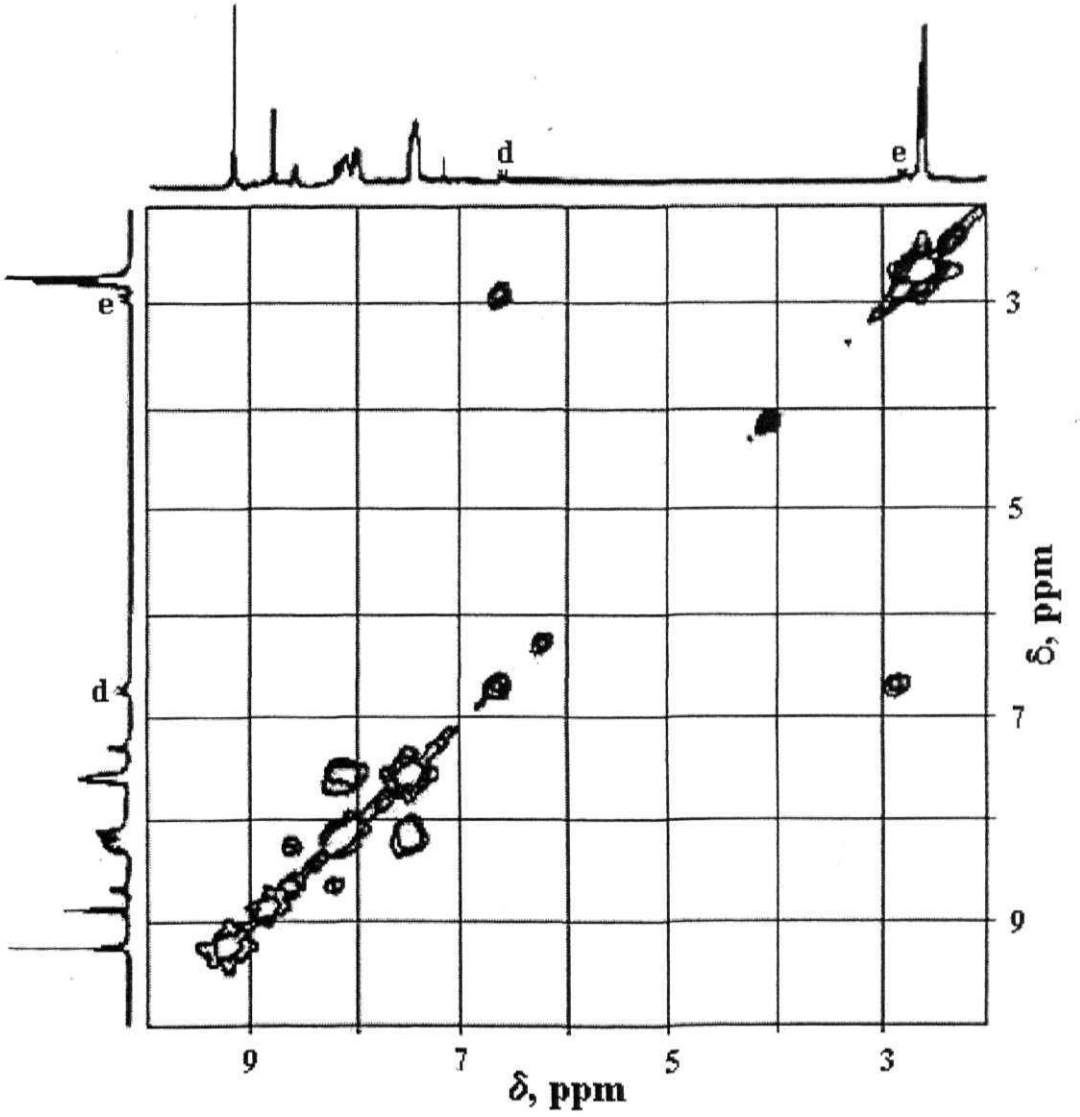

Fig. 3.4 ^{1}H-^{1}H COSY NMR spectrum of dimer (**H_2-Al**) in $CDCl_3$, TMS (300 K, 200 MHz).

As seen from the Fig. 3.3 and data given in Table 3.4, the resonance positions of the protons on the basal Al(III) porphyrin and free base porphyrin components (protons **g, h** and **i**; see Schemes 3.1 & 3.2) of **H_2-Al** and **H_2-Al_2** are more or less similar to those of **[L^1AlOH]** and **H_2L^2/H_2L^3**. **Zn-Al**, **Zn-Al_2** also exhibited similar shielding and splitting patterns in their ^{1}H NMR spectra with the exception that the spectra of metallo arrays were devoid of the inner imino protons resonance, Table. 3.4.

Interestingly, resonance due to the inner imino protons of the axial free-base porphyrin are also shielded and appear at –2.86 (s, 2H) for **H_2-Al** and –3.10 ppm (s, 2H) for **H_2-Al_2**, respectively as compared to the corresponding protons of **H_2L^2** and **H_2L^3** both of which resonate at ~–2.75 ppm. The protons on the aryloxy bridges and the imino protons thus simultaneously experience the shielding effect of the aluminium(III) porphyrin and the deshielding effect of the axial porphyrin. The ortho and meta protons present on the two trans aryloxo groups of **H_2-Al_2** are expected to experience the shielding effect by both the axial Al(III) porphyrins (albeit of differing magnitudes, with the 'proximal' Al(III) porphyrin having stronger effect than the 'distal' one for each set of 'trans' ortho and meta protons). On the other hand, corresponding protons of the dimer (and also those on the P(V), Sn(IV) and Ge(IV) porphyrin based trimers shown in Fig. 3.1b) are influenced by the shielding effect of only one basal porphyrin.[65,66]

Several diagnostic features in the NMR spectra of the arrays have been helpful in elucidating their gross structure. Specifically, resonance positions and splitting patterns observed for the pyrrole-β protons of the axial porphyrin and protons of the aryloxo bridge are characteristic of these arrays. These protons simultaneously experience the shielding effect of the aluminium(III) porphyrin and the deshielding effect of the axial porphyrin suggesting that the orientation between the π-planes is of 'vertical' type and certainly not face-to-face. It is

expected that an additive shielding effect, as reported for the axial protons of the "wheel-and-axial" type porphyrins, should be noticed for any porphyrin ensemble having the 'face-to-face' juxta position of the interacting monomeric subunits.[37-39,82,83] This interpretation is consistent with results of ESR and UV-visible data discussed above.

Overall, the spectroscopic and electrochemical results obtained for these new 'axial-bonding' type systems are reminiscent of those obtained for the several P(V), Sn(IV) and Ge(IV) based porphyrin trimeric, hexameric and nonameric arrays reported by us earlier.[65,66,68] These results are also consistent with the fact that there is minimal perturbation of electronic structures of the individual macrocyclic π-systems in **H_2-Al** and **H_2-Al_2** and their Cu(II) and Zn(II) derivatives. Specifically, there exists no indication of the presence of exciton coupling between the porphyrin rings.

3.3.3 Singlet state properties

Unlike the case with the ground state properties described above, major differences have been noticed between the singlet state activities of the arrays and their corresponding constituent monomers. From the UV-visible data given in Fig. 3.2 and Table 3.1 it is clear that, axial free base porphyrin of **H_2-Al** and **H_2-Al_2** which are exclusively addressable by excitation at ca. 650 nm, their exists no distinct Q-band(s) that is (are) solely ascribable to the individual monomeric units of a given array. As seen in Fig. 3.5, while excitation at 550 nm (where both free base and Al(III) porphyrins absorb; see Table 3.1) results in the appearance of fluorescence bands due to free base (bands II and III) and Al(III) porphyrin (bands I and II) components, that at 650 nm region (where only free base porphyrin absorbs; see Table 3.1) shows a band exclusively due to the free base component at ~ 720 nm (band III) region. Representative spectra of **H_2-Al** and

H_2-Al_2 measured in toluene are illustrated in Fig. 3.5. Analogous spectra were obtained in CH_2Cl_2, CH_3CN and DMF.

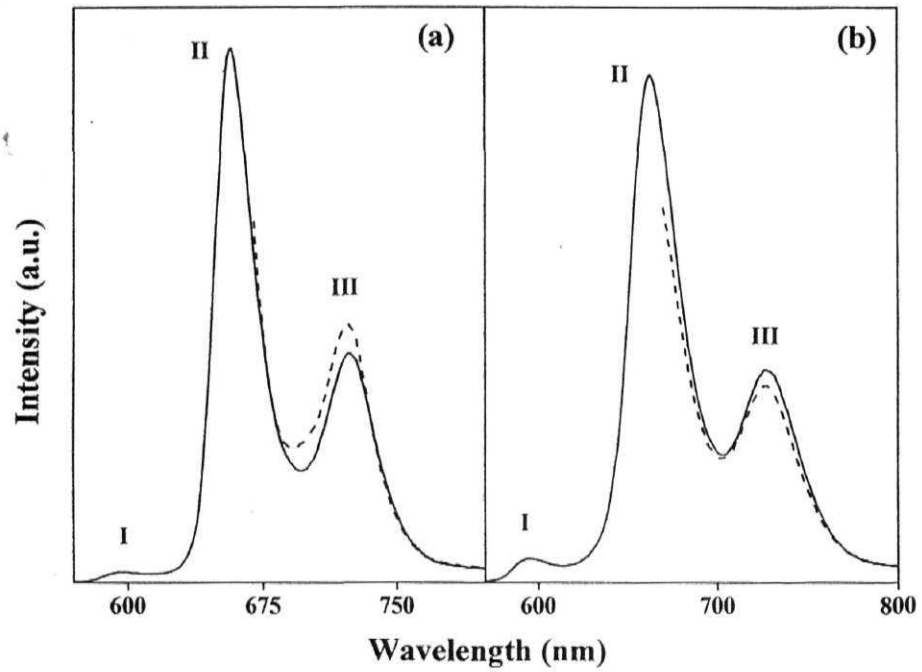

Fig. 3.5 Fluorescence spectra of (a) **H_2-Al** and (b) **H_2-Al_2** in toluene: (——) λ_{ex} = 550 nm and (-------) λ_{ex} = 650 nm.

It was found that while the fluorescence band maxima of Al(III)- and free base components are quite close to those of **H_2L^1** or **[L^1AlOH]** respectively, the fluorescence quantum yields of both the components are quenched in comparison with the reference compounds mentioned above. Arrays containing the Cu(II) porphyrins are found to be either weakly luminescent or totally non-luminescent under these experimental conditions of solvent and excitation wavelengths. Based on the quantum yield data, % quenching efficiencies %Q(Al) (from data obtained upon excitation at 550 nm and emission monitored in the band I region) and %Q(H_2) from data obtained upon excitation at 650 nm and emission monitored in

the band III region) were calculated and are summarized in Table 3.5. The quenching efficiency values (Q) have been evaluated using the quantum yield data, eqn. 3.1

$$Q = (\phi_{ref} - \phi_{array}) / \phi_{ref} \quad (3.1)$$

Where, ϕ_{array} and ϕ_{ref} refers to the quantum yields of a given array and the appropriate reference compound, respectively. **H_2TPP** or **ZnTPP** has been chosen as the common reference compound for studies with excitation into the 550 nm bands. The %Q values thus calculated range between 45-84 (Table 3.5). Inspection of the data presented in Table 3.5 reveals that the %Q(Al) values are invariably higher than the %Q(H_2) values for both **H_2-Al** and **H_2-Al_2** in each solvent. The time-resolved fluorescence data also suggest the same as described below.

While emission decays of **H_2L^1** and the free-base components of **H_2-Al** and **H_2-Al_2** were monitored at 720 nm, those of **[L^1AlOH]** and the Al(III) porphyrin components of **H_2-Al** and **H_2-Al_2** were conveniently monitored at 600 nm. Fluorescence lifetimes (τ/ns) of **H_2L^1**, **[L^1AlOH]**, **H_2-Al** and **H_2-Al_2** measured in toluene and DMF are summarized in Table 3.6. The fluorescence decay curves for **H_2-Al** and **H_2-Al_2** arrays and its reference compounds **[L^1AlOH]** or **H_2L^1** in toluene are shown in Fig. 3.6. As seen from the data given in this Table 3.6, the decays monitored at 600 nm for **H_2-Al** and **H_2-Al_2** showed an additional quenched component each in comparison with the decay of **[L^1AlOH]**. Decays monitored at 720 nm of these arrays also showed a quenched component in them but both the extent of lifetime quenching and % contribution of this component was low. Overall, the time-resolved results corroborate with the steady

Table 3.5 Fluorescence data of dimer, trimer and their monomeric analogues [a]

Compd.	λ_{em}, nm (ϕ, %Q)							
	Toluene λ_{ex}		CH_2Cl_2 λ_{ex}		CH_3CN λ_{ex}		DMF λ_{ex}	
	550 nm	650 nm	550 nm	650 nm	550 nm	650 nm	550 nm	650 nm
H_2L^1	-	721 (0.14)	-	719 (0.11)	-	717 (0.09)	-	718 (0.14)
$[L^1AlOH]$	597, 647 (0.049)	-	601, 647 (0.059)	-	606, 660 (0.11)	-	608, 663 (0.087)	-
H_2-Al	599, 657, 723 (0.008, 84)	721 (0.13, 7)	601, 656, 721 (0.013, 78)	721 (0.10, 9)	607, 655, 720 (0.023, 79)	719 (0.07, 16)	608, 660, 722 (0.031, 65)	721 (0.12, 14)
H_2-Al_2	595, 663, 727 (0.016, 67)	727 (0.11, 21)	599, 658, 725 (0.033, 45)	725 (0.07, 36)	606, 665, 726 (0.060, 45)	726 (0.05, 44)	609, 675, 732 (0.038, 56)	733 (0.09, 35)

(a) Error limits: λ, ± 1 nm; ϕ, ± 10%

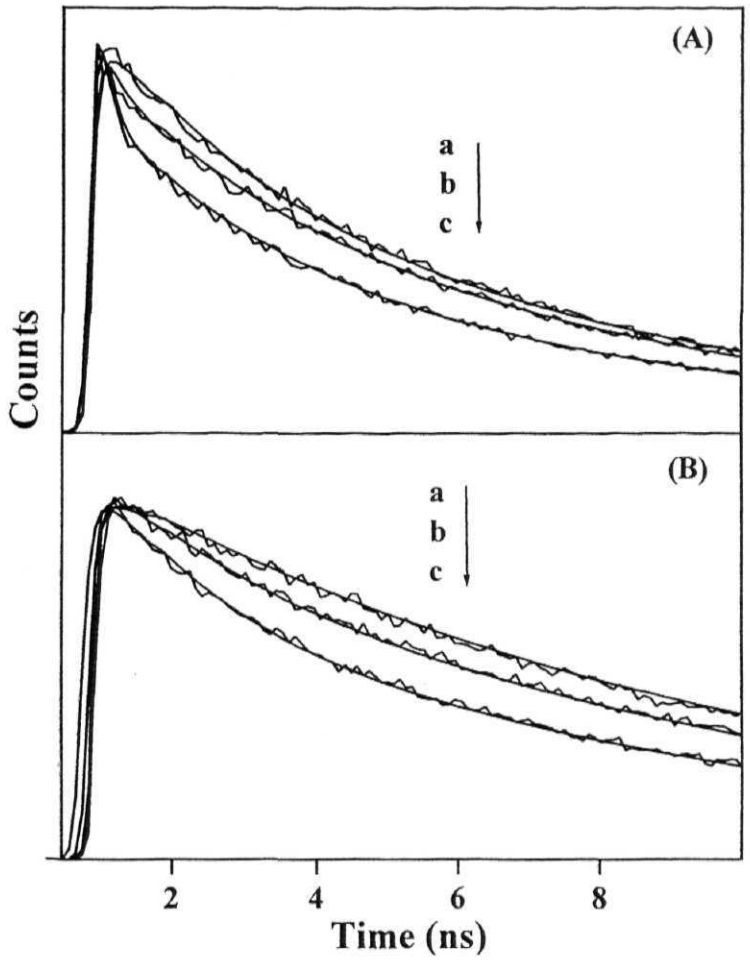

Fig. 3.6 Decay profiles of (A) a: **[L^{1}AlOH]**, b: **H_2-Al_2** and c: **H_2-Al** at λ_{ex} = 575 nm, λ_{em} = 600 nm (B) a: **H_2L^1**, b: **H_2-Al** and c: **H_2-Al_2** at λ_{ex} = 575 nm, λ_{em} = 720 nm in toluene.

state results in that the values of %Q(Al) are higher than the corresponding %Q(H_2).

Various radiative and non-radiative intramolecular processes which include enhanced internal conversion, excitation energy transfer (EET), photoinduced electron transfer (PET) etc. can be conceived to participate in the excited state decay of these hybrid-type, donor-acceptor (D-A) systems. Among

these, an excitation energy transfer from the central porphyrin containing main-group element (**Al**) to the axial free base/zinc(II) porphyrin (**H_2/Zn**) as well as photo induced electron transfer from **H_2/Zn** (ground sate) to the singlet excited state of the central porphyrin (^{1}**Al**) seem to be more probable as revealed by the thermodynamic considerations based on the redox potential (E_{CT}) and singlet state energy ($E_{0\text{-}0}$) data, Fig. 3.7.

Table 3.6 Fluorescence lifetime data of dimer, trimer and their monomeric analogues [a]

Compd.	λ_{em} (nm)	Toluene		DMF	
		τ/ns (%A)	χ^2	τ/ns (%A)	χ^2
H_2L^1	720	9.40 (100)	1.06	10.37 (100)	1.06
[L^1AlOH]	600	6.70 (73), 2.06 (27)	1.11	6.49 (92), 1.33 (8)	1.19
H_2-Al	600	6.80 (35), 2.11 (18), 0.17 (47)	1.06	6.50 (72), 2.07 (6), 0.14 (22)	0.97
	720	9.02 (84), 1.29 (16)	0.98	9.49 (81), 2.45 (19)	1.05
H_2-Al_2	600	6.64 (61), 2.20 (15), 0.26 (24)	1.08	6.34 (84), 1.54 (2), 0.30 (14)	1.02
	720	8.30 (68), 1.45 (32)	1.10	8.79 (53), 5.09 (20), 0.43 (27)	1.07

(a) Error limits: τ, ± 10%. A is a relative amplitude of the decay component and χ^2 values shows the quality of fit.

We analyze, based on the steady state and time resolved fluorescence data, that quenching of the Al(III) porphyrin components in these donor-acceptor (D-A) systems is predominantly due to the electronic energy transfer (EET) from the Al(III) porphyrin to the free-base porphyrin. This EET is a thermodynamically favourable process in both **H_2-Al** and **H_2-Al_2** (singlet state energy (**$E_{0\text{-}0}$**) of Al(III) and free base porphyrins are 2.13 and 1.94 eV, respectively) as is the case with the P(V), Sn(IV) and Ge(IV) porphyrin based arrays investigated by us

earlier.[65,66,68] Indeed, as seen in Fig. 3.5, fluorescence spectra of both **H_2-Al** and **H_2-Al_2** prominently show bands due to the free-base component (i. e. bands II and

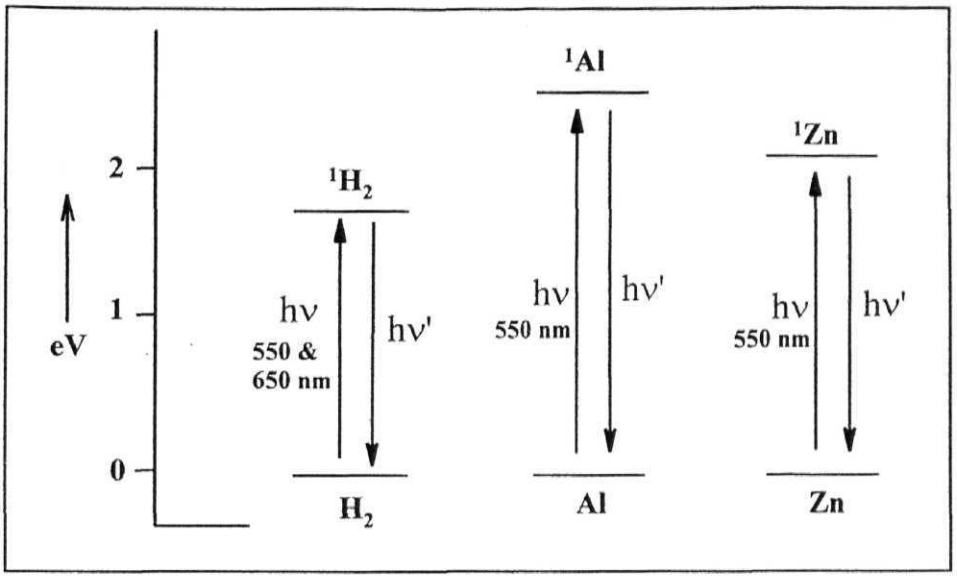

Fig. 3.7 Energy level relationships of aluminium(III) (**Al**), zinc(II) (**Zn**) and free base (**H_2**) porphyrins. Here hν, hν′ (ν > ν′) refers absorption and fluorescence.

III) when excited at 550 nm. In addition, the excitation spectra of **H_2-Al** and **H_2-Al_2** showed bands due to the Al(III) porphyrin when the emission was collected at 720 nm, where the emission is exclusively due to the free-base component of these bichromophoric systems. Overlap of the corrected and normalized excitation spectra with the corresponding absorption spectra revealed that the EET efficiency is 80 ± 7 % and 60 ± 7 % for **H_2-Al** and **H_2-Al_2**, respectively in toluene, Fig. 3.8. These EET efficiencies compare well with the corresponding %Q(Al) values (see Table 3.5). Thus, it appears that the quenching of fluorescence due to the Al(III) porphyrin components of these arrays is almost exclusively due to an EET process.

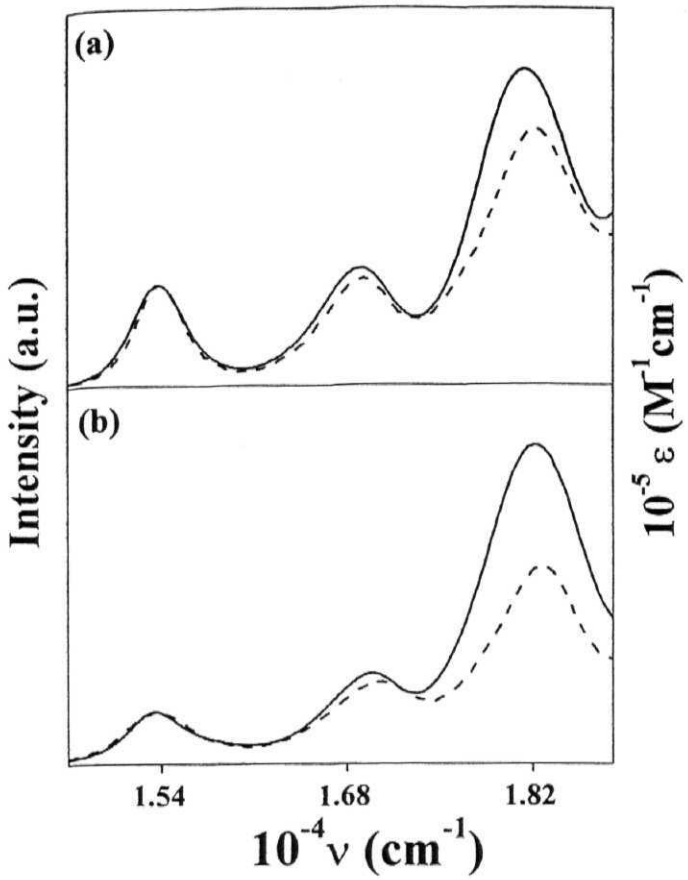

Fig. 3.8 Overlay of the excitation (-------) and absorption (——) spectra of (a) **H_2-Al** and (b) **H_2-Al_2** in toluene (λ_{em} = 720 nm). The excitation spectra were corrected for the instrument response function and were normalized with respect to the absorption spectra between 14727 - 16000 cm^{-1}.

On the other hand, efficiency of the photoinduced electron transfer (PET) from the singlet Al(III) porphyrin to the free base cannot be neglected altogether in high polarity solvents. The free-energy change for this electron transfer process, ($\Delta G(^1\mathbf{Al}\rightarrow\mathbf{H_2})$), eqn. 3.2.

$$\Delta G(^1\mathbf{Al}\rightarrow\mathbf{H_2}) = E_{CT}(\mathbf{Al^+H_2^-})-E_{0\text{-}0}(\mathbf{Al}) \qquad (3.2)$$

The values of $\Delta G(^1\mathbf{Al}\rightarrow\mathbf{H_2})$, as estimated using the $E_{CT}(\mathbf{Al^+H_2^-})$ (Table 3.3) and $E_{0\text{-}0}$ (Al) and the ΔG_{PET} values are weakly exergonic –0.06 and –0.10 eV for **H_2-Al** and **H_2-Al_2**, respectively.

Fluorescence quenching observed upon excitation of axial free base at 650 nm seems primarily due to a PET from singlet excited state of free base porphyrin to ground state of aluminium(III) porphyrin. This is because the energy transfer from the axial free base porphyrin to the aluminium(III) porphyrin is neither thermodynamically feasible nor was it experimentally detected in this study. The PET from $^1\mathbf{H_2}$ to the **Al(III)** has been found to be exoergic for **H_2-Al** and **H_2-Al_2**. The free energy change for this PET, $\Delta G(^1\mathbf{H_2}\rightarrow\mathbf{Al})$, has been estimated using eqn. 3.3

$$\Delta G(^1\mathbf{H_2}\rightarrow\mathbf{Al}) = E_{CT}(^1\mathbf{H_2^+Al^-}) - E_{0\text{-}0}(\mathbf{H_2}) \qquad (3.3)$$

Interestingly, the $\%Q(H_2)$ values listed in Table 3.5 are lower than not only the %Q(Al) values but also the corresponding $\%Q(H_2)$ values observed for the P(V) (93%), Sn(IV) (82%)and Ge(IV) (69%) porphyrin based trimers investigated earlier.[65,66] The free energy changes (ΔG_{PET}) associated with this PET are –0.45, -0.01 and 0.07 eV for P(V), Sn(IV) and Ge(IV) analogues, respectively. The corresponding ΔG_{PET} values in CH_2Cl_2 for **H_2-Al** and **H_2-Al_2** are estimated to be 0.22 and 0.25 eV, respectively. Interestingly, the exoergicity of these PET reactions follow a trend, viz: P(V) >> Sn(IV) > Ge(IV) > Al(III), that is dependent on the electropositivity of the resident metalloid ion in the arrays and is consistent with the magnitudes of the corresponding $\%Q(H_2)$ values. We thus analyze that a PET from the singlet free base porphyrin to the Al(III) porphyrin is weak in both **H_2-Al** and **H_2-Al_2** but can, in principle, explain the low $\%Q(H_2)$ values observed for **H_2-Al** and **H_2-Al_2**. The observed general decrease of the ϕ

values (or the increase in the %Q(H_2) values, see Table 3.5) with increasing polarity of the solvent is consistent with the participation of a charge transfer state in the excited state deactivation of the free base components of these systems.[84] However, an additional pathway for quenching that involves the heavy atom effect due to the presence of Al(III) can not be neglected altogether.[85]

Inspection of the data given in Table 3.5 and 3.6 additionally reveals that, in general, the %Q(Al) (which is due to EET) values are lower and the %Q(H_2) (which is due to PET) values are higher for the trimeric species in comparison with the corresponding values for the dimer. A simplistic analysis indicates that the dimer is a bicomponent D-A system wherein the donor/acceptor ratio is 1:1 for both EET and PET. On the other hand, the trimeric system has two donors (i.e. Al(III) porphyrins) and only one acceptor (i.e. free base porphyrin) for EET and one donor (i.e. free base porphyrin) and two acceptors (i.e. Al(III) porphyrins) for PET. This situation might rationalize the lower %Q(Al) (which is due to EET) and higher %Q(H_2) (which is due to PET) values observed for **H_2-Al_2**.

3.4 Summary

In summary, new 'vertically-linked' dimeric and trimeric species based on the Al(III) porphyrin scaffold have been synthesized and investigated by spectroscopic and electrochemical methods. Their photophysical properties have also been investigated and the results are interpreted in terms of intramolecular electron- and energy transfer mechanisms. Noticeable differences exist between properties of the dimers and trimers. Differences have also been noticed between the properties of the presently investigated trimers and the ones based on the P(V), Sn(IV) and Ge(IV) porphyrins reported by us earlier. These differences seem to arise not only from the differences in the electropositivities of the main

group element ions bound to the porphyrin but also from the different topological features of these 'axial-bonding' type systems.

3.5 References

1. Gust, D.; Moore, T. A. in *The Porphyrin Handbook*; Kadish, K. M.; Smith, K. M.; Guilard, R., Eds.; Academic Press: London, **2000**; vol. 8, p. 153 - 167.
2. Imahori, H. *J. Phys. Chem. B* **2004,** *108,* 6130.
3. Sanders, J. K. M.; Bampos, N.; Clyde-Watson, Z.; Darling, S. L.; Hawley, J. C.; Kim, H.-J.; Mak, C. C.; Webb, S. J. in *The Porphyrin Handbook*; Kadish, K. M.; Smith, K. M.; Guilard, R., Eds.; Academic Press: London, **2000**; vol. 3, p. 1-48.
4. Choi, M.-S.; Yamazaki, T.; Yamazaki, I.; Aida, T. *Angew. Chem., Int. Ed.* **2004**, *43*, 150.
5. Liddell, P. A.; Kodis, G.; de la Garza, L.; Moore, A. L.; Moore, T. A.; Gust, D. *J. Phys. Chem. B* **2004**, *108*, 10256.
6. Sazanovich, I. V.; Kirmaier, C.; Hindin, E.; Yu, L.; Bocian, D. F.; Lindsey, J. S.; Holten, D. *J. Am. Chem. Soc.* **2004**, *126*, 2664.
7. Lensen, M. C.; Dingenen, S. J. Y.; Elemans, J. A. A. W.; Dijkstra, H. P.; Klink, G. P. M. V.; Koten, G. V.; Gerritsen, J. W.; Speller, S.; Nolte, R. J. M.; Rowan, A. E. *Chem. Commun.* **2004**, 762.
8. Peng, X.; Aratani, N.; Takagi, A.; Matsumoto, T.; Kawai, T.; Hwang, I.-W, Ahn, T. K.; Kim, D.; Osuka, A. *J. Am. Chem. Soc.* **2004**, *126*, 4468.
9. Takahashi, R.; Kobuke, Y. *J. Am. Chem. Soc.* **2003**, *125*, 2372.
10. Ikeda, C.; Satake, A.; Kobuke, Y. *Org. Lett.* **2003**, *26*, 4935.
11. Suogu, K.; Sasaki, K.; Kitajima, K.; Iwaki, T.; Kuroda, Y. *J. Am. Chem. Soc.* **2002**, *124*, 1182.

12. Aratani, N.; Osuka, A.; Cho, H. S.; Kim, D. *J. Photochem. Photobiol: C Photochem. Rev.* **2002**, *21*, 1.
13. Choi, M. -S.; Aida, T.; Yamazaki, T.; Yamazaki, I. *Chem. Eur. J.* **2002**, *8*, 2667.
14. Burrell, A. K.; Officer, D. L.; Plieger, P. G.; Reid, D. C. W. *Chem. Rev.* **2001**, *101*, 2751.
15. Yu, L.; Lindsey, J. S. *J. Org. Chem.* **2001**, *66*, 7402.
16. Ambroise, A.; Li, J.; Yu, L.; Lindsey. J. S. *Org. Lett.* **2000**, *2*, 2563.
17. Wojaczynski, J.; Latos-Grazynski, L. *Coord. Chem. Rev.* **2000**, *204*, 113.
18. Imamura, T.; Fukushima, K. *Coord. Chem. Rev.* **2000**, *198*, 133.
19. Karamochi, Y.; Satake, A.; Kobuke, Y. *J. Am. Chem. Soc.* **2004**, *126*, 8668.
20. Yoon, D. H.; Lee, S. B.; Yoo, K.-H.; Kim, J.; Lim, J. K.; Aratani, N.; Tsuda, A.; Osuka, A.; Kim, D. *J. Am. Chem. Soc.* **2003**, *125*, 11062.
21. Aratani, N.; Cho, H. S., Ahn, T. K., Cho, S., Kim, D.; Sumi, H.; Osuka, A. *J. Am. Chem. Soc.* **2003**, *125*, 9668.
22. Nakamura, Y.; Osuka, A. *Chem. Commun.* **2003**, 1096.
23. Kobuke, Y.; Ogawa, K. *Bull. Chem. Soc. Jpn.* **2003**, *76*, 689.
24. Cheng, K. F.; Drain, C. M.; Grohmann, K. *Inorg. Chem.* **2003**, *42*, 2075.
25. Holten, D.; Bocian, D. F.; Lindsey, J. S. *Acc. Chem. Res.* **2002**, *35*, 57.
26. Loewe, R. S.; Lammi, R. K.; Diers, J. R.; Kirmaier, C.; Bocian, D, F.; Holten, D.; Lindsey, J. S. *J. Mater. Chem.*, **2002**, *12*, 1530.
27. Iengo, E.; Zangrando, E.; Minatel, R.; Alessio, E. *J. Am. Chem. Soc.* **2002**, *124*, 1003.
28. Anderson, H. L. *Chem. Commun.* **1999**, 2323.
29. Kieran, A. L.; Bond, A. D.; Belenguer, A. M.; Sanders, J. K. M. *Chem. Commun.* **2003**, 2674.
30. Nakash, M.; Sanders, J. K. M. *J. Org. Chem.* **2000**, *65*, 7266.

31. Nakash, M.; Clyde-Watson, Z.; Feeder, N.; Davies, J. E.; Teat, S. J.; Sanders, J. K. M. *J. Am. Chem. Soc.* **2000**, *122*, 5286.

32. Marty, M.; Clyde-Watson, Z.; Twyman, L. J.; Nakash, M.; Sanders, J. K. M. *Chem. Commun.* **1998**, 2265.

33. Merlau, M. L.; Mejia, M. P.; Nguyen, S. B. T.; Hupp, J. T. *Angew. Chem., Int. Ed.* **2001**, *40*, 4239.

34. Susumu, K.; Kunimoto, K.; Segawa, H.; Shimidzu, T. *J. Photochem. Photobiol. A Chem.* **1995**, *92*, 39.

35. Hirakawa, K.; Segawa, H. *J. Photochem. Photobiol. A Chem.* **1999**, *123*, 67.

36. Susumu, K.; Tanaka, K.; Shimidzu, T.; Takeuchi, Y.; Segawa, H. *J. Chem. Soc. Perkin. Trans. 2* **1999**, 1521.

37. Susumu, K.; Kunimoto, K.; Segawa, H.; Shimidzu, T. *J. Phys. Chem.* **1995**, *99*, 29.

38. Susumu, K.; Segawa, H.; Shimidzu, T. *Chem. Lett* . **1995**, 929.

39. Segawa, H.; Kunimoto, K.; Susumu, K.; Taniguchi, M.; Shimidzu, T. *J. Am. Chem. Soc.* **1994**, *116*, 11193.

40. Arnold, D.; Blok, J. *Coord. Chem. Rev.* **2004**, *248*, 299.

41. Hawley, J. C.; Bampos, N.; Sanders, J. K. M. *Chem. Eur. J.* **2003**, *9*, 5211.

42. Fallon, G. D.; Langford, S. J.; Lee, M. A.-P.; Lygris, E. *Inorg. Chem. Commun.* **2002**, *5*, 715.

43. Fallon, G. D.; Lee, M. A.-P.; Langford, S. J.; Nichols, P. J. *Org. Lett.* **2002**, *4*, 1895.

44. Redmann, J. E.; Feeder, N.; Teat, S. J.; Sanders, J. K. M. *Inorg. Chem.* **2001**, *40*, 2486.

45. Tong, Y.; Hamilton, D. G.; Meillon, J.-C.; Sanders, J. K. M. *Org. Lett.* **1999**, *1*, 1343.

46. Shiragami, T.; Andou, Y.; Hamasuna, Y.; Yamaguchi, F.; Shima, K.; Yasuda, M. *Bull. Chem. Soc. Jpn.* **2002**, *75*, 1577.

47. Andou, Y.; Shiragami, T.; Shima, K.; Yasuda, M. *J. Photochem. Photobiol. A Chem.* **2002**, *147*, 191.

48. Wojaczynski, J.; Latos-Grazynski, L.; Olmstead, M. M.; Balch, A. L. *Inorg. Chem.* **1997**, *36*, 4548.

49. Wojaczynski, J.; Latos-Grazynski, L. *Inorg. Chem.* **1995**, *34*, 1054.

50. Shriver, D. F.; Atkins, P. W.; Langford, C. H. *Inorganic Chemistry*; Oxford University Press: Oxford, **1990**, p. 332.

51. Wada, K.; Mizutani, T.; Kitagawa, S. *J. Org. Chem.* **2003**, *68*, 5123.

52. Aida, T.; Sugimoto, H.; Kuroki, M.; Inoue, S. *J. Phys. Org. Chem.* **1995**, *8*, 249.

53. Komatsu, M.; Aida, T. *J. Am. Chem. Soc.* **1991**, *113*, 8492.

54. Sato, Y.; Arai, T.; Inoue, S. *Chem. Lett.* **1990**, *4*, 551.

55. Konishi, K.; Aida, T.; Inoue, S. *J. Org. Chem.* **1990**, *55*, 816.

56. Konishi, K.; Makita, K.; Aida, T.; Inoue, S. *J. Chem. Soc., Chem. Commun.* **1988**, 643.

57. Fuhrhop, J.-H.; Smith, K. M.; In *Porphyrins and Metalloporphyrins*; Smith, K. M., Ed.; Elsevier: Amsterdam, **1975**; p. 769.

58. Fuhrhop, J.-H.; Smith, K. M. in *Porphyrins and Metalloporphyrins*; Smith, K. M., Ed.; Elsevier: Amsterdam, **1975**; p. 179.

59. Moghadam, G. E.; Ding, L.; Tadj, F.; Meunier, B. *Tetrahedron* **1989**, *45*, 2641.

60. Alder, A. D.; Longo, F. R.; Finarelli, J. D.; Goldmacher, J.; Assour, J.; Korsakoff, L. *J. Org. Chem.* **1967**, *32*, 476.

61. Lindsey, J. S.; Schreiman, I. C.; Hsu, H. C.; Kearney, P. C.; Marguerettaz, A. M. *J. Org. Chem.* **1987**, *52*, 827.

62. Lee, C.-H.; Lindsey, J. S. *Tetrahedron*, **1994**, *50*, 11427.

63. Kaizu, Y.; Misu, N.; Tsuji, K.; Kaneko, Y.; Kobayashi, H. *Bull. Chem. Soc. Jpn.* **1985**, *58*, 103.

64. Harriman, A.; Osborne, A. D. *J. Chem. Soc., Faraday Trans. 1* **1983**, *79*, 765.

65. Rao, T. A.; Maiya, B. G. *Chem. Commun.* **1995**, 939.

66. Giribabu, L.; Rao, T. A.; Maiya, B G. *Inorg. Chem.* **1999**, *38*, 4971.

67. Guilard, R.; Ratti, C.; Barbe, J.-M.; Dubois, D.; Kadish, K. M. *Inorg. Chem.* **1991**, *30*, 1537.

68. Kumar, A. A.; Giribabu, L.; Reddy, D. R.; Maiya, B. G. *Inorg. Chem.* **2001**, *40*, 6757.

69. Maiya, B. G.; Bampos, N.; Kumar, A. A.; Feeder, N.; Sanders, J. K. M. *New J. Chem.* **2001**, 797.

70. Reddy, D. R.; Maiya, B. G. *J. Porphyrins Phthalocyanines,* **2002**, *6*, 3.

71. Kasha, M. *Pure Appl. Chem.* **1965**, *11*, 746.

72. Fujihara, T.; Tsuge, K.; Sasaki, Y.; Kaminaga, Y.; Imamura, T. *Inorg. Chem.* **2002**, *41*, 1170.

73. Fleatcher, J.; Therien, M. J. *Inorg. Chem.* **2002**, *41*, 331.

74. Fleatcher, J.; Therien, M. J. *J. Am. Chem. Soc.* **2002**, *124*, 4298.

75. Subramanian, J. In *Porphryins and Metalloporphyrins*; Smith, K. M., Ed.; Elsevier: Amsterdam, **1975**; p. 555.

76. Kievelson, D.; Lee, S. K. *J. Chem. Phys.* **1964**, *41*, 1896.

77. Assour, J. M. *J. Chem. Phys.* **1965**, *43*, 2477.

78. Eaton, S. S.; Raton, G. R.; Chang, C. K. *J. Am. Chem. Soc.* **1985**, *107*, 3177.

79. Mengersen, C.; Subramanian, J.; Fuhrhop, J.-H. *Mol. Phys.* **1976**, *3*, 893.

80. Nicholson, R. S.; Shain, I. *Anal. Chem.* **1964**, *36*, 706.

81. Abraham, R. J.; Bedford, G. R.; Mc Neillie, D.; Wright, B. *Org. Magn. Reson.* **1980**, *14*, 418.

82. Collman, J. P.; Wagenknecht, P. S.; Hutchison, J. E. *Angew. Chem., Int. Ed. Engl.* **1994**, *33*, 1537.

83. Tran-Thi, T. H.; Lipskier, J. F.; Maillard, P.; momenteau, M.; Lopez-Castillo, J.-M.; Jay-Gerin, J.-P. *J. Phys. Chem.* **1992**, *96*, 1073.

84. Suppan, P. *Chimia* **1988**, *42*, 320.

85. Lakowicz, J. R. in *Principles of Fluorescence Spectroscopy*; 2nd ed.; Plenum Press: New York, **1999**; p. 237-239.

CHAPTER 4

Synthesis and characterization of axial bis(terpyridoxy) Sn(IV) and P(V) Porphyrins: Modulation of PET and EET by transition metal ions.

4.1 Introduction

The 'axial-bonding' theme, which was introduced in the Chapter 3, has been extended to synthesize tin(IV)/phosphorus(V) porphyrin-terpyridine based donor-acceptor (**D-A**) systems during the present study.

Tin(IV) complexes of porphyrin and related macrocyclic systems have several biomedical applications. The major use has been for photodynamic therapy against cancer and non-cancerous proliferative skin conditions.[1-6] Non-cytotoxic antiproliferative action has been applied to the problem of restenosis following angioplasty.[7] A particularly useful property of tin(IV) complexes of natural porphyrins and their allies is their inhibition of heme oxygenase, making them candidates for the treatment of hyperbilirubinemia.[8,9] In addition, they offer protection against acute oxidative injury.[10] Tin(IV) porphyrins have also been included, with other metalloporphyrins, in studies of antiviral action, particularly for preventing HIV infection.[11,12] Tin(IV) porphyrin studied extensively for electrochemical and fluorescence sensors for various substrates[13,14] and as catalysts for photooxidation/photoreduction reactions of water as well as a variety of organic reactants.[15-17] More recent applications of tin(IV) macrocycles built on the porphyrin framework are concerned with their ability to act as NMR shift reagents and key components in functional supramolecular assemblies.[18-24]

On the other hand phosphorus(V) porphyrins have unique spectroscopic and redox properties and can also form stable axial bonds.[25-36] Utilizing these

properties of phosphorus(V) porphyrins, multiporphyrin arrays and D-A systems including 'molecular photoswitching' devices have been constructed recently.[33-36]

All the above applications of these macrocyclic systems largely rely on their favorable chemical and spectroscopic properties.[37-54] Thus, interest in the chemistry of tin(IV)/phosphorus(V) porphyrins has originated from the realization that their attractive redox and photochemical properties can be harnessed for performing potentially useful functions.

On the basis of photochemical and photophysical properties of terpyridine based transition metal complexes, $[\mathbf{M(ptp)_2}^{2+}]$-porphyrin based D-A systems are synthesized and studied extensively.[55-59] Here **ptp** = terpyridine and M = $\mathbf{Ru}^{2+}$, $\mathbf{Os}^{2+}$, $\mathbf{Rh}^{2+}$ and $\mathbf{Ir}^{2+}$ ions. Branda *et al.* reported axially coordinated $\mathbf{M(ptp)_2}^{2+}$ (M = $\mathbf{Ru}^{2+}$ or $\mathbf{Os}^{2+}$) complex with Ru(II) porphyrin based **D-A** system.[60] In addition, it appears that no effort has been made so far to covalently linked the **ptp** donor at the axial site of a metallo/metalloid porphyrin, where **ptp** is a strong chelating ligand towards the transition metal ions.[61-68] This has been accomplished during the present study, and this Chapter reports on the design, synthesis, spectral characterization and elucidation of **PET** and **EET** reactions of $\mathbf{[L^1Sn(O\text{-}ptp)_2]}$ and $\mathbf{[L^1P(O\text{-}ptp)_2]}$, where **Sn(IV)/P(V)** porphyrins endowed with the **ptp** donor subunits at the porphyrin axial positions. Synthesis and structures of these D-A systems are shown in Scheme 4.3 and the structure of $\mathbf{[L^1Sn(O\text{-}ptp)_2]}$ was determined by X-ray crystallographic methods. Finally, the chelating property of **ptp** with various transition metal ions was studied by proton NMR (^{1}H and ^{1}H-^{1}H COSY), UV-visible and fluorescence methods.

4.2 Experimental details

5,10,15,20-tetraphenylporphyrinatozinc(II) (**ZnTPP**) and 4′-(4-methoxyphenyl)-2,2′:6′,2″-terpyridine (**OMe-ptp**) the fluorescence standards

employed during this investigation, was synthesized as reported.[69,70] The precursor compounds 5,10,15,20-tetra(4-methylphenyl) porphyrin ($\mathbf{H_2L^1}$) was synthesized as described in Chapter 3 (section 3.2.1).

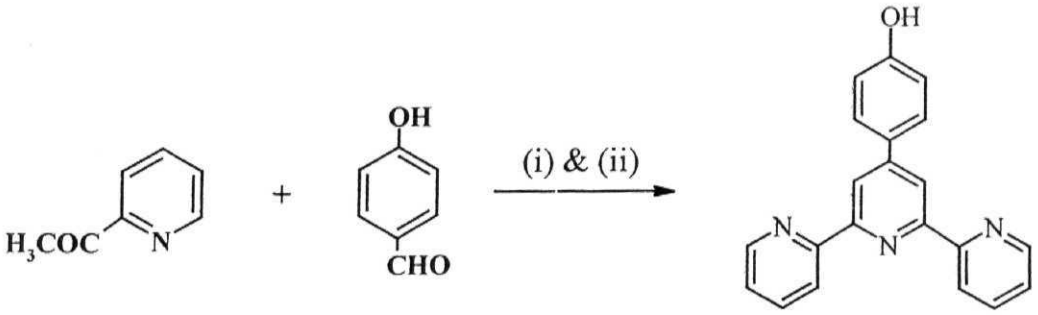

Scheme 4.1 Synthesis of 4′-(4-hydroxyphenyl)-2,2′:6′,2″-terpyridine (**OH-ptp**). Reaction conditions: (i) acetamide, ammonium acetate, NaOH, 48% HBr (ii) $FeCl_2$, 30% H_2O_2.

4.2.1 Synthesis of 4′-(4-hydroxyphenyl)-2,2′:6′,2″-terpyridine [OH-ptp] [70]

A mixture of acetamide (35.5 g), ammonium acetate (23 g), 4-hydroxybenzaldehyde (2.45 g) and 2-acetylpyridine (4.85 g) was heated (170-180°C) for 2 h. and cooled to 120°C. An aqueous solution of NaOH (35 g in 75 ml of water) was added and the solution was maintained at 120°C for 2 h. without stirring and then cooled to room temperature. The brown solidified paste that separated out was filtered, washed with water and dissolved in acetic acid (60 ml). The hydrobromide salt was precipitated with 47% HBr (60 ml), filtered off, and dissolved in water (200 ml). The pH of the aqueous solution was adjusted to 5-6 with 4N KOH. The suspension obtained was extracted with n-butanol (3x100 ml). After evaporation of the solvent, the residue was recrystallized from butanol-ethanol (1:1) to give white needles (1.4 g, 4.3 mmol, 22%).

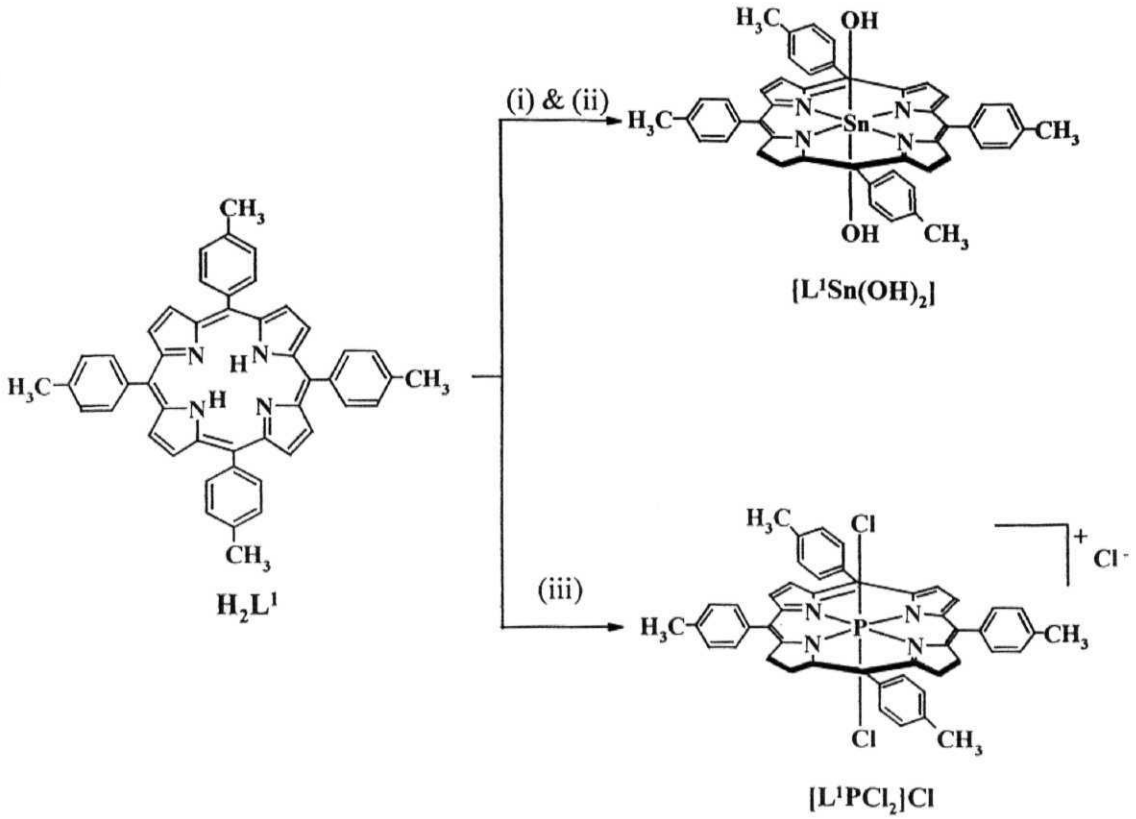

Scheme 4.2 Synthesis of reference compounds tin(IV) and phosphorus(V) porphyrins. Reaction conditions: (i) $SnCl_2$, dry pyridine, reflux, 3 h. (ii) aq. NH_3, (iii) $POCl_3$, dry pyridine, reflux, 24 h.

At this stage, TLC (Al_2O_3, $CHCl_3$-CH_3OH) and ^1H NMR revealed the presence of two compounds. The needles obtained were dissolved in CH_3CN, and $FeCl_2$ was added to give immediately a purple solution. The solution was filtered to remove excess of $FeCl_2$, to the filtrate was added an aqueous solution of NH_4PF_6. The precipitate was collected and recrystallized twice from CH_3CN-ether solution. A solution of **$[Fe(OH\text{-}ptp)_2(PF_6)_2]$** (500 mg, 0.5mmol) in aqueous CH_3CN (1:1) was made alkaline by the addition of aqueous KOH (600 mg in 2 ml H_2O) followed by the dropwise addition of aqueous H_2O_2 solution (30%) until the purple color had been discharged. The suspension was filtrated to remove iron

oxides, and the filtrate extracted with n-butanol (3x100 ml). The extracts were concentrated and to it was added an equal volume of ethanol to give a pale yellow needles. Yield = 405 mg (1.24 mmol, 81%).

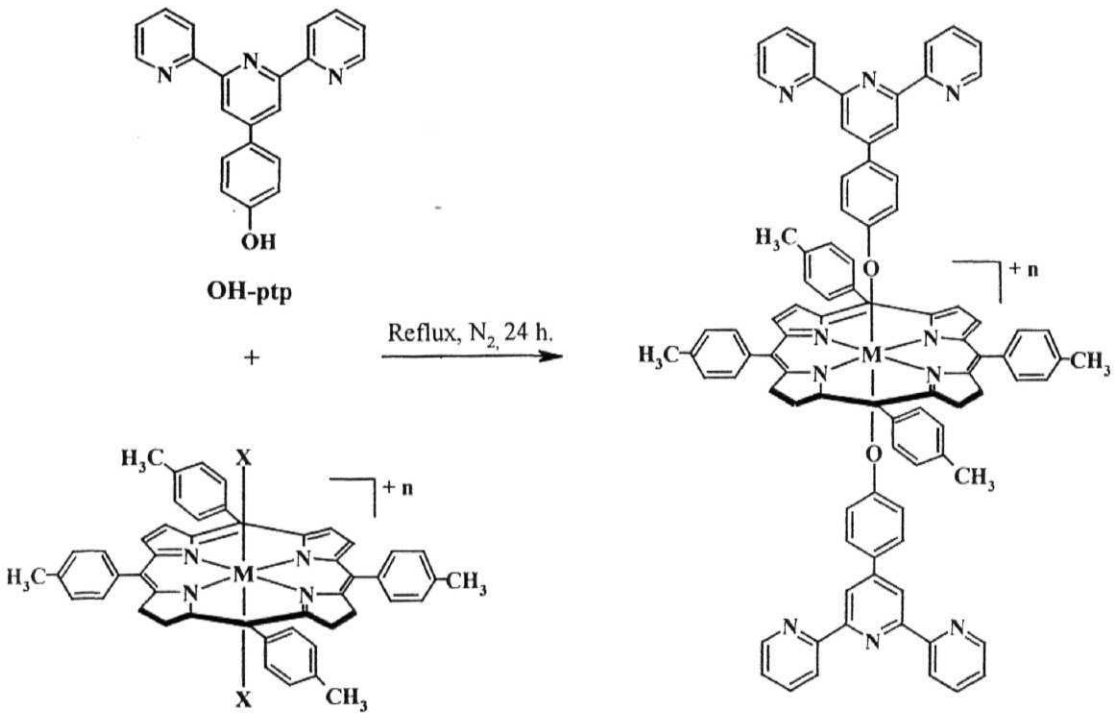

Scheme 4.3 Synthesis of tin(IV)/phosphorus(V)-(terpyridoxy)$_2$ porphyrins, **[L^{1}Sn(O-ptp)$_2$]** and **[L^{1}P(O-ptp)$_2$]$^+$**. Reaction conditions for **[L^{1}Sn(O-ptp)$_2$]**: **[L^{1}Sn(OH)$_2$]** (M = Sn(IV), X = OH, n = 0) in benzene and for **[L^{1}P(O-ptp)$_2$]OH**: **[L^{1}PCl$_2$]Cl** (M = P(V), X = Cl, n = 1) in pyridine.

4.2.2 Synthesis of 5,10,15,20-tetra(4-methylphenyl)porphyrinatodihydroxide tin(IV) [L^{1}Sn(OH)$_2$] [71,72]

2.0 g (3.0 mmol) sample of **H$_2$L^1** and 2.0 g (8.0 mmol) of $SnCl_2$ were taken up in 40 ml of pyridine. The reaction mixture was refluxed for 2 h. To this, 5 ml of aq. ammonia was added and the resulting mixture was stirred for 1 h. at 50°C. The solvent was evaporated to dryness under reduced pressure. The residue

was dissolved in ca. 50 ml of $CHCl_3$ and was washed repeatedly with water. The $CHCl_3$ solution was dried over anhydrous Na_2SO_4, after which it was evaporated to ca. 5 ml. This solution was applied on to a neutral alumina column. The desired product was eluted using $CHCl_3$-CH_3OH (97:3, v/v). Solvents were evaporated and the product was precipitated from CH_2Cl_2-hexane. Yield = 2.4 g (3 mmol, 90 %).

4.2.3 Synthesis of 5,10,15,20-tetra(4-methylphenyl)porphyrinatodichloro phosphorus(V) chloride $[L^1PCl_2]Cl$ [29]

Phosphorus oxychloride (8.8 g, 57 mmol) was added to $\mathbf{H_2L^1}$ (2.0 g, 3 mmol) in dry pyridine (30 ml) in an atmosphere of nitrogen. The mixture was refluxed for 24 h. The solvent pyridine and excess $POCl_3$ were removed under reduced pressure. The solid obtained was chromatographed on a silica gel column. Elution with $CHCl_3$-CH_3OH (10:1, v/v) gave desired product as a green solid. Yield = 1.2 g (1.5 mmol, 50%).

4.2.4 Synthesis of 5,10,15,20-tetra(4-methylphenyl)porphyrinatodihydroxide phosphorus(V) hydroxide $[L^1P(OH)_2]OH$ [29]

$\mathbf{[L^1PCl_2]Cl}$ (200 mg, 0.26 mmol) was dissolved in a solvent system consisting of pyridine (50 ml) and water (5 ml) and was refluxed for 12 h. Over this period, the solution changed color from dark purple to dark crimson. Pyridine and water were removed under reduced pressure, and the red residue obtained was chromatographed on silica. Elution with $CHCl_3$-CH_3OH (10:1, v/v) removed the desired red band. The solvents were removed under reduced pressure to give red glassy solid, which was recrystallized with benzene to yield $\mathbf{[L^1P^V(OH)_2]OH}$ as small red crystals. Yield = 180 mg (0.24 mmol, 89%).

4.2.5 Synthesis of tin(IV) porphyrin-(terpyridoxy)$_2$ triad [L^1Sn(O-ptp)$_2$]

[L^1Sn(OH)$_2$] (100 mg, 0.12 mmol) and **OH-ptp** (250 mg, 0.80 mmol) were dissolved in 50 ml of benzene and the resulting solution was refluxed for 24 h. After cooling to room temperature, the excess **OH-ptp** was removed by filtration through sintered crucible. The solvent was removed under reduced pressure and the crude solid was dissolved in minimum amount of CH_2Cl_2. This solution was precipitated by addition of CH_3CN and heated to 80 °C for 1 h. It was then filtered in hot condition to remove traces of **OH-ptp**. This process was repeated several times to get **OH-ptp** free compound. Finally it was crystallized from $CHCl_3$-CH_3CN to give the desired product. Yield = 140 mg (0.1 mmol, 80%).

4.2.6 Synthesis of phosphorus(V) porphyrin-(terpyridoxy)$_2$ triad [L^1P(O-ptp)$_2$]OH

[L^1PCl_2]Cl (200 mg, 0.26 mmol) was taken up in dry pyridine (30 ml). Large excess of **OH-ptp** (2.0 g, 14 mmol) was added and the mixture was refluxed under the nitrogen atmosphere for 24 h. Pyridine was evaporated under reduced pressure and the crude product was chromatographed on silica gel. Elution with $CHCl_3$-CH_3OH (98:2, v/v) removed a faint red fraction, which was discarded. Changing the solvent to $CHCl_3$-CH_3OH (90:10, v/v) eluted the desired product. Finally it was chromatographed on neutral alumina to remove little impurity of **[L^1P(OH)$_2$]OH** and **OH-ptp**. It was precipitated from CH_2Cl_2-hexane to yield = 200 mg (0.15 mmol, 55%).

4.2.7 X-ray crystallography

The fine and dark red single crystals of **[L^1Sn(O-ptp)$_2$]** was obtained by slow evaporation of CH_3CN layered $CHCl_3$ solution. This crystal was mounted to

the instrument Bruker Smart and primary unit cell constants were determined with a set of 30 narrow frame scans. This compound crystallized in the triclinic system (space group, P $\bar{1}$). The data were collected at low temperature (100 K) using Bruker Smart software. Bruker Saint version was employed for the data reduction. Semiempirical absorption correction was applied. The solution and refinement for the crystal data was performed using SHELXL-97 programme. The crystallographic parameters of **[L^1Sn(O-ptp)$_2$]** are summarized in Table 4.1, and the molecular structures is shown in Fig. 4.1. The metal centers of **[L^1Sn(O-ptp)$_2$]** are coordinated octahedrally via the four inner peripheral nitrogens of the porphyrin ligand the two **ptp** oxygen atoms. The **ptp** groups lie in an *anti* orientation with respect to each other. Other details of the crystal data are summarized in Appendix 1.

Table 4.1 Crystal data and structure refinement for **[L^1Sn(O-ptp)$_2$]**

Identification code	**[L^1Sn(O-ptp)$_2$]**
Empirical formula	C_{45} H_{32} N_5 O $Sn_{0.5}$
Formula weight	715.10
Temperature	100(2) K
Wavelength	0.71073 Å
Crystal system, space group	Triclinic, P $\bar{1}$
Unit cell dimensions	a = 11.2359(15) A, α = 79.716(2)°
	b = 11.8613(16) A, β = 78.803(2)°
	c = 14.2220(19) A, γ = 65.364(2)°
Volume	1679.9 (4) $Å^3$
Z, Calculated density	2, 1.451 gmL^{-1}
Absorption coefficient	0.447 mm^{-1}

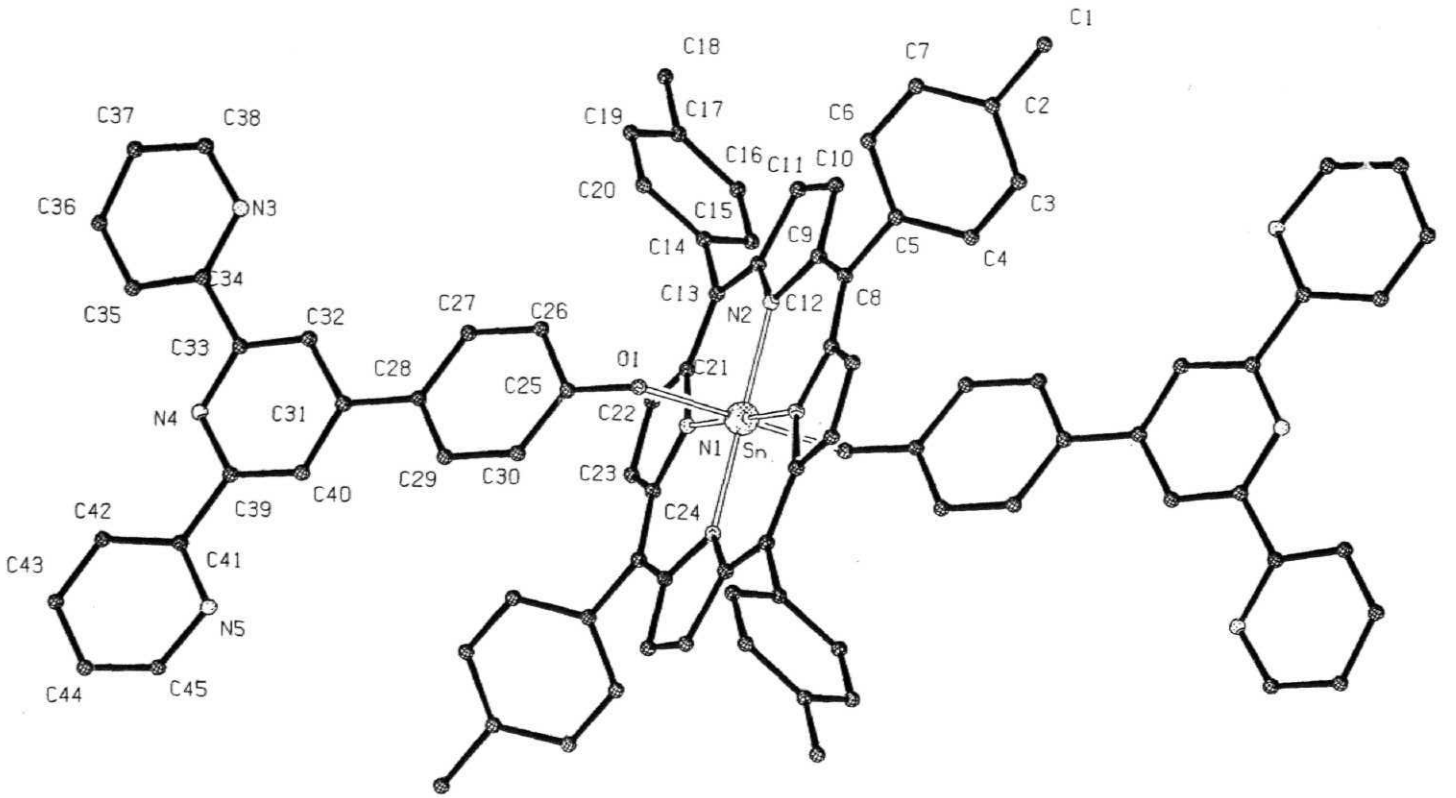

Fig. 4.1 Solid-style diagram of **[L^1Sn(O-ptp)$_2$]**. Hydrogen atoms are omitted for clarity.

F(000)	756
Crystal size	0.40 x 0.07 x 0.04 mm
Theta range for data collection	1.47 to 28.28°
Limiting indices	$-14 \leq h \leq 14, -15 \leq k \leq 15, -18 \leq l \leq 18$
Reflections collected / unique	19596 / 7811 [R(int) = 0.0445]
Completeness to theta = 28.28	93.7 %
Absorption correction	Semi-empirical
Max. and min. transmission	0.9823 and 0.8414
Refinement method	Full-matrix least-squares on F^2
Data / restraints / parameters	7811 / 0 / 475
Goodness-of-fit on F^2	1.173
Final R indices [I>2sigma(I)]	$R_1 = 0.0719$, $wR_2 = 0.1750$
R indices (all data)	$R_1 = 0.0812$, $wR_2 = 0.1796$
Largest diff. peak and hole	2.425 and -0.982 $e.A^{-3}$

All the spectroscopic and electrochemical experiments have been carried out as described in Chapter 2.

4.3 Results and discussion

The well-known oxophilicity of tin(IV) and phosphorus(V) porphyrins have been exploited to synthesize functionally-active, 'axial-bonding' type tin(IV) porphyrin-(terpyridoxy)$_2$ **[L^{1}Sn(O-ptp)$_2$]** and phosphorus(V) porphyrin-(terpyridoxy)$_2$ **[L^{1}P(O-ptp)$_2$]$^+$** triads, where terpyridine is capable of forming stable chelate complexes with a variety of transition metal ions. Details of spectroscopic, electrochemical and fluorescence properties of these triads are described below. Finally, metal (i.e. **Zn^{2+}**, **Cd^{2+}**, **Hg^{2+}**, **Cu^{2+}**, **Cu^{1+}**, **Ag^{1+}**, **Ni^{2+}**, **Co^{2+}**, **Fe^{2+}** and **Mn^{2+}**) ion titrations were carried out for **[L^{1}P(O-ptp)$_2$]$^+$** by ^{1}H

NMR, UV-visible and fluorescence methods using metal acetates/triflates/ chlorides. Binding constants were calculated from UV-visible and fluorescence titrations.

4.3.1 Design and Synthesis

The Schemes leading to synthesis of new compounds is shown in Scheme 4.3. Reaction of excess of 4′-(4-hydroxyphenyl)-2,2′:6′,2″-terpyridine **[OH-ptp]** with metal/metalloid porphyrins in refluxing in benzene or pyridine offered desired compounds. By simple recrystallization process, in suitable solvents spectroscopic grade pure compound **[L^1Sn(O-ptp)$_2$]** was obtained, whereas **[L^1P(O-ptp)$_2$]$^+$** was obtained as hydroxide salt by column chromatography, followed by recrystallization. Relying largely on oxophilicity of the Sn(IV) and P(V) ion, synthesis of **[L^1Sn(O-ptp)$_2$]** and **[L^1P(O-ptp)$_2$]$^+$** has been accomplished here, in good-to-moderate yields, following a step-wise protocol that we had adopted earlier for the synthesis Sn(IV) and P(V) porphyrin triads.[34-36,41,42]

4.3.2 Ground state properties

In mass (MALDI) spectroscopy, **[L^1Sn(O-ptp)$_2$]** triad was not shown the expected molecular ion peak whereas **[L^1P(O-ptp)$_2$](OH)** triad showed a less intense molecular ion peak. In both triads peaks are obtained due to fragments upon successive removal of the one/two axial terpyridoxy (**-O-ptp**) subunits. **[L^1Sn(O-ptp)$_2$]:** $[M-(C_{21}H_{14}N_3O)]^+ = 1111$, $[M-2(C_{21}H_{14}N_3O)]^+ = 788$, **[$L^1$P(O-ptp)$_2$](OH):** $[M]^+ = 1364$, $[(M-OH)+4H]^+ = 1351$, $[M-2(C_{21}H_{14}N_3O)]^+ = 699$.

The ^{31}P NMR signal due to the central phosphorus atom in **[L^1P(O-ptp)$_2$]$^+$** appear at –201.2 ppm. These values are shifted downfield compared to the ^{31}P resonance of **[L^1PCl_2]Cl** (δ = –233.2 ppm), but are within the typical range expected for hexa-coordinated diaryloxo phosphorus(V) porphyrins.[33-36,73] The ^{1}H

NMR spectrum of each new porphyrin synthesized during this study was analyzed with the proton assignments being made on the basis of both integrated intensity data and ^{1}H-^{1}H coupling patterns observed in the 2D (^{1}H-^{1}H COSY) spectra. Fig. 4.2 illustrates the various types of protons present in the investigated compounds.

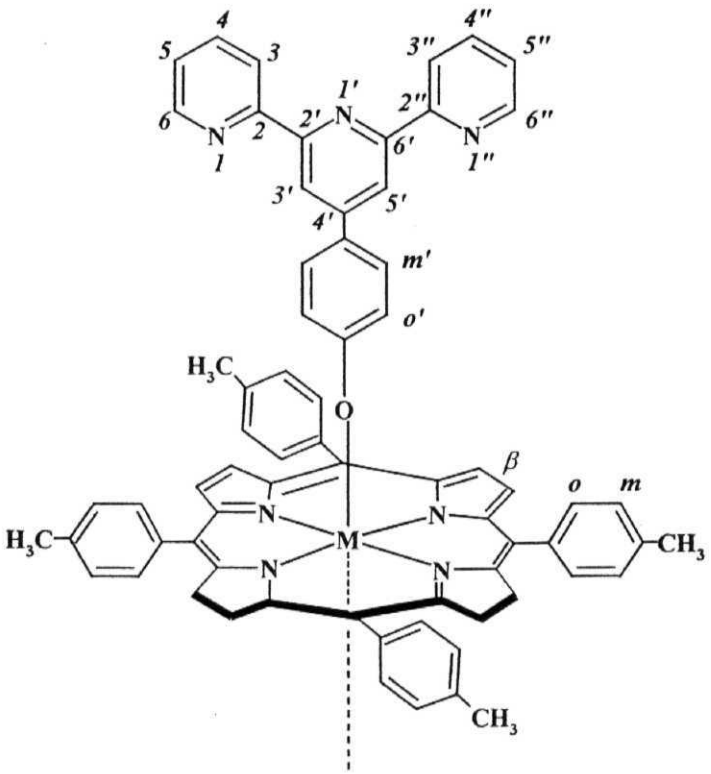

Fig. 4.2 Illustration of the various types of protons present in the newly investigated triads.

The 1D spectra of **[L^{1}Sn(O-ptp)$_2$]**, **[L^{1}P(O-ptp)$_2$]$^+$** and **OH-ptp** are shown in Fig. 4.3, and data summarized in Table 4.2. Each complex showed features typical of a diamagnetic porphyrin and, moreover, it was possible to distinguish between the resonances due to protons present on the porphyrin ring and those on the axial ligands, as was the case with the tin(IV) and phosphorus(V)

porphyrins reported earlier.[33-36,41,42] Resonance due to the β-pyrrole protons of **[L^{1}Sn(O-ptp)$_2$]** and **[L^{1}P(O-ptp)$_2$]$^+$** appear in the region 9.14 and 9.08 ppm as singlet with two minor peaks and multiplet, respectively. These minor peaks are due to the ^{117,119}Sn-H coupling and the coupling constants span a range of 12-15 Hz consistent with what was reported earlier for analogous aryloxo derivatives.[74,75] Resonance due to protons on the meso-tolyl rings of **[L^{1}Sn(O-ptp)$_2$]** and **[L^{1}P(O-ptp)$_2$]$^+$** triads are not much influenced by type of the axial ligand and appear as a pair of sharp doublets, see Table 4.2. The singlets observed at 2.66 and 2.60 ppm are due to the methyl protons of tolyl groups of **[L^{1}Sn(O-ptp)$_2$]** and **[L^{1}P(O-ptp)$_2$]$^+$** triads, respectively.

Dramatic shielding effects have been noticed for the ^{1}H NMR resonance of protons on the axial aryloxo subunits. For example, resonances due to protons ortho and meta to the axial oxo group in compound **[L^{1}Sn(O-ptp)$_2$]** (labeled as ***o′*** and ***m′***, respectively in Fig. 4.2), which were appearing at 6.91 and 7.75 ppm in the **OH-ptp**, now appear at 1.84 and 6.18 ppm respectively due to the ring current effect of the basal porphyrin(i.e. tin(IV) porphyrin) macrocycle.[76] Similarly, resonances due to the protons ***5′***(or ***3′***) of this compound are upfield shifted compared to the corresponding resonances in the spectrum of **OH-ptp**. The Δδ values (i.e. $\delta_{\text{OH-ptp}}-\delta_{\text{triad}}$) are a function of their separation distance from the porphyrin ring (see Table 4.2), as expected. Similar results were obtained for **[L^{1}P(O-ptp)$_2$]$^+$** from ^{1}H NMR as shown in Fig 4.3. Analysis of the ^{1}H NMR spectrum of **[L^{1}Sn(O-ptp)$_2$]** and **[L^{1}P(O-ptp)$_2$]$^+$** proved to be inconclusive with respect to assigning the axial ligand proton resonances and hence a ^{1}H-^{1}H COSY spectrum was run for these complexes. Resonances due to the axial ligand protons could be readily assigned based on the ^{1}H-^{1}H correlation patterns observed in the 2D spectrum. The representative ^{1}H-^{1}H COSY spectra of **[L^{1}P(O-ptp)$_2$]$^+$** is displayed in Fig. 4.4.

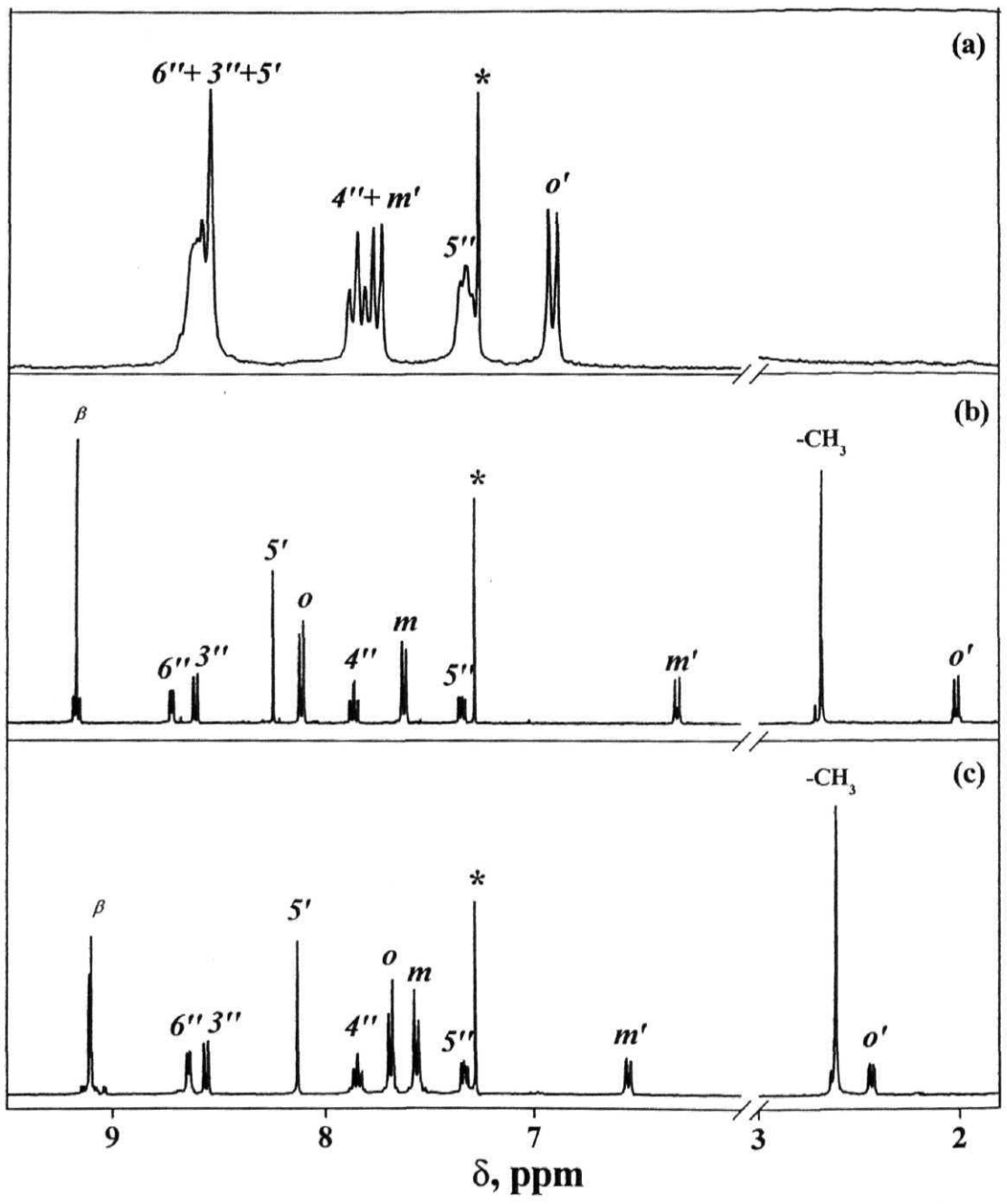

Fig. 4.3 ^{1}H NMR spectra of (a) **OH-ptp** in $CDCl_3$ + few drops of CD_3OD and (b) **[L^1Sn(O-ptp)]** (c) **[L^1P(O-ptp)$_2$]$^+$** are in $CDCl_3$, TMS (400 MHz, 300K) (* peak is due to solvent).

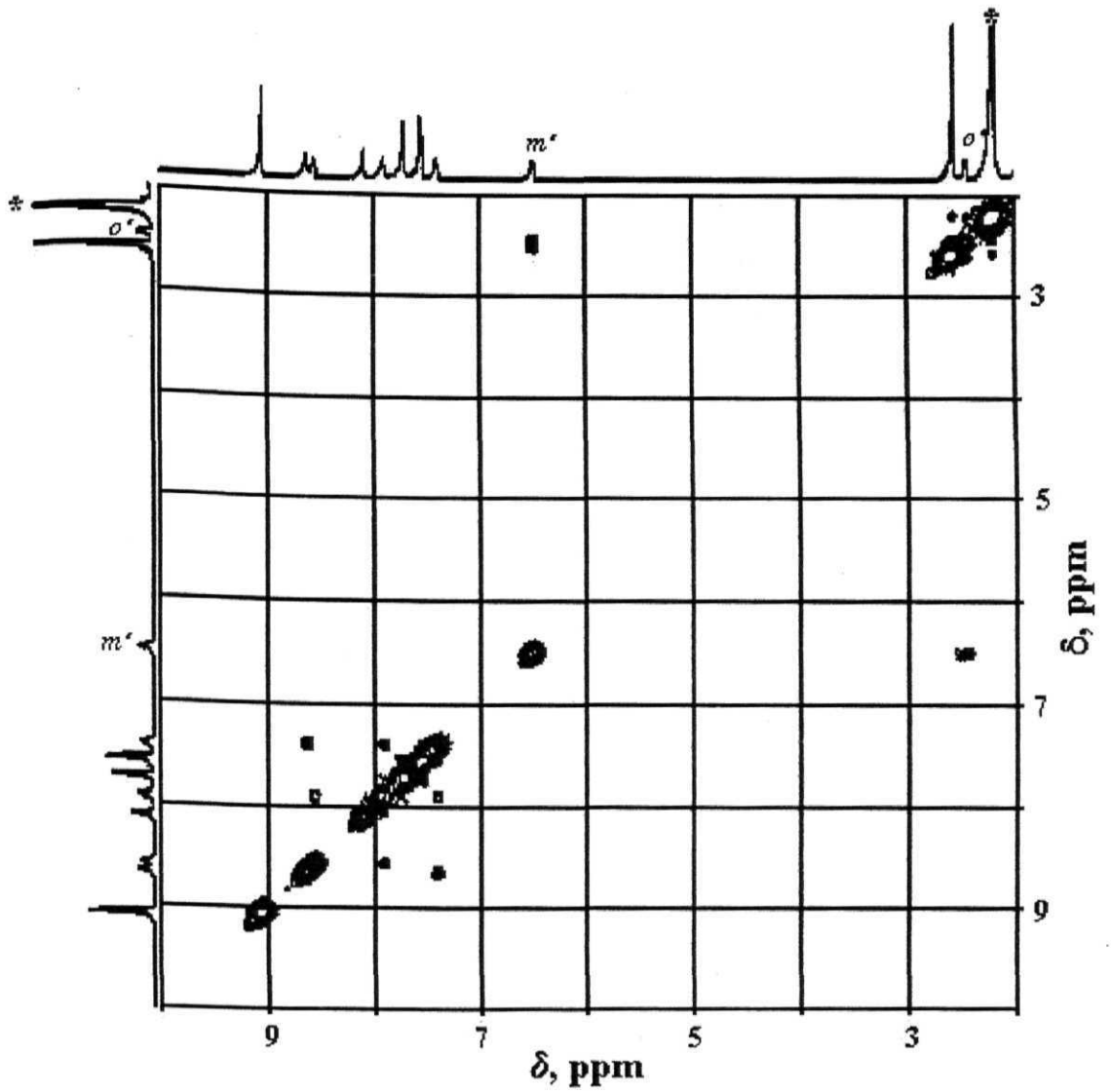

Fig. 4.4 ^{1}H-^{1}H COSY NMR spectrum of $[L^{1}P(O\text{-}ptp)_2]^{+}$ in CD_3CN (400 MHz, 300K) (* peak is due to solvent).

The absorption spectra of the $[L^{1}Sn(O\text{-}ptp)_2]$ and $[L^{1}P(O\text{-}ptp)_2]^{+}$ are shown in Fig. 4.5. The wavelengths of maximum absorbance (λ_{max}) and molar extinction coefficient (ε) values of both the triads (i.e. $[L^{1}Sn(O\text{-}ptp)_2]$ and $[L^{1}P(O\text{-}ptp)_2]^{+}$) and those of their constituent individual components (**OH-ptp**,

Table 4.2 ^{1}H NMR data of $[L^{1}Sn(O\text{-}ptp)_2]$, $[L^{1}P(O\text{-}ptp)_2]^{+}$ and their reference compounds [a]

Compd.	δ, ppm								
	Porphyrin			ptp group					
	β-pyrrole	*meso-tolyl*	*-CH$_3$*	*6 & 6″*	*3 & 3″*	*3′ & 5′*	*4 & 4″*	*5 & 5″*	*Bridging aryloxo (m′ & o′)*
OH-ptp [b]	-	-	-	8.60 (m, 2H)	8.58 (m, 2H)	8.54 (s, 2H)	7.84 (t, 2H)	7.32 (t, 2H)	7.75 (d, 2H$_{m'}$) 6.91 (d, 2H$_{o'}$) J = 8.2 Hz
$[L^{1}Sn(OH)_2]$	9.14 (s, 8H)	8.23 (d, 8H$_o$) 7.63 (d, 8H$_m$) J = 7.8 Hz	2.74 (s, 12H)	-	-	-	-	-	-
$[L^{1}PCl_2]^{+}$	9.12 (m, 8H)	7.86 (d, 8H) 7.58 (d, 8H) J = 7.8 Hz	2.62 (s, 12H)	-	-	-	-	-	-
$[L^{1}Sn(O\text{-}ptp)_2]$	9.14 (s, 8H)	8.07 (d, 8H$_o$) 7.59 (d, 8H$_m$) J = 8.0 Hz	2.66 (s, 12H)	8.70 (d, 4H) J = 4.8 Hz	8.59 (d, 4H) J = 8.4 Hz	8.22 (s, 4H) [0.32] [c]	7.83 (t, 4H)	7.32 (t, 4H)	6.28 (d, 4H$_{m'}$) [1.47] 1.99 (d, 4H$_{o'}$) [4.92] J = 8.8 Hz
$[L^{1}P(O\text{-}ptp)_2]^{+}$	9.08 (m, 8H)	7.67 (d, 8H$_o$) 7.55 (d, 8H$_m$) J = 8.0 Hz	2.60 (s, 12H)	8.63 (d, 4H) J = 5.2 Hz	8.54 (d, 4H) J = 7.6 Hz	8.11 (s, 4H) [0.43]	7.83 (t, 4H)	7.32 (t, 4H)	6.53 (d, 4H$_{m'}$) [1.22] 2.42 (d, 4H$_{o'}$) [4.49] J = 7.6 Hz

(a) Error limits: δ, ± 0.01 ppm, J: ± 1 Hz, spectra were recorded in $CDCl_3$, TMS (b) Spectrum was recorded in $CDCl_3$ + few drops of CD_3OD (c) Numbers within the square parentheses refer to the Δδ values (i.e. $\delta_{OH\text{-}ptp} - \delta_{triad}$; see text for details).

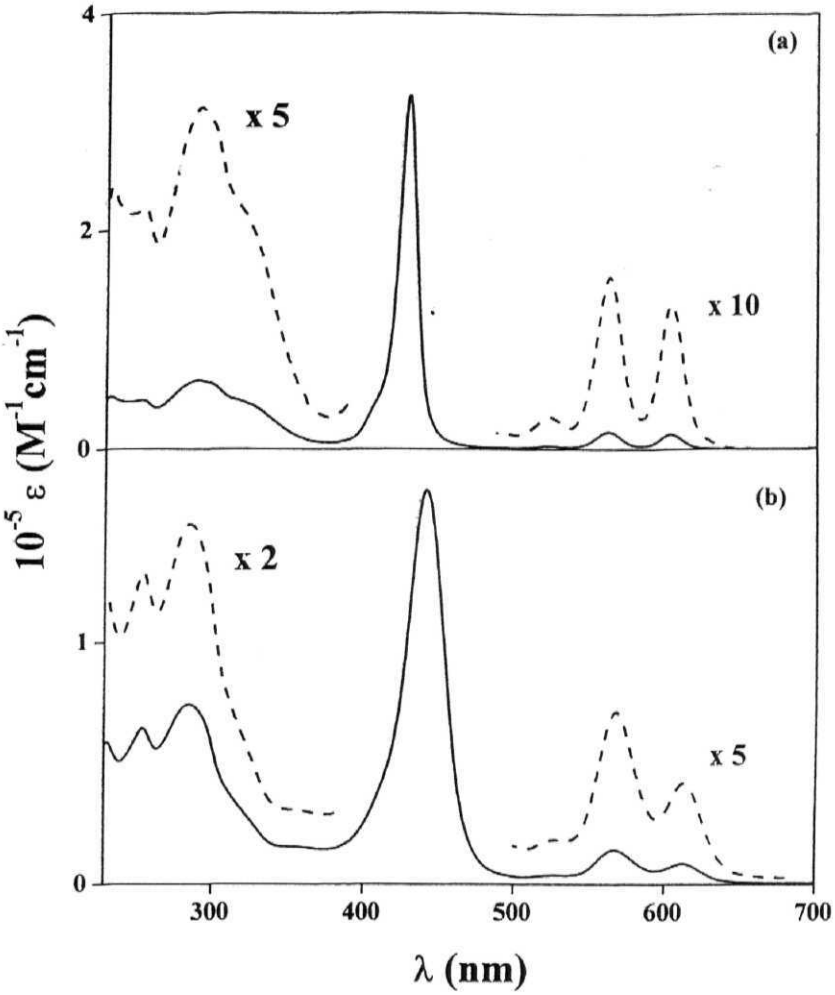

Fig. 4.5 UV-visible spectra of (a) **[L^1Sn(O-ptp)$_2$]** and (b) **[L^1P(O-ptp)$_2$]$^+$** in CH_2Cl_2.

and **[L^1Sn(OH)$_2$]/[L^1P(OH)$_2$]$^+$**), as obtained from the UV-visible studies, are summarized in Table 4.3. Comparison of spectra and the data given in Table 4.3 suggests that the axially connected **OH-ptp** subunit in these compounds dominantly absorbs between ca. 230-350 nm, a region in which porphyrin part of each molecule shows its so-called N and L bands. A band at λ<300 nm for each compound corresponds largely to the absorbance (π-π* transition) of the **OH-ptp**

moiety because the N and L bands are quite weak compared to the **OH-ptp** absorbance in this wavelength region. On the other hand, porphyrin parts of these compounds show two less intense Q-bands and one intense Soret band (B-band) in the wavelength region (400-700 nm) where the **OH-ptp** part of each molecule does not absorb.

Table 4.3 UV-visible data of newly synthesized triads and its reference compounds in CH_2Cl_2 [a]

Compd.	λ_{max}, nm (log ε)		
	B-band	**Q-bands**	**ptp**
OH-ptp [b]	-	-	290 (4.57)
OMe-ptp	-	-	255 (4.35), 287 (4.60)
$[L^1Sn(OH)_2]$	428 (5.75)	524 (3.57), 563 (4.29), 604 (4.24)	-
$[L^1P(OH)_2]^+$	432 (5.31)	557 (4.14), 598 (3.81)	-
$[L^1PCl_2]^+$	445 (5.35)	571 (4.09), 618 (3.95)	-
$[L^1Sn(O\text{-}ptp)_2]$	427 (5.50)	522 (3.60), 562 (4.30), 603 (4.21)	253 (4.63), 290 (4.89)
$[L^1P(O\text{-}ptp)_2]^+$	441 (5.21)	568 (4.14), 613 (3.91)	255 (4.80), 285 (4.86)

(a) Error limits: λ_{max}, ± 1 nm, log ε, ± 10% (b) Spectrum recorded in DMSO.

Dilute solutions containing 1:2 molar equivalents of **$[L^1Sn(OH)_2]$** and **OH-ptp** generate UV-visible spectra that is close to the spectra of **$[L^1Sn(O\text{-}ptp)_2]$**. The absorption maxima (λ_{max}) and molar extinction coefficient (ε) values of the Soret and Q-bands in this triad were not shifted from those of respective bands in reference compounds suggest that there exist no π-π interaction between

porphyrin and **ptp** subunits in the ground state. Whereas in absorption spectra of $[L^1P(O\text{-}ptp)_2]^+$, the wavelength maxima of the Soret and Q bands are red shifted from respective bands in the 1:2 physical mixture spectra of $[L^1P(OH)_2]^+$ and **OH-ptp**. The absorption spectra of $[L^1P(O\text{-}ptp)_2]^+$ and its monomers ($[L^1P(OH)_2]^+$, **OH-ptp**) in DMSO, are shown in Fig. 4.6, suggest the electronic (π-π) interactions between axial terpyridine and porphyrin subunits. The intensity of the Soret band is slightly diminished and the full width at half maximum (FWHM) of the Soret band is increased. The absorption maxima (λ_{max}) and molar extinction coefficient (ε) values of $[L^1P(O\text{-}ptp)_2]^+$ triad and its monomer $[L^1P(OH)_2]^+$ in difference solvents are summarized in Table 4.4.

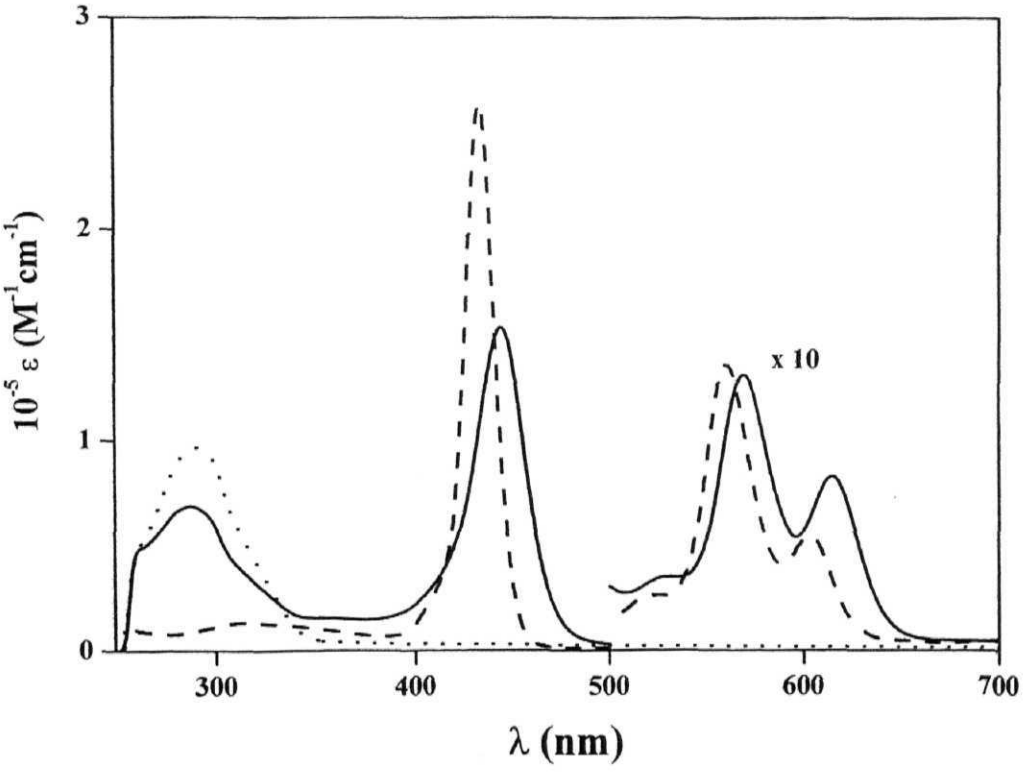

Fig. 4.6 Absorption spectra of triad $[L^1P(O\text{-}ptp)_2]^+$ (——) and its monomeric compounds $[L^1P(OH)_2]^+$ (------), **OH-ptp** (·····) in DMSO.

Table 4.4 UV-visible data of $[L^1P(OH)_2]^+$ and $[L^1P(O\text{-}ptp)_2]^+$ in different solvents [a]

Compd.	λ_{max}, nm (log ε)		
	B-band	**Q-bands**	**ptp**
$[L^1P(OH)_2]^+$			
Toluene	433 (5.40)	601 (3.58), 560 (4.15)	-
CH_3CN	428 (5.43)	594 (3.78), 554 (4.16)	-
DMF	432 (5.39)	603 (3.70), 560 (4.10)	-
DMSO	435 (5.41)	603 (3.74), 561 (4.13)	-
CH_3OH	428 (5.41)	599 (3.63), 557 (4.11)	-
$[L^1P(O\text{-}ptp)_2]^+$			
Toluene	446 (5.08)	616 (3.84), 571 (4.04)	289 (4.72)
CH_3CN	439 (5.13)	611 (3.80), 566 (4.04)	284 (4.80)
DMF	443 (5.17)	615 (3.88), 569 (4.08)	286 (4.80)
DMSO	445 (5.19)	615 (3.92), 570 (4.12)	287 (4.84)
CH_3OH	438 (5.16)	611 (3.82), 566 (4.07)	286 (4.81)

(a) Error limits: λ_{max}, ± 1 nm, log ε, ± 10%

Table 4.5 summarizes the redox potential data (CH_2Cl_2, 0.1 M TBAP) of $[L^1Sn(O\text{-}ptp)_2]$ and $[L^1P(O\text{-}ptp)_2]^+$ along with the reference compounds $[L^1Sn(OH)_2]$, $[L^1P(OH)_2]^+$ or $[L^1PCl_2]^+$ and **OH-ptp** investigated in this study. Fig. 4.7 illustrates the cyclic and differential pulse voltammograms of $[L^1Sn(O\text{-}ptp)_2]$ and $[L^1P(O\text{-}ptp)_2]^+$. As seen in Fig. 4.7, each triad undergoes two stepwise reduction reactions. Wave-analysis (from cyclic voltammetry) suggested that both these electrode processes are reversible (i_{pc}/i_{pa} = 0.9 - 1.0) and diffusion controlled ($i_{pc}/\nu^{1/2}$ = constant in the scan rate (ν) range 50 - 500 mV s^{-1}) one-electron transfer (ΔEp = 60 - 70 mV; ΔEp = 65 ± 3 mV for Fc^+/Fc couple) reactions.[77] Based on the redox potential data reported earlier for 'axial-bonding' type tin(IV) and phosphorus(V) porphyrins,[27,32,34,41-43] and also on the basis of the

diagnostic criteria developed by Fuhrhop, Kadish and Davis for porphyrin ring reduction[78] ($\Delta E_{1/2}$ i.e. the difference in potential between the first one-electron and second one-electron addition = 0.42 ± 0.05 V; see Table 5.2 where $\Delta E_{1/2}$ = 0.42 - 0.48 V), the first two reduction waves observed for the D-A conjugates investigated here can be assigned to successive, one-electron additions to the porphyrin ring. Reduction peak due to the terpyridine subunits was not observed for these compounds, within the solvent window.

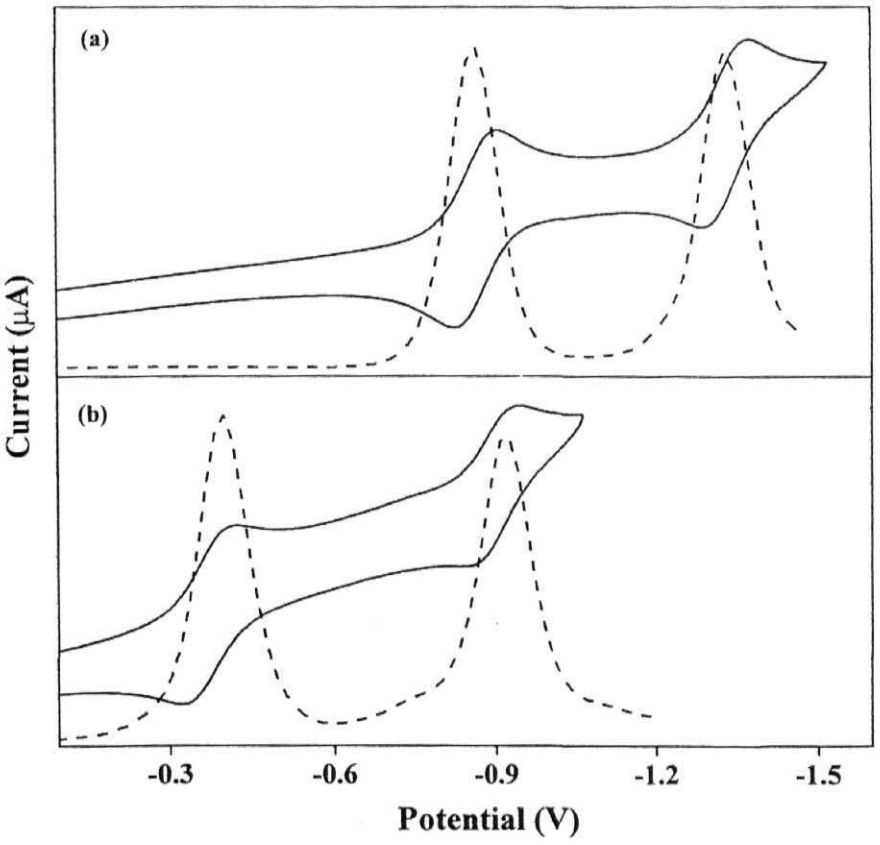

Fig. 4.7 Cyclic (——) and differential pulse (·····) voltammograms of (a) **[L^{1}Sn(O-ptp)$_2$]** and (b) **[L^{1}P(O-ptp)$_2$]$^+$** in CH_2Cl_2, 0.1 M TBAP (scan rate = 100 mVs^{-1}, modulation amplitude = 10 mV).

Scanning the potential in the positive range (0-1.8 V) for solutions containing the investigated **[L^{1}Sn(O-ptp)$_2$]** and **[L^{1}P(O-ptp)$_2$]$^+$** triads gave ill-defined voltammograms with a large background current. However, terpyridine (**OH-ptp**) employed here for synthesis of the aryloxo porphyrins could be irreversibly oxidized in DMSO, 0.1 M TBAP. During the anodic scan, irreversible oxidation responses was seen at 1.16 V for **[L^{1}Sn(O-ptp)$_2$]**. Comparing differential voltammograms and redox data of **[L^{1}Sn(O-ptp)$_2$]** with its reference compounds **OH-ptp** and **[L^{1}Sn(OH)$_2$]**, it was found that the observed oxidation peak is the combination of the first oxidation of terpyridine (**OH-ptp**) and first oxidation of **[L^{1}Sn(OH)$_2$]** porphyrin. Based on the knowledge that phosphorus(V) porphyrins are hard to oxidize[26,27,78] and the observation that both **[L^{1}PCl$_2$]$^+$** and **[L^{1}P(OH)$_2$]$^+$** did not show any oxidation response up to +1.8 V under our experimental conditions, the peaks seen for **[L^{1}P(O-ptp)$_2$]$^+$** can be ascribed to electron abstraction from the appended terpyridine subunit. These potentials are anodically shifted compared to those of the corresponding free terpyridine (see Table 4.5).

Analysis of the data given in Table 4.5 reveals that, the electrochemical redox potentials of the **[L^{1}Sn(O-ptp)$_2$]** are in the same range as those of the corresponding reference compounds **HO-ptp** and **[L^{1}Sn(OH)$_2$]** porphyrins. This is not the case for **[L^{1}P(O-ptp)$_2$]$^+$**, whereas the redox peaks are anodically shifted compared to the reference compound **[L^{1}P(OH)$_2$]$^+$**, suggesting that the oxidation and reduction potentials of the present triads are dependent on the metal ion present in the cavities of the porphyrin thus enabling a facile modulation of the ground state properties. As will be shown in the next section, the excited state redox properties of these arrays are also dependent on the type of metal/metalloid ion present in the porphyrin cavities. Finally, energies of the possible charge transfer states (i.e. E_{CT}(**M$^+$ptp$^-$**) and E_{CT}(**M$^-$ptp$^+$**) where M = Sn(IV) and P(V) of

the photoactive compounds, as evaluated from the redox potentials data are also summarized Table 4.5. These E_{CT} values are useful quantities in analyzing the photochemical data of the triads (see in the next section).

Table 4.5 Redox potential data in CH_2Cl_2, 0.1 M TBAP [a]

Compd.	Potential ($E_{1/2}$) mV vs SCE		M*→Ptp (555 nm)		Ptp*→M (280/300 nm)
	Oxidation	Reduction	$\Delta G(M^+Ptp^-)$ eV	$\Delta G(M^-Ptp^+)$ eV	$\Delta G(Ptp^+M^-)$ eV
OH-ptp [b]	1004	-	-	-	-
$[L^1Sn(OH)_2]$	1440	-920, -1325	-	-	-
$[L^1P(OH)_2]^+$	-	-520, -1002	-	-	-
$[L^1PCl_2]^+$	-	-290, -780	-	-	-
$[L^1Sn(O\text{-}ptp)_2]$	1160	-860, -1330	0.92	-0.02	-1.73
$[L^1P(O\text{-}ptp)_2]^+$	1650	-390, -920	1.60	0.04	-1.71

(a) Error limits: $E_{1/2}$, ± 15 mV (b) Measured in DMSO, 0.1 M TBAP.

4.3.3 Singlet state properties

The UV-visible spectral data of **$[L^1Sn(O\text{-}ptp)_2]$** and **$[L^1P(O\text{-}ptp)_2]^+$** indicate that it is possible to address photochemistry of the porphyrin and the terpyridine subunits in these bichromophoric systems. Steady state fluorescence spectra of these D-A systems have been measured in different solvents by exciting the solutions at 555 nm (exclusively porphyrin absorption) and 280/300 nm (predominantly terpyridine absorption). The resulting spectra are compared with those of the corresponding individual components constituting them, i.e. **$[L^1Sn(OH)_2]$/$[L^1P(OH)_2]^+$** and **OH-ptp**. In Fig. 4.8, the steady state fluorescence

spectra of these compounds measured in toluene are compared with spectra of the corresponding individual components. Upon excitation at 555 nm, porphyrin component of each compound showed fluorescence spectrum that is typical of a hexa-coordinated tin(IV)/phosphorus(V) porphyrin, respectively.[33-36,41-43] Spectral shapes and wavelengths of emission maxima (λ_{em}) of **[L^{1}Sn(O-ptp)$_2$]** is seen to be similar to the spectrum of **[L^{1}Sn(OH)$_2$]** whereas for **[L^{1}P(O-ptp)$_2$]$^+$** triad fluorescence peaks are result in broaden and red shifted compared to the **[L^{1}P(OH)$_2$]$^+$**.

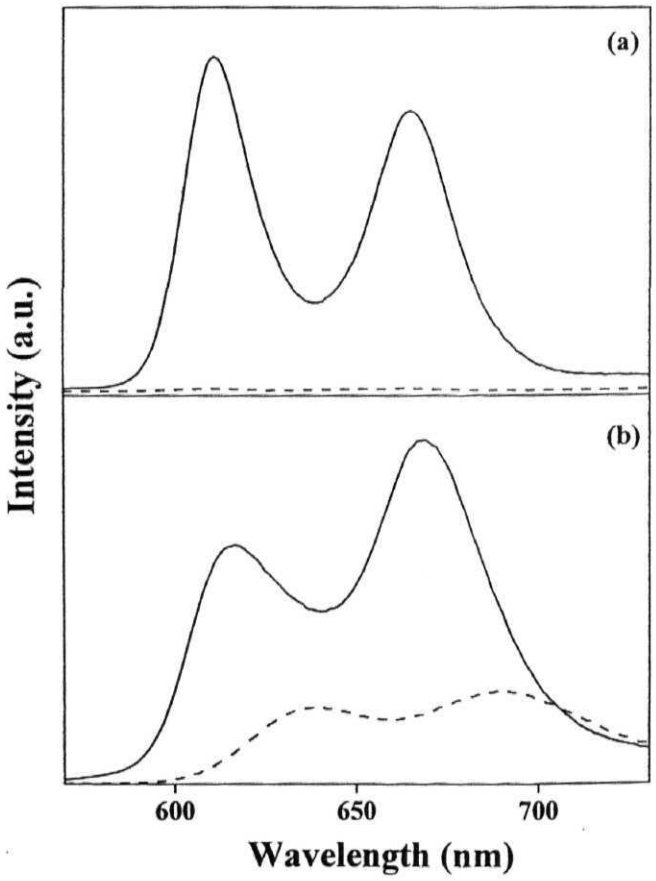

Fig. 4.8 Fluorescence spectra (equimolar solutions, ~0.2 OD at λ_{ex} = 555 nm) of (a) **[L^{1}Sn(OH)$_2$]** (———) and **[L^{1}Sn(O-ptp)$_2$]** (.....) (b) **[L^{1}P(OH)$_2$]$^+$** (———) and **[L^{1}P(O-ptp)$_2$]$^+$** (.....) in toluene.

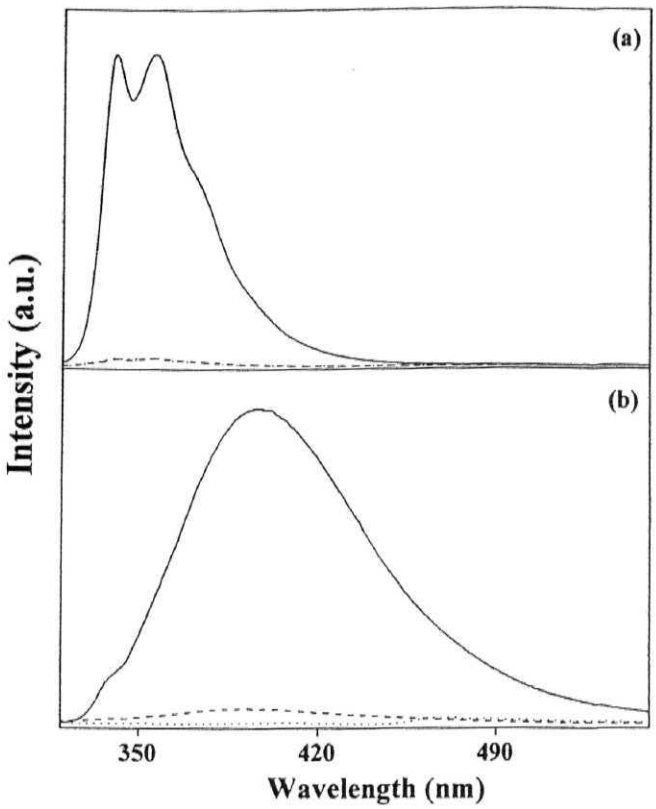

Fig. 4.9 Fluorescence spectra (equimolar solutions, ~0.2 OD) of (a) λ_{ex} = 300 nm: **OH-ptp** (———), **[L^{1}Sn(O-ptp)$_2$]** (--------) and **[L^{1}P(O-ptp)$_2$]$^+$** (·····) in toluene; (b) λ_{ex} = 280 nm: **OH-ptp** (———), **[L^{1}Sn(O-ptp)$_2$]** (--------) and **[L^{1}P(O-ptp)$_2$]$^+$** (·····) in CH_3CN.

Fig 4.9 shows, excitation at 280/300 nm (dominant terpyridine absorption) resulted in quenching of both the compounds in comparison with the reference **OH-ptp**. From an overlay of the absorption and fluorescence spectra of these D-A systems, the 0-0 spectroscopic transition energies ($E_{0\text{-}0}$) of the **OH-ptp** (3.75 ± 0.04 eV) and tin(IV) porphyrin (2.04 ± 0.04 eV) moieties have been estimated and found to be close to those of the corresponding unlinked chromophores. But whereas for **[L^{1}P(O-ptp)$_2$]$^+$** triad $E_{0\text{-}0}$ value (2.00 ± 0.04 eV) found to be different

from its reference compound $[L^1P(OH)_2]^+$ (i.e. 2.06 ± 0.04 eV). This difference may be due to the π-π interaction between porphyrin and **ptp** chromophores. The quenching efficiency values (Q) have been calculated with eqn. 4.1 in different solvents using the quantum yield data, and are summarized in Tables 4.6 & 4.7.

$$Q = (\phi_{ref} - \phi_{triad}) / \phi_{ref} \quad (4.1)$$

Where, ϕ_{triad} and ϕ_{ref} refers to the quantum yields of given triad and the appropriate reference compound, respectively.

Table 4.6 Fluorescence data of triads and their monomeric analogues (λ_{ex} = **555 nm**) [a]

Compd.	λ_{em}, nm (ϕ, %Q)				
	Toluene	**CH_2Cl_2**	**CH_3CN**	**DMSO**	**DMF**
$[L^1Sn(OH)_2]$	611, 665 (0.039)	612, 666 (0.04)	610, 664 (0.03)	614, 668 (0.044)	613, 668 (0.045)
$[L^1P(OH)_2]^+$	617, 669 (0.049)	618, 671 (0.045)	617, 670 (0.054)	622, 673 (0.06)	621, 672 (0.051)
$[L^1Sn(O\text{-}ptp)_2]$	609, 663 (0.0006, 98)	611, 664 (0.0003, 99)	609, 664 (0.0005, 98)	613, 667 (0.0004, 99)	610, 666 (0.0009, 98)
$[L^1P(O\text{-}ptp)_2]^+$	639, 690 (0.018, 61)	634, 686 (0.022, 52)	631, 677 (0.016, 70)	638, 689 (0.026, 58)	637, 688 (0.026, 51)

(a) Error limits: λ, ± 1 nm; ϕ, ± 10%

A variety of excited state processes including EET, enhanced internal conversion and intersystem crossing, ion-association, PET etc. can be thought to be operative in the quenching of fluorescence observed in these D-A systems. Obviously, it is not going to be easy to estimate the contribution from each of

these excited state processes. However, the possibilities of both EET and PET quenching processes (eqns. 4.2 - 4.6) are discussed below.

Table 4.7 Fluorescence data of triads and their monomeric analogues (λ_{ex} = 280/300 nm) [a]

Compd.	λ_{em}, nm (ϕ, %Q)			
	Cyclo -hexane (λ_{ex} = 280 nm)	Toluene (λ_{ex} = 300 nm)	CH_2Cl_2 (λ_{ex} = 280 nm)	CH_3CN (λ_{ex} = 280 nm)
OMe-ptp	337, 352 (0.29)	341, 356 (0.31)	342, 358 (0.28)	387 (0.24)
OH-ptp	337, 351 (0.154)	340,355 (0.30)	339, 355 (0.26)	397 (0.20)
$[L^1Sn(O\text{-}ptp)_2]$	336, 352 (0.005, 96)	340, 355 (0.008, 96)	340, 355 (0.015, 94)	391 (0.012, 94)
$[L^1P(O\text{-}ptp)_2]^+$	421 (0.005, 96)	340, 355 (0.009, 96)	398 (0.0061, 97)	409, 471 (0.0038, 98)

(a) Error limits: λ, ± 1 nm; ϕ, ± 10%. **OMe-ptp** was used as a standard for calculating the quantum yields.[79]

$$M\text{-}Ptp \xrightarrow{555\ nm} M^*\text{-}Ptp \xrightarrow{\textbf{PET 1}} M^+\text{-}Ptp^- \quad \text{---------- (4.2)}$$

$$M\text{-}Ptp \xrightarrow{555\ nm} M^*\text{-}Ptp \xrightarrow{\textbf{PET 2}} M^-\text{-}Ptp^+ \quad \text{---------- (4.3)}$$

$$M\text{-}Ptp \xrightarrow{280/300\ nm} M\text{-}Ptp^* \xrightarrow{\textbf{PET 3}} M^-\text{-}Ptp^+ \quad \text{---------- (4.4)}$$

$$M\text{-}Ptp \xrightarrow{555\ nm} M^*\text{-}Ptp \xrightarrow{\textbf{EET 1}} M\text{-}Ptp^* \quad \text{---------- (4.5)}$$

$$M\text{-}Ptp \xrightarrow{280/300\ nm} M\text{-}Ptp^* \xrightarrow{\textbf{EET 2}} M^*\text{-}Ptp \quad \text{---------- (4.6)}$$

In eqns 4.2 - 4.6, **M*** and **Ptp*** stands for the singlet excited state of Sn(IV)/P(V) porphyrin and terpyridine subunits, respectively. The free energy changes (ΔG_{PET}) required for the three PET reactions between two chromophores (eqns. 4.2 - 4.4) are calculated by the simplified Rehm-Weller method, [80] eqn. 4.7.

$$\Delta G_{PET} = E_{CT} - E_{0\text{-}0} \qquad (4.7)$$

Where E_{CT} refers to energy of the charge transfer state (see Table 4.5) and $E_{0\text{-}0}$ is energy of the singlet state of the porphyrin/terpyridine units.

The ΔG_{PET} values thus obtained for processes 4.2, 4.3 and 4.4 are summarized in Table 4.5. In these calculations, oxidation potential of the phosphorus(V) porphyrin and reduction potential of terpyridine subunit are assumed to be anodic to +1.8 V and cathodic to -1.8 V, respectively (solvent limit). The positive ΔG_{PET} (0.92 eV and 1.60 eV for **$[L^1Sn(O\text{-}ptp)_2$** and **$[L^1P(O\text{-}ptp)_2)]^+$**, respectively) values for processes 4.2 suggest that, PET processes are thermodynamically unfavorable processes in both the compounds and it is consistent with the 'hard to oxidize' nature of the phosphorus(V) porphyrins in **$[L^1P(O\text{-}ptp)_2)]^+$** triad. On the other hand, eqns. 4.3 and 4.4 are thermodynamically favorable processes and the extent of exoergicity (i.e. –0.02 / 0.04 and –1.73 / –1.71 eV for **$[L^1Sn(O\text{-}ptp)_2]/[L^1P(O\text{-}ptp)_2]^+$**, respectively) suggests that these processes can, in principle, occur in these new D-A systems. For processes 4.3, due to slightly positive ΔG_{PET} value or nearly zero (0.04 eV) in triad **$[L^1P(O\text{-}ptp)_2]^+$**, explain low quenching values compared with **$[L^1Sn(O\text{-}ptp)_2]$** triad.

As far as the EET processes are concerned, it should be noted that energies of the singlet excited states of terpyridine and the porphyrin subunits rule out the EET to occur from the singlet porphyrin to the terpyridine chromophore (eqn.

4.5). The occurrence of the reverse process, i.e. ^{1}(terpyridine) → porphyrin (eqn. 4.6), is a distinct possibility. The observation is that there exists a considerable overlap between the emission of terpyridine and the absorption of porphyrin in these D-A systems (compare the corresponding spectra in Fig 4.9 & Table 4.3) suggests that quenching of the terpyridine fluorescence observed for **$[L^1Sn(O\text{-}ptp)_2]$** and **$[L^1P(O\text{-}ptp)_2]^+$** may be due to intramolecular EET from the singlet terpyridine to the porphyrin. Indeed, excitation into the terpyridine moieties absorption band at 280/300 nm (where the porphyrin part absorbs weakly) results in the appearance of strong fluorescence bands due to the porphyrin at $\lambda > 600$ nm. This was not the case with **$[L^1Sn(OH)_2]$**/**$[L^1P(OH)_2]^+$**, which under comparable concentrations used with experiments with **$[L^1Sn(O\text{-}ptp)_2]$**/**$[L^1P(O\text{-}ptp)_2]^+$**, showed only weak fluorescence at $\lambda > 600$ nm. Conclusive evidence for intramolecular EET comes from the excitation spectral measurements. When emission was recorded at the porphyrin emission maximum (670 nm for both **$[L^1Sn(O\text{-}ptp)_2]$** and **$[L^1P(O\text{-}ptp)_2]^+$**), the excitation spectra of these D- A systems showed bands characteristic of terpyridine absorption. The corrected and normalized excitation spectra of these dyads were overlayed with the corresponding absorption spectra. Fig 4.10 shows a comparison of **$[L^1P(O\text{-}ptp)_2]^+$** spectra in the 3.9×10^4 - 3.0×10^4 cm^{-1} region gave 61% energy transfer efficiencies in CH_3CN. By using the same method the % energy transfer was calculated for both **$[L^1Sn(O\text{-}ptp)_2]$** and **$[L^1P(O\text{-}ptp)_2]^+$** in solvents like cyclohexane, CH_2Cl_2, DMF, and DMSO gave 68-76% energy transfer efficiency.

Fig. 4.11 shows the possible relaxation process of the excited states of **$[L^1Sn(O\text{-}ptp)_2]$** and **$[L^1P(O\text{-}ptp)_2]^+$**. Thus, the quenching of fluorescence when excitation at 555 nm due to a PET (reductive electron transfer, Fig. 4.11) from the ground state terpyridine to the singlet porphyrin whereas that at 280/300 nm results in a PET from the excited state terpyridine to the ground state porphyrin

compete with an EET from the terpyridine to the porphyrin in both the D-A systems and it can explain the high %Q values (~96%), see Table 4.7.

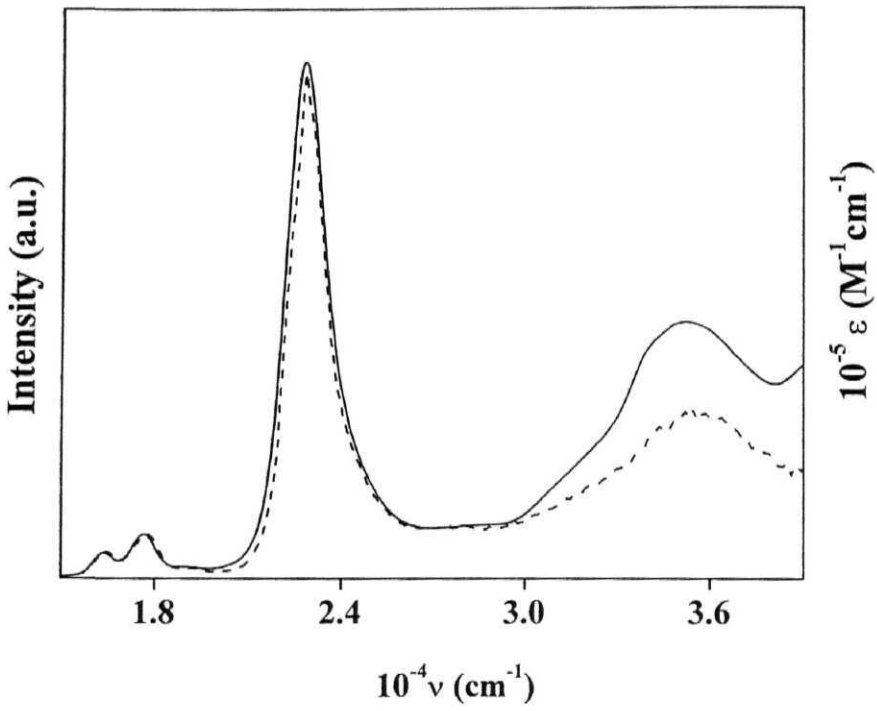

Fig 4.10 Overlay of $[L^1P(O\text{-}ptp)_2]^+$ excitation (-----) and absorption (——) spectra in CH_3CN, λ_{em} = 670 nm. The excitation spectra were corrected for the instrument response function and were normalized with respect to the absorption spectra between 15500 -16800 cm^{-1}.

It is interesting to note that, in newly investigated $[L^1Sn(O\text{-}ptp)_2]$ and $[L^1P(O\text{-}ptp)_2]^+$ triads both energy and electron transfer processes are reported to occur from axial terpyridine subunits to basal porphyrin (Sn(IV)or P(V)). Finally, in $[L^1P(O\text{-}ptp)_2]^+$ triad porphyrin fluorescence bands are red shifted and this proved that there is a π-π interaction between terpyridine subunit and porphyrin moiety.

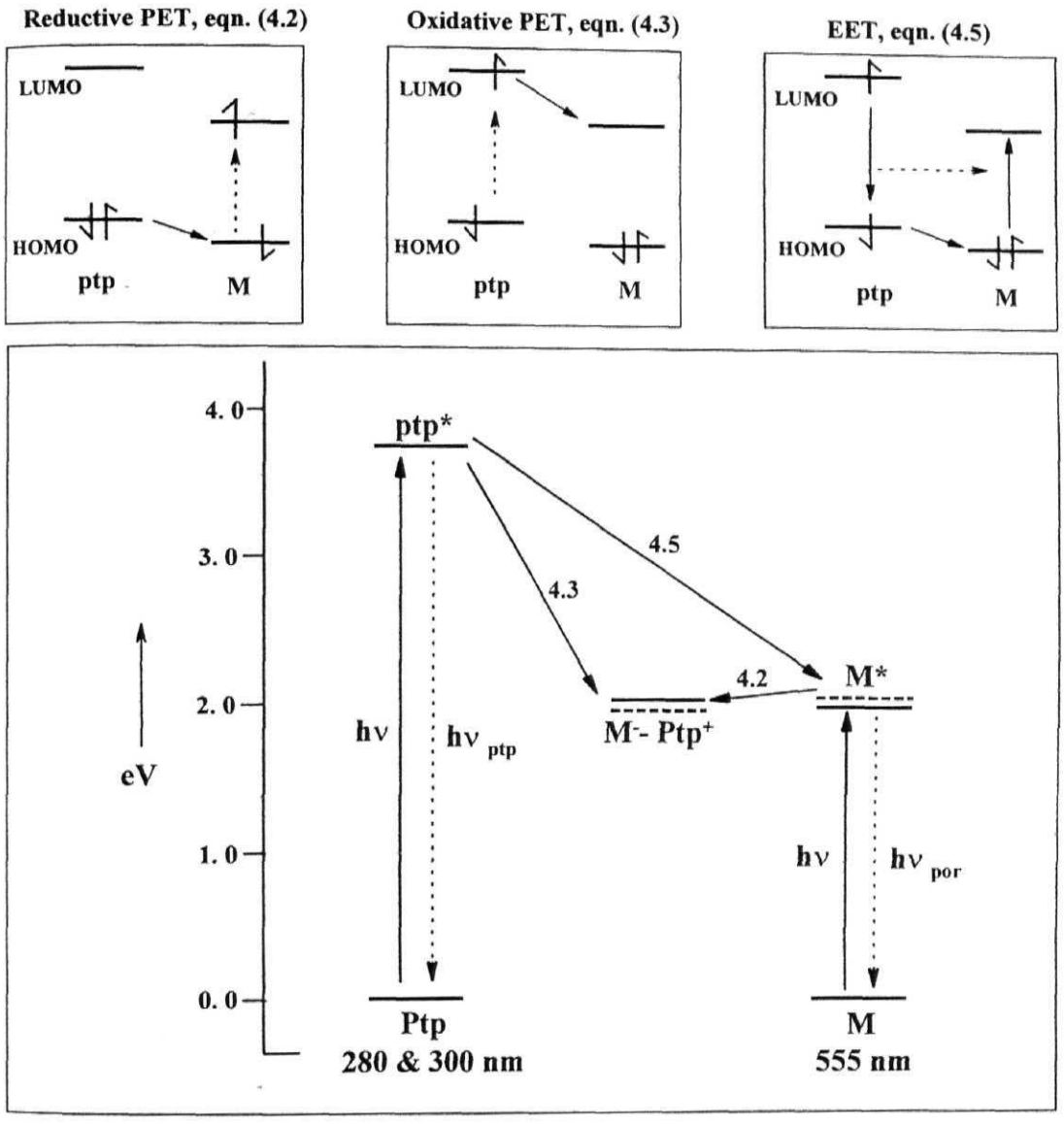

Fig. 4.11 Energies of the singlet and charge transfer states pertaining to the bis(terpyridine) derivatives of Sn(IV) (·····) / P(V) (——) porphyrin triads investigated in this study. Here ptp*, M*, hν, $h\nu_{ptp}$ and $h\nu_{por}$ refer to singlet state of terpyridine, singlet state of porphyrin, terpyridine/porphyrin absorption, terpyridine fluorescence and porphyrin fluorescence, respectively.

4.4 Transition metal ion titrations

Terpyridine ligands are known for very effective and stable complexing agents for transition metals.[61-68] However, only a very few porphyrin based D-A systems are reported that use these units as building blocks through metal coordination. Branda and his co-workers reported synthesis of axially coordinated **Ru(II)** or **Os(II)** terpyridine complex-porphyrin systems.[60] In this part, we focus on the complexation behavior of terpyridine-containing **[L^{1}Sn(O-ptp)$_2$]** and **[L^{1}P(O-ptp)$_2$]$^+$** triads. This was complexed with a variety of transition metals such as **Zn^{2+}**, **Cd^{2+}**, **Hg^{2+}**, **Cu^{2+}**, **Cu^{1+}**, **Ag^{1+}**, **Ni^{2+}**, **Co^{2+}**, **Fe^{2+}** and **Mn^{2+}** ions by using their corresponding acetates/triflates/chlorides. The complexation behavior was studied in detail by means of ^{1}H NMR, UV-visible and fluorescence spectroscopy.

4.4.1 ^{1}H NMR titration

^{1}H NMR spectroscopy was the first method employed in this case in order to study the complexation behavior of the **[L^{1}Sn(O-ptp)$_2$]** and **[L^{1}P(O-ptp)$_2$]$^+$**. It was found that in triad **[L^{1}Sn(O-ptp)$_2$]**, axial Sn-O bond was unstable towards acid (i.e. acetic/triflic acid), this was proved from ^{1}H and ^{1}H-^{1}H COSY NMR spectroscopy whereas in **[L^{1}P(O-ptp)$_2$]$^+$**, axial P-O bond found to be highly stable. Thus, ^{1}H NMR titrations carried out using various concentration of **Zn(OTf)$_2$**, **Zn(OAc)$_2$** and **Ag(OAc)** and constant concentration of **[L^{1}P(O-ptp)$_2$]$^+$**. The Schematic representation of **[L^{1}P(O-ptp)$_2$]$^+$** complexation with **Zn(OAc)$_2$** and **Zn(OTf)$_2$** are shown in Scheme 4.4. Fig. 4.12 illustrates the ^{1}H NMR titration of **[L^{1}P(O-ptp)$_2$]$^+$** triad with **Zn(OTf)$_2$** in CD_3CN. The spectra clearly shows the formation of the complex with **Zn^{2+}** results appearance of complexed peaks (*o$_c$′*, *m$_c$′*, *5$_c$″*, *4$_c$″*, *5$_c$′*, *3$_c$″* and *6$_c$″*), disappearance of the un-complexed **ptp** peaks (*o′*, *m′*, *5″*, *4″*, *5′*, *3″* and *6″*) and at a **[L^{1}P(O-ptp)$_2$]$^+$:Zn**

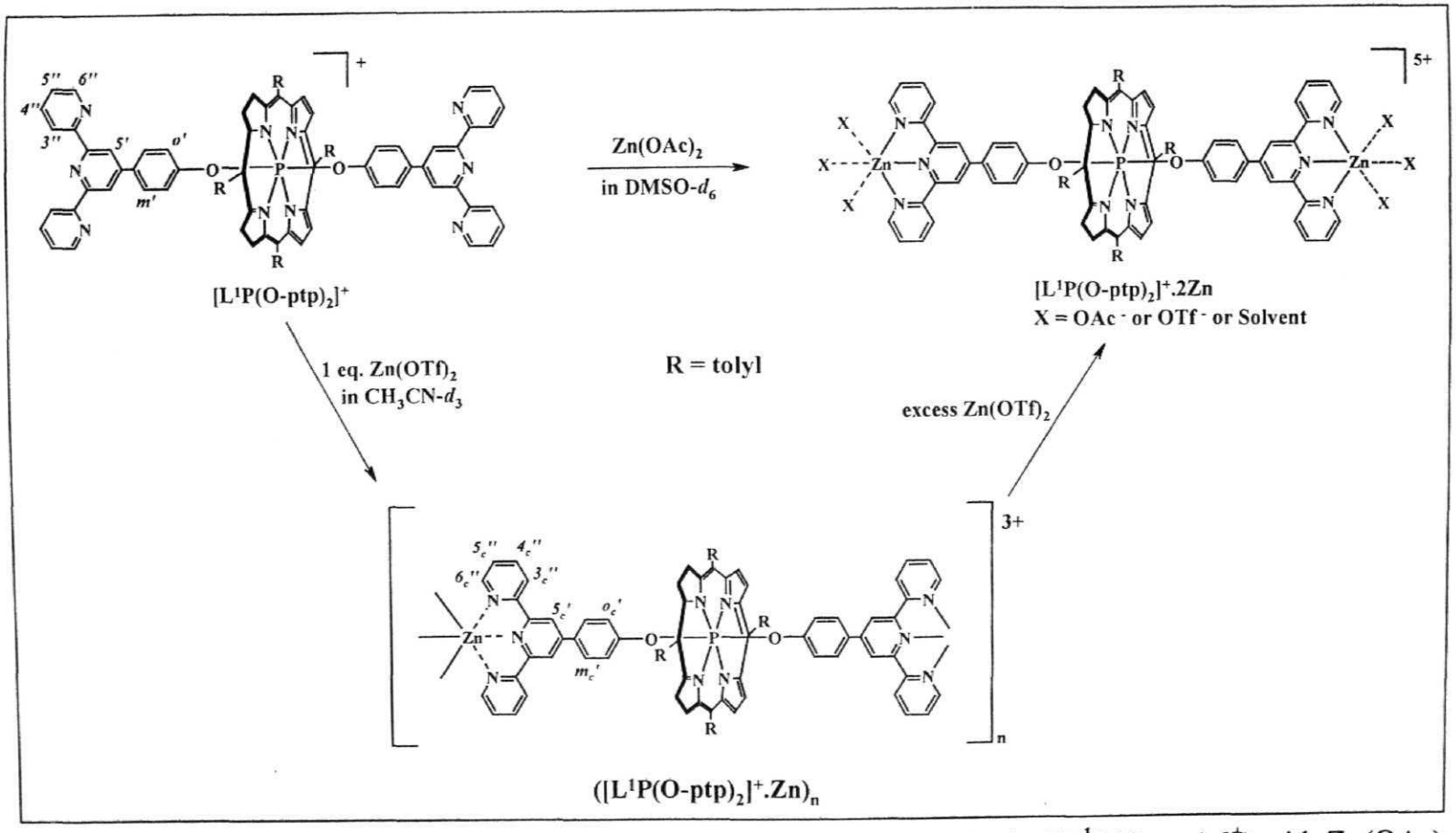

Scheme 4.4 Complexation of terpyridine functionalized phosphorus(V) porphyrin ($[\mathbf{L^1P(O\text{-}ptp)_2}]^+$) with $\mathbf{Zn(OAc)_2}$ in DMSO-d_6 and $\mathbf{Zn(OTf)_2}$ in CD_3CN.

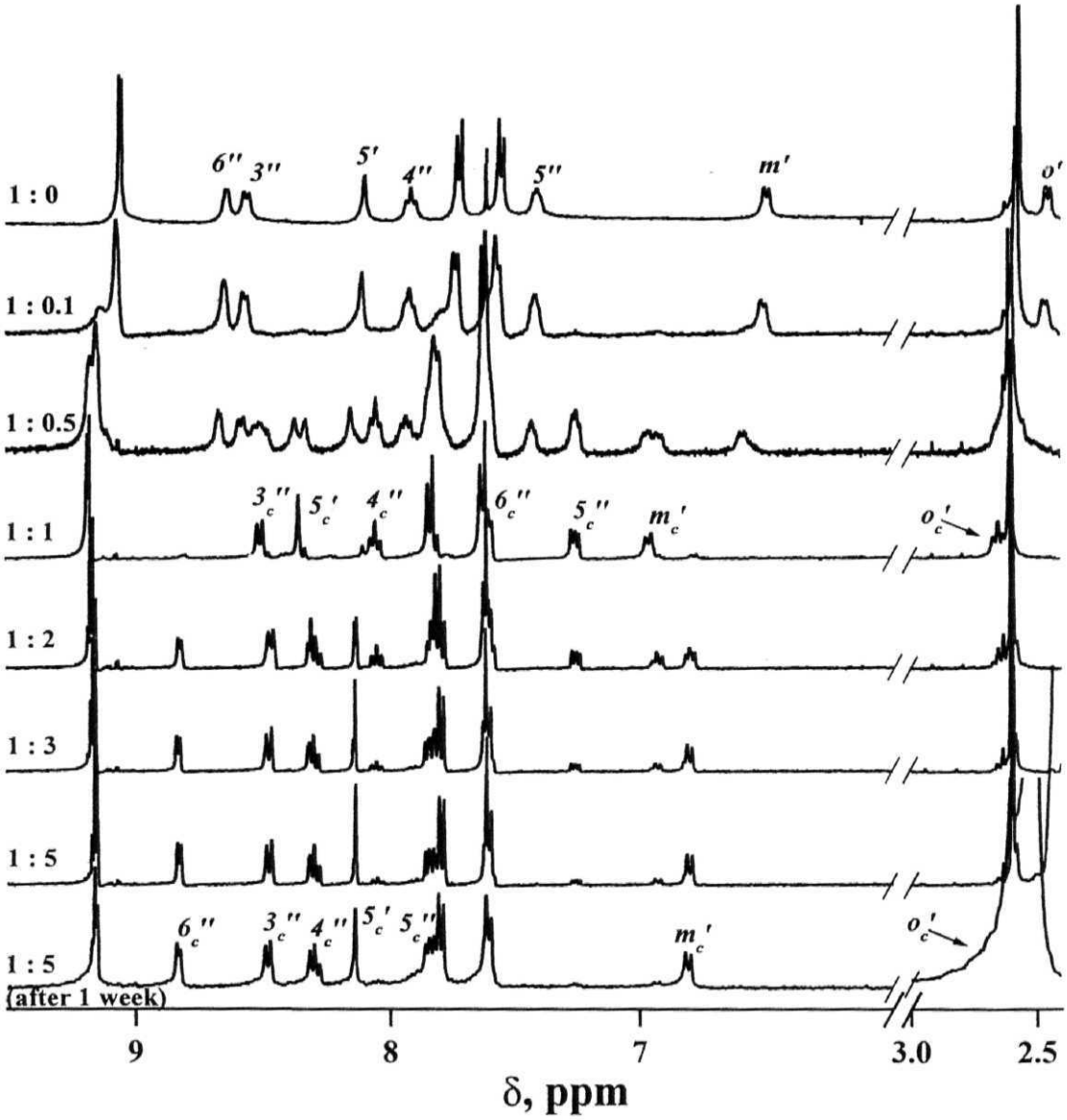

Fig. 4.12 ^{1}H NMR titration of $[L^1P(O\text{-}ptp)_2]^+$ (3.66 x 10^{-3} M) in CD_3CN upon aliquot addition of $Zn(OTf)_2$ (3.25 x 10^{-2} M) with corresponding $[L^1P(O\text{-}ptp)_2]^+$: Zn^{2+} ratios. In last spectrum (1:5 ratio) singlet seen at 2.50 ppm is due to the solvent (400 MHz, 300 K).

ratio of 1:1 uncomplexed **ptp** protons are completely disappeared. From this data the formation of coordination polymer $([L^1P(O\text{-}ptp)_2]^+.Zn)_n$ can be inferred.[63]

Interestingly, the addition of an excess amount of **$Zn(OTf)_2$** gives rise to a second process in which complex **$([L^1P(O\text{-}ptp)_2]^+.Zn)_n$** is dissociated again in favour of an open form **$[L^1P(O\text{-}ptp)_2]^+.2Zn$** with the **$Zn^{2+}$** ion only attached to one **ptp** subunit and its other coordination sites are presumably saturated by solvent molecules.

As illustrated in Fig. 4.13, all species can be distinguished and their concentrations can be quantified by integration of the NMR signals (for example, *m*- and m_c-protons).

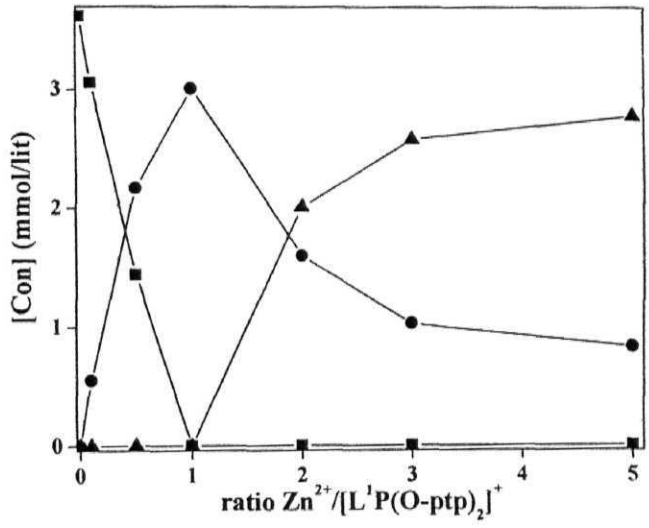

Fig. 4.13 Concentration of **$[L^1P(O\text{-}ptp)_2]^+$** (■), polymer (•) and the open form (▲) upon addition of **$Zn(OTf)_2$** to a 3.6 x 10^{-3} M solution of **$[L^1P(O\text{-}ptp)_2]^+$** in CD_3CN calculated from integrated ^1H NMR signals (*m*- and m_c-protons).

The same NMR titration were carried out for **$[L^1P(O\text{-}ptp)_2]^+$** using **$Zn(OAc)_2$** in DMSO-d_6. Before recording NMR, after each addition, the sample was kept overnight for the complete complexation. The spectra Fig. 4.14 shows analogous changes of the chemical shifts upon complexation and the

disappearance of ligand signals exactly at a 1:2 ratio. The titration curve Fig. 4.15 shows the concentrations of the different species during the titration experiment. These results suggest that the $[L^1P(O\text{-}ptp)_2]^+$ is not forming polymer (i.e. $\{([L^1P(O\text{-}ptp)_2]^+.Zn)_n\}$) upon complexation with Zn^{2+} ions, instead open form $[L^1P(O\text{-}ptp)_2]^+.2Zn$ complex is forming. Here, Zn^{2+} ion expected to be coordinating with only one **ptp** subunit and remaining sites are coordinated with OAc or solvent molecules.

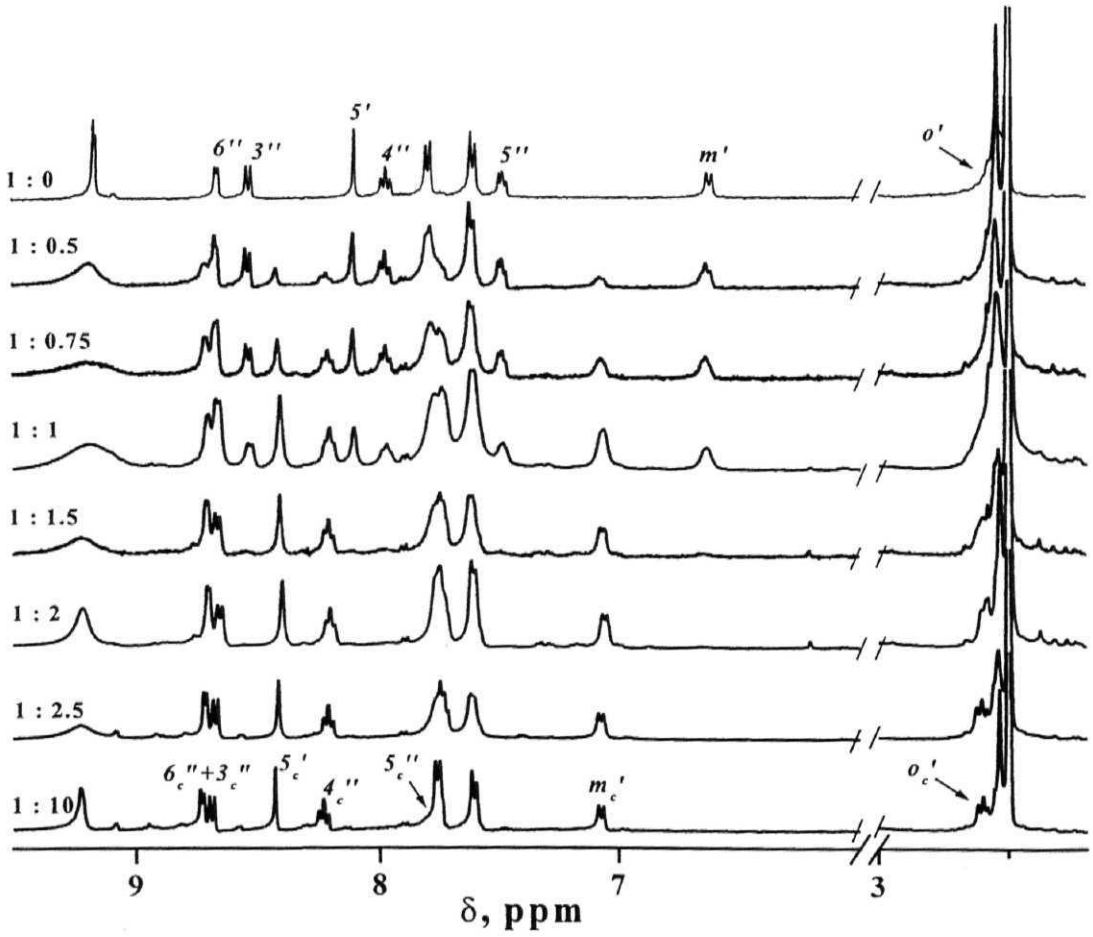

Fig. 4.14 ^{1}H NMR titration of $[L^1P(O\text{-}ptp)_2]^+$ (4.4×10^{-3} M) in DMSO-d_6 upon aliquot addition of $Zn(OAc)_2$ (9.13×10^{-2} M) with corresponding $[L^1P(O\text{-}ptp)_2]^+$:Zn^{2+} ratios. Singlet seen at 2.50 ppm is due to the solvent (400 MHz, 300 K).

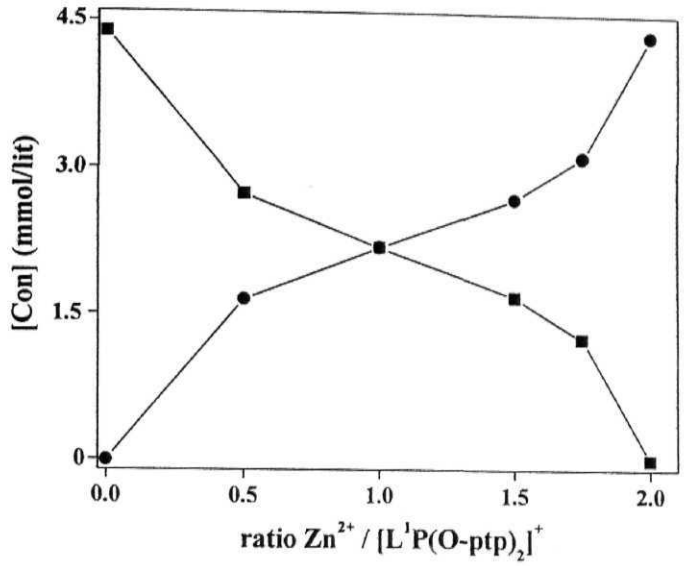

Fig. 4.15 Concentration of $[\mathbf{L^1P(O\text{-}ptp)_2}]^+$ (■) and the open form (•) upon addition of $\mathbf{Zn(OAc)_2}$ to a 4.3 x 10^{-3} M solution of $[\mathbf{L^1P(O\text{-}ptp)_2}]^+$ in DMSO-d_6 calculated from integrated ^{1}H NMR signals (*m*- and m_c-protons).

This complexation differences of $[\mathbf{L^1P(O\text{-}ptp)_2}]^+$ with $\mathbf{Zn(OTf)_2}$ in CD_3CN and $\mathbf{Zn(OAc)_2}$ in DMSO-d_6 was explained by nothing that both acetate and DMSO are much better ligands for $\mathbf{Zn^{2+}}$ than the triflate and CH_3CN. Finally, in addition of $\mathbf{Zn(OTf)_2}$ or $\mathbf{Zn(OAc)_2}$, slight down field shift in the porphyrin peaks (i.e. β-pyrrole, *o*-, *m*- and -CH_3) was observed and peak broadening as is expected for NMR signals of polymers. This complexation, however, does not seem to have any influence on the axial **P-O** bond of $[\mathbf{L^1P(O\text{-}ptp)_2}]^+$, because **P-O** bonds are highly stable in the presence of acids.[33] This was proved by recording ^{1}H-^{1}H COSY NMR spectrum for saturated solution and shown in Fig. 4.16. The ^{31}P NMR signals due to the central phosphorus atoms in $[\mathbf{L^1P(O\text{-}ptp)_2}]^+$**.2Zn** complex appear at –197.04 ppm (with $\mathbf{Zn(OTf)_2}$) and –197.94 ppm ($\mathbf{Zn(OAc)_2}$), respectively. Titration with **Ag(OAc)**, $\mathbf{Ag^{1+}}$ does not show

significant affinity towards **ptp**, hence in ^{1}H NMR spectroscopy the $\Delta\delta$ values are very less.

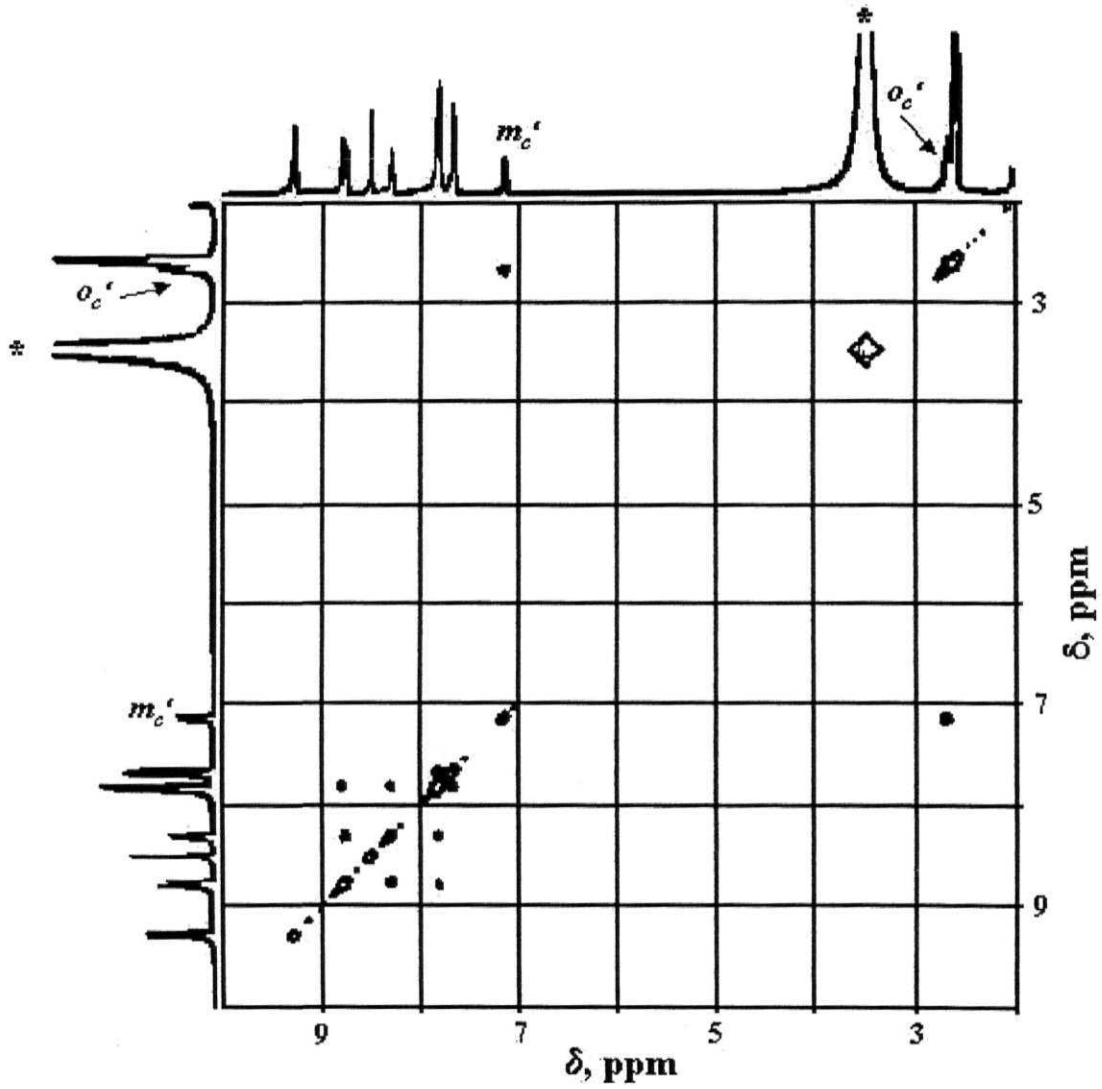

Fig. 4.16 ^{1}H-^{1}H COSY NMR of **[L^{1}P(O-ptp)$_2$]$^+$.2Zn** complex (ratio = 1:10) in DMSO-d_6 (* peak is due to solvent, 400 MHz, 300 K).

4.4.2 UV-visible titrations

Fig. 4.17 shows, UV-visible spectral changes of constant concentration of **[L^{1}P(O-ptp)$_2$]$^+$** with **Zn(OAc)$_2$/Co(OAc)$_2$** acetates in DMSO. Upon titration

there was slight decrease in the intensity of porphyrin Soret band whereas Q-bands almost unchanged at wavelengths > 500 nm. At shorter wavelengths, *i.e.* 250-300 nm characteristic ligand centered **ptp** band intensity decreases and red shifted, simultaneously a new band comes up between 300-400 nm, which is attributed to **ptp** complexation.[62,65] The similar changes were noticed when $[L^1P(O\text{-}ptp)_2]^+$ was titrated with $Ni(OAc)_2$, $Cu(OAc)_2$ and $Cd(OAc)_2$. While titrating with $FeCl_2$ (Fig.4.18) spectral changes observed in the shorter wavelength region remains same with other metals, whereas an increases in absorption intensity was observed in porphyrin Soret and Q-band regions. This change in absorption is attributed to the MLCT band of $[Fe(ptp)_2]^{2+}$ complex.[64,66] By observing the absorption changes of $[L^1P(O\text{-}ptp)_2]^+$ triad at shorter wavelengths with different metal ions (i.e. Zn^{2+}, Cu^{2+}, Co^{2+}, Ni^{2+}, Cd^{2+}, Fe^{2+}), a titration curve was obtained and the binding constants (K) were calculated for 1:1 binding profile by using eqn. 4.8 [81] and are summarized in Table 4.8.

$$\frac{\Delta A}{b} = \frac{S_t K \Delta\varepsilon [L]}{1 + K [L]} \qquad (4.8)$$

Here, ΔA refers to the change in absorbance from initial value at the required wavelength, b is cuvette path length (in cm), S_t is total concentration of $[L^1P(O\text{-}ptp)_2]^+$, K is the apparent binding constant, $\Delta\varepsilon$ is change in extinction coefficient between free and bound $[L^1P(O\text{-}ptp)_2]^+$ and [L] is concentration of the titrating metal ion. On the other hand very weak binding was observed for $[Cu(CH_3CN)_4](PF_6)$, $Mn(OAc)_2$, $Hg(OAc)_2$ and **Ag(OAc)** in UV-visible titrations.

Addition of metal to the solution containing a constant concentration of $[L^1P(O\text{-}ptp)_2]^+$ resulted in a red shift of **ptp** peak and a new peak was observed

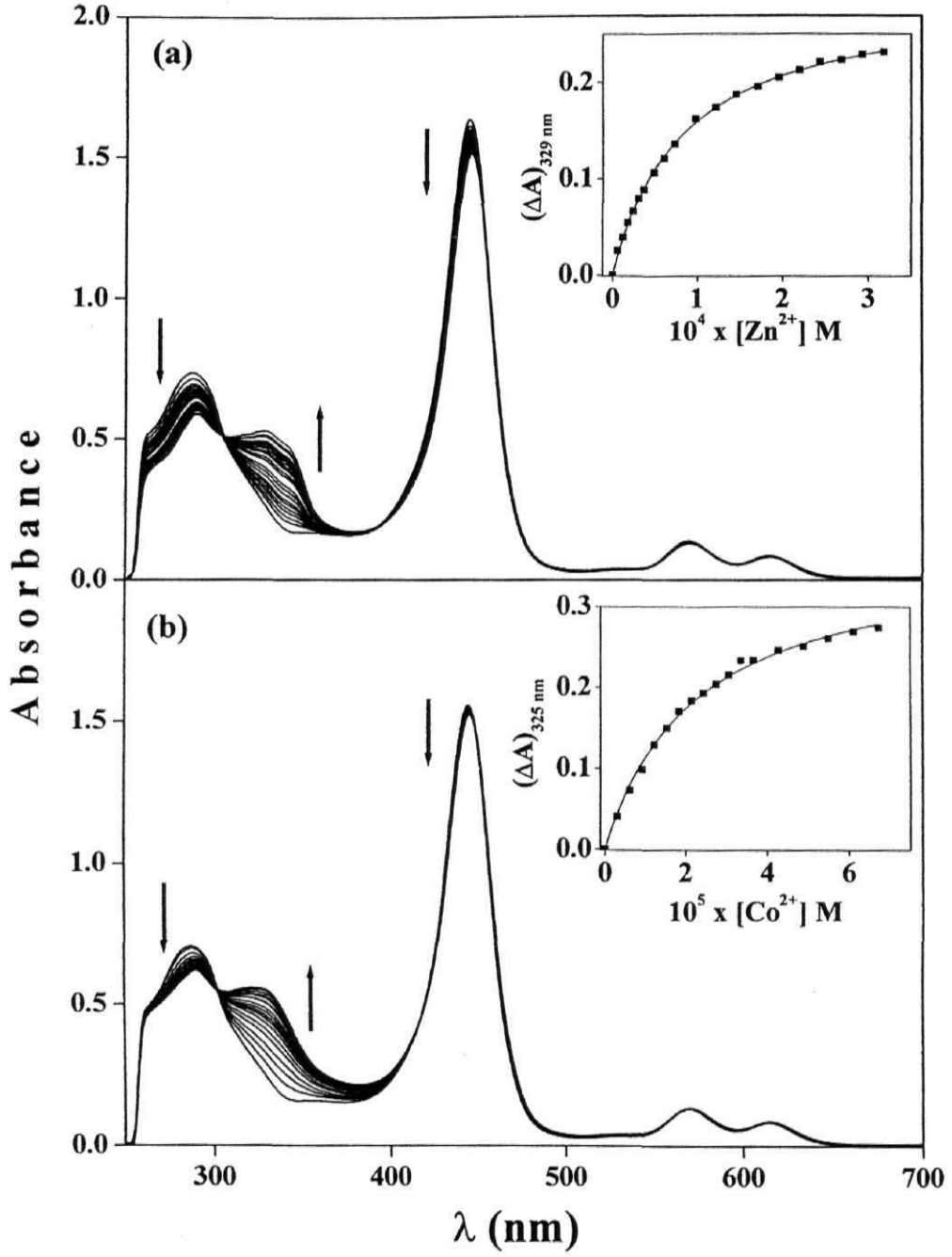

Fig. 4.17 UV-visible titration of $[L^1P(O\text{-}ptp)_2]^+$ (1.066 x 10^{-5} M) with (a) $Zn(OAc)_2$ (1.23 x 10^{-3} M) and (b) $Co(OAc)_2$ (6.15 x 10^{-4} M) in DMSO. The inset in each case shows a fit of the experimental data to a 1:1 binding profile (see, eqn. 4.8).

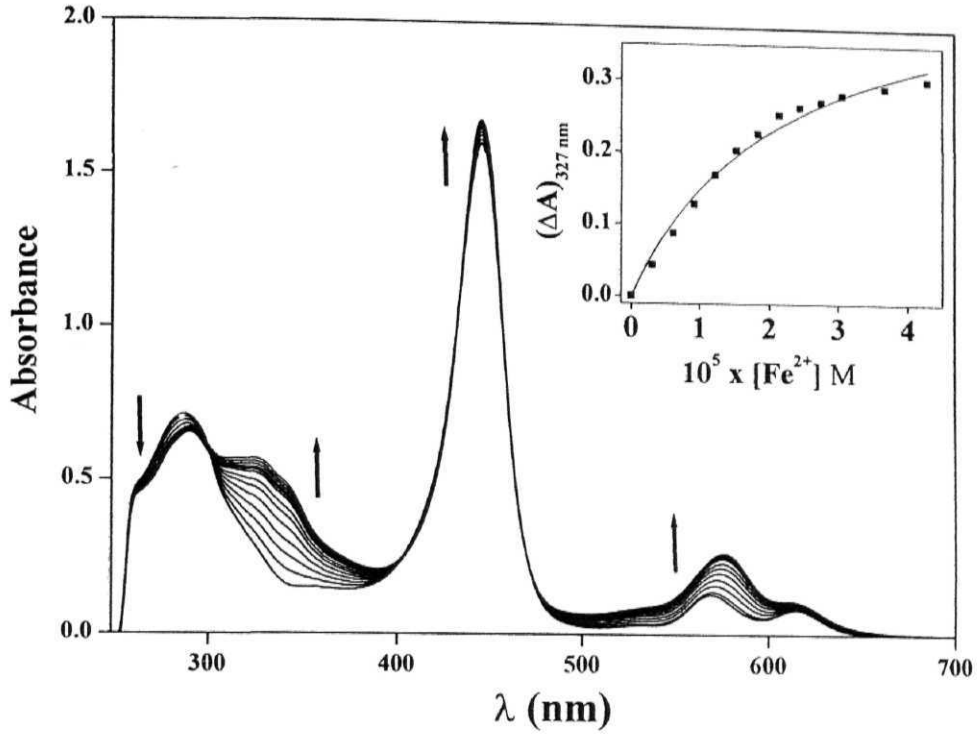

Fig. 4.18 UV-visible titration of $[L^1P(O\text{-}ptp)_2]^+$ (1.066 x 10^{-5} M) with $FeCl_2$ (6.15 x 10^{-4} M) in DMSO. The inset shows a fit of the experimental data to a 1:1 binding profile (see, eqn. 4.8).

between 300-400 nm, suggesting complexation of the appended **ptp** subunit with metal ion.[62,65] After a linear increase of the absorption with the concentration, the equivalence point was reached, indicating that the axial **ptp** groups were complexed completely. No significant change of the absorption bands was observed upon further titration. Although the coordination of metal ions to the **ptp** units of $[L^1P(O\text{-}ptp)_2]^+$ is strong, there is little electronic interaction between the metal-complex and the porphyrin chromophore according to UV-visible spectroscopy. Similar changes were observed when $[L^1P(O\text{-}ptp)_2]^+$ triad was titrated with $Zn(OTf)_2$ or $Cu(OTf)_2$ in CH_3CN.

4.4.3 Fluorescence titrations

Fig. 4.19 illustrates the metal ion (($\mathbf{Zn(OAc)_2}$ and $\mathbf{Co(OAc)_2}$)) induced fluorescence of $\mathbf{[L^1P(O\text{-}ptp)_2]^+}$ triad in DMSO. Interestingly, addition of the $\mathbf{Zn(OAc)_2}$, enhancement of the porphyrin fluorescence intensity and red shift of the spectral maximum was observed. At the saturated point, the calculated fluorescence quantum yield, is found to be 0.038 and is nearly 20% enhancement with respective that of reference compound $\mathbf{[L^1P(OH)_2]^+}$ (ϕ = 0.06 in DMSO). Similar fluorescence enhancement (quantum yields) was observed with $\mathbf{Cd(OAc)_2}$ titrations. On the other hand titration with $\mathbf{Zn(OTf)_2}$ in CH_3CN, enhancement of the porphyrin fluorescence slightly more, compare to that of $\mathbf{Zn(OAc)_2/Cd(OAc)_2}$ titrations. At saturation point, the quantum yield was found to be 0.034 which is 34% enhancement with respective that of reference compound $\mathbf{[L^1P(OH)_2]^+}$ (ϕ = 0.054 in CH_3CN).

This fluorescence enhancement is probably due to the fact that PET between the **ptp** and porphyrin is forbidden by the complexation of **ptp** subunit. After forming the complex with metals, **ptp** becomes electron deficient compared to free **ptp**, results the oxidation potential of the complexed **ptp** is expected to be shift towards more positive side [82,83] (>1650 mV) than the corresponding **ptp** peak in $\mathbf{[L^1P(O\text{-}ptp)_2]^+}$ and the resultant free energy change (ΔG_{PET}) for this process become more positive (>0.04 eV) or endergonic. As a result, the added $\mathbf{Zn^{2+}/Cd^{2+}}$ upon complexing with **ptp**, inhibits the excited state electron transfer (i.e. reductive electron transfer) and consequently enhances the porphyrin fluorescence emission.

On the other hand titration with $\mathbf{Cu^{2+}}$, $\mathbf{Ni^{2+}}$, $\mathbf{Co^{2+}}$ and $\mathbf{Fe^{2+}}$ ions fluorescence intensity was quenched in CH_3CN or DMSO due to the paramagnetic effect, whereas there was no change in fluorescence intensity with $\mathbf{Mn^{2+}}$, $\mathbf{Cu^{1+}}$, $\mathbf{Ag^{1+}}$ and $\mathbf{Hg^{2+}}$ indicating very weak complexation with **ptp** subunit.

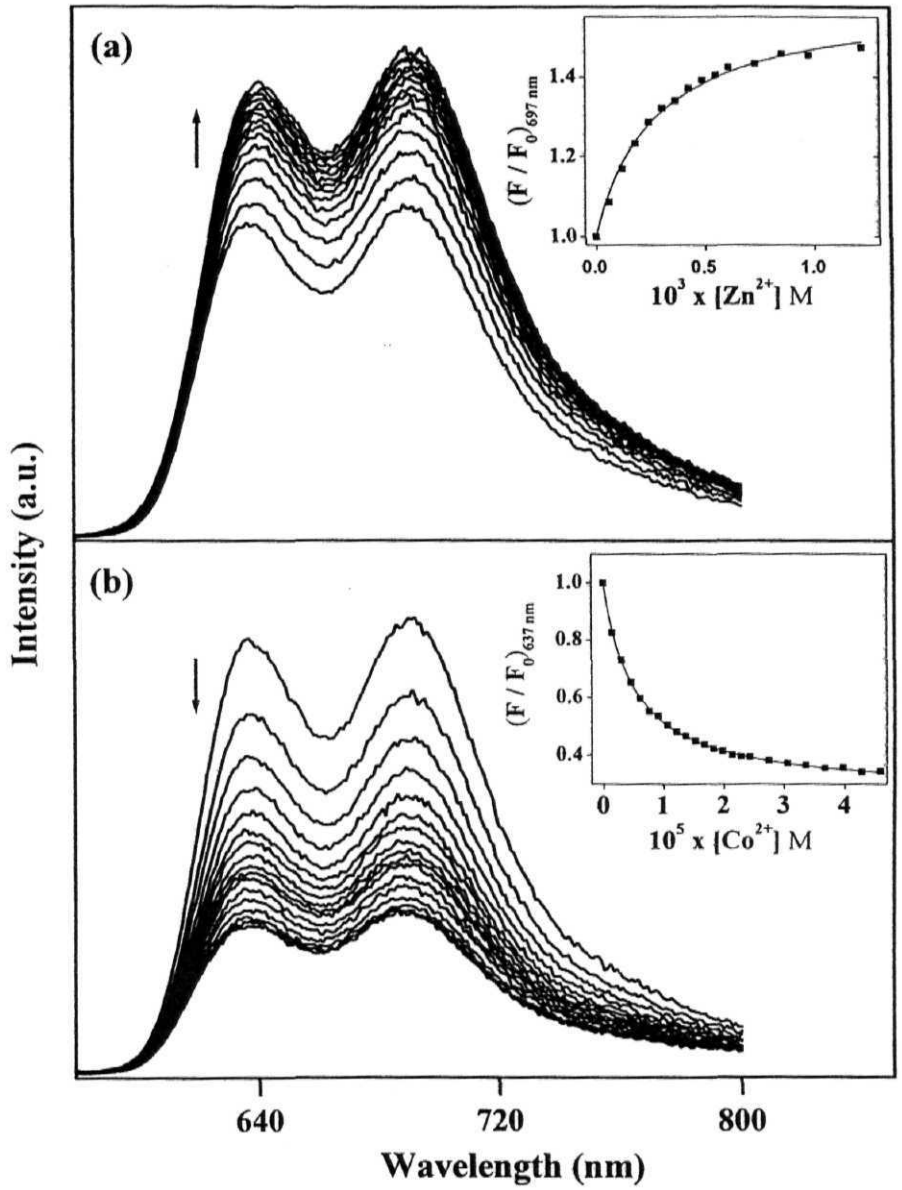

Fig. 4.19 Fluorescence titration of $[L^1P(O\text{-}ptp)_2]^+$ (1.066 x 10^{-5} M) with (a) $Zn(OAc)_2$ (1.23 x 10^{-2} M) and (b) $Co(OAc)_2$ (6.15 x 10^{-4} M) in DMSO at λ_{ex} = 566 nm. Inset shows plots for the enhancing/quenching of $[L^1P(O\text{-}ptp)_2]^+$ by addition of Zn^{2+} and Co^{2+} ions. The inset shows a fit of the experimental data to a 1:1 binding profile (see, eqn. 4.9).

Inset in Fig 4.19 shows the variation of fluorescence intensity with increasing metal ion concentration, where F_0 is the initial fluorescence intensity and F, the fluorescence intensity after each metal ion addition. The binding constants (K) were calculated for 1:1 binding profile by using eqn. 4.9 [84] and are summarized in Table 4.8.

$$\frac{F}{F_0} = \frac{1 + (k_{11}/k_s)\, K\, [L]}{1 + K\, [L]} \qquad (4.9)$$

Here k_{11} is proportionality constant of the bound complex and k_s is the the proportionality constant for $[L^1P(O\text{-}ptp)_2]^+$ triad.

Table 4.8 Binding constants of $[L^1P(O\text{-}ptp)_2]^+$ with various metal ions obtained from UV-visible and steady-state fluorescence measurements [a]

Metal	UV-visible	Fluorescence
Zn^{2+}	1.27×10^4 4.03×10^4 [b]	3.60×10^3
Cu^{2+}	5.7×10^3 3.35×10^4 [b]	4.55×10^4 9.10×10^4 [b]
Ni^{2+}	1.40×10^4	4.84×10^4
Co^{2+}	4.30×10^4	1.96×10^5
Fe^{2+}	4.44×10^4 [c]	-
Cd^{2+}	5.9×10^3	1.7×10^3

(a) Error limits: $K \pm 10\%$. (b) with metal triflates (c) with $FeCl_2$.

Fig. 4.20 shows changes in fluorescence when excited at the isosbestic point, 300 nm (which was obtained from UV-visible titration, where the complexed and un-complexed equilibrium exist) in presence of $\mathbf{Zn^{2+}}$ or $\mathbf{Cd^{2+}}$ ions and there was a fluorescence enhancement was observed in porphyrin emission bands. After each addition of $\mathbf{Zn(OTf)_2}$ to the solution $\mathbf{[L^1P(O\text{-}ptp)_2]^+}$ in CH_3CN, it was excited at an isosbestic point 300 nm where the ratio of light absorbed by the **ptp** subunit and the porphyrin unit is 67:33. The enhancement in fluorescence intensity of $\mathbf{[L^1P(O\text{-}ptp)_2]^+}$ is accounted for by the direct excitation of porphyrin and also excitation energy transfer from **ptp** to porphyrin moiety. After reaching the saturation point, the absorption and excitation spectra were recorded. When emission was recorded at the porphyrin emission maximum (670 nm), the excitation spectra of these saturated solution showed bands characteristic of complexed **ptp** absorption peaks. Fig. 4.21 shows the corrected and normalized excitation spectrum overlayed with the corresponding absorption spectra in CH_3CN. A comparison of these spectra in the $4.0 \times 10^4 - 2.6 \times 10^4$ cm^{-1} region gave almost 100% energy transfer efficiencies in this case.

As discussed in previous section 4.3.3, upon excitation of **ptp** subunit in compound $\mathbf{[L^1P(O\text{-}ptp)_2]^+}$, there was 98 ± 10% fluorescence quenching observed. This was explained by excitation energy and photoinduced electron transfer from excited singlet state of **ptp** subunit to the ground state of the porphyrin. From the excitation spectra (Fig. 4.10), only 61 ± 10% is assigned due to EET and balance 38 ± 10% could be from PET. Whereas here, from Fig. 4.21, excitation of **ptp** subunit with addition of $\mathbf{Zn^{2+}}$ ion have shown that there is a 100 ± 10% energy transfer from the excited state of **ptp** to the ground state of porphyrin. These results suggest that due to complexation of **ptp** subunits, the PET is dominated by the EET.

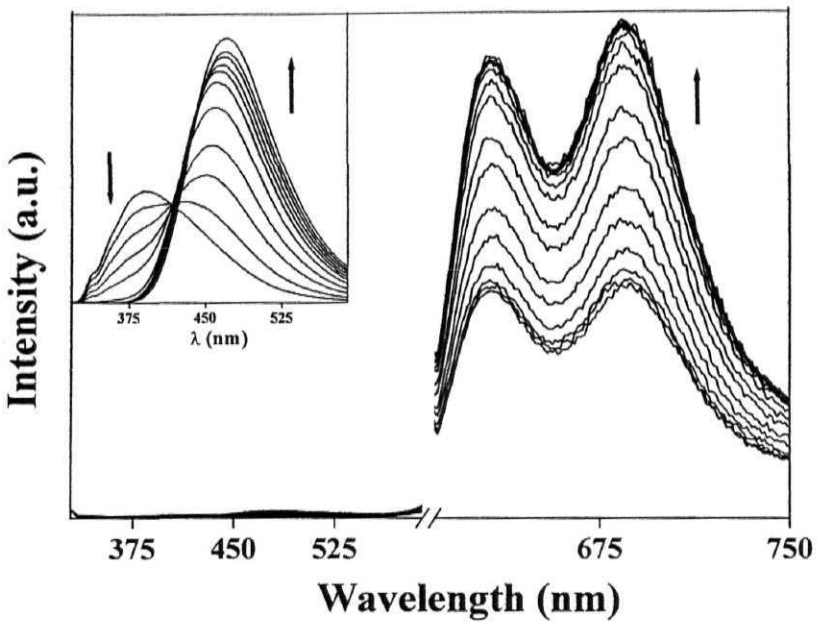

Fig. 4.20 Fluorescence titration of $[L^1P(O\text{-}ptp)_2]^+$ (6.08 x 10^{-6} M) with $Zn(OTf)_2$ (1.27 x 10^{-4} M) in CH_3CN at isosbestic point, λ_{ex} = 300 nm. The inset shows a fluorescence titration of **OMe-ptp** (6.2 x 10^{-6} M) with $Zn(OTf)_2$ (1.3 x 10^{-4} M) in CH_3CN at λ_{ex} = 300 nm.

In Fig. 4.20 inset shows the fluorescence spectra of **OMe-ptp** with the Zn^{2+} ion addition in CH_3CN. By aliquot addition of Zn^{2+} to the solution of **OMe-ptp**, the fluorescence intensity is increasing with large red shift (~80 nm) in fluorescence maximum.[62] The observation that there exists a considerable spectral overlap integral (J) increases between the emission of **ptp** and the absorption of porphyrin in this D-A systems (compare the corresponding spectra in Fig 4.20 & Table 4.3). According to both Forster[85] and Dextor[86] mechanisms, the rate of energy transfer is proportional to spectral overlap integral (J) of the donor emission and acceptor absorption. Thus, we analyzed based on these mechanisms, energy transfer increases (enhancement in fluorescence intensity of porphyrin

bands) with J and it reaches 100% at saturated point (i.e. complete complexation of **ptp** units).

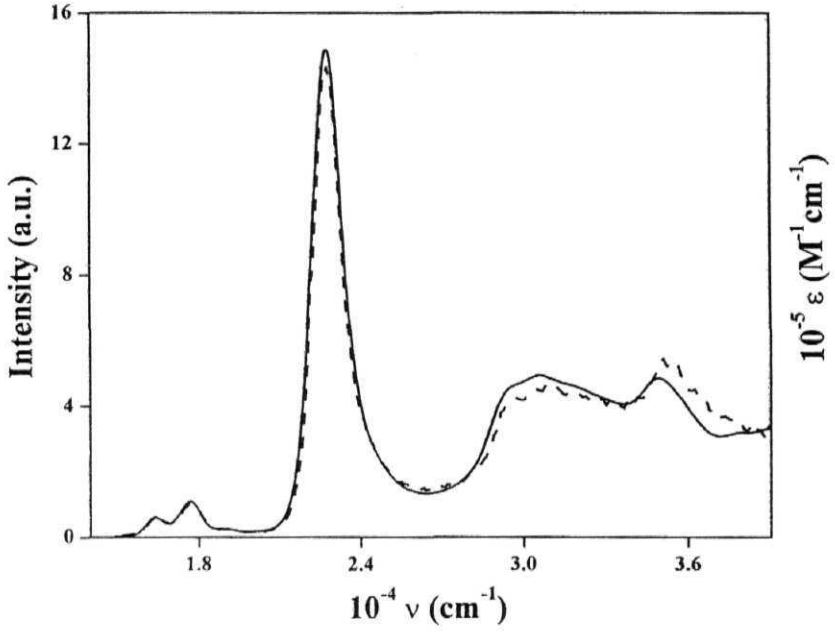

Fig. 4.21 Overlay of **$[L^1P(O\text{-}ptp)_2]^+.2Zn$** complex excitation (-------) and absorption (——) spectra in CH_3CN, λ_{em} = 670 nm. The excitation spectra were corrected for the instrument response function and were normalized with respected to the absorption spectra between 15500-17000 cm^{-1}.

4.5 Summary

In summary, a new axial-bonding type 'porphyrin-terpyridine' triads based on the Sn(IV)/P(V) porphyrin systems have been synthesized and characterized by spectral and electrochemical methods. UV-visible and redox data of these D-A systems suggest the absence or intramolecular π-π interaction between the porphyrin and the terpyridine. Photophysical properties have also been investigated and the results are interpreted in terms of intramolecular electron and energy transfer mechanisms. In both mechanisms axial **ptp** subunit

act as a donor and Sn(IV) or P(V) porphyrin as a acceptor. ^{1}H NMR and UV-visible titrations suggest that although the coordination of metal ions to the **ptp** units of $[L^1P(O\text{-}ptp)_2]^+$ is strong, there is little electronic interaction between the metal-complex and the porphyrin chromophore. In fluorescence titrations it was found that the PET and EET reactions are controlled by metal ion coordination with **ptp** subunits. A schematic representation of these PET and EET processes are shown in Fig. 4.22. When excited at 566 nm with addition of Zn^{2+} or Cd^{2+}, PET process was inhibited from ground state of **ptp** subunit to excited state of porphyrin, results enhancement in porphyrin fluorescence. On the other hand when excited at the isosbestic point at 300 nm, PET was suppressed and EET from excited **ptp** subunit to the ground state of porphyrin was enhanced.

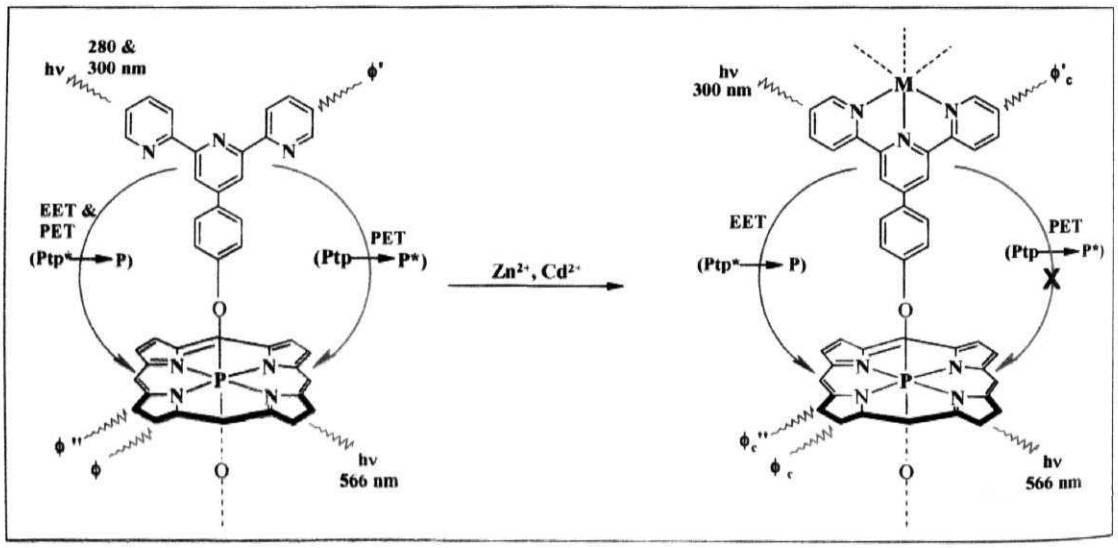

Fig. 4.22 A Schematic diagram shows the modulation of PET and EET by transition metal (Zn^{2+}, Cd^{2+}) ions. Where ϕ, ϕ' and ϕ'' are fluorescence quantum yield of phosphorus(V) porphyrin (at λ_{ex} = 566 nm), **ptp** (at λ_{ex} = 280 or 300 nm) and phosphorus(V) porphyrin (at λ_{ex} = 280 or 300 nm), respectively. $\phi_c(>\phi)$, ϕ'_c and $\phi''_c(>\phi''_c)$ also refers same but it corresponds to metal-complex triad.

4.6 References

1. Dierickx, C. C. *Compr. Ser. Photosci.* **2001**, *2*, 271.
2. Pogue, B. W.; Ortel, B.; Chen, N.; Redmond, R. W.; Hasan, T. *Cancer Res.* **2001**, *61*, 717.
3. Renno, R. Z.; Miller, J. W. *Adv. Drug Deliv. Rev.* **2001**, *52*, 63.
4. Kaplan, M. J.; Somers, R. G.; Greenberg, R. H.; Ackler, J. *J. Surg. Oncol.* **1998**, *76*, 121.
5. Kessel, D.; Morgan, A.; Garbo, G. M. *Photochem. Photobiol.* **1991**, *54*, 193.
6. Embleton, M. L.; Nair, S. P.; Cookson, B. D.; Wilson, M. *J. Antimicrob. Chemother.* **2002**, *50*, 857.
7. Coates Jr. W. D.; Currie, J. W.; Mejias, Y.; Narciso, H. L.; Faxon, D. P. *Biochem. Cell Biol.* **1996**, *74*, 325.
8. Philippova, T. O.; Galkin, B. N.; Golovenko, N. Y.; Zhilina, Z. I.; Vodzinskii, S. V. *J. Porphyrins Phthalocyanines* **2000**, *4*, 243.
9. Drummond, G. S.; Smith, T. J.; Kappas, A. *Pharmacology* **1996**, *52*, 178.
10. Dwyer, B. E.; Lu, S.-Y.; Laitinen, J. T.; Nishimura, R. N. *J. Neurochem.* **1998**, *71*, 2497.
11. Compans, R. W.; Marzilli, L. G.; Sears, A. E.; Dixon, D. W. *International Patent WO 0*, **2003**, *357*, 176.
12. Neurath, A. R.; Jiang, S.; Debnath, A. K. *International Patent WO 9*, **1995**, *517*, 893.
13. Chaniotakas, N. A.; Park, S. B.; Meyerhoff, M. E. *Anal. Chem.* **1989**, *61*, 566.
14. Grigg, R.; Norbert, W. D. J. A. *Chem. Commun.* **1992**, 1298.
15. Szulbinski, W.; Strojek, J. W. *Inorg. Chim. Acta.* **1986**, *118*, 91.
16. Harel, Y.; Manassen, J. *J. Am. Chem. Soc.* **1977**, *99*, 5817.
17. Whitten, D. G.; You, J. C.; Carroll, F. A. *J. Am. Chem. Soc.* **1971**, *93*, 2291.

18. Tong, Y.; Hamilton, D. G.; Meillon, J.-C.; Sanders, J. K. M. *Org. Lett.* **1999**, *1*, 1343.

19. Hawley, J. C.; Bampos, N.; Abraham, R. J.; Sanders, J. K. M. *Chem. Commun.* **1998**, 661.

20. Kim, H.-J.; Bampos, N.; Sanders, J. K. M. *J. Am. Chem. Soc.* **1999**, *121*, 8120.

21. Redman, J. E.; Feeder, N.; Teat, S. J.; Sanders, J. K. M. *Inorg. Chem.* **2001**, *40*, 2486.

22. Webb, S. J.; Sanders, J. K. M. *Inorg. Chem.* **2000**, *39*, 5920.

23. Fallon, G. D.; Langford, S. J.; Lee, M. A.-P.; Lygris, E. *Inorg. Chem. Commun.* **2002**, *5*, 715.

24. Crossley, M. J.; Thordarson, P.; Wu, R. A.-S. *J. Chem. Soc., Perkin Trans. 1* **2001**, 2294.

25. Sayer, P.; Gouterman, M.; Connell, C. R. *Acc. Chem. Res.* **1982**, *15*, 73.

26. Mangani, S.; Meyer, E. F.; Cullen, D. L.; Tsutsui, M.; Carrano, C. J. *Inorg. Chem.* **1983**, *22*, 400.

27. Marrese, C. A.; Carrano, C. J. *Inorg. Chem.* **1984**, *23*, 3961.

28. Pandian, R. P.; Chandrashekar, T. K.; Chandrashekar, V. *Ind. J. Chem.* **1991**, *30A*, 579.

29. Barbour, T.; Belcher, W. J.; Brothers, P. J.; Rickard, C. E. F.; Ware, D. C. *Inorg. Chem.* **1992**, *31*, 746.

30. Lin, Y.-H.; Lin, C.-C.; Chen, J.-H.; Zeng, W.-F.; Wang, S.-S. *Polyhedron* **1994**, *13*, 2887.

31. Lin, Y.-H.; Sheu, M.-T.; Lin, C.-C.; Chen, J.-H.; Wang, S.-S. *Polyhedron* **1994**, *13*, 3091.

32. Liu, Y.-H.; Benassy, M.-F.; Chojnacki, S.; D'Souza, F.; Barbour, T.; Belcher, J. W.; Brothers, P. J.; Kadish, K. M. *Inorg. Chem.* **1994**, *33*, 4480.

33. Rao, T. A.; Maiya, B. G. *Chem. Commun.* **1995**, 939.
34. Rao, T. A.; Maiya, B. G. *Inorg. Chem.* **1996**, *35*, 4829.
35. Reddy, D. R.; Maiya, B. G. *Chem. Commun.* **2001**, 117.
36. Reddy, D. R.; Maiya, B. G. *J. Phys. Chem. A* **2003**, *107*, 6326.
37. Arnold, D. P.; Blok, J. *Coord. Chem. Rev.* **2004**, *248*, 299.
38. Hawley, J. C.; Bampos, N.; Sanders, J. K. M. *Chem. Eur. J.* **2003**, *9*, 5211.
39. Fallon, G. D.; Lee, M. A.-P.; Langford, S. J.; Nichols, P. *J. Org. Lett.* **2002**, *4*, 1895.
40. Smith, G.; Arnold, D. P.; Kennard, C. H. L.; Mak, T. C. W. *Polyhedron* **1991**, *10*, 509.
41. Reddy, D. R.; Maiya, B. G. *J. Porphyrins Pthalocyanines* **2002**, *6*, 3.
42. Giribabu, L.; Kumar, A. A.; Neeraja, V.; Maiya, B. G. *Angew. Chem., Int. Ed.* **2001**, *40*, 3621.
43. Kumar, A. A.; Giribabu, L.; Reddy, D. R.; Maiya, B. G. *Inorg. Chem.* **2001**, *40*, 6757.
44. Segawa, H.; Kunimoto, K.; Nakamoto, A.; Shimidzu, T. *J. Chem. Soc. Perkin Trans. 1* **1992**, 939.
45. Segawa, H.; Nakamoto, A.; Shimidzu, T. *Chem. Commun.* **1992**, 1066.
46. Segawa, H.; Kunimoto, K.; Susumu, K.; Taniguchi, M.; Shimidzu, T. *J. Am. Chem. Soc.* **1994**, *116*, 11193.
47. Susumu, K.; Kunimoto, K.; Segawa, H.; Shimadzu, T. *J. Phys. Chem.* **1995**, *99*, 29.
48. Susumu, K.; Segawa, H.; Shimadzu, T. *Chem. Lett.* **1995**, 929.
49. Hirakawa, K.; Segawa, H. *J. Photochem. Photobiol. A Chem.* **1999**, *123*, 67.
50. Yamamoto, A.; Satoh, W.; Yamamoto, Y.; Akiba, K.-Y. *Chem. Commun.* **1999**, 147.

51. Yamaguchi, H.; Kamachi, M.; Harada, A. *Angew. Chem., Int. Ed.* **2000**, *39*, 3829.
52. Yamamoto, Y.; Akiba, K.-Y. *J. Organomet. Chem.* **2000**, *611*, 200.
53. Akiba, K.-Y.; Nadano, R.; Satoh, W.; Yamamoto, Y.; Nagase, S.; Ou, Z.; Tan, X.; Kadish, K. M. *Inorg. Chem.* **2001**, *40*, 5553.
54. Delaere, D.; Nguyen, M. T. *Chem. Phys. Lett.* **2003**, *376*, 329.
55. Baranoff, E.; Collin, J.-P.; Flamigni, L.; Sauvage, J.-P. *Chem. Soc. Rev.* **2004**, *33*, 147.
56. Flamigni, L.; Barigelletti, F.; Armaroli, N.; Collin, J.-P.; Dixon, I. M.; Sauvage, J.-P. Williams, J. A. G. *Coord. Chem. Rev.* **1999**, *190-192*, 671.
57. Sauvage, J.-P.; Harriman, A. *Chem. Soc. Rev.* **1996**, *25*, 41.
58. Uyeda, H. T.; Zhao, Y.; Wostyn, K.; Asselberghs, I.; Clays, K.; Persoons, A.; Therien, M. J. *J. Am. Chem. Soc.* **2002**, *124*, 13806.
59. Norsten, T. B.; Chichak, K.; Branda, N. R. *Chem. Commun.* **2001**, 1794.
60. Chichak, K.; Branda, N. R. *Chem. Commun.* **1999**, 523.
61. Barigelletti, F.; Flamigni, L.; Calogero, G.; Hammarström, L.; Sauvage, J.-P.; Collin, J.-P. *Chem. Commun.* **1998**, 2333.
62. Goodall, W.; Williams, J. A. G. *Chem. Commun.* **2001**, 2514.
63. Hofmeier, H.; El-ghayoury, A.; Schenning, A. P. H. J.; Schubert, U. S. *Chem. Commun.* **2004**, 318.
64. Dobrawa, R.; Wurthner, F. *Chem. Commun.* **2002**, 1878.
65. Turbnek, M. L.; Moore, P.; Errington, W. *J. Chem. Soc., Dalton Trans.* **2000**, 441.
66. Hofmeier, H.; Schubert, U. S. *Macromol. Chem. Phys.* **2003**, *204*, 1391.
67. Moutet, J.-C.; Saint-Aman, E.; Royal, G.; Tingry, S.; Ziessel, R. *Eur. J. Inorg. Chem.* **2002**, 692.

68. Ziener, U.; Breuning, E.; Lehn, J.-M.; Wegelius, E.; Rissanen, K.; Baum, G.; Fenske, D.; Vaughan, G. *Chem. Eur. J.* **2000**, *6*, 4132.

69. Fuhrhop, J.-H.; Smith, K. M.; In *Porphyrins and Metalloporphyrins*; Smith, K. M.; Ed.; Elsevier: Amsterdam, **1975**; p. 179.

70. Spahni, W.; Calzaferri, G. *Helv. Chim. Acta* **1984**, *67*, 450.

71. Kadish, K. M.; Xu, Q. Y. Y.; Maiya, B. G.; Barbe, J.-M.; Guilard, R. *J. Chem. Soc., Dalton Trans.* **1989**, 1531.

72. Corwin, A. H.; Collins III, O. D. *J. Org. Chem.* **1962**, *27*, 3060.

73. *Multinuclear NMR*; Mason, J., Ed.; Plenum Press: New York, **1987**; p. 369.

74. Arnold, D. P. *Polyhedron* **1986**, *5*, 1957.

75. Arnold, D. P.; Bartley, J. P. *Inorg. Chem.* **1994**, *33*, 1486.

76. Abraham, R. J.; Bedford, G. R.; McNeillie, D.; Wright, B. *Org. Magn. Reson.* **1980**, *14*, 418.

77. Nicholson, R. S.; Shain, I. *Anal. Chem.* **1964**, *36*, 706.

78. Fuhrhop, J. H.; Kadish, K. M.; Davis, D. G. *J. Am. Chem. Soc.* **1973**, *95*, 5140.

79. Mutai, T.; Cheon, J.-D.; Arita, S.; Araki, K. *J. Chem. Soc., Perkin Trans. 2* **2001**, 1045.

80. Rehm, D.; Weller, A. *Isr. J. Chem.* **1970**, *8*, 259.

81. Connors, K. A. *Binding constants:* John Wiley and Sons: New York, **1987**, p. 141.

82. Yoshikawa, N.; Matsumura-Inoue, T. *Analytical Science* **2003**, *19*, 761.

83. Prasanna de Silva, A.; Dixon, I. M.; Gunaratne, H. Q. N.; Gunnlaugsson, T.; Maxwell, P. R. S.; Rice, T. E. *J. Am. Chem. Soc.* **1999**, *121*, 1393.

84. Connors, K. A. *Binding constants:* John Wiley and Sons: New York, **1987**, p. 340.

85. Forster, Th. *Discuss. Faraday Soc.* **1959**, *27*, 7.

86. Dexter, D. L. *J. Chem. Phys.* **1953**, *21*, 836.

CHAPTER 5

Porphyrin dyads and triads with ruthenium(II) bis-terpyridine complex: Synthesis, spectroscopy and photochemistry.

5.1 Introduction

It is of interest to know whether such a preference over the 'axial pathway', for intramolecular EET and PET in a porphyrin-based D-A system as described above, can occur in a system wherein the terpyridine is connected at the meso-position/s of a porphyrin. For this reason a new D-A systems, in which Ru(II) bis-terpyridine complex **[Ru]**$^{2+}$ have been connected *via* flexible ethylene bridges at the meso positions of either free base or zinc(II) porphyrins, have been synthesized in this Chapter.

Multi-porphyrin systems hold promise for intramolecular photoinduced energy and electron transfer processes.[1-7] Information obtained from the study of such molecules is of interest not only for understanding photosynthesis and devising new approaches to solar energy conversion, but also for the design of molecule-based opto-electronic devices.[8-24] In order to understand the primary photophysical processes involved, it is important to gain knowledge, and thereby control, of the parameters that influence energy and electron transfer rates. To investigate the mechanisms of photoinduced excitation energy and electron transfer, various supramolecular complexes have been constructed so far, having porphyrins linked either covalently *via* flexible hydrocarbon chains, more rigid aliphatic or aromatic spacers, or hydrogen bonds formed between complementary nucleic bases or amino acids.[25-43] In this context polypyridyl transition metal complex connected porphyrin systems were prepared, where the photochemical and photophysical properties of polypyridyl complexes are promising

photosensitizers.[44-55] In most of the models (dyads and triads) elaborated by the Sauvage group, porphyrin modules are connected to transition metal complexes with rigid σ-bonds.[56-61] But in this Chapter, we describe the synthesis of multicomponent dyads and triads assembled *via* a flexible -OCH_2CH_2O- spacer between ruthenium(II) bis-terpyridine complex $\mathbf{[Ru]^{2+}}$ and free base/zinc(II) porphyrins (i.e. $\mathbf{H_2L^2/ZnL^2}$). The dyads ($\mathbf{[H_2Ru]^{2+}}$, $\mathbf{[ZnRu]^{2+}}$) and triads ($\mathbf{[H_2RuH_2]^{2+}}$, $\mathbf{[ZnRuH_2]^{2+}}$, $\mathbf{[ZnRuZn]^{2+}}$), as well as the individual components $\mathbf{[Ru]^{2+}}$, $\mathbf{H_2Br}$ and **ZnBr** have been synthesized and characterized by various analytical techniques including electrochemistry and photochemistry, Schemes 5.1, 5.2 and 5.3.

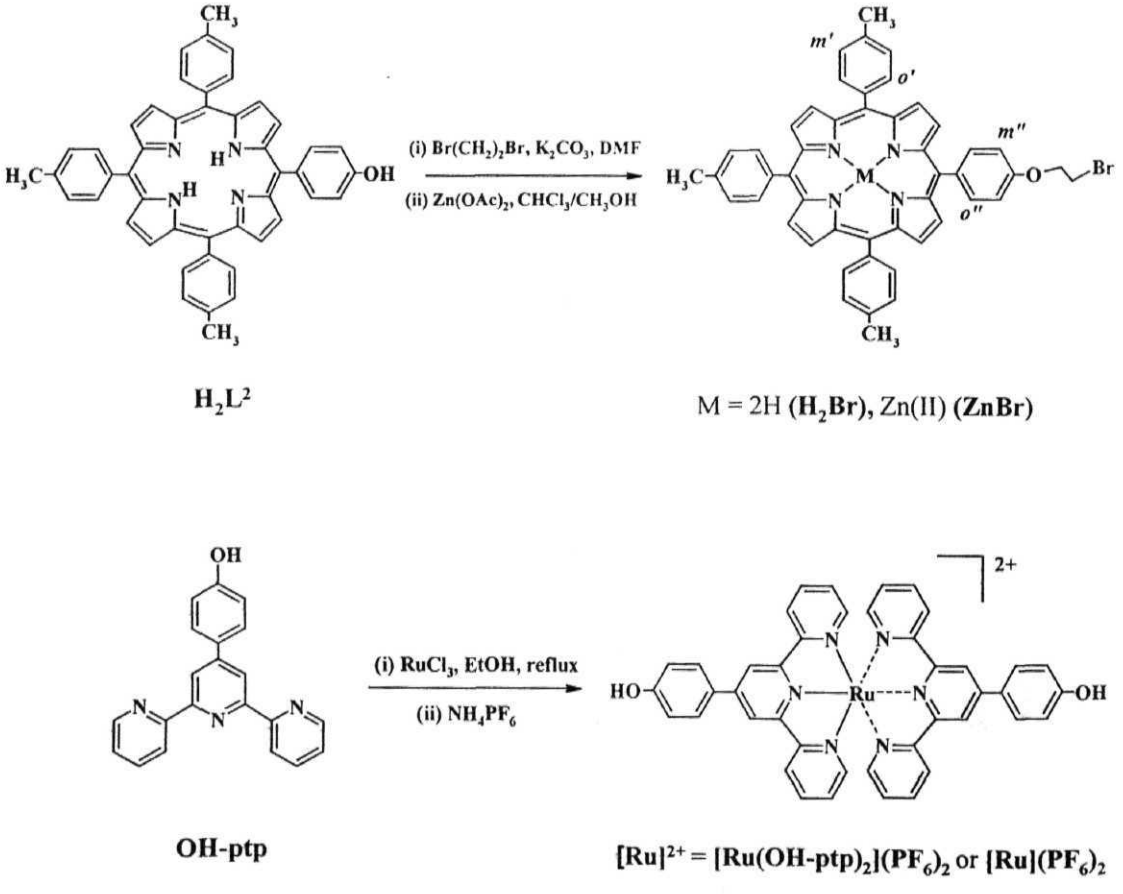

Scheme 5.1 Synthesis of precursor compounds $\mathbf{H_2Br}$, **ZnBr** and $\mathbf{[Ru]^{2+}}$.

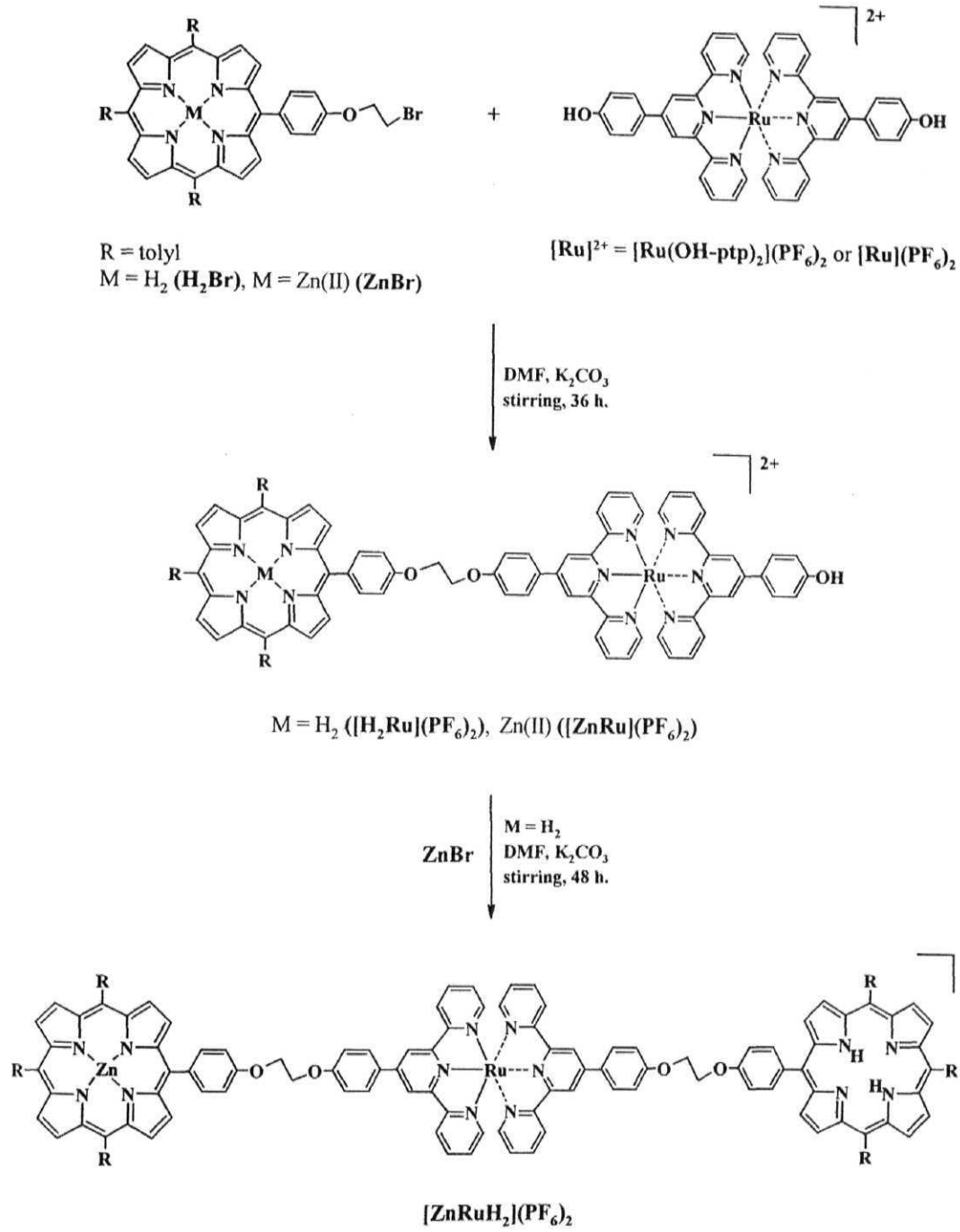

Scheme 5.2 Synthesis of dyads $[H_2Ru]^{2+}$, $[ZnRu]^{2+}$ and triad $[ZnRuH_2]^{2+}$.

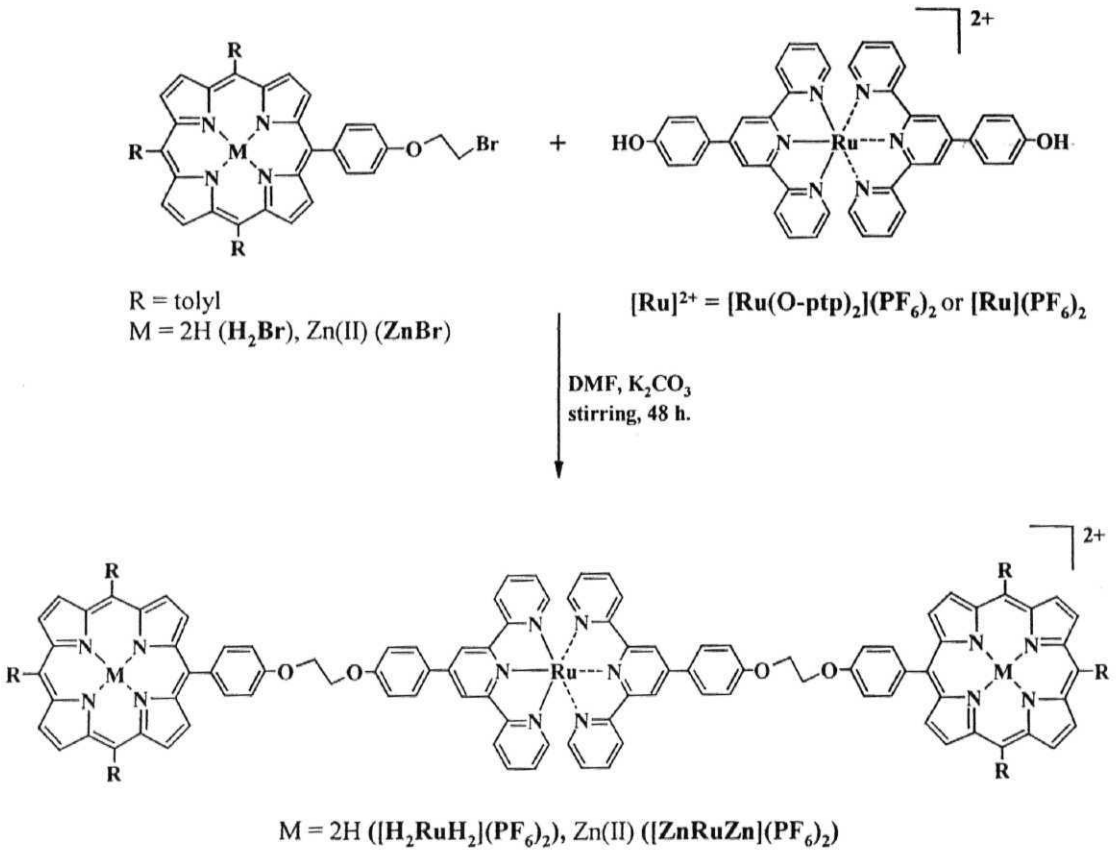

Scheme 5.3 Synthesis of triads $[H_2RuH_2]^{2+}$ and $[ZnRuZn]^{2+}$.

5.2 Experimental details

5.2.1 Synthesis

The precursor compounds meso-5-(4-hydroxyphenyl)-10,15,20-tri(4-methylphenyl) porphyrin (H_2L^2) and 4′-(4-hydroxyphenyl)-2,2′:6′,2″ terpyridine [**OH-ptp**] was synthesized as described in Chapter 3, section 3.2.1 and Chapter 4, section 4.2.1, respectively. 5,10,15,20-tetraphenylporphyrin (**H_2TPP**) and its zinc(II) derivative (**ZnTPP**), the reference compound used during the fluorescence studies, was synthesized as reported.[62,63]

5.2.2 Synthesis of $[Ru(OH\text{-}ptp)_2](PF_6)_2$ or $[Ru](PF_6)_2$ [64,65]

To 60 ml of absolute ethanol was added 200 mg (0.96 mmol) of $RuCl_3.3H_2O$ and 740 mg (2.28 mmol) of **OH-ptp**. The mixture was refluxed for 6 h. The reaction mixture was filtered and the filtrate was concentrated. To this aqueous NH_4PF_6 was added and keep at 10 °C for overnight. The precipitate was collected and recrystallized three to four times with CH_3CN-ether mixture. Yield = 480 mg (0.46 mmol, 20%).

5.2.3 Synthesis of 5-(4-(2-bromoethoxy)phenyl)-10,15,20-tri-(4-methyl phenyl)porphyrin [H_2Br] [66]

A mixture of $\mathbf{H_2L^2}$ (2.0 g, 3 mmol), 1, 2-dibromoethane (4.1 g, 22 mmol) and 3.0 g of anhydrous K_2CO_3 was stirred magnetically in 50 ml of dry DMF for 48 h. at room temperature under nitrogen atmosphere. The reaction mixture was then poured into a solvent mixture containing 170 ml water and 30 ml methanol. The precipitated porphyrin was filtered off, washed successively with water and methanol and dried under vacuum. It was loaded onto a neutral alumina column. Elution with $CHCl_3$ gave **H_2Br**. Yield = 2.20 g (2.8 mmol, 95%).

5.2.4 Synthesis of 5-(4-(2-bromoethoxy)phenyl)-10,15,20-tri-(4-methylphenyl) porphyrinatozinc(II) [ZnBr]

ZnBr was prepared by metallating **H_2Br** with the corresponding zinc(II) acetates by the standard methods.[63] Typically, 100 mg (0.12 mmol) of **H_2Br** and 100 mg (0.45 mmol) of zinc(II) acetate were stirred in $CHCl_3/CH_3OH$ mixture for 30 min. The solvents were evaporated and the residue was washed with water and dried. Purification by column chromatography ($CHCl_3$; alumina, activity 1) furnished the pure product, yield = 108 mg (0.12 mmol, 95%).

5.2.5 Synthesis of [H_2Ru](PF_6)$_2$

[Ru]$(PF_6)_2$ (50 mg, 0.048 mmol) and **H_2Br** (30 mg, 0.038 mmol) were dissolved in 60 ml of dry DMF. The resulting solution was added K_2CO_3 (7 mg, 0.048 mmol) and stirred under the nitrogen atmosphere for 36 h. The reaction mixture was poured into 100 ml of H_2O and the precipitate was filtered. Dissolve the precipitate in CH_2Cl_2 and chromatographed twice on silica (100-200 mesh). Elute the column first with $CHCl_3/CH_3CN/CH_3OH$ (70/20/10) and collect the unreacted porphyrin **H_2Br** and less polar triad (i.e. **[H_2RuH_2]$(PF_6)_2$**, see in next pages), respectively. Finally the desired dyad was collected as a red-brown band with solvent polarity raises upto $CHCl_3/CH_3CN/CH_3OH$ (50/30/20). Evaporation of the solvent gave a brown solid, which was precipitated twice from CH_2Cl_2-hexane to give **[H_2Ru]$(PF_6)_2$** in pure form. Yield = 42 mg (0.024 mmol, 63 %).

5.2.6 Synthesis of [ZnRu]$(PF_6)_2$

This compound was prepared, starting with **[Ru]$(PF_6)_2$**, (50 mg, 0.048 mmol) and **ZnBr** (30mg, 0.036 mmol) in a manner analogous to that described above for **[H_2Ru]$(PF_6)_2$**. Yield = 46 mg (0.025 mmol, 71%).

5.2.7 Synthesis of [H_2RuH_2]$(PF_6)_2$

[Ru]$(PF_6)_2$, (50 mg, 0.048 mmol) and **H_2Br** (373 mg, 0.48 mmol) were dissolved in 30 ml of dry DMF. An excess of K_2CO_3 was added and stirred under the nitrogen atmosphere for 48 h. The reaction mixture was poured into 100 ml of H_2O and the precipitate was filtered. The precipitate was dissolved in CH_2Cl_2 and chromatographed twice on silica (100-200 mesh). The column was first run with $CHCl_3/CH_3CN$ (80/20) and the excess unreacted porphyrin, **H_2Br** was collected. The polarity was then increased to $CHCl_3/CH_3CN/CH_3OH$ (70/20/10), and the desired triad collected as a red-purple band. Evaporation of

the solvent gave a purple solid, which was precipitated twice from CH_2Cl_2-hexane to give **$[H_2RuH_2](PF_6)_2$** in pure form. Yield = 80 mg (0.032 mmol, 68%).

5.2.8 Synthesis of $[ZnRuZn](PF_6)_2$

This compound was prepared, starting with **$[Ru](PF_6)_2$**, (50 mg, 0.048 mmol) and **ZnBr** (404 mg, 0.48 mmol) in a manner analogous to that described above for **$[H_2RuH_2](PF_6)_2$**. Yield = 90 mg (0.035 mmol, 73%).

5.2.9 Synthesis of $[ZnRuH_2](PF_6)_2$

$[H_2Ru](PF_6)_2$ (50 mg, 0.028 mmol) and **ZnBr** (120 mg, 0.14 mmol) were dissolved in 30 ml of dry DMF. To the resulting solution was added excess of K_2CO_3 and the solution was stirred under the nitrogen atmosphere for 48 h. The reaction mixture was poured into 100 ml of H_2O and the precipitate was filtered. The precipitate was dissolved in CH_2Cl_2 and chromatographed twice on silica (100-200 mesh). The column was run first with $CHCl_3/CH_3CN$ (80/20) and the excess unreacted porphyrin, **ZnBr** was collected. The polarity was increased to $CHCl_3/CH_3CN/CH_3OH$ (70/20/10), and the triad collected as a red-purple band. Evaporation of the solvent gave a purple solid, which was precipitated twice from CH_2Cl_2-hexane to give **$[ZnRuH_2](PF_6)_2$** in pure form. Yield = 46 mg (0.018 mmol, 64%).

5.3 Results and discussion

Synthesis of all the five new compounds have been accomplished here, in good-to-moderate yields, by a simple condensation between the ethylbromo porphyrin (**H_2Br/ZnBr**) derivatives and **$[Ru](PF_6)_2$** complex having an hydroxy groups. Reaction of excess **H_2Br** or **ZnBr** with **$[Ru](PF_6)_2$** in presence of K_2CO_3 and DMF gives triads **$[H_2RuH_2]^{2+}$** or **$[ZnRuZn]^{2+}$**, respectively. To get the dyads

(i.e. $\mathbf{[H_2Ru]^{2+}}$ and $\mathbf{[ZnRu]^{2+}}$), **H_2Br/ZnBr** was reacted with an excess of $\mathbf{[Ru]^{2+}}$. Triad $\mathbf{[ZnRuH_2]^{2+}}$ was synthesized starting from $\mathbf{[H_2Ru]^{2+}}$, with excess of **ZnBr** in DMF. These compounds have been fully characterized by mass (MALDI), UV-visible, ^{1}H NMR (1D and ^{1}H-^{1}H COSY) spectroscopies and also by the cyclic and differential pulse voltammetric techniques as described below.

5.3.1 Mass spectral data (MALDI)

$[H_2Ru](PF_6)_2$: $[M-2PF_6]^+$ = 1449, $[M-2PF_6-C_{49}H_{39}N_4O]^+$ = 750; **$[ZnRu](PF_6)_2$:** $[M-2PF_6]^+$ = 1512, $[M-2PF_6\text{-}C_{49}H_{37}N_4OZn]^+$ = 750; **$[H_2RuH_2](PF_6)_2$:** $[M-2PF_6]^+$ = 2147, $[M-2PF_6-C_{49}H_{39}N_4O]^+$ = 1448, $[M-2PF_6-2(C_{49}H_{39}N_4O)]^+$ = 749; **$[ZnRuZn](PF_6)_2$:** $[M-2PF_6]^+$ = 2273, $[M-2PF_6-C_{49}H_{37}N_4OZn]^+$ = 1511, $[M-2PF_6-2(C_{49}H_{37}N_4OZn)]^+$ = 749; **$[ZnRuH_2](PF_6)_2$:** $[M-2PF_6]^+$ = 2210, $[M-2PF_6-C_{49}H_{37}N_4OZn]^+$ = 1448, $[M-2PF_6-2(C_{49}H_{39}N_4O)]^+$ = 749.

5.3.2 Ground state properties

The mass spectrum of each of these compounds showed peak due to the $[M\text{-}2PF_6]^+$ ion and the peaks due to those fragments obtained upon elimination of the successive **H_2/Zn** porphyrin were found. ^{1}H NMR spectral data of all the five compounds along with their individual constituents are summarized in Table 5.1 and the spectra of $\mathbf{[H_2Ru]^{2+}}$, $\mathbf{[H_2RuH_2]^{2+}}$ and $\mathbf{[ZnRuH_2]^{2+}}$ are displayed in Fig. 5.1. Fig. 5.2 illustrates the various protons present on the $\mathbf{[Ru]^{2+}}$ complex. Spectra were analyzed based on the resonance position and integrated intensity data as well as the proton-to-proton connectivity information revealed in the COSY spectra (Fig. 5.3) to arrive at the structure of these compounds. A comparison of these spectra with those of **H_2Br**, **ZnBr** and $\mathbf{[Ru]^{2+}}$ reveals that the resonance positions of the various protons present either on the porphyrin

macrocycle or the $[Ru]^{2+}$ complex are not shifted considerably upon linking the two chromophores *via* the $-OCH_2CH_2O-$ spacer.

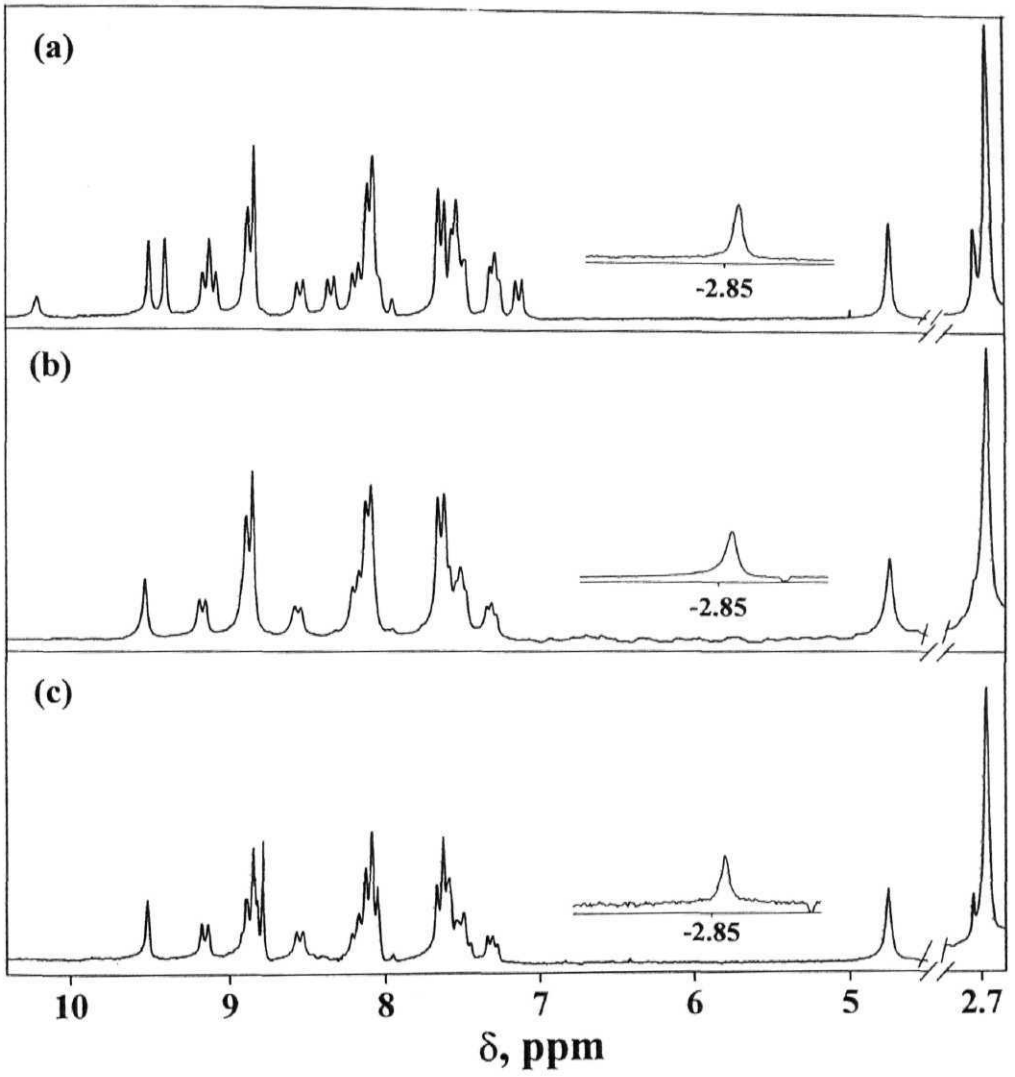

Fig. 5.1 ^{1}H NMR spectra of (a) $[H_2Ru]^{2+}$ (b) $[H_2RuH_2]^{2+}$ and (c) $[ZnRuH_2]^{2+}$ in DMSO-d_6 (200 MHz, 300 K).

The wavelengths of maximum absorbance (λ_{max}) and molar extinction coefficient (ε) values of the three new dyads, triads and those of their constituent

individual components (i.e. **H_2Br**, **ZnBr** and **$[Ru]^{2+}$**), as obtained from the UV-visible studies, are summarized in Table 5.2. UV-visible spectra of **$[H_2Ru]^{2+}$**, **$[H_2RuH_2]^{2+}$** and **$[ZnRuZn]^{2+}$** are shown in Fig. 5.4. Comparison of these spectra and the data given in Table 5.2 suggests that the **$[Ru]^{2+}$** chromophore in **$[H_2Ru]^{2+}$**, **$[ZnRu]^{2+}$**, **$[H_2RuH_2]^{2+}$**, **$[ZnRuZn]^{2+}$** and **$[ZnRuH_2]^{2+}$** dominantly absorbs between ca. 290-370 nm and 380-600 nm. The peaks at ~ 310 and ~495

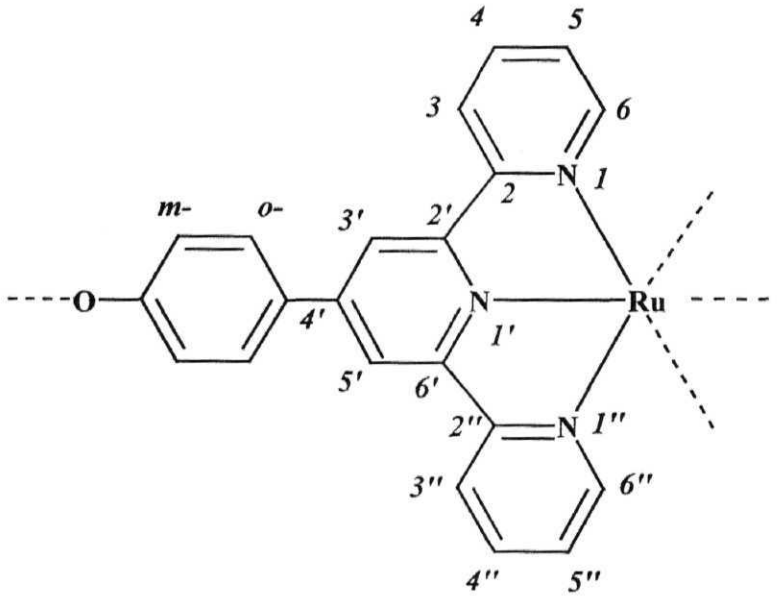

Fig. 5.2 Illustration of the various type protons of **$[Ru]^{2+}$** complex in the investigated compounds.

nm for each compound corresponds to the absorbance of the terpyridine ligand moiety and metal-to-ligand charge transfer (MLCT) absorption band, respectively. On the other hand, porphyrin parts of these five compounds show four/two less intense Q-bands and one intense Soret band (B-band) in the wavelength region (400 - 700 nm) where the **$[Ru]^{2+}$** complex MLCT band also absorb. Both porphyrin and **$[Ru]^{2+}$** chromophores of these compounds are seen to

absorb between ca. 380 - 600 nm resulting in the broadening of the peaks as well as appearance of MLCT band in the porphyrin Q-band region. Spectral data given in the Table 5.2 further reveals that, in general, both λ_{max} and log ε values of each dyad are within the same range as those of the constituent individual components. Finally, it was observed that the λ_{max} and spectral shapes of the bands of these newly synthesized compounds are more or less similar to individual components, implying that the π-electronic systems are not significantly perturbed.

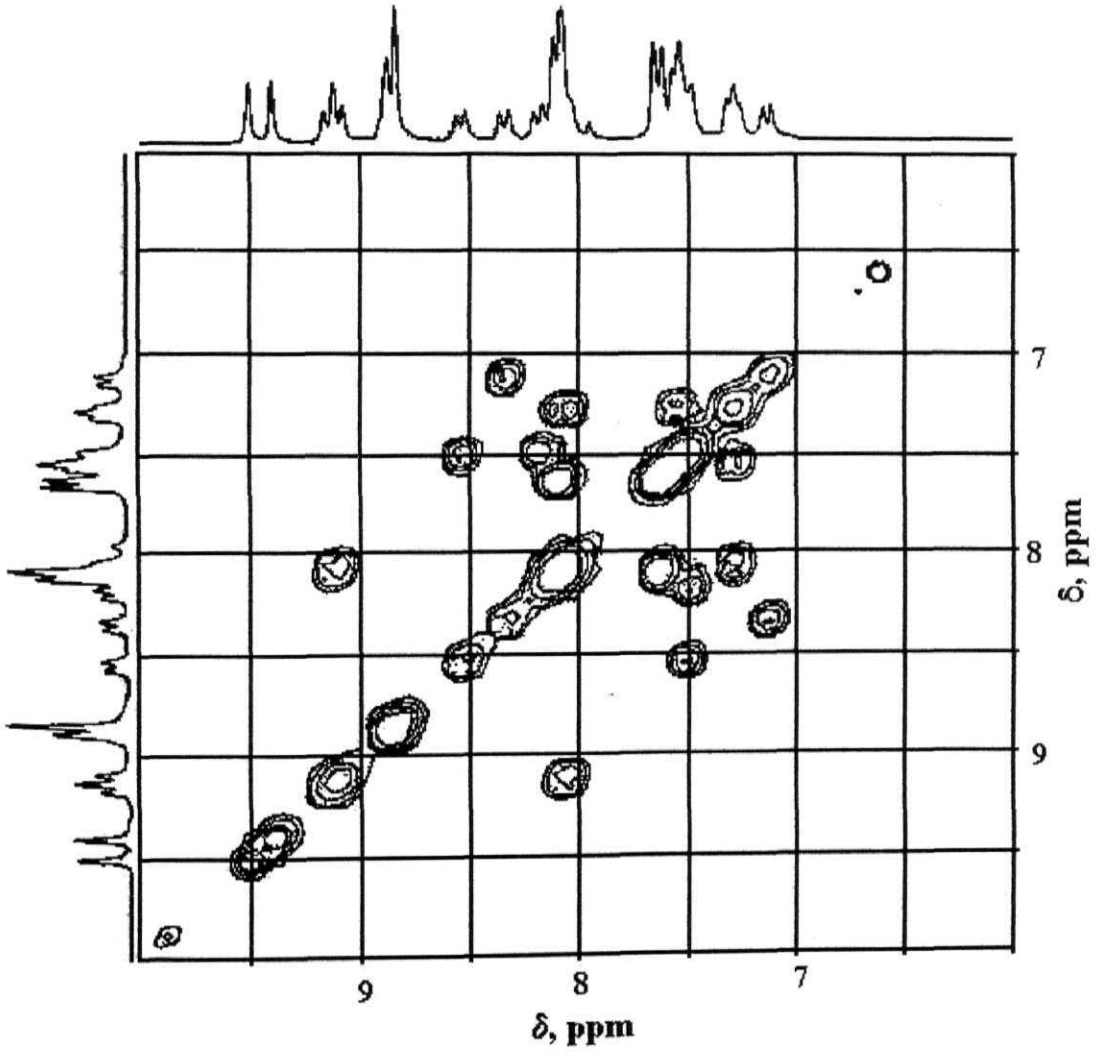

Fig. 5.3 ^{1}H-^{1}H COSY NMR spectrum of **[HRu]**$^{2+}$ in DMSO-d_6 (200 MHz, 300K).

Table 5.1 ^{1}H NMR data of dyads, triads and its monomeric analogues [a]

Compd.	Porphyrin	----CH_2-O-ptp/OH-ptp
$[Ru]^{2+}$		9.36 (s, 4H, $H_{3'}$+$H_{5'}$), 9.06 (d, 4H, $2H_3$+$2H_{3''}$) [8.0], 8.31 (d, 4H_o) [9.0], 8.04 (t, 4H, $2H_4$+$2H_{4''}$), 7.52 (d, 4H, $2H_6$+$2H_{6''}$), 7.26 (t, 4H, $2H_5$+$2H_{5''}$), 7.12 (d, 4H_m)
H_2Br [b]	8.86 (s, 8H_β), 8.11 (d, 8$H_{o'}$) [7.8], 7.56 (d, 6$H_{m'}$) [7.8], 7.28 (d, 2$H_{m''}$), 4.55 (t, 2H_{-OCH}), 3.83 (t, 2H_{-CHBr}), 2.71 (s, 9H_{-CH}), -2.75 (s, 2H_{-NH})	
ZnBr [b]	8.97 (s, 8H_β), 8.12 (m, 8$H_{o'}$), 7.56 (d, 6$H_{m'}$) [7.8], 7.29 (d, 2$H_{m''}$) [7.6], 4.59 (t, 2H_{-OCH}), 3.85 (t, 2H_{-CHBr}), 2.72 (s, 9H_{-CH})	-
$[H_2Ru]^{2+}$	8.86 (d, 8H_β) [7.8], 8.19 (d, 2$H_{o''}$) [7.8], 8.10 (d, 6$H_{o'}$) [7.0], 7.64 (d, 6$H_{m'}$) [7.8], 7.59- 7.43 (m, 2$H_{m''}$), 4. 74 (bs, 4H_{-OCH}), 2.73 (s, 9H_{-CH}), 2.67 (s, 6H_{-CH}), -2.89 (s, 2H_{-NH})	10.2 (s, **1**H_{-OH}), 9.49 (s, 2H, $H_{3'}$+$H_{5'}$), 9.39 (s, 2H, **$H_{3'}$**+**$H_{5'}$**), 9.12 (m, 4H, H_3+$H_{3''}$+**H_3**+**$H_{3''}$**), 8.54 (d, 2H_o) [8.8], 8.34 (d, **2H_o**) [8.6], 8.14-7.91 (m, 4H, H_4+$H_{4''}$+**H_4**+**$H_{4''}$**), 7.59-7.43 (m, 6H, 2H_m+H_6+$H_{6''}$+**H_6**+**$H_{6''}$**), 7.28 (m, 4H, H_5+$H_{5''}$+**H_5**+**$H_{5''}$**), 7.13 (d, **2H_m**) [7.4]
$[ZnRu]^{2+}$	8.81(d, 8H_β) [7.6], 8.08 (m, 8$H_{o'}$), 7.70-7.39 (m, 8$H_{m'}$), 4.74 (bs, 4H_{-OCH}), 2.67 (s, 9H_{-CH})	10.2 (s, **1**H_{-OH}), 9.50 (s, 2H, $H_{3'}$+$H_{5'}$), 9.40 (s, 2H, **$H_{3'}$**+ **$H_{5'}$**), 9.12 (m, 4H, H_3+$H_{3''}$+**H_3**+**$H_{3''}$**), 8.54 (d, 2H_o) [8.8], 8.34 (d, **2H_o**) [8.6], 8.22-7.96 (m, 4H, H_4+$H_{4''}$+**H_4**+**$H_{4''}$**), 7.66-7.42 (m, 6H, 2H_m+H_6+$H_{6''}$+**H_6**+**$H_{6''}$**), 7.28 (m, 4H, H_5+$H_{5''}$+**H_5**+**$H_{5''}$**), 7.13 (d, **2H_m**) [7.6]
$[H_2RuH_2]^{2+}$	8.86 (d, 16H_β) [7.8], 8.19 (d, 4$H_{o''}$) [7.8], 8.11 (d, 12$H_{o'}$) [7.8], 7.64 (d, 12$H_{m'}$) [7.8], 7.56-7.43 (m, 4$H_{m''}$), 4.75 (bs, 8H_{-OCH}), 2.67 (s, 18H $_{-CH}$)	9.52 (s, 4H, $2H_{3'}$+$2H_{5'}$), 9.17 (d, 4H, $2H_3$+$2H_{3''}$) [7.8], 8.56 (d, 4H_o) [7.8], 8.09 (m, 4H, $2H_4$+$2H_{4''}$), 7.51 (m, 4H, $2H_6$+$2H_{6''}$), 7.31 (m, 4H, $2H_5$+$2H_{5''}$)

.....continued

.....**Table 5.1**

$[ZnRuH_2]^{2+}$	8.85 (m, 16H$_\beta$), 8.31 (m, 16H$_{o'}$), 7.63 (m, 12H$_{m'}$), 7.49 (m, 4H$_{m''}$), 4.75 (bs, 8H$_{-OCH}$), 2.67 (s, 18H$_{-CH}$)	9.51 (s, 4H, 2H$_3$+2H$_{5'}$), 9.16 (d, 4H, 2H$_3$+2H$_{3''}$) [8.0], 8.55 (d, 4H$_o$) [8.0], 8.09 (m, 4H, 2H$_4$+2H$_{4''}$), 7.49 (m, 4H, 2H$_6$+2H$_{6''}$), 7.31 (m, 4H, 2H$_5$+2H$_{5''}$)
$[ZnRuZn]^{2+}$	8.82 (m, 16H$_\beta$), 8.14 (d, 4H$_{o''}$) [7.8], 8.06 (d, 12H$_{o'}$) [7.8], 7.61 (d, 12H$_{m'}$) [7.6], 7.49 (m, 4H$_{m''}$), 4.75 (bs, 8H$_{-OCH}$), 2.67 (s, 18H$_{-CH}$)	9.51 (s, 4H, 2H$_3$+2H$_{5'}$), 9.16 (d, 4H, 2H$_3$+2H$_{3''}$) [7.0], 8.55 (d, 4H$_o$) [8.0], 8.16 (m, 4H, 2H$_4$ +2H$_{4''}$), 7.49 (m, 4H, 2H$_6$ +2H$_{6''}$), 7.30 (m, 4H, 2H$_5$ +2H$_{5''}$)

(a) Error limits: δ, ± 0.01 ppm, J: ± 1Hz. Spectra were recorded in DMSO-d_6 and bolded protons corresponds to free **OH-ptp** group in complex moiety. (b) Spectra were recorded in $CDCl_3$, TMS.

Table 5.2 UV-visible data of dyads, triads and its monomeric analogues [a]

Compd.	Porphyrin		$[Ru]^{2+}$	
	B-band	Q-bands	ptp	MLCT
H_2Br	420 (5.53)	648 (3.60), 592 (3.63), 553 (3.90), 517 (4.15)	-	-
ZnBr	421 (5.73)	588 (3.76), 549 (4.36), 513 (3.53)	-	-
[b]$[Ru]^{2+}$	-	-	283 (4.66), 309 (4.79)	494 (4.46)
$[H_2Ru]^{2+}$	420 (5.48)	650 (3.65), 593 (3.76), 554 (4.12), 515 (4.44)	309 (4.80)	498 (4.42)
$[ZnRu]^{2+}$	421 (5.70)	591 (4.05), 551 (4.57)	286 (4.98), 309 (5.03)	499 (4.75)
$[H_2RuH_2]^{2+}$	420 (5.75)	648 (3.78), 591 (3.89), 552 (4.22), 515 (4.53)	285 (4.78), 310 (4.85)	498 (4.42)
$[ZnRuH_2]^{2+}$	421 (5.91)	648 (3.71), 596 (4.09), 555 (4.43), 513 (4.57)	286 (4.91), 309 (5.01)	501 (4.56)
$[ZnRuZn]^{2+}$	421 (5.94)	594 (4.13), 553 (4.59)	286 (4.88), 310 (4.98)	497 (4.56)

(a) Error limits: λ_{max}, ± 1 nm, log ε, ± 10%. Spectra were measured in CH_2Cl_2 (b) measured in CH_3CN.

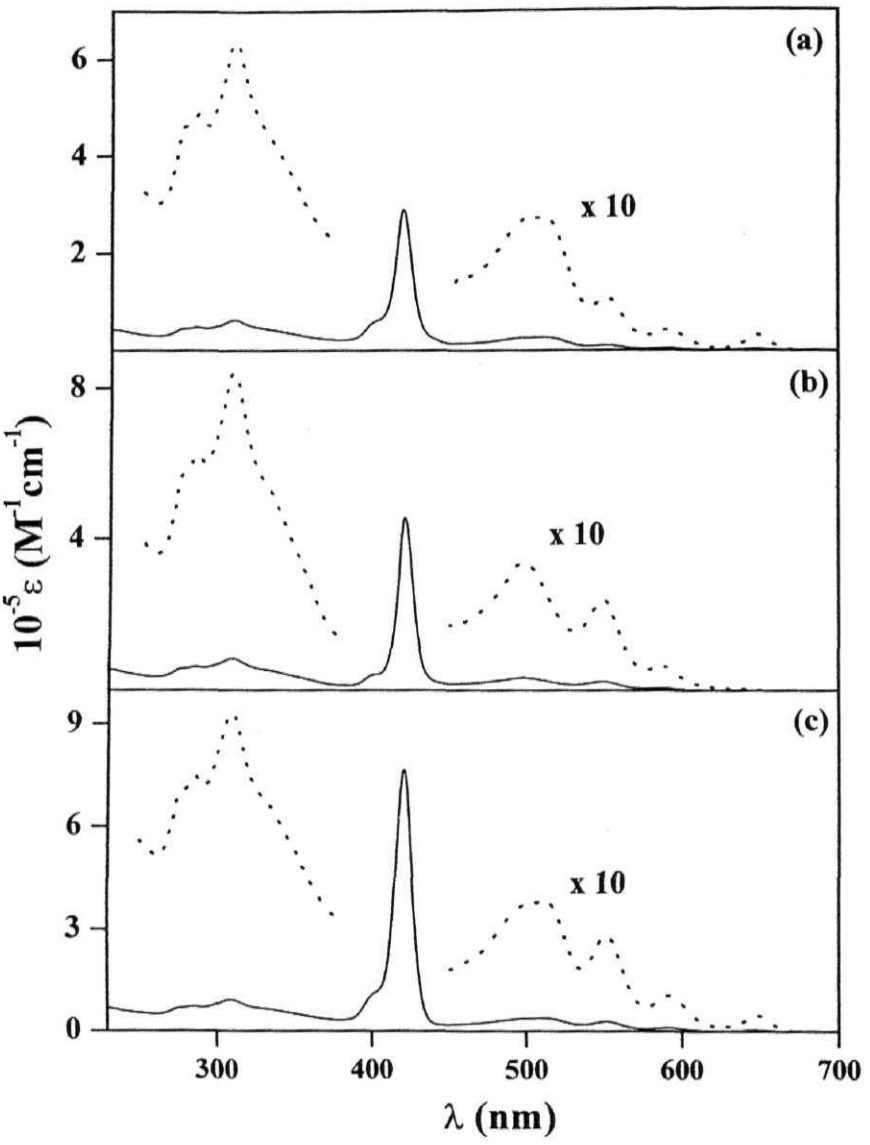

Fig. 5.4 UV-visible spectra of (a) $[H_2Ru]^{2+}$ (b) $[ZnRu]^{2+}$ and (c) $[ZnRuH_2]^{2+}$ in CH_2Cl_2.

The redox characteristic of the dyads ($[H_2Ru]^{2+}$, $[ZnRu]^{2+}$), triads ($[H_2RuH_2]^{2+}$, $[ZnRuH_2]^{2+}$, $[ZnRuZn]^{2+}$) and the reference compounds (**H_2Br**, **ZnBr**, $[Ru]^{2+}$) examined by cyclic and differential pulse voltammetry in CH_2Cl_2 (oxidation) and DMF (reduction) are reported in Table 5.3. Due to limitations

Table 5.3 Redox potential data [a]

Compd.	Potential ($E_{1/2}$) mV vs SCE	
	Oxidation [b]	**Reduction** [d]
H_2Br	950, 1170	-1020, -1475
ZnBr	750, 1065	-1300, -1705
$[Ru]^{2+}$ [c]	1210	-1195, -1480
$[H_2Ru]^{2+}$	970, 1235	-1000, -1175, -1470
$[ZnRu]^{2+}$	760, 1050, 1224	-1160, -1315, -1470
$[H_2RuH_2]^{2+}$	930, 1144, 1285	-1020, -1135, -1370, -1495
$[ZnRuH_2]^{2+}$	670, 910, 1155, 1260	-1040, -1160, -1385, -1505, -1730
$[ZnRuZn]^{2+}$	640, 985, 1260	-1160, -1325, -1720

(a) Error limits, $E_{1/2}$, ± 15 mV (b) measured in 0.1 M CH_2Cl_2, (c,d) measured in 0.1 M DMF.

imposed by solvent potential, the reduction potentials of dyads and triads could not be obtained in CH_2Cl_2. In view of this, reduction potentials of each dyads and triads were investigated in DMF solvent with a broader negative potential window. Fig. 5.5 illustrates the differential pulse voltammograms of **$[H_2Ru]^{2+}$**, **$[ZnRu]^{2+}$** and **$[ZnRuH_2]^{2+}$**. As seen in Fig. 5.5 and also data given in Table 5.3, each investigated new compound shows up to two to four oxidation and two to five reduction peaks under the experimental conditions employed in this study. Wave analysis suggested that while the first two oxidation and first three reduction processes represent reversible (i_{pc}/i_{pa} = 0.9 - 1.0) and diffusion controlled ($i_{pc}/\upsilon^{1/2}$ = constant in the scan rate (υ) range 50 - 500 mV/s) one-electron transfer (ΔE_P = 60 - 70 mV; ΔE_P = 65 ± 3 mV for Fc^+/Fc couple)

reactions, left over electrode processes are either quasi-reversible (i_{pc}/i_{pa} = 0.6 - 0.8 and ΔE_P = 80 - 150 mV) or irreversible under similar experimental conditions.[67]

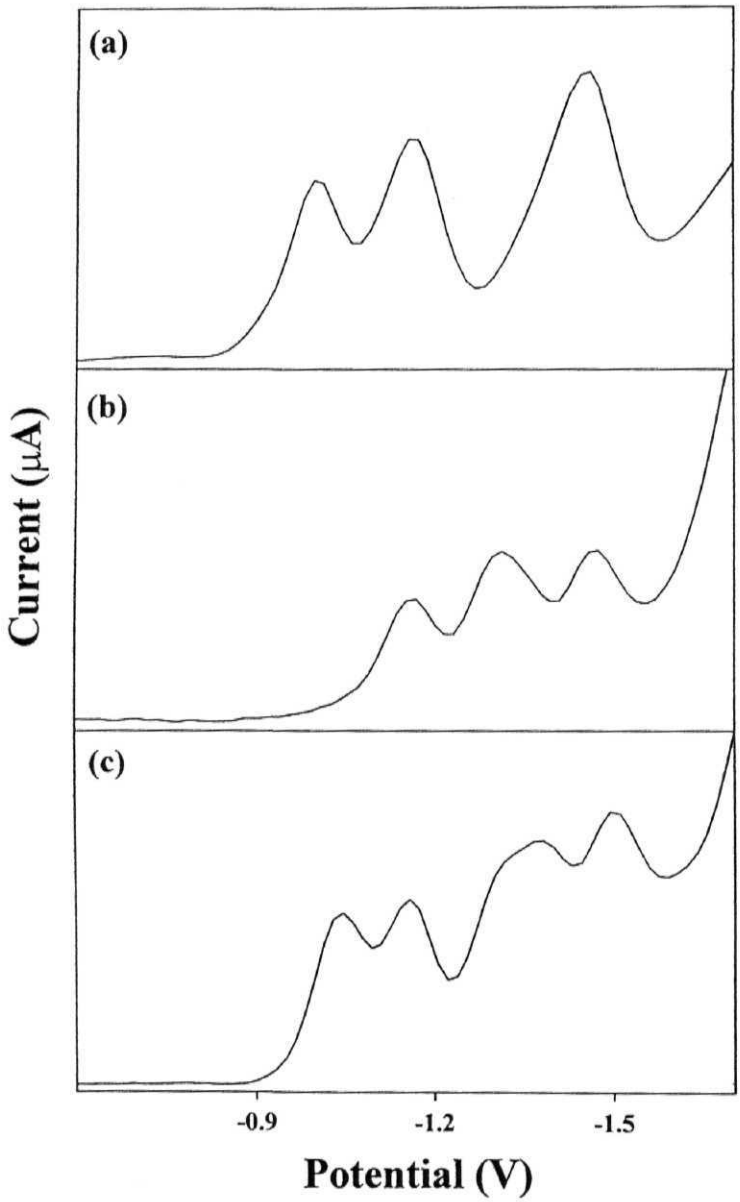

Fig. 5.5 Differential pulse voltammograms of (a) $[H_2Ru]^{2+}$ (b) $[ZnRu]^{2+}$ and (c) $[ZnRuH_2]^{2+}$ in DMF, 0.1 M TBAP (scan rate = 100 mVs^{-1}, modulation amplitude = 10 mV).

Analysis of the data given in Table 5.3 reveals that the redox potentials of dyads and triads are essentially close to those of the corresponding reference compounds. From the differential pulse voltammetric experiments, the current values corresponding to oxidation and reduction peaks of the **H_2/Zn(II)** porphyrin components of the triads ($[H_2RuH_2]^{2+}$/$[ZnRuZn]^{2+}$) are higher than those of the corresponding dyads ($[H_2Ru]^{2+}$/$[ZnRu]^{2+}$).

Overall, the spectroscopic and electrochemical results obtained for these dyads and triads are suggest that there is minimal perturbation of electronic structure of the individual macrocyclic π-systems.

5.3.3 Singlet state properties

The UV-visible spectral data of dyads and triads indicate that it is possible to address photochemistry of the porphyrin and the $[Ru]^{2+}$ complex in these systems. $[Ru]^{2+}$ complex was found to be totally non-luminescent in all solvents presumably because of a fast deactivation *via* an upper lying metal-centered state that favours non-radiative decay of the excited state.[68] Steady state fluorescence spectra of these D-A systems have been measured in different solvents by exciting the solutions at 420 nm (predominantly porphyrin absorption (**H_2/Zn**)) and 650 nm (exclusively for free base porphyrin (**H_2**) absorption, see Table 5.2 & Fig. 5.4). Fig. 5.6 illustrates the steady-state fluorescence spectra of dyads ($[H_2Ru]^{2+}$, $[ZnRu]^{2+}$), triads ($[H_2RuH_2]^{2+}$, $[ZnRuZn]^{2+}$) and its reference (**H_2Br**, **ZnBr**) compounds in CH_3CN. Analogous spectra were obtained in CH_2Cl_2, DMF and CH_3OH. In Fig. 5.6, the steady state fluorescence spectra of these compounds are compared with spectra of the corresponding individual components constituting them. Spectral shapes and wavelengths of maximum emission (λ_{em}) of these D-A systems, when they were irradiated at the porphyrin absorption band (λ_{ex} = 420 nm), are seen to be similar to the spectrum of either **H_2Br** or **ZnBr**.

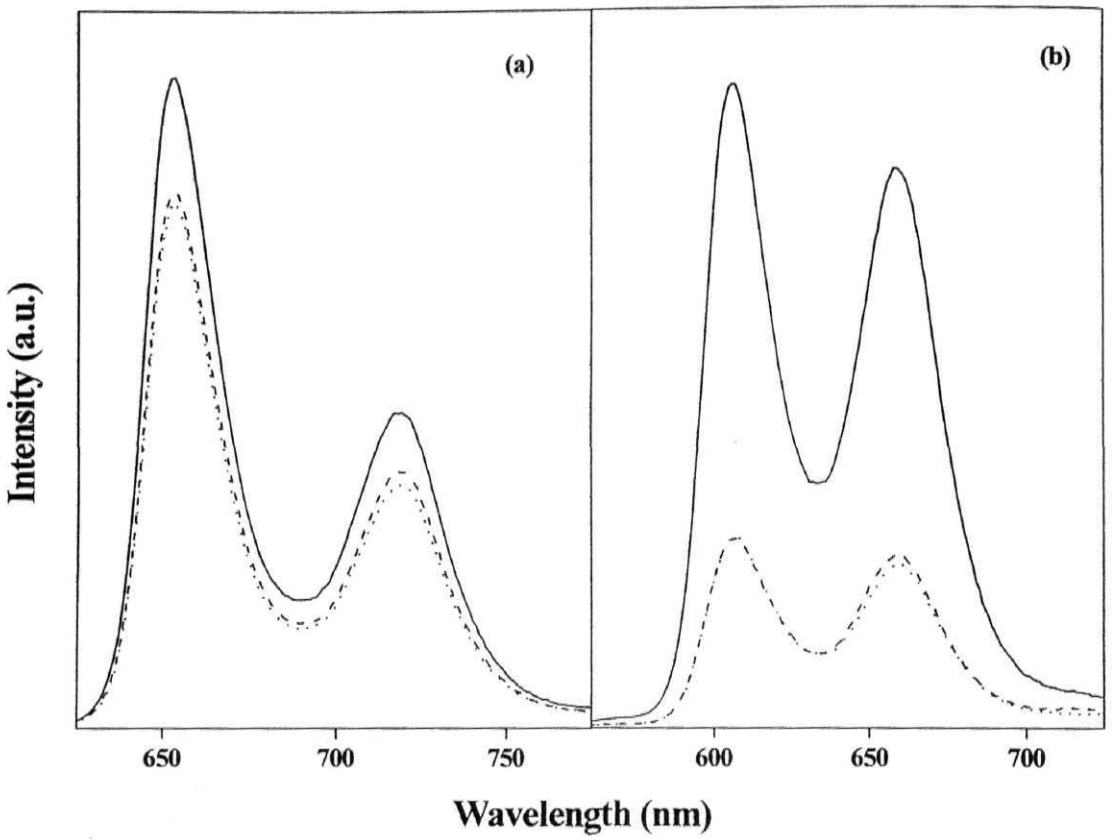

Fig. 5.6 Fluorescence spectra (O.D. ≈ 0.2 at λ_{ex} = 420 nm) of (a) **H_2Br** (———), **$[H_2Ru]^{2+}$** (--------) and **$[H_2RuH_2]^{2+}$** (·····) (b) **ZnBr** (———), **$[ZnRu]^{2+}$** (------) and **$[ZnRuZn]^{2+}$** (·····) in CH_3CN.

The fluorescence quantum yield (ϕ) for excitation into the porphyrin part of **$[H_2Ru]^{2+}$**, **$[H_2RuH_2]^{2+}$** was not quenched much, whereas it was found to be strongly quenched in **$[ZnRu]^{2+}$**, **$[ZnRuZn]^{2+}$**. Fluorescence quantum yields (ϕ) and quenching efficiency values (%Q) of these new compounds in different solvents are summarized in Table 5.4. The quenching efficiency values (Q) have been evaluated using the quantum yield data, eqn. 5.1.

$$Q = (\phi_{ref} - \phi_{dyad/triad})/ \phi_{ref} \qquad (5.1)$$

Where, $\phi_{dyad/triad}$ and ϕ_{ref} refers to the quantum yields of a given dyad/triad and the reference compound, respectively. Based on the electrochemical data (Table 5.3), singlet state and triplet state energies, a schematic energy level diagram is shown in Fig. 5.7. It should be noted that the triplet excited state energies of **[Ru]$^{2+}$** (the energy level of the **^{3}Ru** state, which could not be directly measured because of the absence of any emission from this moiety was assumed to be placed at 2 eV)[69] slightly above the singlet state of free base (**^{1}H$_2$**) porphyrin (1.90 eV) suggest the very weak EET can occur from the singlet porphyrin to **^{3}Ru** in both **[H$_2$Ru]$^{2+}$**, **[H$_2$RuH$_2$]$^{2+}$** compounds.[69] Energy transfer from **^{1}H$_2$** to **^{3}Ru** that is, between states of different multiplicity, can occur because of the perturbed nature of the ^{3}MLCT state of the ruthenium complex, which is only formally a triplet.

Table 5.4 Fluorescence data of dyads, triads and their monomeric analogues in various solvents (λ_{ex} = **420 nm**) [a]

Compd.	λ_{em} (ϕ, %Q)			
	CH_2Cl_2	CH_3CN	DMF	CH_3OH
H$_2$Br	654, 720 (0.108)	653, 719 (0.097)	655, 721 (0.141)	653, 718 (0.093)
ZnBr	598, 648 (0.033)	607, 658 (0.035)	609, 661 (0.049)	608, 655 (0.038)
[H$_2$Ru]$^{2+}$ (99:1) [b]	654, 720 (0.083, 23)	653, 718 (0.08, 16)	655, 721 (0.12, 15)	653, 718 (0.082, 12)
[ZnRu]$^{2+}$ (99:1) [b]	599, 651 (0.01, 70)	607, 658 (0.011, 70)	610, 661 (0.016, 67)	606, 658 (0.012, 68)
[H$_2$RuH$_2$]$^{2+}$ (99:1) [b]	655, 720 (0.083, 23)	652, 719 (0.078, 19)	655, 721 (0.119, 16)	653, 718 (0.075, 19)
[ZnRuZn]$^{2+}$ (99:1) [b]	599, 650 (0.009, 72)	606, 660 (0.011, 70)	610, 661 (0.017, 66)	606, 658 (0.011, 71)

(a) Error limits: λ, ± 1 nm; ϕ, ± 10%. (b) The partition of % absorption (or photons) of **H$_2$**, **Zn(II)** porphyrins and **[Ru]$^{2+}$** complex at 420 nm calculated on the basis of the absorption coefficients of the reference compounds.

On the other hand positive ΔG_{PET} values suggest that photoinduced electron transfer (PET) from the singlet free base porphyrin to the $[Ru]^{2+}$ complex thermodynamically unfavourable processes in both $[H_2Ru]^{2+}$, $[H_2RuH_2]^{2+}$ compounds. The PET from $^1H_2$ to the ^3Ru has been found to be exoergic for $[H_2Ru]^{2+}$ and $[H_2RuH_2]^{2+}$. The free-energy change for this electron transfer process, ($\Delta G(^1H_2 \rightarrow Ru)$) was calculated by the simplified Rehm-Weller treatment,[70] eqn. 5.2.

$$\Delta G_{PET}(^1H_2 \rightarrow Ru) = E_{CT}(H_2^+Ru^-) - E_{0\text{-}0}(H_2) \qquad (5.2)$$

Where $E_{CT}(H_2^+Ru^-) = E_{1/2}^{ox}(H_2) - E_{1/2}^{red}(Ru)$, the corresponding ΔG_{PET} values for $[H_2Ru]^{2+}$ and $[H_2RuH_2]^{2+}$ are estimated to be 0.24 and 0.18 eV, respectively. Thus, we analyze that the EET from the singlet free base porphyrin to the $[Ru]^{2+}$

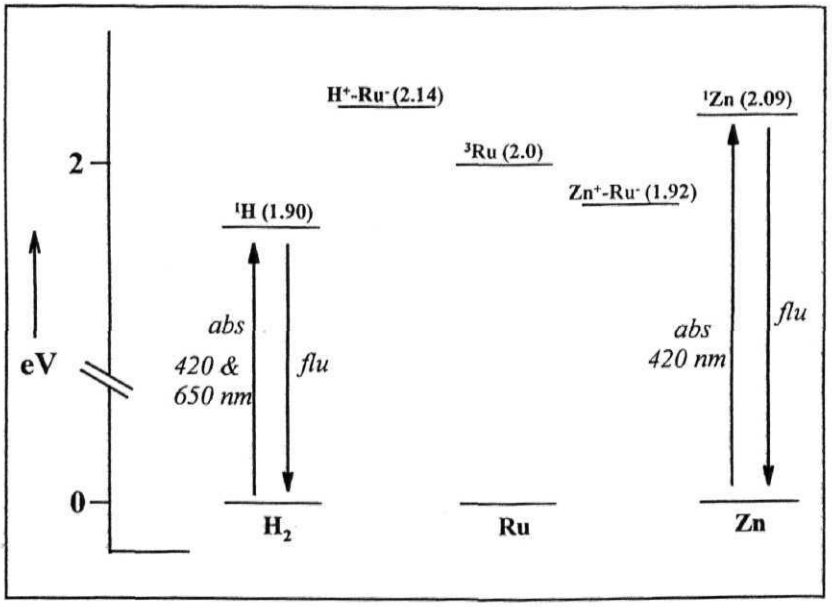

Fig. 5.7 Schematic energy-level diagram of dyads $[H_2Ru]^{2+}$and $[ZnRu]^{2+}$. Here *abs* and *flu* refers absorption and fluorescence, respectively.

complex is very weak in both $[H_2Ru]^{2+}$ and $[H_2RuH_2]^{2+}$ and it can explain the low %Q values. When excitation at 650 nm the fluorescence quantum yields and % quenching efficiency values for $[H_2Ru]^{2+}$ and $[H_2RuH_2]^{2+}$, were found to be similar to the one detected in the case of the 420 nm excitation, Table 5.6.

The fluorescence quantum yields (ϕ) for excitation into the porphyrin part of $[ZnRu]^{2+}$and $[ZnRuZn]^{2+}$ were quenched upto 72-66%, when excited at 420 nm. Fluorescence quantum yields (ϕ) and quenching efficiency values (%Q) of these new compounds in different solvents are summarized in Table 5.4. This quenching is explained in terms of PET mechanism from singlet excited state zinc(II) porphyrin (^{1}**Zn**) to $[Ru]^{2+}$ complex. The energy level diagram (Fig. 5.7) of $[ZnRu]^{2+}$ differ from the corresponding free base dyad (i.e. $[H_2Ru]^{2+}$), the presence of the charge-transfer (CT) excited state corresponding to the transfer of an electron from the singlet excited state zinc(II) porphyrin to the $[Ru]^{2+}$ moiety. Such a CT excited state, indicated as Zn^+-Ru^- ($E_{CT}(Zn^+Ru^-) = E_{1/2}^{ox}(Zn) - E_{1/2}^{red}(Ru)$), has an energy of 1.92 eV judging from the electrochemical data (Table 5.3), i.e. it can be placed below the ^{3}MLCT level of $[Ru]^{2+}$ moiety and the ^{1}**Zn** ($E_{0\text{-}0}$ = 2.09 eV). The free-energy change for this electron transfer process ($\Delta G_{PET}(^1Zn \rightarrow Ru)$) for $[ZnRu]^{2+}$ and $[ZnRuZn]^{2+}$ are estimated to be –0.17, –0.20 eV, respectively by using eqn. 5.3

$$\Delta G_{PET}(^1Zn \rightarrow Ru) = E_{CT}(Zn^+Ru^-) - E_{0\text{-}0}(Zn) \qquad (5.3)$$

Whereas triad $[ZnRuH_2]^{2+}$ fluorescence properties was explained based on singlet state properties of dyads, $[H_2Ru]^{2+}$ and $[ZnRu]^{2+}$. From the UV-visible data given in Fig. 5.4 and Table 5.2 it is clear that, in the free base porphyrin of $[ZnRuH_2]^{2+}$ which is exclusively addressable by excitation at ca. 650 nm, there exists no distinct Q-bands(s) that is solely ascribable to the

individual monomeric units of $[\mathbf{ZnRuH_2}]^{2+}$. Representative spectra of $[\mathbf{ZnRuH_2}]^{2+}$ measured in CH_3CN are illustrated in Fig. 5.8. Analogous spectra were obtained in CH_2Cl_2, DMF and CH_3OH. As seen in Fig. 5.8, while excitation at 420 nm (where both free base and zinc(II) porphyrins absorb; see Tables 5.2 & Fig. 5.4) results in the appearance of fluorescence bands due to free base (bands II and III) and zinc(II) porphyrin (bands I and II) components.

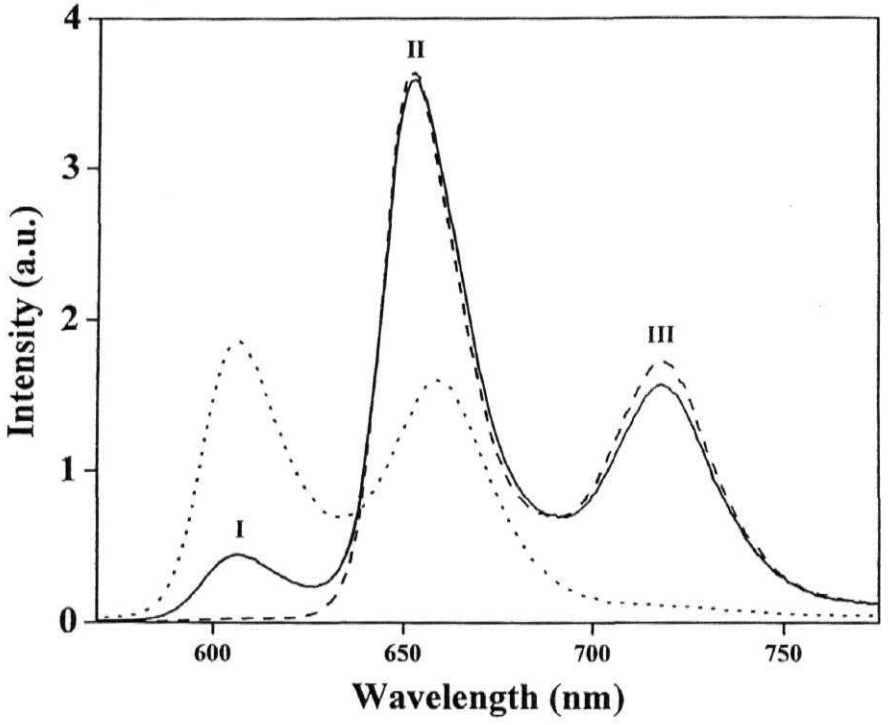

Fig. 5.8 Fluorescence spectra (at λ_{ex} = 420 nm) of $[\mathbf{ZnRuH_2}]^{2+}$ (———) (O.D. ≈ 0.2), $\mathbf{H_2Br}$ (--------) (O.D. ≈ 56% in 0.2) and **ZnBr** (·····) (O.D. ≈ 43% in 0.2) in CH_3CN.

It was found that the fluorescence band maxima of zinc(II) and free base components are quite close to those of **ZnBr** or $\mathbf{H_2Br}$ respectively. Similarly, like in dyads $[\mathbf{ZnRu}]^{2+}$and $[\mathbf{H_2Ru}]^{2+}$ the fluorescence quantum yield of zinc(II) and free base component is quenched in comparison with the reference compound

ZnBr and **H_2Br**, respectively. Based on the quantum yield data, % quenching efficiencies %Q(Zn) (from data obtained upon excitation at 420 nm and emission monitored in the band I region) and %Q(H_2) (from data obtained upon excitation at 420 nm and emission monitored in the band III region) were calculated and are summarized in Table 5.5.

Table 5.5 Fluorescence data of **$[ZnRuH_2]^{2+}$** (at λ_{ex} = **420 nm**) [a]

$[ZnRuH_2]^{2+}$ (56:1:43) [b]	λ_{em} (ϕ, %Q)			
	CH_2Cl_2	**CH_3CN**	**DMF**	**CH_3OH**
Zn-component	599 (0.0063, 81)	606 (0.0086, 75)	611 (0.0072, 85)	606 (0.0099, 74)
H_2-component	720 (0.086, 20)	718 (0.0089, 8)	721 (0.09, 15)	718 (0.069, 26)

(a) Error limits: λ, ± 1 nm; ϕ, ± 10% (b) The % absorption (or photons) of **Zn(II)**, **$[Ru]^{2+}$** and **H_2** components at 420 nm was calculated on the basis of the absorption coefficients of the reference compounds.

Inspection of Fig. 5.9 and based on the steady state properties of dyad (**$[H_2Ru]^{2+}$** and **$[ZnRu]^{2+}$**), that quenching of the zinc(II) component in this triad **$[ZnRuH_2]^{2+}$** is predominantly due to the photoinduced electron transfer (PET) from the **^{1}Zn** to the **$^3[Ru]^{2+}$** complex. The free-energy change for this process (ΔG_{PET}(**^{1}Zn** → **Ru**)) is estimated to be –0.23 eV. On the other hand the excitation energy transfer (EET) from the **^{1}Zn** to the **$^3[Ru]^{2+}/H_2$** cannot be neglected because energy levels of **^{1}Zn**, **$^1H_2$** porphyrins and **$^3[Ru]^{2+}$** complex are 2.09, 1.94 and 2.0 eV, respectively. When excited at 420 nm where the ratio of light absorbed by the zinc(II) and the free base component is 56:43, the free base component (monitored at ~720 nm or band III) fluorescence intensity of **$[ZnRuH_2]^{2+}$** is 92%

of that of **H_2Br**. From that more than 80% is accounted for by the direct excitation of free base moiety. For example the free base component fluorescence intensity in **[H_2Ru]$^{2+}$** dyad was found to be ~81% to that of **H_2Br**, when excited at 650 nm or 420 nm. Based on this in triad remaining ~ 11% is probably due to excitation

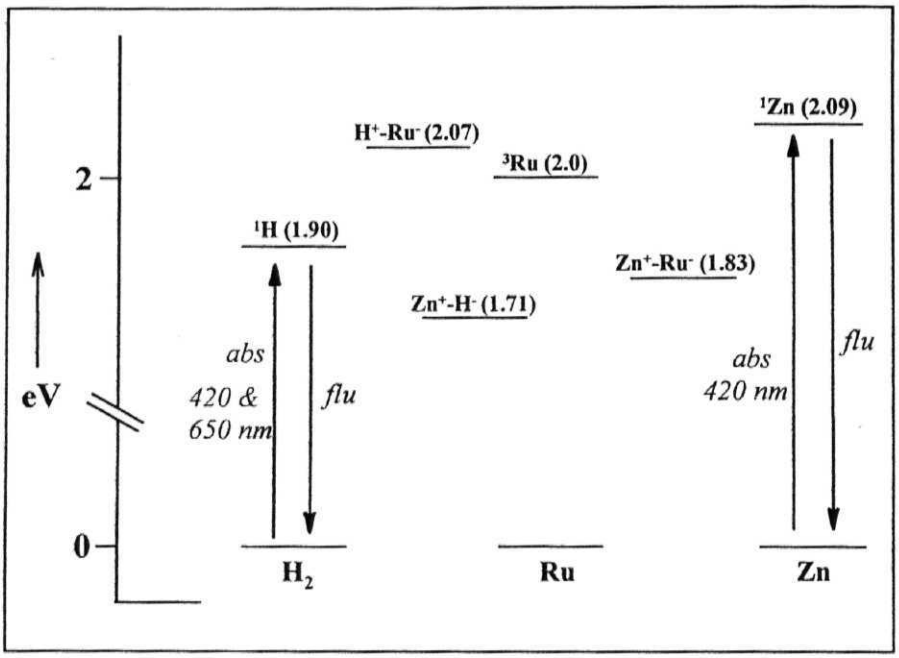

Fig. 5.9 Schematic energy-level diagram of **[ZnRuH_2]$^{2+}$**. Here *abs* and *flu* refers absorption and fluorescence, respectively.

energy transfer originate from the excited singlet state of the zinc(II) component to free base porphyrin in triad **[ZnRuH_2]$^{2+}$**. Even though there is a large distance between zinc(II) porphyrin and free base porphyrin, this EET processes is taking place probably because of flexible nature of the –OCH_2CH_2O– bridge. This will allow the donor (zinc(II) porphyrin) and acceptor (free base porphyrin) moieties to come close, such that EET can take place.[26] We thus analysed that a EET from the singlet Zn(II) porphyrin to the free base porphyrin is weak in **[ZnRuH_2]$^{2+}$** but

can, in principle, explain the high %Q(Zn) values than $[ZnRu]^{2+}$ and $[ZnRuZn]^{2+}$ observed for $[ZnRuH_2]^{2+}$. And finally, the fluorescence quantum yields and quenching efficiency %Q(H_2) of $[ZnRuH_2]^{2+}$ when excited at 650 nm are summarized in Table 5.6, were similar to those of $[H_2Ru]^{2+}$ and $[H_2RuH_2]^{2+}$.

Table 5.6 Fluorescence data of dyads and triads (at λ_{ex} = **650 nm**) [a]

Compd.	λ_{em} (ϕ, %Q)			
	CH_2Cl_2	CH_3CN	DMF	CH_3OH
H_2L^1	720 (0.115)	719 (0.104)	721 (0.161)	718 (0.113)
$[H_2Ru]^{2+}$	720 (0.099, 14)	719 (0.095, 19)	721 (0.136, 14)	718 (0.104, 8)
$[H_2RuH_2]^{2+}$	720 (0.091, 21)	719 (0.087, 16)	721 (0.133, 18)	719 (0.103, 9)
$[ZnRuH_2]^{2+}$	720 (0.092, 20)	719 (0.082, 21)	721 (0.129, 20)	719 (0.102, 10)

(a) Error limits: λ, ± 1 nm; ϕ, ± 10%.

5.4 Summary

In summary, dyads and triads with -OCH_2CH_2O- spacer/s have been synthesized and investigated by spectroscopic and electrochemical methods. Their photophysical properties have also been investigated and the results are interpreted in terms of intramolecular energy and electron transfer mechanisms. These dyads and triads exhibit interesting photochemical properties. In the case of $[H_2Ru]^{2+}$/$[H_2RuH_2]^{2+}$, the singlet state of free base porphyrin is weakly quenched by energy transfer to Ru(II) moiety. Whereas in compounds $[ZnRu]^{2+}$/$[ZnRuZn]^{2+}$, deactivation of singlet excited state of zinc(II)porphyrin occurs essentially by electron transfer to give the CT level that deactivates to ground state. Similar to the dyads ($[H_2Ru]^{2+}$ and $[ZnRu]^{2+}$), the triad $[ZnRuH_2]^{2+}$

also exhibit same singlet state properties but the additional quenching is explained by energy transfer from singlet excited state of Zn(II)porphyrin to free base porphyrin.

5.5 References

1. Harvey, P. D. In *The Porphyrin Handbook*; Kadish, K. M., Smith, K. M., Guilard, R., Eds.; Academic Press: San Diego, CA, **2003**; Vol. 18, p. 63.
2. Connolly, J. S.; Bolton, J. R. In *Photoinduced Electron Transfer*; Fox, M. A.; Chano, M., Eds.; Elsevier: New York, **1988**; Part D.
3. Balzani, V.; Scandola, F. In *Comprehensive Supramolecular Chemistry*; Reinhoudt, D. N., Ed.; Pergamon: Oxford, **1996**; Vol. 10, p. 1.
4. Burrell, A. K.; Officer, D. L.; Plieger, P. G.; Reid, D. C. W. *Chem. Rev.* **2001**, *101*, 2751.
5. Ward, M. D. *Chem. Soc. Rev.* **1997**, *26*, 365.
6. Wasielewski, M. R. *Chem. Rev.* **1992**, *92*, 435.
7. Gust, D.; Moore, T. A.; Moore, A. L. *Acc. Chem. Res.* **1993**, *26*, 198.
8. Chen. A. J.; Burrell, A. K.; Campbell, W. M.; Officer, D. L.; Too, C. O.; Wallace, G. G. *Electrochim. Acta* **2004**, *49*, 329.
9. Kobuke, Y.; Ogawa, K. *Bull. Chem. Soc. Jpn.* **2003**, *76*, 689.
10. Takahashi, R.; Kobuke, Y. *J. Am. Chem. Soc.* **2003**, *125*, 2372.
11. Otsuki, J.; Yasuda, A.; Takido, T. *Chem. Commun.* **2003**, 608.
12. Yoon, D. H.; Lee, S. B.; Yoo, K.-H.; Kim, J.; Lim, J. K.; Aratani, N.; Tsuda, A.; Osuka, A.; Kim, D. *J. Am. Chem. Soc.* **2003**, *125*, 11062.
13. Yu, L.; Lindsey, J. S. *J. Org. Chem.* **2001**, *66*, 7402.
14. Seth, J.; Palaniappan, V.; Johnson, T. E.; Prathapan, S.; Lindsey, J. S.; Bocian, D. F. *J. Am. Chem. Soc.* **1994**, *116*, 10578.
15. Davila, J.; Harriman, A.; Milgrom, L. *Chem. Phys. Lett.* **1987**, *136*, 427.

16. Chernook, A. V.; Rempel, U.; von Borczyskowski, C.; Shulga, A. M.; Zenkevich, E. I. *Chem. Phys. Lett.* **1996**, *254*, 229.
17. Kurreck, H.; Huber, M. *Angew. Chem., Int. Ed. Engl.* **1995**, *34*, 849.
18. Gust, D.; Moore, T. A.; Moore, A. L. *Pure Appl. Chem.* **1998**, *70*, 2189.
19. Hu, Y. Z.; Tsukiji, S.; Shinkai, S.; Oishi, S.; Hamachi, I. *J. Am. Chem. Soc.* **2000**, *122*, 241.
20. Fungo, F.; Otero, L. A.; Sereno, L.; Silber, J. J.; Durantini, E. N. *J. Mater. Chem.* **2000**, *10*, 645.
21. Moore, T. A.; Gust, D.; Mathis, P.; Mialocq, J.-C.; Chachaty, C.; Bensasson, R. V.; Land, E. J.; Doizi, D.; Liddell, P.; Lehman, W. R.; Nemeth, G. A.; Moore, A. L. *Nature* **1984**, *307*, 630.
22. Nagata, T.; Osuka, A.; Muruyama, *J. Am. Chem. Soc.* **1990**, *112*, 3054.
23. Reddy, D. R.; Maiya, B. G. *J. Phys. Chem. A* **2003**, *107*, 6326.
24. Reddy, D. R.; Maiya, B. G. *Chem. Commun.* **2000**, 117.
25. Harriman, A.; Heitz, V.; Sauvage, J.-P. *J. Phys. Chem.* **1993**, *97*, 5940.
26. Brookfield, R. L.; Ellul, H.; Harriman, A.; Porter, G. *J. Chem. Soc., Faraday Trans. 2* **1986**, *82*, 219.
27. Chambron, J.-C.; Heitz, V.; Sauvage, J.-P.; Pierre, J.-L.; Zurita, D. *Tetrahedron Lett.* **1995**, *36*, 9321.
28. Sylvie, C.-N.; Sauvage, J.-P.; Mathis, P. *Angew. Chem., Int. Ed. Engl.* **1989**, *28*, 593.
29. Chambron, J.-C, Harriman, A.; Heitz, V.; Sauvage, J.-P. *J. Am. Chem. Soc.* **1993**, *115*, 7419.
30. Helms, A.; Heiler, D.; McLendon, G. *J. Am. Chem. Soc.* **1992**, *114*, 6227.
31. Osuka, A.; Tanabe, N.; Kawabata, S.; Yamazaki, I.; Nishimura, Y. *J. Org. Chem.* **1995**, *60*, 7177.

32. A. Harriman, V. Heitz, M. Ebersole, H. van Willigen, *J. Phys. Chem.* **1994**, *98*, 4982.

33. Kilsa, K.; Kajanus, J.; Martensson, J.; Albinsson, B. *J. Phys. Chem. B* **1999**, *103*, 7329.

34. Jensen, J. J.; van Berlekom, S. N.; Kajanus, J.; Martensson, J.; Albinsson, B. *J. Phys. Chem. A* **1997**, *101*, 2218.

35. Kilsa, K.; Kajanus, J.; Larsson, S.; Macpherson, A. N.; Martensson, J.; Albinson, B. *Chem. Eur. J.* **2001**, *7*, 2122.

36. Yang, S. I.; Seth, J.; Balasubramanian, T.; Kim, D.; Lindsey, J. S.; Holten, D.; Bocian, D. F. *J. Am. Chem. Soc.* **1999**, *121*, 4008.

37. Asano-Someda, M.; Kaizu, Y. *Inorg. Chem.* **1999**, *38*, 2303.

38. Brun, A. M.; Harriman, A.; Heitz, V.; Sauvage, J.-P. *J. Am. Chem. Soc.* **1991**, *113*, 8657.

39. de Rege, P. J. F.; Williams, S. A.; Therien, M. J. *Science* **1995**, *269*, 1409.

40. Sazanovich, I. V.; Balakumar, A.; Muthukumaran, K.; Hindin, E.; Kirmaier, C.; Diers, J. R.; Lindsey, J. S.; Bocian, D. F.; Holten, D. *Inorg. Chem.* **2003**, *42*, 6616.

41. Harriman, A.; Magda, D. J.; Sessler, J. L. *J. Chem. Soc., Chem. Commun.* **1991**, 345.

42. Tamiaki, H.; Nomura, K.; Maruyama, K. *Bull. Chem. Soc. Jpn.* **1993**, *66*, 3062.

43. Kumar, A. A.; Giribabu, L.; Reddy. D. R.; Maiya, B. G. *Inorg. Chem.* **2001**, *40*, 6757.

44. Cheng, K. F.; Drain, C. M.; Grohmann, K. *Inorg. Chem.* **2003**, *42*, 2075.

45. Kalyanasundaram, K. *Photochemistry of Polypyridine and Porphyrin Complexes*; Academic Press: London, **1992**.

46. Sauvage, J.-P.; Harriman, A. *Chem. Soc. Rev.* **1996**, *25*, 41.

47. Hamilton, A. D.; Rubin, H. D.; Bocarsley, A. B. *J. Am. Chem. Soc.* **1984**, *106*, 7255.

48. Sessler, J. L.; Capuano, V. L.; Burell, A. K. *Inorg. Chim. Acta* **1993**, *204*, 93.

49. Balzani, V.; Juris, A.; Venturi, M.; Campagna, S.; Serroni, S. *Chem. Rev.* **1996**, *96*, 759.

50. Flamigni, L.; Barigelletti, F.; Armaroli, N.; Collin, J.-P.; Dixon, I. M.; Sauvage, J.-P.; Williams, J. A. G. *Coord. Chem. Rev.* **1999**, *190 -192*, 671.

51. Chichak, K.; Branda, N. R. *Chem. Commun.* **1999**, 523.

52. Durr, H.; Bossman, S. *Acc. Chem. Res.* **2001**, *34*, 905.

53. LeGourrierec, D.; Andersson, M.; Davidsson, J.; Mukhtar, E.; Sun, L.; Hammarstrom, L. *J. Phys. Chem. A* **1999**, *103*, 557.

54. Brum, A. M.; Atherton, S. J.; Harriman, A.; Heitz, V.; Sauvage, J.-P. *J. Am. Chem. Soc.* **1992**, *114*, 4632.

55. Araki, K.; Losco, P.; Engelmann, F. M.; Winnischofer, H.; Toma, H. E. *J. Photochem. Photobiol. A Chem.* **2001**, *142*, 25.

56. Baranoff, E.; Collin, J.-P.; Flamigni, L.; Sauvage, J.-P. *Chem. Soc. Rev.* **2004**, *33*, 147.

57. Collin, J.-P; Harriman, A.; Heitz, V.; Obodel, F.; Sauvage, J.-P. *J. Am. Chem. Soc.* **1994**, *116*, 5679.

58. Dixon, I. M.; Collin, J.-P.; Sauvage, J.-P.; Flamigni, L. *Inorg. Chem.* **2001**, *40*, 5507.

59. Harriman, A.; Odobel, F.; Sauvage, J.-P. *J. Am. Chem. Soc.* **1995**, *117*, 9461.

60. Collin, J.-P.; Heitz, V.; Sauvage, J.-P. *Tetrahedron Lett.* **1991**, *32*, 5977.

61. Falmigni, L.; Armaroli, N.; Barigeiietti, F.; Balzani, V.; Collin, J.-P.; Dalbavie, J.-O.; Heitz, V.; Sauvage, J.-P. *J. Phys. Chem. B* **1997**, *101*, 5936.

62. Fuhrhop, J.-H.; Smith, K. M. in *Porphyrins and Metalloporphyrins*, Smith, K. M.; Ed.; Elsevier: Amsterdam, **1975**; p. 769.

63. Fuhrhop, J.-H.; Smith, K. M.; In *Porphyrins and Metalloporphyrins*; Smith, K. M.; Ed.; Elsevier: Amsterdam, **1975**; p. 179.

64. Klassen, D. M.; Hudson, C. W.; Shaddix, E. L. *Inorg. Chem.* **1975**, *14*, 2733.

65. Belser, P.; Von Zelewsky, A. *Helv. Chim. Acta* **1980**, *63*, 1675.

66. Little, R. G. *J. Heterocycl. Chem.* **1978**, *15*, 203.

67. Nicholson, R. S.; Shain, I. *Anal. Chem.* **1964**, *36*, 706.

68. Maestri, M.; Armaroli, N.; Balzani, V.; Constable, E. C.; Thompson, A. M. C. C. *Inorg. Chem.* **1995**, *34*, 2759.

69. Flamigni, L.; Barigelletti, F.; Armaroli, N.; Collin, J.-P.; Sauvage, J.-P.; Williams, J. A. G. *Chem. Eur. J.* **1998**, *4*, 1744.

70. Rehm, D.; Weller, A. *Isr. J. Chem.* **1970**, *8*, 259.

CHAPTER 6

Porphyrin-pyrene and porphyrin-anthraquinone dyads: Synthesis, spectroscopy and photochemistry

6.1 Introduction

It is interesting to see whether PET and EET reactions occur when either donor or acceptor molecules are connected at the peripheral positions of porphyrin. For this reason, we had synthesized porphyrin-pyrene and porphyrin-anthraquinone having an azomethine group separating the two subunits, which have been discussed in this Chapter.

In view of their importance in both biological and abiological applications, such as biomimetic photosynthesis, molecular electronics etc., studies on EET and PET reactions occurring in porphyrin based donor-acceptor (D-A) systems are increasingly being pursued in recent years.[1-21] We have been interested in the design, synthesis and mechanistic elucidation of the PET and EET reactions of intramolecular hybrid porphyrin systems in which a tetraaryl porphyrin is linked to either nitroaromatic or anthracene subunit/s.[22-30] Of specific relevance to this Chapter are our recent reports on the intramolecular EET and PET reactions of a pentad system in which a porphyrin is endowed with four anthracene donor subunits,[24] a series of covalently linked isomeric porphyrin -anthracene dyads,[25] a non-covalent D-A systems assembled *via* complementary nucleic acid base-pairing[26] and a recently reported tin(IV) porphyrin that is appended with anthracene donor subunits at both the axial and peripheral positions.[27] Besides

these, there are a number of reports from other workers on EET and PET occurring in D-A systems.[31-37]

EET reactions of porphyrin-anthracene systems are attractive largely due to the facts that (i) anthracene is a good energy donor and its singlet excited state lies above that of the porphyrin and (ii) it has well defined spectral and electrochemical signatures.[38] Pyrene, the next hydrocarbon to anthracene in the homologous series, also possesses photophysical and spectral qualities similar to those of anthracene. On the other hand PET reactions in porphyrin-quinone/anthraquinone molecules have been studied as model for the light-initiated charge separation in photosynthesis.[39-54] Many of these reports are concerned with in order to understand the role of distance, orientation, energetics, and the role of the medium on the rate of intramolecular PET. With the above considerations in mind, we tried to synthesize trichromophoric species having 'pyrene-porphyrin-anthraquinone' where porphyrin functions as a donor/acceptor, pyrene as a donor and anthraquinone as an acceptor. But we could not succeed to synthesize this triad, instead, we successfully prepared 'porphyrin-pyrene' and 'porphyrin-anthraquinone' dyads. Finally, we discuss the synthesis and intramolecular EET/PET mechanisms of an azomethine bridged porphyrin-pyrene/anthraquinone dyads (**H_2-Py/H_2-AQ**) and its copper(II) (**Cu-Py/Cu-AQ**) and zinc(II) (**Zn-Py/Zn-AQ**) derivatives, Schemes 6.1 & 6.2.

6.2 Experimental details

5,10,15,20-tetraphenylporphyrin (**H_2TPP**) and its zinc(II) complex (**ZnTPP**), the reference compounds used during the fluorescence studies were synthesized as reported.[55,56]

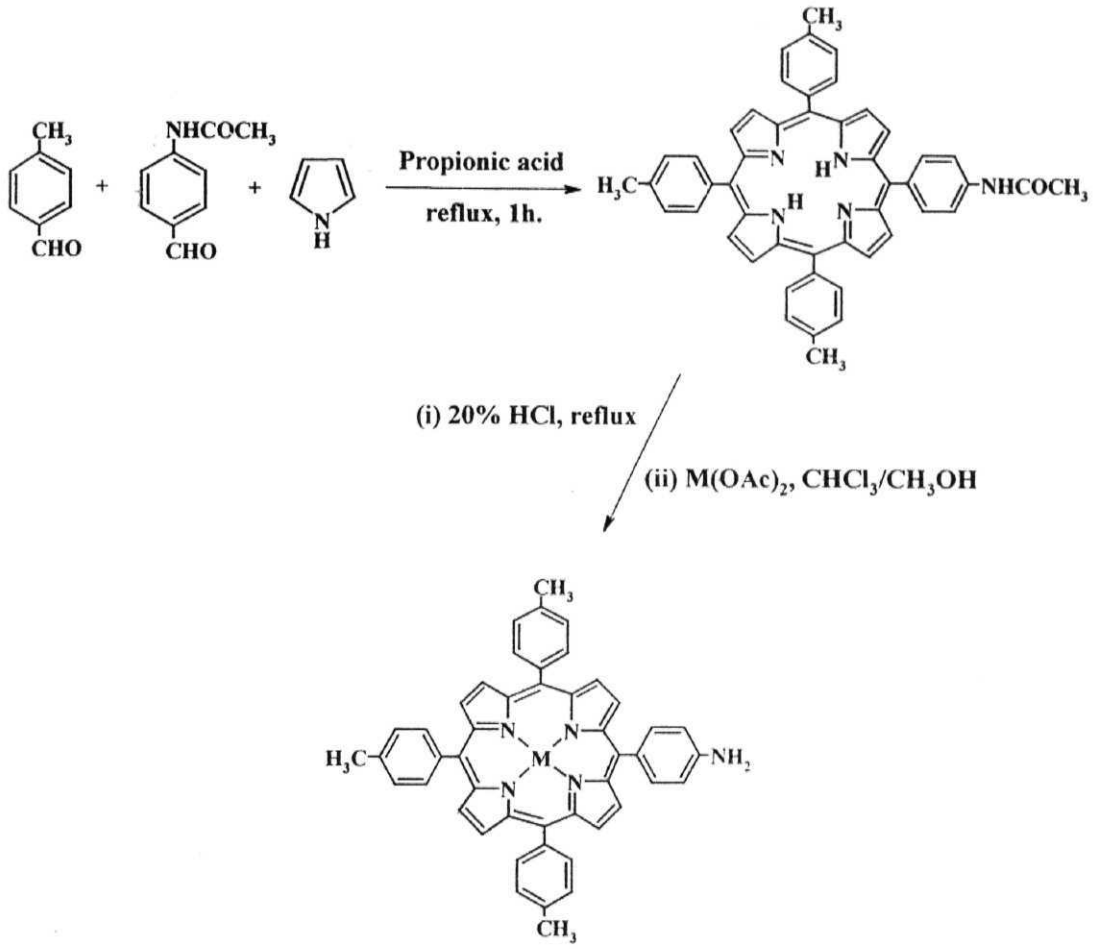

Scheme 6.1 Synthesis of meso-5-(4-aminophenyl)-10,15,20-tri(4-methylphenyl) porphyrin ($\mathbf{H_2L^4}$) and its Cu(II), Zn(II) derivatives, i.e. $\mathbf{CuL^4}$ and $\mathbf{ZnL^4}$.

6.2.1 Synthesis of anthraquinone-2-aldehyde [AQ-2-CHO] [57]

AQ-2-CHO was prepared starting from **2-MeAQ** by standard reported procedure. 5 ml concentrated sulphuric acid was added to a stirring solution of 24 ml of acetic anhydride and 4 g (18 mmol) of **2-MeAQ**. When the temperature was

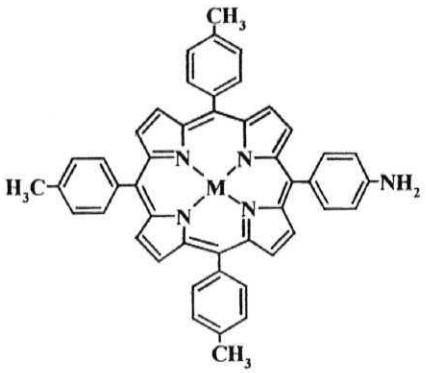

M = 2H (**H_2L^4**), Cu(II) (**CuL^4**), Zn(II) (**ZnL^4**)

Py-1-CHO **AQ-2-CHO**

toluene, 4 Å molecular sieves, 12-24 h., reflux, N_2.

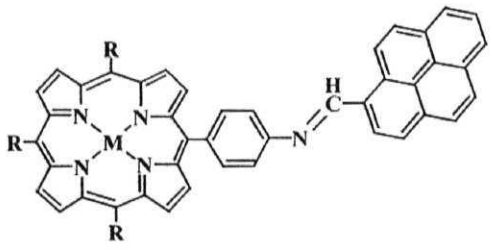

M = 2H (**H_2-Py**), Cu(II) (**Cu-Py**), Zn(II) (**Zn-Py**)

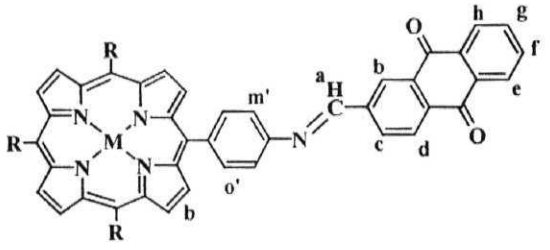

M = 2H (**H_2-AQ**), Cu(II) (**Cu-AQ**), Zn(II) (**Zn-AQ**)

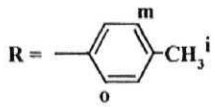

Scheme 6.2 Synthesis of new 'porphyrin-pyrene' and 'porphyrin-anthraquinone' dyads.

lowered to 0 °C, added slowly with stirring a solution of 5 g (50 mmol) of chromium trioxide in 23 ml of acetic anhydride, at such a rate that the temperature does not exceed 10 °C. Stirring was continued further 2 h. This mixture was poured into a 3 L. beaker containing crushed ice and cold water. The precipitate was collected by filtration and washed with cold water until the washings are colourless. The precipitate, thus obtained was refluxed with a mixture of 7 ml of ethanol, 7 ml of water and 1 ml of concentrated sulphuric acid for 30 minutes and this was filtered through a fluted filter-paper and cooled the filtrate in ice. The crystals were collected by suction filtration, washed with cold water and dried in vacuum desiccator. Yield = 2.33 g (8.8 mmol, 55%).

6.2.2 Synthesis of meso-5-(4-aminophenyl)-10,15,20-tri(4-methylphenyl) porphyrin [H_2L^4]

The precursor porphyrin used for the synthesis of the present dyads was prepared by a reported method.[58] 5.37 g (80 mmol) pyrrole was added to a refluxing solution of 7.21 g (60 mmol) 4-methylbenzaldehyde and 3.23 g (20 mmol) 4-acetamidobenzaldehyde in 1.5 L. propanoic acid. After complete addition of the pyrrole, the reaction mixture was refluxed for 1 h. The mixture was cooled, and left for 12 h. at room temperature. The propanoic acid was removed by distillation and the residue was dried at 100 °C in vacuum and chromatographed on a silica gel column with CH_2C1_2 as eluent. The first fraction collected was 5,10,15,20-tetra(4-methylphenyl)porphyrin. After isolation of first fraction, 5% ethyl acetate was added to the eluent. The second fraction collected was compound 5-(4-acetamidophenyl)-10,15,20-tri(4-methylphenyl) porphyrin. Yield = 368 mg (0.5 mmol, 17%).

A suspension of 5-(4-acetamidophenyl)-10,15,20-tri(4-methylphenyl) porphyrin (368 mg, 0.39 mmol) was refluxed for 5 h. in 20% HCl. The solution was cooled and neutralized carefully by adding 10% KOH solution. The neutralized solution was extracted several times with CH_2Cl_2. The combined organic layers were dried (Na_2S0_4), the solvent evaporated and the residue chromatographed on a silica gel column using CH_2C1_2 as eluent. Yield = 310 mg (0.46 mmol, 90%).

6.2.3 Synthesis of 5-(4-aminophenyl)-10,15,20-tri(4-methylphenyl)porphyrina -tocopper(II)/zinc(II) [CuL^4/ZnL^4]

CuL^4 and **ZnL^4** were prepared by metallating **H_2L^4** with the corresponding metal(II) acetates by the standard methods.[56] Typically, 100 mg (0.15 mmol) of **H_2L^4** and ~100 mg of either copper(II) acetate or zinc(II) acetate were stirred in $CHCl_3/CH_3OH$ mixture for 1 h. The solvents were evaporated and the residue was washed with water and dried. Purification by column chromatography (silica, 100-200 mesh) furnished the pure product in each case. Yields: **CuL^4** = 98 mg (0.13 mmol, 90%) and **ZnL^4** = 100 mg (0.14 mmol, 95%).

6.2.4 Synthesis of 'free base porphyrin-pyrene' dyad [H_2-Py]

H_2L^4 (50 mg, 0.074 mmol) and 1-pyrenecarboxaldehyde, **Py-1-CHO**, (85 mg, 0.37 mmol) were dissolved in 40 ml of dry toluene containing 4 Å molecular sieves. The resulting solution was refluxed under the nitrogen atmosphere for 12 h. The solvent was removed and the crude product was dissolved in CH_2Cl_2 and filtered. Evaporation of the solvent gave a purple solid, which was precipitated

twice from CH_2Cl_2-CH_3CN to give **H_2-Py** in pure form. Yield = 55 mg (0.06 mmol, 83%).

6.2.5 Synthesis of 'metallo porphyrin-pyrene' dyad [Cu/Zn-Py]

These compounds were prepared, starting with **CuL^4** or **ZnL^4** (25 mg, ~ 0.034 mmol) and **Py-1-CHO** (40 mg, 0.17 mmol), in a manner analogous to that described above for **H_2-Py**. Yields: **Cu-Py** = 28 mg (0.029 mmol, 86%), **Zn-Py** = 25 mg (0.026 mmol, 78%).

6.2.6 Synthesis of 'free base porphyrin-anthraquinone' dyad [H_2-AQ]

H_2L^4 (50 mg, 0.074 mmol) and **AQ-2-CHO** (87 mg, 0.37 mmol) were dissolved in 40 ml of dry toluene containing 4 Å molecular sieves. The resulting solution was refluxed under the nitrogen atmosphere for 8 h. The solvent was removed and the crude product was dissolved in CH_2Cl_2 and filtered. Evaporation of the solvent gave a purple solid, which was recrystallized twice from CH_2Cl_2-CH_3OH to give **H_2-AQ** in pure form. Yield = 53 mg (0.06 mmol, 80%).

6.2.7 Synthesis of 'metallo porphyrin-anthraquinone' dyad [Cu/Zn-AQ]

These compounds were prepared, starting with **CuL^4** or **ZnL^4** (25 mg ~ 0.034 mmol) and **AQ-2-CHO** (40 mg, 0.17 mmol), in a manner analogous to that described above for **H_2-AQ**. Yields: **Cu-AQ** = 27 mg (0.028 mmol, 82%), **Zn-AQ** = 25 mg (0.026 mmol, 77%).

6.3 Results and discussion

Synthesis of all the new compounds has been accomplished here, in good-to-moderate yields, by a simple schiff base condensation between the aminoporphyrin ($\mathbf{L^4}$) derivatives and **Py-1-CHO/AQ-2-CHO**. These compounds have been fully characterized by FAB-MS, IR, UV-visible, ESR and ^{1}H NMR spectroscopies and also by the cyclic and differential pulse voltammetric techniques as described below.

6.3.1 Ground state properties

H_2-Py and **H_2-AQ** showed the expected mass spectral pattern with the parent ion peak (m/z) appearing at $(M+H)^+$ = 884 and 890, respectively. Peaks due to elimination of the pyrene/anthraquinone unit appear at 672, i.e. $M-C_{17}H_{11}$ or $M-C_{15}H_8O_2$, respectively. The C=N frequencies found from Infrared spectra of various compounds are summarized in Table 6.1

Table 6.1 Infrared data of newly synthesized compounds and their aldehyde precursors [a]

Compd. → $\gamma_{str}(cm^{-1})$ ↓	Py-1-CHO	H_2-Py	Cu-Py	Zn-Py	AQ-2-CHO	H_2-AQ	Cu-AQ	Zn-AQ
$\gamma_{C=O}$	1680	-	-	-	1678	1674	1674	1672
$\gamma_{C=N}$	-	1581	1585	1585	-	1591	1589	1593

(a) Spectra were recorded in KBr pellet.

The ^{1}H NMR spectrum of each new dyad was analyzed based on the resonance position and integrated intensity data as well as the proton-to-proton

connectivity information revealed in the ^{1}H-^{1}H COSY spectra to arrive at the structure of these compounds. The ^{1}H NMR spectra of **H_2-Py**, **H_2-AQ** and **Zn-AQ** are shown in Fig. 6.1 and data for newly investigated compounds along with their individual constituents (i.e. **H_2L^4**, **ZnL^4**, **Py-1-CHO** and **AQ-2-CHO**) are summarized in Table 6.2. A comparison of **H_2-Py** spectrum with those of reference compounds reveals that the resonance positions of the various protons

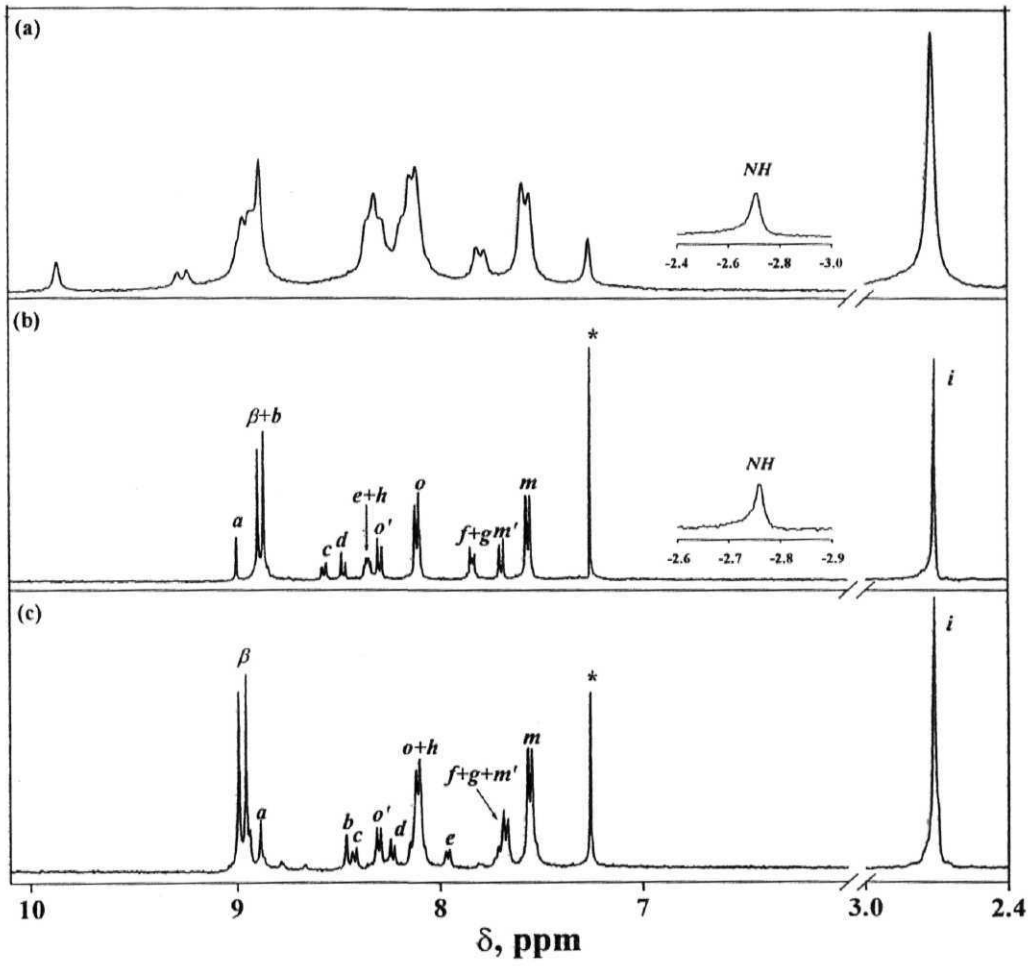

Fig. 6.1 ^{1}H NMR spectra of (a) **H_2-Py** (200 MHz) (b) **H_2-AQ** (400 MHz) and (c) **Zn-AQ** (400 MHz) in $CDCl_3$, TMS at 300 K (* peak is due to solvent).

Table 6.2 ^{1}H NMR data of dyads and their precursors [a]

Compd.	δ, ppm					
	Porphyrin					Py/AQ
	β-pyrrole	meso-tolyl	CH_3	NH_2/NH	HC=O/ CH=N	
H_2L^4	8.90 (m, 8H)	8.10 (d, 6H) 8.01 (d, 2H) 7.55 (d, 6H) J = 7.4 Hz 7.07 (d, 2H) J = 7.9 Hz	2.71 (s, 9H)	4.03 (s, 2H) -2.74 (s, 2H)	-	-
ZnL^{4b}	8.96 (m, 8H) 8.87 (d, 4H) J = 4.4 Hz 8.82 (d, 4H) J = 5.0 Hz	8.15 (d, 8H) J = 8.0 Hz 8.07 (d, 8H) J = 7.8 Hz 7.58 (dd, 4H) J = 8.4, 3.2Hz 5.64 (d, 4H) J = 7.8 Hz	2.70 (s, 9H) 2.66 (s, 9H)	-	-	-
Py-1-CHO	-	-	-	-	10.78 (s, 1H)	9.41 (d, 1H) J = 9.7 Hz 8.45 (d, 1H) 8.31 (d, 1H) J = 8.7 Hz 8.26 (m, 5H) 8.11 (m, 2H)
AQ-2-CHO	-	-	-	-	10.24 (s, $1H_a$)	8.80 (s, $1H_b$) 8.48 (d, $1H_c$) J = 8.0 Hz 8.32 (m, $3H_{d+e+h}$) 7.89 (m, $2H_{f+g}$)
H_2-Py	8.88 (m, 8H)	8.31 (m, 2H) 8.11 (m, 6H) 7.80 (d, 2H) 7.58 (d, 6H) J = 6.8 Hz	2.72 (s, 9H)	-2.71 (s, 2H)	9.87 (s, 1H)	9.25 (d, 1H) J = 8.8 Hz 8.99 (m, 1H) 8.31 (m, 5H) 8.21 (m, 1H) 8.13 (m, 1H)

.....Continued

.....Table 6.2

Zn-Py	8.97 (m, 8H)	8.32 (m, 2H) 8.12 (m, 6H) 7.80 (d, 2H) J = 7.9 Hz 7.57 (d, 6H) J = 7.5 Hz	2.73 (s, 9H)	-	9.87 (s, 1H)	9.24 (d, 1H) J = 8.8 Hz 8.93 (m, 1H) 8.32 (m, 5H) 8.18 (m, 1H) 8.07 (m, 1H)
H_2-AQ	8.87 (m, 8H)	8.29 (m, $2H_{o'}$) 8.11 (d, $6H_o$) 7.69 (d, $2H_{m'}$) J = 8.0 Hz 7.57 (d, $6H_m$) J = 7.2 Hz	2.72 (s, 9H)	-2.76 (s, 2H)	8.99 (s, $1H_a$)	8.87 (s, $1H_b$) 8.56 (d, $1H_c$) J = 8.0 Hz 8.47 (d, $1H_d$) J = 7.6 Hz 8.36 (m, $2H_{e+h}$) 7.83 (m, $2H_{f+g}$)
Zn-AQ	8.97 (m, 8H)	8.31 (m, $2H_{o'}$) 8.11 (d, $6H_o$) 7.68 (d, $2H_{m'}$) J = 7.8 Hz 7.56 (d, $6H_m$) J = 7.8 Hz	2.72 (s, 9H)	-	8.88 (s, $1H_a$)	8.46 (s, $1H_b$) 8.42 (m, $1H_c$) J = 8.0 Hz 8.24 (d, $1H_d$) J = 8.0 Hz 7.96 (d, $1H_e$) J = 7.2 Hz 8.11 (m, $1H_h$) 7.68 (m, $2H_{f+g}$)

(a) Spectra were recorded in $CDCl_3$, TMS. Error limits: δ, ± 0.01 ppm, J: ± 1 Hz.

(b) Due to self-assembly it is showing more signals than corresponding free base porphyrin (**H_2L^4**). [59]

present either on the porphyrin macrocycle or the pyrene subunit are not shifted considerably upon linking the two chromophores *via* the azomethine spacer. This is reasonable if one considers that the two aromatic rings are at a 'trans' configuration with respect to the C=N spacer, avoiding the steric interaction. Similar results were obtained for **Zn-Py** and **H_2-AQ** from ^{1}H NMR spectroscopy. The structure of **H_2-Py** and **H_2-AQ** derived from the molecular mechanics (PCM) calculations indeed suggests the same.

Interestingly the anthraquinone peak positions in **Zn-AQ** undergo a high field shift without perturbing appreciably the peak position of the porphyrin ring, Figs. 6.1& 6.2. For example resonance due to protons **d, b, e** and **h** (see Scheme

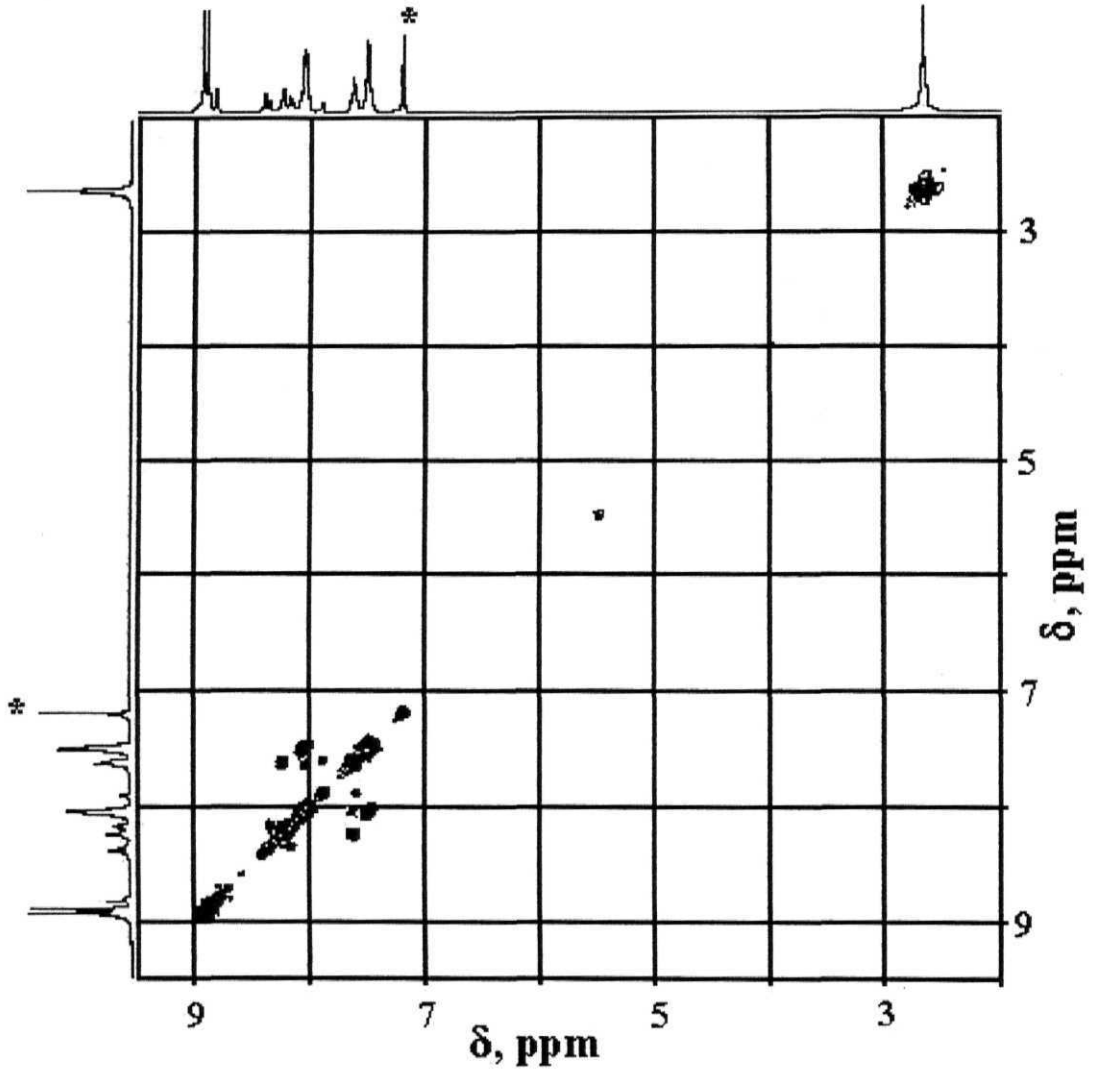

Fig. 6.2 ^{1}H-^{1}H COSY NMR spectrum of **Zn-AQ** in $CDCl_3$ (* peak is due to solvent).

6.2) which were appearing at 8.47, 8.87, 8.36 and 8.36 ppm in **H_2-AQ**, whereas in **Zn-AQ** appear at 8.23, 8.46, 7.96 and 8.11 ppm respectively, Similarly, resonances due to the protons **a**, **c**, **f** and **g** of this compound are upfield shifted compared to the corresponding resonances in the spectrum of **H_2-AQ**. This changes could be interpreted in terms of ligation of the anthraquinone carbonyl group (C=O) with the central zinc(II) porphyrin.[60,61] This would bring the protons present on the anthraquinone subunit into the shielding region of the coordinated porphyrin's ring current.[62]

In addition, the spin Hamiltonian parameters ($g_{\parallel}$, $g_{\perp}$ and $A_{\parallel}^{Cu}$, $A_{\perp}^{Cu}$, $A_{\parallel}^{N}$ and $A_{\perp}^{N}$ derived from the ESR spectrum of **Cu-Py** and **Cu-AQ** (toluene, 100 ± 3 K) are also quite close to those of **CuL^4** or **CuTPP**.[63] Fig. 6.3 illustrates the ESR spectra of **Cu-Py** and **Cu-AQ** and ESR parameters are summarized in Table 6.3.

Table 6.3 ESR spectral data in toluene at 100 ± 3K [a]

Compd.	$g_{\parallel}$	$g_{\perp}$	x 10^4 cm^{-1}			
			$A_{\parallel}^{Cu}$	$A_{\perp}^{Cu}$	$A_{\parallel}^{N}$	$A_{\perp}^{N}$
CuTPP	2.145	2.029	207	32.8	13.9	16.4
CuL^1	2.160	2.028	202	33.0	14.2	16.5
Cu-Py	2.176	2.035	204	33.0	14.6	16.5
Cu-AQ	2.148	2.020	215	33.2	14.2	16.6

(a) Error limits: g = ± 0.005; A = ± 10%.

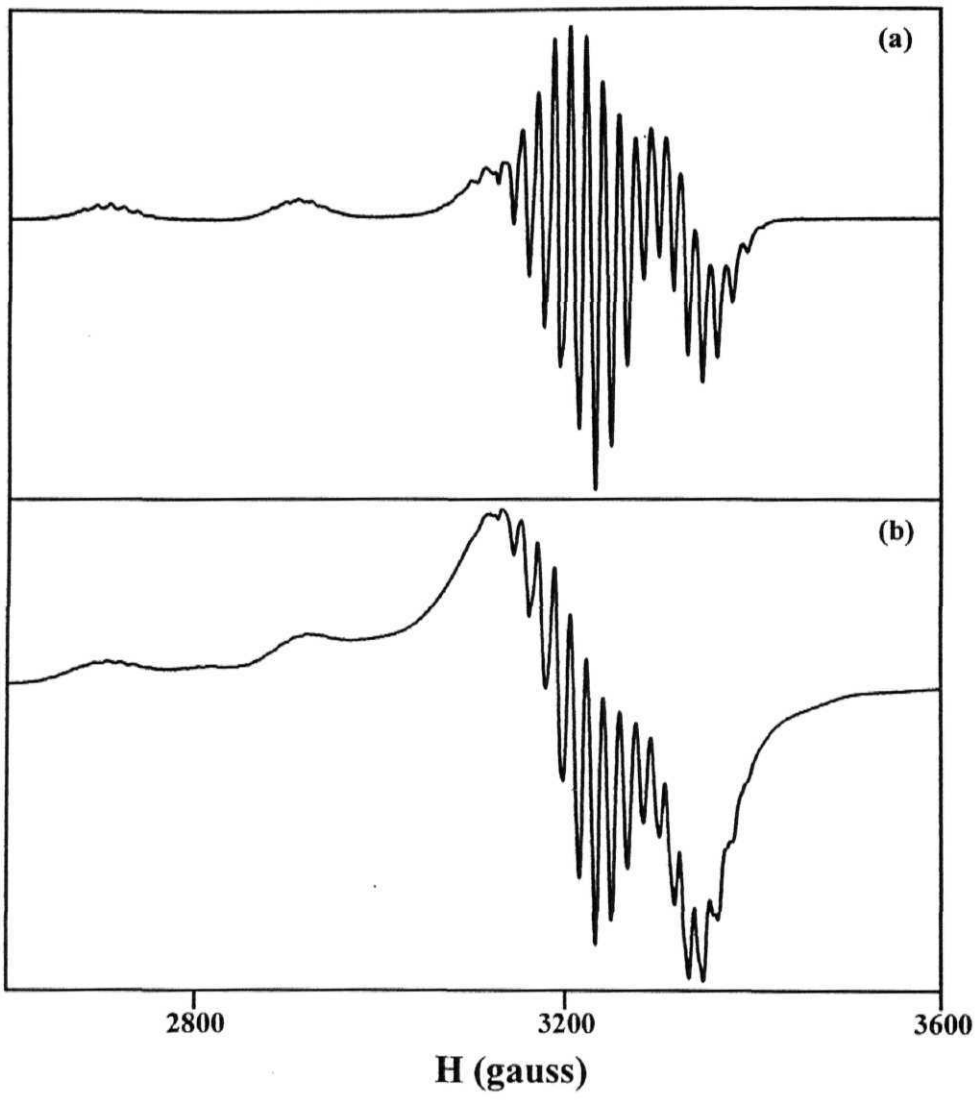

Fig. 6.3 ESR spectra of (a) **Cu-Py** and (b) **Cu-AQ** in toluene at 100 ± 3 K.

The wavelengths of maximum absorbance (λ_{max}) and molar extinction coefficient (ε) values of the new dyads and those of their constituent individual components (i.e. $\mathbf{H_2L^4}$, $\mathbf{CuL^4}$, $\mathbf{ZnL^4}$, **Py-1-CHO** and **2-MeAQ**), as obtained from

the UV-visible studies are summarized in Table 6.4 and spectra were shown in Fig. 6.4. UV-visible spectra of all the new compounds and the data given in Table 6.4 suggests that the appended pyrene/anthraquinone chromophore dominantly absorbs between ca. 230-350 nm, a region in which porphyrin part of each molecule shows its so-called N and L bands. Nonetheless, the peak at 260-290 nm for each dyad corresponds largely to the absorbance of the pyrene/anthraquinone moiety because the N and L bands are quite weak compared to the pyrene/anthraquinone in this wavelength region. On the other hand, porphyrin parts of **H_2-Py/AQ, Cu-Py/AQ** and **Zn-Py/AQ** show four/two Q-bands in the wavelength region (500-700 nm) where the pyrene/anthraquinone part of each molecule does not absorb. Both porphyrin and pyrene chromophores of **H_2-Py, Cu-Py** and **Zn-Py** compounds are seen to absorb between ca. 350-420 nm resulting in the broadening of the peaks as well as appearance of pyrene bands in the porphyrin Soret band (B-band) region.

Spectral data given in the Table 6.4 further reveals that, in general, both λ_{max} and log ε values of each dyad are within the same range as those of the constituent individual components. Finally, it was observed that the λ_{max} and spectral shapes of the bands of all the new compounds are more or less similar to those of solutions containing one mole equivalent each of **H_2L^4 / CuL^4 / ZnL^4** and **Py-1-CHO/2-MeAQ**.

Table 6.5 summarizes redox potential data (CH_2Cl_2, 0.1 M TBAP) of the D-A systems investigated in this study along with that of the corresponding reference compounds. Fig. 6.5 illustrates the cyclic and differential pulse voltammograms of newly synthesized pyrene dyads. Each investigated new compound shows two to three reduction and three oxidation peaks under the

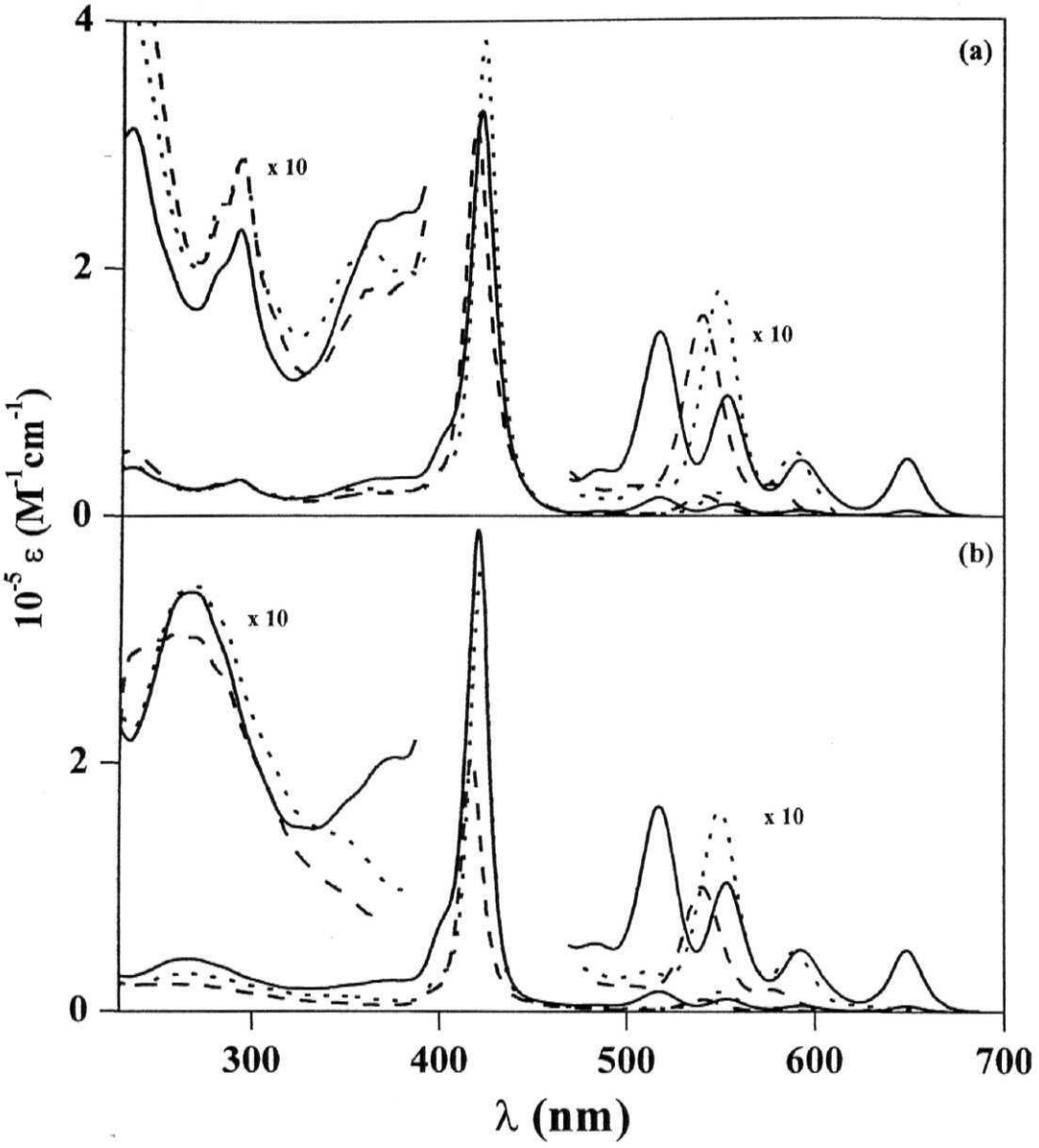

Fig. 6.4 UV-visible spectra of (a) **H_2-Py** (——), **Cu-Py** (-------) and **Zn-Py** (·····) and (b) **H_2-AQ** (——), **Cu-AQ** (-------) and **Zn-AQ** (·····) in CH_2Cl_2.

Table 6.4 UV-visible data of dyads and its monomeric analogues in CH_2Cl_2 [a]

Compd.	λ_{max}, nm (log ε)		
	B-band	Q-bands	AQ/Py
H_2L^4	421 (5.44)	650 (3.65), 594 (3.62), 555 (3.94), 518 (4.12)	-
CuL^4	418 (5.47)	578 (3.51), 541 (4.22), 506 (3.48)	-
ZnL^4	422 (5.51)	590 (3.71), 550 (4.20)	-
Py-1-CHO	-	-	397 (4.36), 375 (4.39), 364 (4.40), 289 (4.55)
2-MeAQ	-	-	329 (3.87), 278 (4.39), 258 (4.84)
H_2-Py	422 (5.52)	649 (3.67), 593 (3.66), 554 (3.99), 518 (4.17)	378 (4.39), 367 (4.38), 292 (4.36)
Cu-Py	419 (5.50)	577 (3.50), 541 (4.22), 502 (3.49)	364 (4.27), 292 (4.45)
Zn-Py	423 (5.58)	589 (3.80), 550 (4.30), 512 (3.51)	379 (4.34), 362 (4.37), 292 (4.48)
H_2-AQ	421 (5.59)	649 (3.70), 593 (3.70), 554 (4.02), 517 (4.22)	268 (4.53)
Cu-AQ	418 (5.31)	577 (3.44), 541 (4.16), 498 (3.52)	260 (4.48)
Zn-AQ	422 (5.56)	589 (3.68), 550 (4.21)	271 (4.53)

(a) Spectra were measured in CH_2Cl_2. Error limits: λ_{max}, ± 1 nm, log ε, ± 10%

experimental conditions employed in this study. Wave analysis suggested that first two reduction and two oxidation processes represent reversible (i_{pc}/i_{pa} = 0.9-1.0) and diffusion controlled ($i_{pc}/\upsilon^{1/2}$ = constant in the scan rate (υ) range 50 - 500 mV/s) one-electron transfer (ΔE_P = 60 - 70 mV; ΔE_P = 65 ± 3 mV for Fc^+/Fc couple) reactions, the third electrode process is either quasi-reversible (i_{pc}/i_{pa} = 0.6 – 0.8 and ΔE_P = 80 - 150 mV) or irreversible under similar experimental conditions.[64] While the peaks occurring at potentials that are less anodic than 1.40 V are ascribed to successive one-electron oxidations of the porphyrin parts of **H_2-Py**, **Cu-Py** and **Zn-Py**, the peak occurring at more anodic potential represents the oxidation of the appended pyrene moiety. Similarly, while the first reduction peak corresponds to the reduction of the porphyrin ring, the remaining peak/s are assigned to electron addition to the porphyrin/pyrene moiety.

Whereas anthraquinone derivatives in CH_2Cl_2, 0.1 TBAP M shows two oxidation and three to four reduction peaks under the experimental conditions employed in this study (see Fig. 6.6 and data given in Table 6.5). Wave analysis suggest that the first two oxidation and first three reduction processes are reversible and remaining are either quasi-reversible or irreversible. Comparing cyclic and differential voltammograms of **H_2-AQ** with its reference compounds **2-MeAQ** and 5,10,15,20-tetra(4-methylphenyl)porphyrin (**H_2TTP**), it is found that the reduction potentials for first peak and third peak are close to that for the first reduction of **2-MeAQ** and second reduction of porphyrin (**H_2TTP**) ring. While second reduction peak is more complex, its peak current value is twice that of first peak. Since there is only one kind of substance in solution, the results indicate that two reduction (AQ moiety and porphyrin ring) of the molecule occurs with one electron each and at same potential.[65]

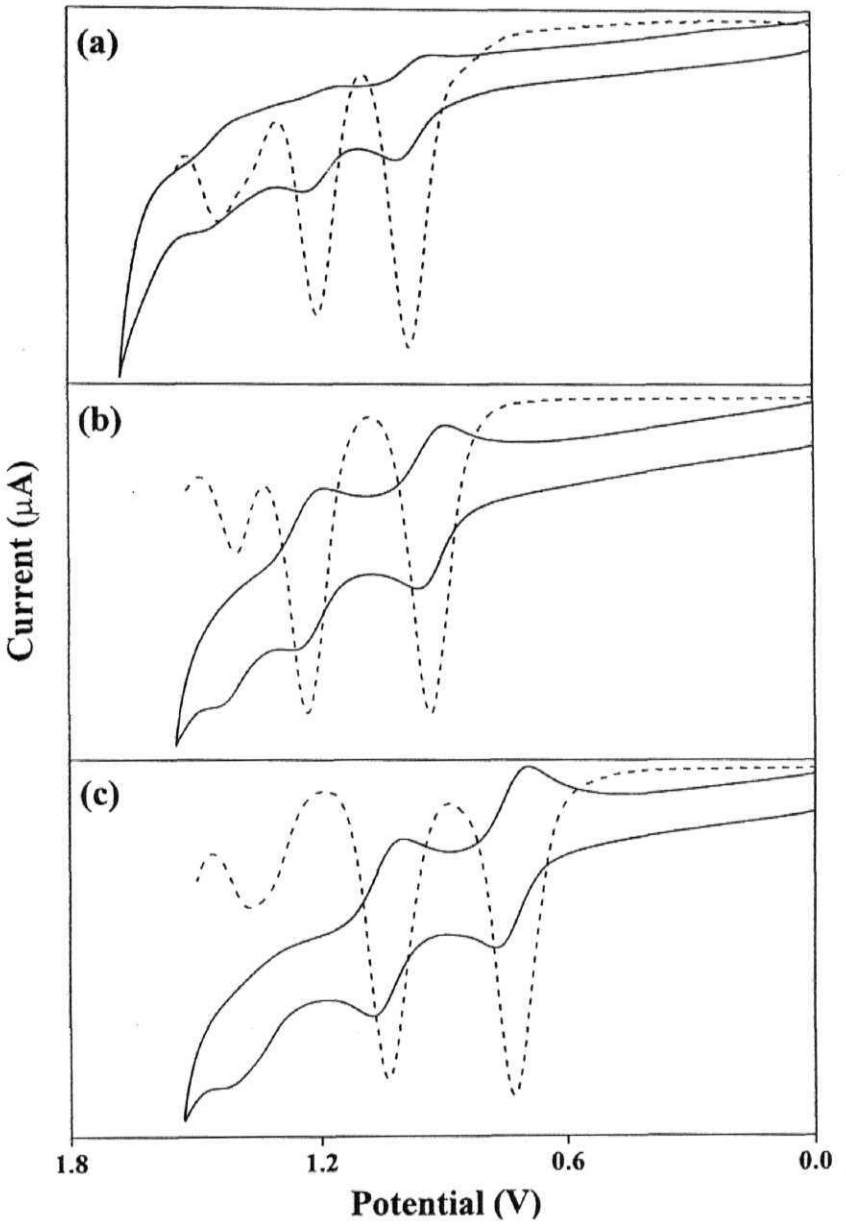

Fig. 6.5 Cyclic and differential pulse voltammograms of (a) **H_2-Py** (b) **Cu-Py** and (c) **Zn-Py** in CH_2Cl_2, 0.1 M TBAP (scan rate = 100 mV s^{-1}, modulation amplitude = 10 mV).

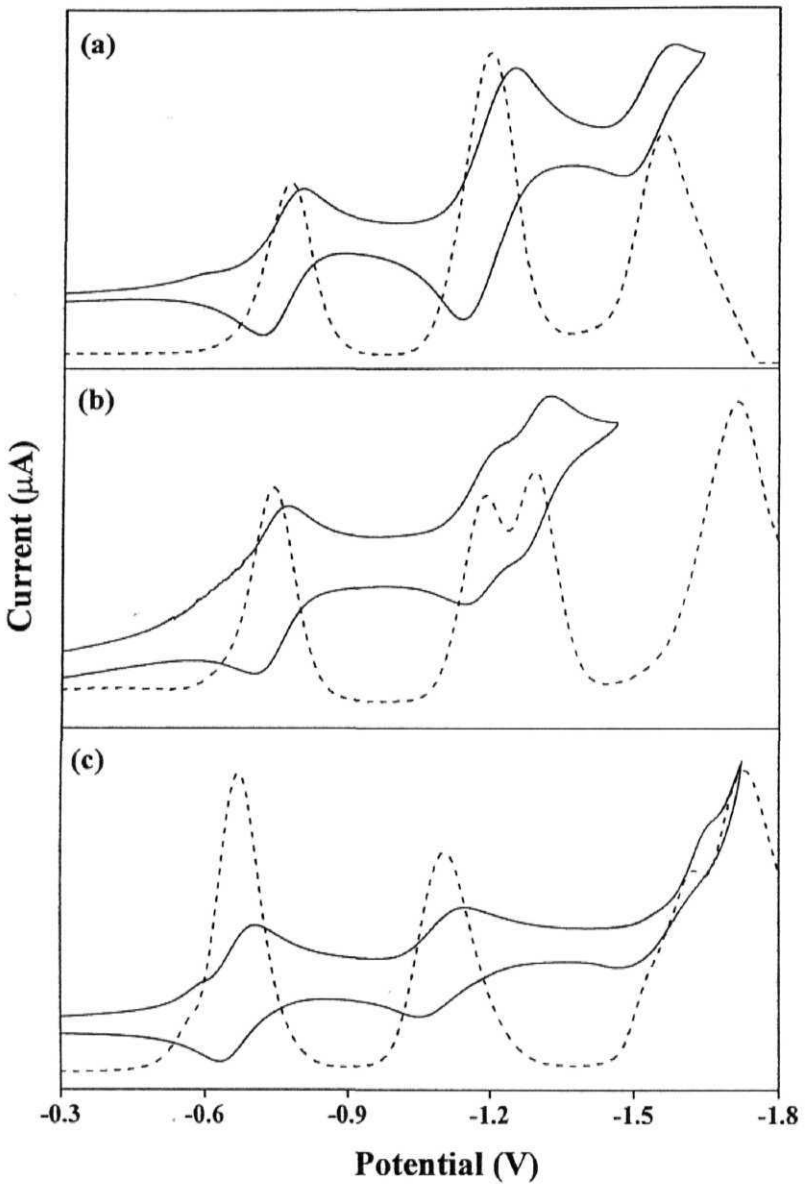

Fig. 6.6 Cyclic and differential pulse voltammograms of (a) **H_2-AQ** (b) **Cu-AQ** and (c) **Zn-AQ** in CH_2Cl_2, 0.1 M TBAP (scan rate = 100 mV s^{-1}, modulation amplitude = 10 mV).

Table 6.5 Redox potential data in CH_2Cl_2, 0.1 M TBAP [a]

Compd.	Potential ($E_{1/2}$) (mV vs SCE)		$\Delta G(^1P \rightarrow AQ)$ (eV) [c]
	Oxidation	Reduction	
Py-1-CHO	1510	-1410	-
2-MeAQ	-	-920, -1375	-
H_2TTP [b]	880, 1125	-1230, -1570	-
CuTTP [b]	930, 1250	-1300, -1720	-
ZnTTP [b]	790, 1085	-1310, -1550	-
H_2-Py	980, 1200, 1435	-1150, -1475	-
Cu-Py	930, 1230, 1400	-1295, -1520	-
Zn-Py	730, 1040, 1380	-1330, -1485, -1570	-
H_2-AQ	940, 1165	-770, -1200, -1560	-0.19
Cu-AQ	950, 1230	-740, -1190, -1290, -1725	-
Zn-AQ	750, 1050	-670, -1110, -1645, -1730	-0.65

(a) Error limits: $E_{1/2}$, ± 15 mV (b) $\mathbf{H_2L^1}$ (see Chapter 3) and its metal(II) derivatives gave ill-defined voltammograms. Hence, **TTP** [5,10,15,20-tetra(4-methylphenyl) porphyrin] derivatives are employed as reference compounds. (c) For a discussion see section 6.3.2.2.

This analysis, which is based on a comparison between the voltammograms of the dyads and those of the reference compounds, reveals that the redox potentials of the two subunits in the dyads are essentially close to those of the corresponding reference compounds.

6.3.2 Singlet state properties

The spectroscopic and electrochemical features described above suggest that the electronic communication between the porphyrin and pyrene/anthraquinone chromophores is quite negligible in these new conjugates. More importantly, the UV-visible data suggests that it is possible to individually address photochemistry of the porphyrin and the pyrene/anthraquinone subunits in these bichromophoric systems. In steady state fluorescence studies **Cu-Py** and **Cu-AQ** were found to be totally non-emissive probably due the paramagnetic nature of these complexes, but **H_2-Py, Zn-Py, H_2-AQ** and **Zn-AQ** were found to be photochemically active species.

6.3.2.1 Porphyrin-pyrene dyads

In Fig. 6.7, the steady state fluorescence spectra of these compounds measured in CH_2Cl_2 are compared with spectra of the corresponding individual components. Spectral shapes and wavelengths of maximum emission (λ_{em}) of these D-A systems, when they were irradiated at the porphyrin absorption band (λ_{ex} = 550 nm), are seen to be similar to the spectrum of either **H_2L^4** or **ZnL^4**. However, excitation at 290 nm (dominant pyrene absorption) resulted in broadening and marginal red shifts of the fluorescence bands in both the compounds in comparison with the fluorescence due to **Py-1-CHO**. From an overlay of the absorption and fluorescence spectra of these D-A systems, the 0-0 spectroscopic transition energies ($E_{0\text{-}0}$) of the pyrene (3.56 ± 0.05 eV) and the porphyrin moieties (1.90 ± 0.04 eV for **H_2-Py** and 2.09 ± 0.04 eV for **Zn-Py**) were obtained, and these values are found to be close to those of pyrene and **H_2TTP / ZnTTP**, respectively.

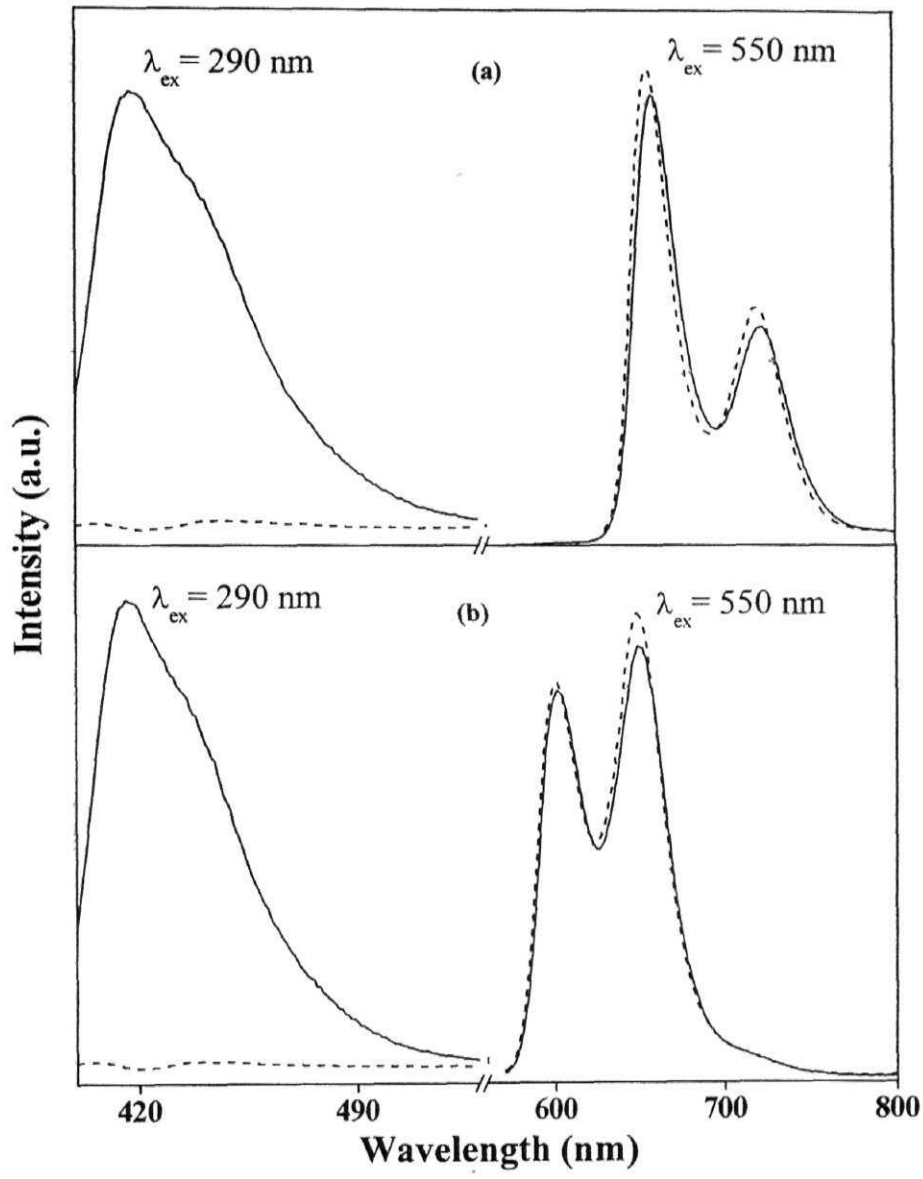

Fig. 6.7 Fluorescence spectra (CH_2Cl_2, O. D. = 0.2 at each λ_{ex}) of (a) λ_{ex} = 290 nm: **Py-1-CHO** (———) and **H_2-Py** (-------); λ_{ex} = 550 nm: **H_2L^4** (———) and **H_2-Py** (-------) (b) λ_{ex} = 290 nm: **Py-1-CHO** (———) and **Zn-Py** (-------); λ_{ex} = 550 nm: **ZnL^4** (———) and **Zn-Py** (--------).

Whereas the fluorescence quantum yield (ϕ) for excitation into the porphyrin part of each dyad was similar to that of the unlinked porphyrin (i.e. ϕ(**H_2-Py**) = 0.15 ± 0.01 and ϕ(**Zn-Py**) = 0.048 ± 0.005), fluorescence from the pyrene part was found to be strongly quenched, in comparison with the fluorescence of free **Py-1-CHO** (or pyrene), Fig. 6.7. The quenching efficiency values (Q),

$$Q = [\phi(\textbf{Py-1-CHO}) - \phi(\textbf{H}_2\textbf{-Py/Zn-Py})] / \phi(\textbf{Py-1-CHO}) \qquad (6.1)$$

(where ϕ(**Py-1-CHO**) and ϕ(**H_2-Py/Zn-Py**) refer to the fluorescence quantum yields for **Py-1-CHO** and the D-A systems **H_2-Py/Zn-Py**, respectively; λ_{ex} = 290 nm) have been calculated by using eqn. 6.1, in different solvents (cyclohexane, CH_3CN, CH_3OH) and are summarized in Table 6.6. These values are 98 ± 10% for both **H_2-Py** and **Zn-Py**. The fluorescence decay curves for **H_2-Py** in CH_2Cl_2 were shown in Fig. 6.8. An examination of the fluorescence decay results indicate that lifetimes (τ) of the porphyrin parts of **H_2-Py** (8.09 ns, λ_{ex} = 575 nm) remained quite similar to those of **H_2TTP** (8.43 ns) but, those of their pyrene subunits (λ_{ex} = 290 nm) were found to be considerably shorter (~ 0.1 ns) in comparison with the lifetime of pyrene. Similar trend was observed in **Zn-Py** dyad.

The observation that there exist a considerable overlap between the emission of pyrene and the absorption of porphyrin in these D-A systems (compare the corresponding spectra in Figs. 6.4 & 6.7) suggests that quenching of the pyrene fluorescence observed for **H_2-Py** and **Zn-Py** may be due to

intramolecular EET from the singlet pyrene to the porphyrin, see Fig. 6.9. Indeed, excitation of ca. 10^{-7} M solution of these two D-A systems at 290 nm resulted in an appearance of well-defined porphyrin emission bands in CH_2Cl_2. Conclusive evidence for intramolecular EET comes from the excitation spectral measurements. When emission was recorded at the porphyrin emission maximum

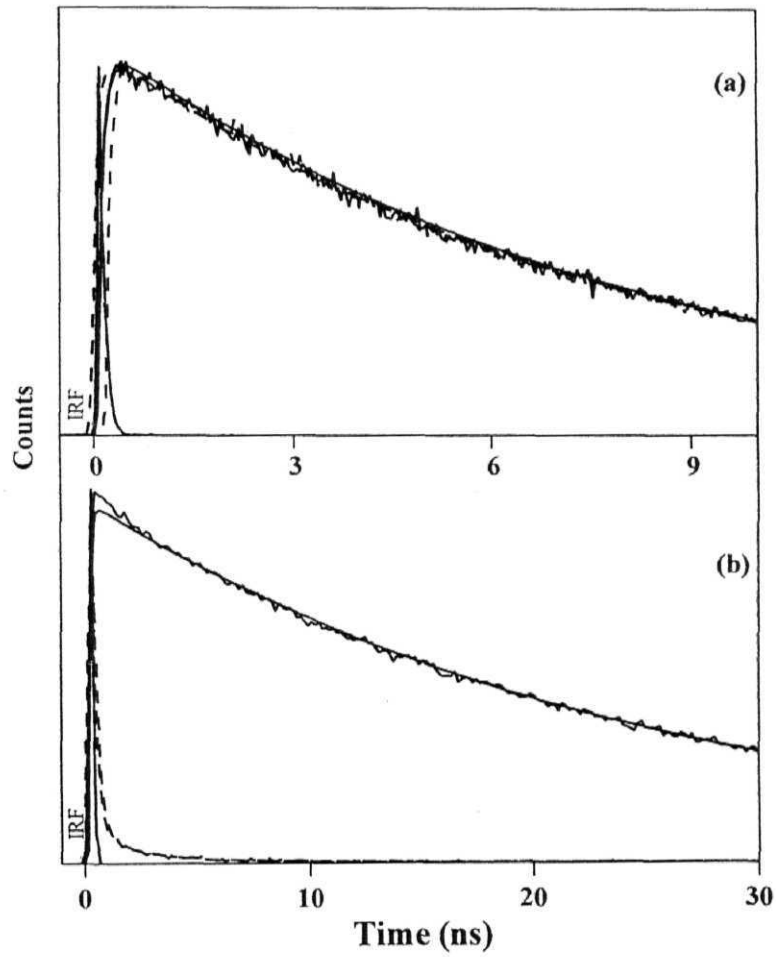

Fig. 6.8 Decays profiles of (a) λ_{ex} = 575 nm, λ_{em} = 650 nm: **H_2TTP** (——) and **H_2-Py** (--------) (b) λ_{ex} = 290 nm, λ_{em} = 430 nm: Pyrene (——) and **H_2-Py** (-------) in CH_2Cl_2.

(720/650 nm for **H_2-Py/Zn-Py**), the excitation spectra of these D-A systems showed bands characteristic of pyrene absorption. The corrected and normalized excitation spectra of these dyads were overlayed with the corresponding absorption spectra in CH_2Cl_2, Fig. 6.10. Excitation spectral data indicates that photons collected by the hydrocarbon subunit are effectively transferred to the porphyrin in both these donor-acceptor systems. A comparison of these spectra in the $4.0x10^4 - 2.6x10^4$ cm^{-1}region gave almost 100% energy transfer efficiencies (%T) in each case. On the other hand from Fig. 6.9, it should be noted that energies of the singlet state of pyrene and the porphyrin (free base or zinc(II)) subunits ruled out the EET to occur from the singlet porphyrin to the pyrene chromophore.

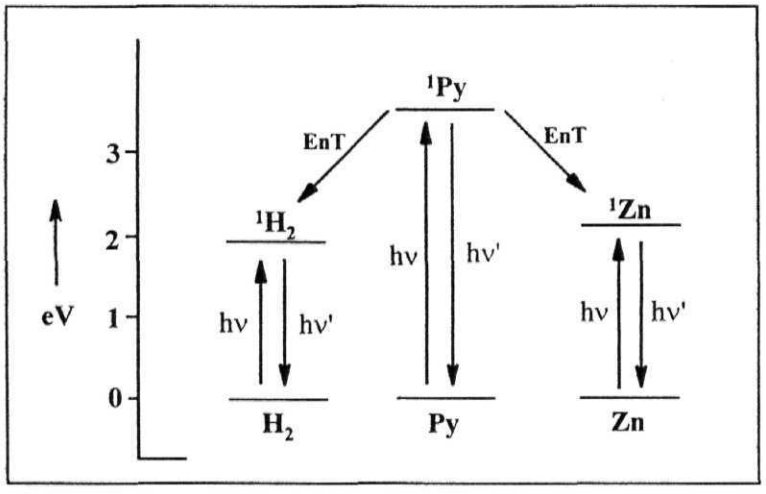

Fig. 6.9 Energy level diagram of free base (**H_2**), zinc(II) (**Zn**) porphyrins and pyrene (**Py**). Here EnT, hν and hν′ represents energy transfer, absorption and fluorescence processes, respectively.

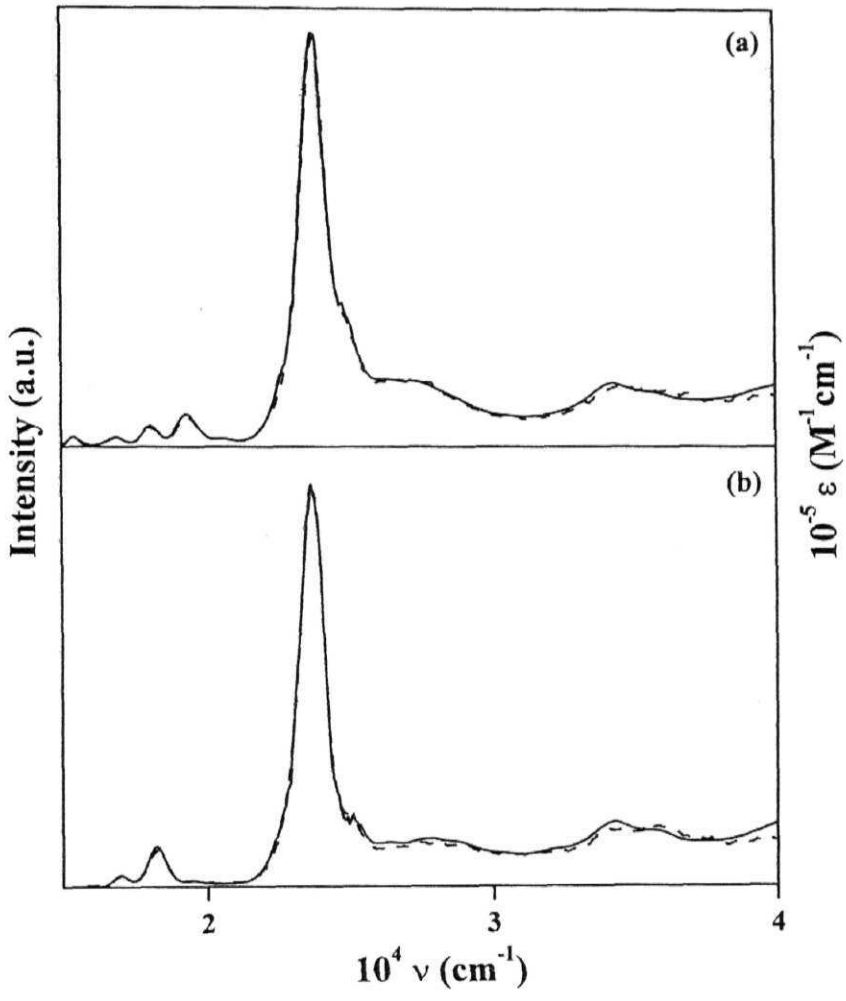

Fig. 6.10 Overlay of the (a) λ_{em} = 720 nm: excitation (-------) and absorption (——) spectra of **H_2-Py** (b) λ_{em} = 650 nm: excitation (--------) and absorption (——) spectra of **Zn-Py** in CH_2Cl_2. The excitation spectra were corrected for the instrument response function and were normalized with respect to the absorption spectra between 14900 - 16050 cm^{-1} and 16200 - 17450 cm^{-1} for **H_2-Py** and **Zn-Py**, respectively.

6.3.2.2 Porphyrin-anthraquinone dyads

Fig. 6.11 shows the steady-state fluorescence spectra of **H_2-AQ** and **Zn-AQ** measured in CH_2Cl_2 and cyclohexane are compared with spectra of the corresponding individual (**H_2L^4/ZnL^4**) components constituting them. Analogous spectra were obtained in CH_3CN and CH_3OH. Spectral shapes and wavelengths of maximum emission (λ_{em}) of these D-A systems, when they were irradiated at the porphyrin absorption band (λ_{ex} = 550 nm), are seen to be similar to the spectrum of either **H_2L^4** or **ZnL^4**. Excitation at 265 nm (predominantly anthraquinone absorption band) did not show any fluorescence in the UV region suggesting that the linked anthraquinone subunit of these conjugates is photochemically inactive under the present set of experimental conditions.

The fluorescence quantum yield (ϕ) for excitation into the porphyrin part of each dyad was similar to that of the unlinked porphyrin in cyclohexane whereas the fluorescence from the porphyrin part was found to be strongly quenched in CH_2Cl_2, CH_3CN and CH_3OH. The quenching efficiency values (Q) for these systems were calculated by using eqn. 6.2, in different solvents and are summarized in Table 6.6.

$$Q = [\phi(\mathbf{H_2L^4/ZnL^4}) - \phi(\mathbf{H_2\text{-}AQ/Zn\text{-}AQ})]/\phi(\mathbf{H_2L^4/ZnL^4}) \qquad (6.2)$$

Where ϕ(**H_2L^4 / ZnL^4**) and ϕ(**H_2-AQ / Zn-AQ**) refer to the fluorescence quantum yields for **H_2L^4 / ZnL^4** and the D-A systems **H_2-AQ / Zn-AQ**, respectively. These values are 84 - 97% for both **H_2-AQ** and **Zn-AQ**. The time-resolved fluorescence data also suggest the same as described below.

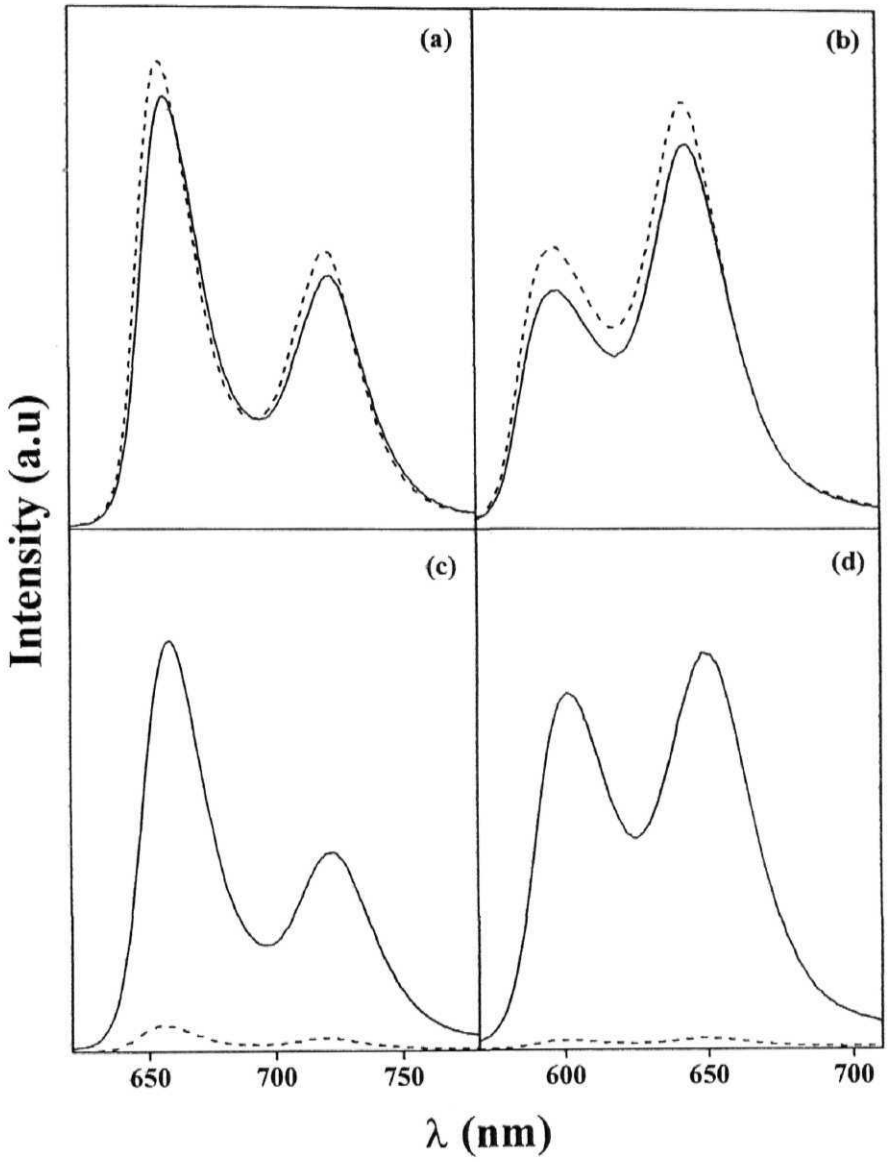

Fig. 6.11 Fluorescence spectra (O.D. ≈ 0.2 at λ_{ex} = 550 nm) of (a) $\mathbf{H_2L^4}$ (———) and **H_2-AQ** (--------) (b) $\mathbf{ZnL^4}$ (———) and **Zn-AQ** (--------) in cyclohexane; (c) $\mathbf{H_2L^4}$ (———) and **H_2-AQ** (--------) (d) $\mathbf{ZnL^4}$ (———) and **Zn-AQ** (--------) in CH_2Cl_2.

Fig 6.12 and Table 6.7 suggest that the time-resolved fluorescence lifetimes, τ, (λ_{ex} = 575 nm & λ_{em} = 650 nm) of the **H_2-AQ** and **Zn-AQ** are quite similar to those of **H_2TTP** and **ZnTTP** in cyclohexane but in CH_2Cl_2, CH_3CN and CH_3OH were found to be show considerably shorter decay times than **H_2TTP** and **ZnTTP**. In **H_2-AQ** case, we were able to fit these decays to bi-exponential expression with a shorter lifetime and a longer lifetime. The shorter lifetime component of the bi-exponential decay was attributed to the deactivation (quenched) of the porphyrin excited state to anthraquinone and the longer lifetime component was assigned either to the unquenched or decay of porphyrin–hydroquinone generated by porphyrin sensitized photoreduction.[51] But **Zn-AQ** decays fit to three-exponential expression composed of one major (see Table 6.7, shorter lifetime) component and two minor components (shorter & longer lifetime). From these data the shorter lifetime with higher amplitude and longer lifetime components are ascribed same as like **H_2-AQ**, but the additional shorter lifetime component is explained in the following manner. The ^{1}H NMR data of for **Zn-AQ** suggest that there is a significant degree of complexation by anthraquinone groups to the zinc(II) porphyrin core. We believe the anthraquinone-ligated state is responsible for the additional short-lived component obtained from the TCSPC experiments.[41,42]

The data in Table 6.7 shows that the shorter lifetime observed for **H_2-AQ** in all solvents (expect cyclohexane) have much larger amplitude relative to that observed for longer lifetime component. Similar features were seen in the **Zn-AQ** derivative.

We analyze, based on the steady state and time resolved fluorescence data, that quenching of the porphyrin components in these dyads is predominantly due

to the PET from the porphyrin singlet state to the anthraquinone subunit. The free energy change for this PET, $\Delta G(^1\mathbf{P} \rightarrow \mathbf{AQ})$, has been estimated using eqn. 6.3, and summarized in Table 6.5.

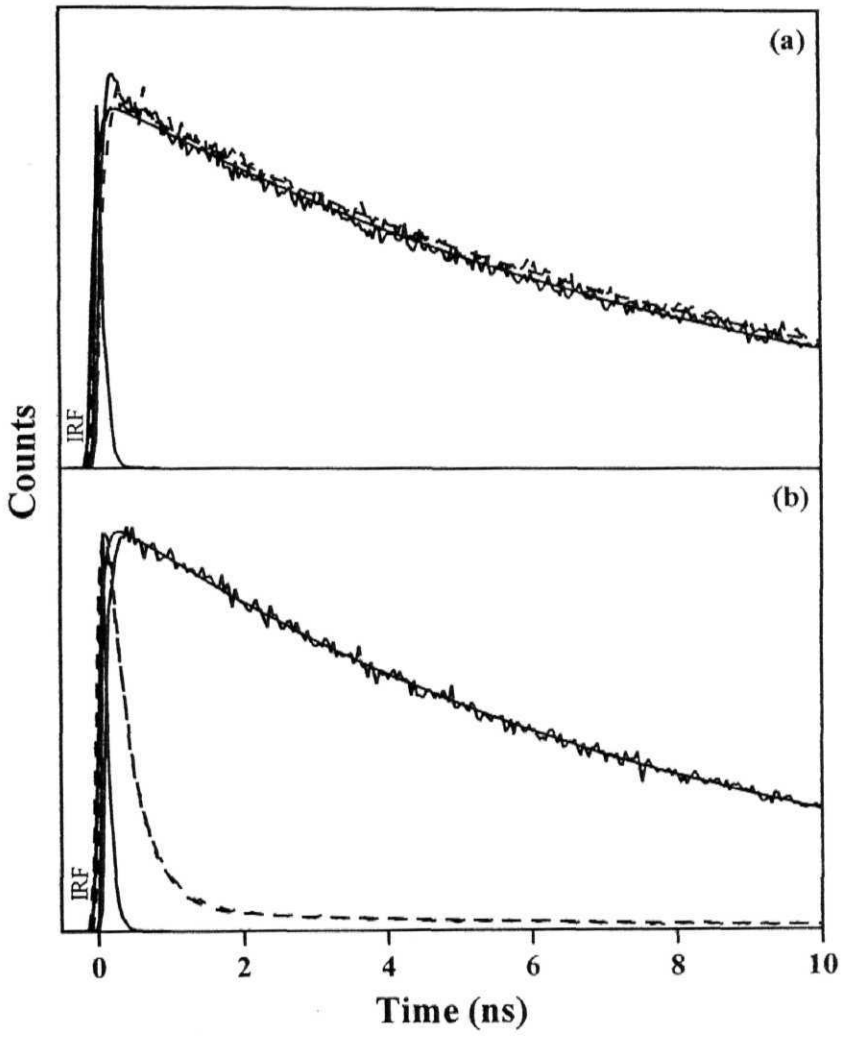

Fig. 6.12 Time-resolved fluorescence decay profiles at λ_{ex} = 575 nm, λ_{em} = 650 nm of (a) **H_2TTP** (——) and **H_2-AQ** (--------) in cyclohexane (b) **H_2TTP** (——) and **H_2-AQ** (--------) in CH_2Cl_2.

Table 6.6. Fluorescence data of dyads and their monomeric analogues in various solvents [a]

Compd.	λ_{em}, (ϕ, %Q)							
	Cyclohexane		CH_2Cl_2		CH_3CN		CH_3OH	
	550 nm	290 nm	550 nm	290 nm	550 nm	290 nm	550 nm	290 nm
H_2L^4	657, 723 (0.11)	-	658, 722 (0.15)	-	659, 723 (0.21)	-	659, 721 (0.11)	-
ZnL^4	599, 644 (0.035)	-	601, 649 (0.045)	-	612, 662 (0.032)	-	611, 661 (0.041)	-
Py-1-CHO	-	406 (1.0)	-	416 (1.0)	-	417 (1.0)	-	454 (1.0)
H_2-Py	655, 721 (0.123)	450 (0.011, 99)	655, 720 (0.15)	445 (0.031, 97)	653, 718 (0.21)	443 (0.053, 95)	653, 718 (0.14)	455 (0.022, 98)
Zn-Py	599, 643 (0.038)	439 (0.008, 99)	601, 648 (0.048)	442 (0.019, 98)	611, 661 (0.036)	448 (0.044, 96)	608, 659 (0.058)	457 (0.014, 99)
H_2-AQ	655, 721 (0.11, 0)	-	656, 720 (0.009, 94)	-	654, 719 (0.025, 88)	-	655, 719 (0.0086, 92)	-
Zn-AQ	598, 642 (0.038, 0)	-	602, 650 (0.002, 96)	-	612, 662 (0.0015, 95)	-	610, 660 (0.001, 97)	-

(a) Error limits: λ, ± 1 nm; ϕ, ± 10%.

Table 6.7 Fluorescence lifetime (τ, ns) data and electron transfer rate constants (k_{ET}, s^{-1}) of **H_2-AQ** and **Zn-AQ** [a]

Compd.	τ, ns (A%) [b] k_{ET}, s^{-1}							
	Cyclo hexane	χ^2	CH_2Cl_2	χ^2	CH_3CN	χ^2	CH_3OH	χ^2
H_2TTP	9.08	0.98	7.97	1.10	8.79	0.99	8.48	1.05
ZnTTP	1.89	1.07	1.61	1.07	1.71	1.20	1.69	1.21
H_2-AQ	9.24	1.02	0.38 (94) 6.68 (6) 2.5×10^9	1.03	0.85 (95) 5.79 (5) 1.1×10^9	1.03	0.42 (95) 6.02 (5) 2.3×10^9	1.02
Zn-AQ	1.78	0.99	0.03 (91) 0.71 (1) 1.68 (8) 3.2×10^{10}	1.26[c]	0.01 (93) 1.26 (6) 2.61 (1) 9.9×10^{10}	1.24[c]	0.01 (86) 0.71 (6) 1.86 (8) 9.9×10^{10}	1.43[c]

(a) Error limits: τ and k_{ET}, ± 10% (b) A is the relative amplitude of the decay component (c) In these cases, a two-exponential fit gave a better χ^2 value, but the lifetime of one of the components was insignificant (more than ZnTTP lifetime).

$$\Delta G_{PET}(^1\mathbf{P} \rightarrow \mathbf{AQ}) = E_{CT}(\mathbf{P}^+\mathbf{AQ}^-) - E_{0\text{-}0}(\mathbf{P}) \qquad (6.3)$$

The value of $\Delta G_{PET}(^1\mathbf{P}\rightarrow\mathbf{AQ})$, as estimated using the $E_{CT}(\mathbf{P}^+\mathbf{AQ}^-)$ [i.e. $E_{1/2}{}^{ox}(\mathbf{P})$–$E_{1/2}{}^{red}(\mathbf{AQ})$, Table 6.4) and singlet state energy (i.e. $E_{0\text{-}0}$ for **H_2-AQ** and **Zn-AQ** are 1.90 and 2.09 eV, respectively). The more efficient quenching of the **Zn-AQ** dyad excited state relative to that of the **H_2-AQ** can be directly attribute to

the significantly more exothermic value of ΔG_{PET} for **Zn-AQ**. The rate constant (k_{ET}) for the $\mathbf{P^+AQ^-}$ were calculated by eqn. 6.4 and summarized in Table 6.7.

$$k_{ET} = (1/\tau_f) - k \qquad (6.4)$$

Where k is the reciprocal of the lifetime of the **H_2TTP/ZnTTP**, τ_f is the lifetime of **H_2-AQ / Zn-AQ**. The k_{ET} values in the range of 1.1 x 10^9 to 9.9 x 10^{10} s^{-1} that were dependent upon the solvent. The observed general increase of the %Q values (see Table 6.6) with increasing polarity of the solvent is consistent with the participation of a charge transfer state in the excited state deactivation of the free-base components of these systems. Fig. 6.13 shows the energy levels of porphyrin singlet excited state and the charge transfer state that participate in the PET processes in porphyrin-anthraquinone dyads.

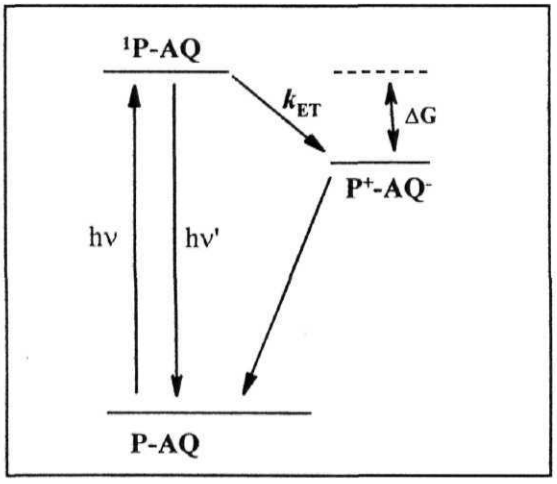

Fig. 6.13 PET mechanism in porphyrin-anthraquinone dyads. Here hν and hν′ refers absorbance and fluorescence, respectively.

6.4 Summary

In summary, new azomethine bridged porphyrin dyads have been synthesized and investigated by spectroscopic and electrochemical methods. These experiments reveal that there exists no π-π interaction between the porphyrin and pyrene/anthraquinone. But, interestingly in the ^{1}H NMR of **Zn-AQ** dyad we found that –C=O of the anthraquinone subunit ligating with another zinc(II) porphyrin moiety. The photophysical (steady-state and time-resolved fluorescence spectroscopy) properties have also been investigated and the results are interpreted in terms of intramolecular energy and electron transfer mechanisms. In photo-excited state of pyrene in **H_2-Py** or **Zn-Py** energy transfer was observed from singlet to ground state porphyrin moiety, whereas for the photo-excited state of porphyrin in **H_2-AQ** or **Zn-AQ** dyads electron transfer mechanism was observed in polar solvents from excited singlet state of porphyrin to anthraquinone subunit. The time resolved fluorescence data were in good agreement with the steady state fluorescence studies. The absence of charge-transfer bands in any of the fluorescence spectra is an indication that no electronic interactions exist in the ground state between the porphyrin and pyrene/anthraquinone.

6.5 References

1. Gust, D.; Moore, T. *The Porphyrin Handbook*, Kadish, K. M.; Smith, K, M.; Guilard, R. Eds.; Academic Press, **2000**.
2. Connolly, J. S.; Bolton, J. R. In *Photoinduced electron transfer*; Fox, M. A.; Chanon, M., Eds.; Elsevier: Amsterdam, **1988**, Part D.
3. Wasielewski, M. R. *Chem. Rev.* **1992**, *92*, 435.

4. Ward, M. D. *Chem. Soc. Rev.* **1997**, *26*, 365.
5. Hayashi, T.; Ogoshi, H. *Chem. Soc. Rev.* **1997**, 355.
6. Piotrowiak, P. *Chem. Soc. Rev.* **1999**, *28*, 143.
7. Sessler, J. L.; Wang, B.; Harriman, A. *J. Am. Chem. Soc.* **1995**, *117*, 704.
8. Wagner, R. W.; Lindsey, J. S.; Sethi, J.; Palaniappan, V.; Bocian, D. F. *J. Am. Chem. Soc.* **1996**, *118*, 3996.
9. Imahori, H.; Hasegawa, M.; Taniguchi, S.; Aoki, M.; Okada, T.; Sakata, Y.; *Chem. Lett.* **1998**, 721.
10. Schmidt, J. A.; McIntosh, A. R.; Weedon, A. C.; Bolton, J. R.; Connolly, J. S.; Hurley, J. K.; Wasielewski, M. R. *J. Am. Chem. Soc.* **1988**, *110*, 1733.
11. Guldi, D. M. *Chem. Soc. Rev.* **2002**, *31*, 22.
12. Otsuki, J.; Suka, A.; Yamazaki, K.; Abe, H.; Araki, Y.; Ito, O. *Chem. Commun.* **2004**, 1290.
13. Sazanovich, I. V.; Kirmaier, C.; Hindin, E.; Yu, L.; Bocian, D. F.; Lindsey, J. S.; Holten, D. *J. Am. Chem. Soc.* **2004**, *126*, 2664.
14. D'Souza, F.; Smith, P. M.; Zandler, M. E.; McCarty, A. L.; Itou, M.; Araki, Y.; Ito, O. *J. Am. Chem. Soc.* **2004**, *126*, 7898.
15. Hayes, R. T.; Walsh, C. J.; Wasielewski, M. R. *J. Phys. Chem. A* **2004**, *108*, 3253.
16. Hayes, R. T.; Walsh, C. J.; Wasielewski, M. R. *J. Phys. Chem. A* **2004**, *108*, 2375.
17. Imahori, H. *Org. Biomol. Chem.* **2004**, *2*, 1425.
18. Tomizaki, K-Y.; Loewe, R. S.; Kirmaier, C.; Schwartz, J. K.; Retsek, J. L.; Bocian, D. F.; Lindsey, J. S. *J. Org. Chem.* **2002**, *67*, 6519.
19. Kurreck, H.; Huber, M. *Angew. Chem., Int. Ed. Engl.* **1995**, *34*, 849.

20. Liddell, P. A.; Kodis, G.; Andreasson, J.; de la Garza, L.; Bandyopadhyay, S.; Mitchell, R. H.; Moore, T. A.; Moore, A. L.; Gust, D. *J. Am. Chem. Soc.* **2004**, *126*, 4803.
21. de Rege, P. J. F.; Williams, S. A.; Therien, M. J. *Science* **1995**, *269*, 1409.
22. Sirish, M.; Maiya, B. G. *J. Photochem. Photobiol. A: Chem.* **1994**, *77*, 189.
23. Maiya, B. G.; Doraiswamy, S.; Periasamy, N.; Venkataraman, B.; Krishnan, V. *J. Photochem. Phtobio. A*: *Chem.* **1994**, *81*, 139.
24. Sirish, M.; Maiya, B. G. *J. Photochem. Photobiol. A: Chem.* **1995,** *85*, 127.
25. Sirish, M.; Maiya, B. G. *J. Photochem. Photobiol. A: Chem.* **1996,** *93*, 129.
26. Sirish, M.; Maiya, B. G. *J Porphyrins Pthalocyanins* **1998**, *2*, 327.
27. Giribabu, L.; Kumar, A. A.; Neeraja, V.; Maiya, B. G. *Angew. Chem., Int. Ed.* **2001**, *40*, 3621.
28. Reddy, D. R.; Maiya, B. G. *J. Porphyrins Pthalocyanins* **2002**, *6*, 3.
29. Kumar, A. A.; Giribabu, L.; Maiya, B. G. *Proc. Ind. Nat. Acad. Sci. Chem. Sci.* **2002**, *114*, 565.
30. Reddy, D. R.; Maiya, B. G. *J. Phys. Chem. A* **2003**, *107*, 6326.
31. Nakajima, S.; Osuka, A. *Tetrahedron Lett.* **1995**, 8457.
32. Hirakawa, K.; Segawa, H. *J. Photochem. Photobiol. A Chem.* **1999**, *123*, 67.
33. Kilsa, K.; Kajanus, J.; Larsson, S.; Macpherson, A. N.; Martensson, J.; Albinsson, B. *Chem. Eur. J.* **2001**, *7*, 2122.
34. Fonda, H. N.; Gilbert, J. V.; Cormier, R. A.; Sprague, J. R.; Kamioka, K.; Connoly, J. S. *J. Phys. Chem.* **1993**, *97*, 7024.
35. Rempel, U.; Maltzan, B. V.; Borczyskowski, C. V. *Chem. Phys. Lett.* **1990**, 347.
36. Harriman, A.; Davlila, J. *Tetrahedron* **1989**, *45*, 4737.

37. Vollmer, M. S.; Wurthner, F.; Effenberger, F.; Emele, P.; Meyer, D. U.; Stumpfig, T.; Port, H.; Wolf, H. C. *Chem. Eur. J.* **1998**, *4*, 260.

38. Murov, S. L. *Hand book of Photochemsitry*, Marcell Dekker, New York, **1973**.

39. Mehta, G.; Muthusamy, S.; Maiya, B. G.; Arounaguiri, S. *J. Chem. Soc., Perkin. Trans. 1* **1999**, 2177.

40. Mehta, G.; Muthusamy, S.; Maiya, B. G.; Arounaguiri, S. *Tetrahedron Lett.* **1997**, *38*, 7125.

41. Rubstov, I. V.; Kang, Y. K.; Redmore, N. P.; Allen, R. M.; Zheng, J.; Beratan, D. N.; Therien, M. J. *J. Am. Chem. Soc.* **2004**, *126*, 5022.

42. Capitosti, G. J.; Guerrero, C. D.; Binkley, Jr. D. E.; Rajesh, C. S.; Modarelli, D. A. *J. Org. Chem.* **2003**, *68*, 247.

43. Rajesh, C. S.; Capitosti, G. J.; Cramer, S. J.; Modarelli. D. A. *J. Phys. Chem. B* **2001**, *105*, 10175.

44. Capitosti, G. J.; Cramer, S. J.; Rajesh, C. S.; Modarelli. D. A. *Org. Lett.* **2001**, *3*, 1645.

45. D'Souza, F.; Deviprasad, G. R. *J. Org. Chem.* **2001**, *66*, 4601.

46. Kamioka, K.; Cormier, R. A.; Lutton, T. W.; Connolly, J. S. *J. Am. Chem. Soc.* **1992**, *114*, 4414.

47. Hamaoue, K.; Nakayama, T.; Nanshow, H.; Ushida, K.; Naruta, Y.; Kodo, T.; Maruyama, K. *Chem. Phys. Lett.* **1991**, *187*, 409.

48. Li, L.; Shen, S.; Yu, Q.; Zhou, Q.; Xu, H. *J. Chem. Soc., Chem. Commun.* **1991**, 619.

49. Lin, Z.-M.; Feng, W.-Z.; Leung, H.-K. *J. Chem. Soc., Chem. Commun.* **1991**, 209.

50. Cormier, R. A.; Posey, M. R.; Bell, W. L.; Fonda, H.; N.; Connolly, J. S. *Tetrahedron* **1989**, *45*, 4831.

51. Harriman, A.; Kubo, Y.; Sessler, J. L. *J. Am. Chem. Soc.* **1992**, *114*, 388.

52. Kang, Y. K.; Rubstov, I. V.; Iovine, P. M.; Chen, J.; Therien, M. J. *J. Am. Chem. Soc.* **2002**, *124*, 8275.

53. Sen, A.; Krishnan, V. *J. Photochem. Photobiol. A: Chem.* **1999**, *123*, 77.

54. Nishitani, S.; Kurata, N.; Sakata, Y.; Misumi, S. *J. Am. Chem. Soc.* **1983**, *105*, 7771.

55. Fuhrhop, J.-H.; Smith, K. M.; In *Porphyrins and Metalloporphyrins*; Smith, K. M., Ed.; Elsevier: Amsterdam, **1975**; p. 769.

56. Fuhrhop, J.-H.; Smith, K. M. in *Porphyrins and Metalloporphyrins*; Smith, K. M., Ed.; Elsevier: Amsterdam, **1975**; p. 179.

57. Vogel *Textbook of Practical Organic Chemistry*, Great Britain, England, 1989, p. 1000.

58. Hombrecher, H. K.; Ludtke, K. *Tetrahedron* **1993**, *49*, 9489.

59. Gardner, M.; Guerin, A. J.; Hunter, C. A.; Michelson, U.; Rotger, C. *New J. Chem.* **1999**, 309.

60. Senge, M. O.; Soeck, M.; Wiehe, A.; Dieks, H.; Aguirre, S.; Kurreck, H. *Photochem. Photobiol.* **1999**, *70*, 206.

61. Hayashi, T.; Takimura, T.; Hitomi, Y.; Ohara, T.; Ogoshi, H. *J. Chem. Soc., Chem. Commn.* **1995**, 545.

62. Abraham, R. J.; Bedford, G. R.; Mc Neillie, D.; Wright, B. *Org. Magn. Reson.* **1980**, *14*, 418.

63. Subramanian, J. In *Porphryins and Metalloporphyrins*; Smith, K. M., Ed.; Elsevier: Amsterdam, **1975**; p. 562.

64. Nicholson, R. S.; Shain, I. *Anal. Chem.* **1964**, *36*, 706.

65. Zhang, J.; Sun, H.-R.; Yang, G.-Y.; Wen, K.; Yu, L.-X.; Cao, X.-Z. *Electrochem. Acta* **1998**, *43*, 2693.

CHAPTER 7

Conclusions

Photochemically active porphyrin arrays and porphyrin-based donor-acceptor (D-A) systems are of immense utility in various research areas including biomimetic photosynthesis, molecular catalysis, molecular electronics, photodynamic therapy etc. Over the last two decades, a great variety of monomeric and oligomeric porphyrin species bearing electron donor/acceptor groups at their peripheral or axial positions have been synthesized and their photochemical activity investigated. Literature on recently reported systems that bear relevance to the present thesis have been reviewed in Chapter 1. Results obtained during the present investigation that deal with the design, synthesis, characterization and photochemical properties of porphyrin arrays and D-A systems derived from 'axial' or 'peripheral' site substitution of free base, metallo- and metalloid porphyrins are reported in Chapters 3, 4, 5 and 6.

7.1 Axial-bonding type porphyrin arrays and D-A systems

While the majority of the reported porphyrin arrays have been obtained *via* cumbersome and often, low-yielding organic synthesis protocols which involve manipulation at either the pyrrole-β or the meso-phenyl position/s of the monomers,[1] relatively less such studies have been carried out on the so-called 'axial bonding' type systems. In addition, less attention seems to have been paid towards the construction of functionally active, hybrid systems. During the course of the present investigation, it was realized that a five coordinated, axially ligated aluminium(III) porphyrin can be conveniently employed for the synthesis of 'vertically linked', homologous porphyrin arrays and that a proper choice of two different porphyrins should result in the formation of hybrid analogues. Indeed, it

has been recently demonstrated by our group that photochemically active, 'vertically-linked' porphyrin trimers/hexamers/nonamers can be readily constructed by utilizing the axial-bonding capability of phosphorus(V), tin(IV) and germanium(IV) porphyrins.[2,3]

The present work has been undertaken to extend the scope of this method and to evaluate the ability of aluminium(III) porphyrins to act as the basal scaffolds. Details of the design, synthesis, spectroscopy, electrochemistry and singlet state activity of 'axial-bonding' type three dimeric (**H_2-Al**, **Cu-Al** and **Zn-Al**) and three trimeric (**H_2-Al_2**, **Cu-Al_2** and **Zn-Al_2**) hybrid porphyrin arrays are discussed in Chapter 3 of this thesis. Finally, a comparison is made between the presently synthesized aluminium(III) porphyrin based arrays and the previously reported analogous arrays based on tin(IV), germanium(IV) and phosphorus(V) porphyrins with regard to their architectural features, spectroscopic properties and photochemical activities.

Each synthetic step involved during the construction of the arrays investigated in the present study is straightforward and provides good yields of the desired products in pure form. There, however, exist important differences between these old and new arrays with regard to their design and architectural features. The ground state spectroscopic and redox data of dimers and trimers, as probed by the UV-visible, ^{1}H NMR and differential pulse voltammetric techniques, collectively indicate that there exists minimum interaction between π-planes of the constituent monomeric porphyrins in this 'axial-bonding' type array. Thus, an architecture involving a symmetric but, a non-parallel disposition of the axial porphyrin with respect to plane of the central aluminium(III) porphyrin is appropriate for this arrays. Similarly, ESR spectral parameters of paramagnetic **Cu-Al** and **Cu-Al_2** are also similar to those of the monomeric copper(II) porphyrins.

Analysis of the emission and excitation spectral data suggested that an electronic energy transfer (EET) from the central aluminium(III) porphyrin to the axial free base as well as the photoinduced electron transfer (PET) from axial free base (ground state) to the singlet state of the central aluminium(III) porphyrin occur in this arrays. Time-resolved studies also suggest the same. The %Q(Al) (which is due to EET) values are lower and the %Q(H_2) (which is due to PET) values are higher for the trimeric species in comparison with the corresponding values for the dimer. A simplistic analysis indicates that the dimer is a bicomponent D-A system wherein the donor/acceptor ratio is 1:1 for both EET and PET. On the other hand, the trimeric system has two donors (i.e. Al(III) porphyrins) and only one acceptor (i.e. free base porphyrin) for EET and one donor (i.e. free base porphyrin) and two acceptors (i.e. Al(III) porphyrins) for PET. This situation might rationalize the lower %Q(Al) (which is due to EET) and higher %Q(H_2) (which is due to PET) values observed for **H_2-Al_2**. Interestingly, the exoergicity of these PET reactions follow a trend, viz: P(V) >> Sn(IV) > Ge(IV) > Al(III), that is dependent on the electropositivity of the resident metalloid ion in the arrays and is consistent with the magnitudes of the corresponding %Q(H_2) values.

The 'axial-bonding' strategy has been extended in the next Chapter for the construction of tin(IV)/phosphorus(V) porphyrin based terpyridine containing **[L^1Sn(O-ptp)$_2$]** and **[L^1P(O-ptp)$_2$]$^+$** triads. During the course of the present work, it was realized that all of the previously reported porphyrin-terpyridine (D-A) systems[4,5] have the terpyridine linked at the porphyrin meso position/s and that it would be of interest to 'link' the terpyridine at the 'axial' sites of a metalloid porphyrin and investigate the phototuning function of the ensuing D-A derivatives. Chapter 5 presents the design, synthesis, spectral characterization and

transition metal ion induced luminescence of 'axial-bonding' type, hexa coordinated D-A conjugates.

Relying largely on oxophilicity of the phosphorus(V)/tin(IV) ion, synthesis of the new D-A triads, had been accomplished here in good-to-moderate yields. The fine and dark red crystals of **$[L^1Sn(O\text{-}ptp)_2]$** were obtained and the crystal structure showed that the two terpyridine subunits are in anti position with respect to the each other. Each new compound was fully characterized by MALDI-MS, UV-visible and ^1H NMR (1D and ^1H-^1H COSY) & ^{31}P NMR methods. Porphyrin ring current induced upfield shifts have been noticed for the protons on the axial terpyridine subunits with the magnitude of shift for a given proton ($\Delta\delta = \delta_{OH\text{-}ptp} - \delta_{triad}$) being a function of its separation distance from the porphyrin π-plane. The UV-visible and redox data collectively reveal that there exist π-π overlap between porphyrin and terpyridine subunits in **$[L^1P(O\text{-}ptp)_2]^+$** compared to **$[L^1Sn(O\text{-}ptp)_2]$**. Analysis of the emission and excitation spectral data suggested that electronic energy transfer (EET) from terpyridine to the porphyrin and PET from the ground state terpyridine to the singlet porphyrin and also a PET from the excited state terpyridine to the ground state porphyrin are possible in both these D-A systems.

Further, the complexation of **$[L^1P(O\text{-}ptp)_2]^+$** triad with transition metal ions (**Zn^{2+}**, **Cd^{2+}**, **Hg^{2+}**, **Cu^{2+}**, **Cu^{1+}**, **Ag^{1+}**, **Ni^{2+}**, **Co^{2+}**, **Fe^{2+}** and **Mn^{2+}**) has been studied in detail by ^1H NMR, UV-visible and fluorescence spectroscopies. ^1H NMR and UV-visible titrations suggest that although the coordination of metal ions to the **ptp** units of **$[L^1P(O\text{-}ptp)_2]^+$** is strong, there is little electronic interaction between the metal-complex and the porphyrin chromophore. In fluorescence titrations it was found that the PET and EET reactions are controlled by metal ion coordination with **ptp** subunits. When excited at 566 nm with

addition of Zn^{2+} or Cd^{2+}, PET process was inhibited from ground state of **ptp** subunit to excited state of porphyrin which results enhancement in porphyrin fluorescence. Upon complexation **ptp** becomes electron deficient, as a result it inhibits the excited state electron transfer (i.e. reductive electron transfer) process and consequently enhances the porphyrin fluorescence emission. On the other hand when excited at the isosbestic point (300 nm), PET was suppressed and EET from excited **ptp** subunit to the ground state of porphyrin was enhanced. This results from an increase in the spectral overlap (J) between terpyridine and porphyrin subunits upon complexation.

7.2 Peripherally substituted porphyrin based D-A systems

It is of interest to know whether such a preference over the 'axial pathway', for intramolecular EET and PET in a porphyrin-based D-A system as described above, can occur in a system wherein the terpyridine is connected at the meso-position/s of a porphyrin. For this reason a new D-A systems, in which Ru(II) bis-terpyridine complex $[Ru]^{2+}$ have been connected *via* flexible ethylene bridges at the meso positions of either free base or zinc(II) porphyrins, have been synthesized during this study (Chapter 5).

These molecular dyads ($[H_2Ru]^{2+}$, $[ZnRu]^{2+}$) and triads ($[H_2RuH_2]^{2+}$, $[ZnRuZn]^{2+}$ and $[ZnRuH_2]^{2+}$) have been fully characterized by mass (MALDI), UV-visible and ^1H NMR spectroscopic methods. UV-visible and ^1H NMR data of these dyads and triads reveal the presence of minimum intramolecular ground-state interaction between the porphyrin and $[Ru]^{2+}$ complex π-planes. In the steady state fluorescence studies, $[H_2Ru]^{2+}$ and $[H_2RuH_2]^{2+}$, when the excitation wavelength correspond to the porphyrin band maximum (420 nm), show a weak quenching of fluorescence in comparison with the fluorescence due to free base

porphyrin. Whereas, in the case of **[ZnRu]**$^{2+}$ and **[ZnRuZn]**$^{2+}$, considerable quenching of fluorescence due to zinc(II) porphyrin was observed. Based on the redox data and singlet state energy data the quenching of fluorescence is due to the intramolecular electron transfer from zinc(II) porphyrin to the **[Ru]**$^{2+}$. On the other hand, the hetero triad **[ZnRuH$_2$]**$^{2+}$, shows combined fluorescence properties of dyads **[H$_2$Ru]**$^{2+}$ and **[ZnRu]**$^{2+}$. Similar to **[ZnRu]**$^{2+}$ dyad in this triad also PET processes from zinc(II) porphyrin to **[Ru]**$^{2+}$ complex is a major processes and additionally there exist intramolecular EET from zinc(II) porphyrin to free base porphyrin.

It is interesting to see whether PET and EET reactions occurred when either donor or acceptor molecules are connected at the peripheral positions of porphyrin. For this reason, we had constructed (Chapter 6) porphyrin-pyrene (**H$_2$-Py**, **Cu-Py** and **Zn-Py**) and porphyrin-anthraquinone (**H$_2$-AQ**, **Cu-AQ** and **Zn-AQ**) having an azomethine group separating the two subunits have been synthesized and fully characterized by mass (FAB), IR, UV-visible, ^{1}H NMR and ESR spectroscopies and also by the cyclic and differential pulse voltammetric methods. An analysis of the data reveals that the spectral and electrochemical properties of the individual chromophoric entities are retained and that there exists no specific π-π interaction between the porphyrin and pyrene/anthraquinone subunits in these dyads.

Excitation of **H$_2$-Py** and **Zn-Py** derivatives at 550 nm (where porphyrin absorbs predominantly) results in no quenching of fluorescence due to the porphyrin moiety, but that at 290 nm (pyrene absorbs predominantly) results in a quenching of fluorescence due to the appended pyrene moiety. The fluorescence life times (τ) of the porphyrin parts of both **H$_2$-Py** and **Zn-Py** (λ_{ex} = 411 nm) remained quite similar to those of **H$_2$TTP** and **ZnTTP** but those of their pyrene

subunits (λ_{ex} = 290 nm) were found to be considerably shorter in comparison with the lifetime of pyrene. An intramolecular EET mechanism is proposed for the substantial decrease in fluorescence in both **H_2-Py** and **Zn-Py** derivatives. **H_2-AQ** and **Zn-AQ** were shown to exhibit substantial quenching of the porphyrin fluorescence as measured against the monomeric analogues in steady-state fluorescence experiments. Thermodynamic considerations based on the redox potential and singlet state energy data indicate an intramolecular PET from the excited state of porphyrin to anthraquinone in both derivatives. This was further proved by the time-resolved fluorescence decay experiments and the electron-transfer rate constants, k_{ET} were found to dependent on the solvent. It is also possible that the bridging azomethine group may have a role to play in the efficient EET or PET observed in the present set of dyads, but it is not apparent from the results obtained in this study. Studies addressing this issue are currently in progress.

7.3 Future scope

The present study has been helpful, to some extent, not only in formulating strategies towards the design of new types of porphyrin arrays and D-A systems but also in probing certain intricacies involved in the PET and EET reactions in these compounds. Notwithstanding this fact, an in-depth analysis of the results described in various Chapters of this thesis suggests that a lot more remains to be done to generate more sophisticated D-A compounds/arrays and to arrive at a better understanding of the EET and PET mechanisms. For example, more elaborate photophysical experiments involving the time-resolved absorption and fluorescence techniques can be carried out to learn more about the mechanistic details of the PET and EET reactions occurring in these D-A systems. Axial-bonding type, D-A systems based-on metallo/metalloid porphyrins having rigid

spacers can be built and the intricacies involved in the PET and EET reactions occurring in them can be compared with those of systems described in Chapters 3 and 4. The experience gained in this study while working on various D-A systems can be advantageously used for the construction of triads/arrays of the type D-A_1-A_2, D_1-A-D_2 and A_1-D-A_1 etc.

The results described in Chapter 3 and 4 provide some insight into the design aspects of new, architecturally more-appealing supramolecular arrays. For example, it should be possible to use other main group element containing porphyrins (e.g. Al(III) or Sb(V)) as the basal scaffolds and generate the 'axial-bonding' type dimers shown in Fig. 7.1. It should also be possible to synthesize a un-symmetrical D-A compounds by utiliizing the axial-bonding capabilities of Sb(V) containing porphyrins.

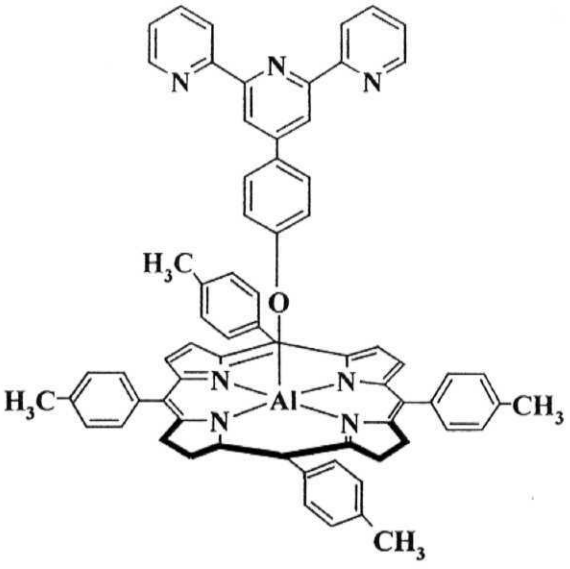

Fig. 7.1

7.4 References

1) Wasielewski, M. R. *Chem. Rev.* **1992**, 92, 435.

2) Kumar, A. A.; Giribabu, L.; Reddy, D. R.; Maiya, B. G. *Inorg. Chem.* **2001**, *40*, 6757.

3) Giribabu, L.; Rao, T. A.; Maiya, B. G. *Inorg. Chem.* **1999**, *38*, 4971.

4) Baranoff, E.; Collin, J.-P.; Flamigni, L.; Sauvage, J.-P. *Chem. Soc. Rev.* **2004**, *33*, 147.

5) Flamigni, L.; Barigelletti, F.; Armaroli, N.; Collin, J.-P.; Dixon, I. M.; Sauvage, J.-P. Williams, J. A. G. *Coord. Chem. Rev.* **1999**, *190-192*, 671.

Appendix I

X-ray crystallographic data of [L^1Sn(O-ptp)$_2$]

Table 1. Atomic coordinates (x10^4) and equivalent isotropic displacement parameters (Å^2 x 10^3) for **[L^1Sn(O-ptp)$_2$]**. U(eq) is defined as one third of the trace of the orthogonalized Uij tensor.

Atom	x	y	z	U(eq)
Sn	0	5000	5000	22(1)
O(1)	1344(3)	3217(3)	5347(2)	30(1)
N(1)	198(3)	5669(3)	6195(2)	24(1)
N(2)	1501(4)	5509(3)	4177(2)	26(1)
C(35)	6447(5)	1389(5)	11071(4)	42(1)
N(4)	4149(4)	1269(4)	10778(3)	34(1)
C(42)	2982(5)	258(5)	12406(4)	44(1)
C(21)	1004(4)	6282(4)	6199(3)	26(1)
C(13)	1913(4)	6465(4)	5428(3)	27(1)
C(12)	2104(4)	6148(4)	4493(3)	27(1)
C(11)	2906(4)	6497(4)	3674(3)	30(1)
C(10)	2743(4)	6104(4)	2888(3)	29(1)
C(9)	1870(4)	5468(4)	3193(3)	27(1)
C(8)	1447(4)	4895(4)	2618(3)	24(1)
C(24)	-543(4)	5672(4)	7084(3)	24(1)
C(23)	-212(4)	6348(4)	7665(3)	27(1)
C(22)	733(4)	6709(4)	7129(3)	29(1)

C(5)	1970(4)	4932(4)	1566(3)	26(1)
C(6)	3318(4)	4416(4)	1257(3)	30(1)
C(7)	3793(4)	4470(4)	283(3)	33(1)
C(2)	2940(5)	5032(5)	-408(3)	34(1)
C(3)	1598(5)	5523(5)	-98(3)	35(1)
C(4)	1104(4)	5484(4)	878(3)	29(1)
C(1)	3475(5)	5128(5)	-1460(3)	44(1)
C(14)	2757(4)	7081(5)	5633(3)	31(1)
C(20)	4040(5)	6351(5)	5811(4)	40(1)
C(19)	4840(5)	6902(6)	5999(4)	47(1)
C(17)	4387(6)	8170(6)	6008(3)	45(1)
C(16)	3099(6)	8886(6)	5845(4)	47(1)
C(15)	2290(5)	8344(5)	5654(3)	38(1)
C(18)	5270(7)	8760(8)	6190(4)	72(2)
C(25)	1817(4)	2849(4)	6200(3)	32(1)
C(26)	2891(5)	3072(5)	6340(3)	37(1)
C(27)	3367(5)	2721(5)	7220(3)	39(1)
C(28)	2778(4)	2147(4)	8013(3)	32(1)
C(29)	1740(4)	1874(4)	7838(3)	31(1)
C(30)	1260(5)	2233(4)	6960(3)	33(1)
C(31)	3238(4)	1851(4)	8967(3)	31(1)
C(32)	4447(4)	1857(4)	9079(3)	32(1)
C(33)	4840(4)	1591(4)	9982(3)	33(1)
C(34)	6105(5)	1633(4)	10132(4)	36(1)
N(3)	6841(4)	1922(4)	9349(3)	39(1)
C(38)	7988(5)	1914(5)	9494(4)	45(1)

C(37)	8450(6)	1625(5)	10374(5)	51(1)
C(36)	7629(6)	1406(6)	11180(5)	54(2)
C(40)	2511(4)	1522(4)	9803(3)	33(1)
C(39)	3004(5)	1215(5)	10682(3)	34(1)
C(41)	2350(5)	737(5)	11564(4)	36(1)
N(5)	1181(4)	708(4)	11526(3)	42(1)
C(45)	658(4)	172(5)	12335(4)	37(1)
C(44)	1199(6)	-298(5)	13147(4)	48(1)
C(43)	2409(7)	-247(6)	13185(4)	55(2)
O(2)	876(11)	11302(11)	4946(10)	208(5)

Table 2. Selected bond lengths [Å] and angles [deg] for **[L^1Sn(O-ptp)$_2$]**

O(1)SnN(1)	93.37(12)
O(1)SnN(2)	91.34(13)
O(1)SnO(1)	180
O(1)SnN(1)	86.63(12)
O(1)SnN(2)	88.66(13)
N(1)SnN(2)	89.97(13)
O(1)SnN(1)	86.63(12)
N(1)SnN(1)	180
N(1)SnN(2)	90.03(13)
O(1)SnN(2)	88.66(13)
N(1)SnN(2)	90.03(13)
N(2)SnN(2)	180
O(1)SnN(1)	93.37(12)

O(1)SnN(2)	91.34(13)
N(1)SnN(2)	89.97(13)
SnO(1)C(25)	122.5(3)
SnN(1)C(21)	125.7(3)
SnN(1)C(24)	125.3(3)
C(21)N(1)C(24)	108.8(3)
SnN(2)C(9)	125.4(3)
SnN(2)C(12)	125.0(3)
C(9)N(2)C(12)	108.6(4)
C(34)N(3)C(38)	115.9(5)
C(33)N(4)C(39)	117.4(4)
C(41)N(5)C(45)	115.9(4)
N(2)C(9)C(8)	124.9(4)
N(2)C(9)C(10)	107.6(4)
N(2)C(12)C(11)	107.7(4)
N(2)C(12)C(13)	126.3(4)
N(1)C(21)C(13)	126.0(4)
N(1)C(21)C(22)	107.8(4)
N(1)C(24)C(23)	107.7(4)
N(1)C(24)C(8)	126.4(4)
O(1)C(25)C(26)	120.6(4)
O(1)C(25)C(30)	121.3(4)
N(4)C(33)C(32)	123.5(5)
N(4)C(33)C(34)	115.0(4)
N(3)C(34)C(33)	116.9(5)
N(3)C(34)C(3)	123.7(5)

N(3)C(38)C(37)	125.1(6)
N(4)C(39)C(40)	122.6(4)
N(4)C(39)C(41)	115.0(4)
N(5)C(41)C(39)	117.8(4)
N(5)C(41)C(42)	121.5(5)
N(5)C(45)C(44)	125.7(5)
SnO(1)	2.062(3)
SnN(1)	2.084(3)
SnN(2)	2.100(3)
SnO(1)	2.062(3)
SnN(1)	2.084(3)
SnN(2)	2.100(3)
O(1)C(25)	1.346(5)
N(1)C(21)	1.378(6)
N(1)C(24)	1.372(5)
N(2)C(9)	1.384(5)
N(2)C(12)	1.380(6)
N(3)C(34)	1.336(7)
N(3)C(38)	1.340(8)
N(4)C(33)	1.334(6)
N(4)C(39)	1.349(8)
N(5)C(41)	1.340(8)
N(5)C(45)	1.365(7)

Symmetry transformations used to generate equivalent atoms: 1-x, -y+1, z+1

Appendix II

List of publications

(* = work not relevant to the present thesis)

1. Aluminium(III) porphyrin based dimers and trimers: synthesis, spectroscopy and photochemistry. **P. Prashanth Kumar** and Bhaskar G. Maiya, *New J. Chem.* **2003,** *27*, 619.
2. Photochemistry of arrays, switches and energy transfer systems based on metalloid porphyrin building blocks. **P. Prashanth Kumar** and Bhaskar G. Maiya, *Proc. Ind. Nat. Sci. Acad. A* **2003**, *69*, 83.
3. Free-base, copper(II) and zinc(II) derivatives of an azomethine bridged 'porphyrin-pyrene' dyad: Synthesis, spectroscopy and photochemistry. **P. Prashanth Kumar** and Bhaskar G. Maiya, *Ind. J. Chem: Section A* **2003**, 2198.
4. Bis(aryloxo) derivatives of azo-benzene bridged tin(IV) porphyrin dimers: Synthesis, spectroscopy and photochemistry. **P. Prashanth Kumar**, G. Premaladha and Bhaskar G. Maiya (*manuscript under preparation*).*
5. Porphyrin-anthraquinone dyads: Synthesis, spectroscopy and photochemistry. **P. Prashanth Kumar** and Bhaskar G. Maiya (*communicated*).
6. Crystal structure of self-assembled 5-(4-aminophenyl)-10,15,20-tritolyl porphyrinatozinc(II). **P. Prashanth Kumar** and Bhaskar G. Maiya (*to be communicated*).

7. Porphyrin dyads and triads with ruthenium(II) bis-terpyridine complex: Synthesis, spectroscopy and photochemistry. **P. Prashanth Kumar** and Bhaskar G. Maiya (*to be communicated*).
8. Synthesis and characterization of axial bis(terpyridoxy) Sn(IV) and P(V) porphyrins: Modulation of electron and energy transfer by transition metal ions. **P. Prashanth Kumar** and Bhaskar G. Maiya (*to be communicated*).
9. Nucleobase appended tricationic water-soluble porphyrins: Synthesis, characterization, binding and photo-cleavage studies with DNA. G. Premaladha, **P. Prashanth Kumar** and Bhaskar G. Maiya (*manuscript under preparation*).*